AD-A059 564 COLORADO UNIV BOULDER DEPT OF ELECTRICAL ENGINEERING F/G 12/2
SYNTHESIS OF MULTIPLE-LOOP FEEDBACK SYSTEMS WITH PLANT MODIFICA--ETC(U)
AUG 78 B WANG, I HOROWITZ AFOSR-76-2946

UNCLASSIFIED AFOSR-TR-78-1341 NL

1 OF 3
AD
A059 564

AFOSR-TR- 78-1341

(2) LEVEL II

AD A059564

DDC FILE COPY

DDC
RECEIVED
OCT 6 1978
B

78 09 13 118

Approved for public release;
distribution unlimited.

DDC FILE COPY AD A059564

(2) LEVEL II

(18) AFOSR (19) TR-78-1341

(6) SYNTHESIS OF MULTIPLE-LOOP FEEDBACK SYSTEMS WITH PLANT MODIFICATION,

by

(10) Bor-Chyun/Wang
Isaac/Horowitz

(16) 2304
(17) A1

Department of Electrical Engineering
University of Colorado
Boulder, Colorado 80309

(9) Interim rept.,

This research was supported by the
AIR FORCE OFFICE OF SCIENTIFIC RESEARCH
under Research Grant (15) AFOSR-76-2946

(11) August 1978

(12) 270 p.

DISTRIBUTION STATEMENT A
Approved for public release;
Distribution Unlimited

DDC
RECEIVED
OCT 6 1978
B

78 09 13 118

088 440

SUMMARY

Consider the constrained part (denoted as the Plant) of a control system, consisting of n cascaded sections, each of whose outputs can be sensed for feedbck purposes. Feedback from these points is to be used to achieve apriori specified tolerances on the system response, despite great uncertainty in plant parameter values. In this first quantitative work of its kind, the feedback is permitted to proceed directly to internal plant variables, constituting "plant modification". The reason is that the internal plant signal levels needed to achieve a specific output are now affected by the feedback loops. This is in contrast to previous quantitative research in which the feedback was confined to the plant input. The plant signal levels needed to achieve a specific output were then not influenced by the feedback.

Plant modification feedback permits greater reduction in the "cost of feedback", in terms of feedback loop bandwidths and effect of sensor noise, at the cost of increase in plant internal signal levels. In this work, the maximum permitted increase Q in signal level, is part of the design specifications. A step by step design procedure is presented for satisfying this Q requirement and the system response tolerances over the given range of plant uncertainty, and doing so at sensibly minimum "cost of feedback". This permits the designer to achieve desired trade-off between increased plant signal level and cost of feedback.

TABLE OF CONTENTS

White Section
Buff Section
ABILITY CODES
d/or SPECIAL
A

LIST OF TABLES

LIST OF FIGURES

CHAPTER 1

STATEMENT OF PROBLEM AND PRELIMINARY BACKGROUND

1.1 Introduction

This work deals with the problem of making a system perform satisfactorily despite uncertainty, in the following context:

Equipment has been assembled by specialists in the area of concern, in order to achieve certain objectives, for example, an airframe and engine for accomplishment of certain aeronautical objectives, a chemical plant for production of certain chemicals, etc. This assembly of equipment is denoted as the plant. The plant has the ability, the muscle so to speak, to achieve the objectives. However, it does not have the accuracy needed. This is manifested by uncertainty in the parameters of the mathematical relations describing the plant. For example in Figure 1.1, suppose the relation

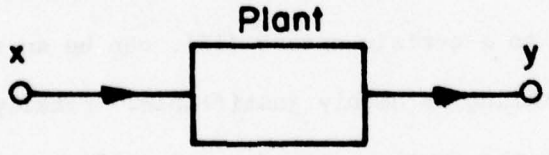

Figure 1-1. Plant

between plant output y and input x is given by a linear time-invariant (&ti) ordinary differential equation

$$y^{(n)} + A_1 y^{(n-1)} + \ldots + A_n y = K[x^{(m)} + B_1 x^{(m-1)} + \ldots + B_m x] \qquad (1.1\text{-}1)$$

i.e., the A_i , B_j are constants. There are q physical parameters $k_1,\ldots,k_q$ and K , A_i , B_j are functions of these parameters. The values of these parameters are not known precisely, but it is known that they lie within certain bounds $k_i \in [k_i^1, k_i^2]$. Hence, each possible parameter vector k , each combination of k_i values $i = 1,\ldots,q$, gives a different plant transfer function, generating a set $\mathcal{P} = \{P(s)\}$ of possible plant transfer functions.

Such a formulation of the uncertainty problem may appear naive because one might argue that often the parameter values change with time-giving uncertain linear time-varying relations, because the rate of variation is uncertain. Also, the ℓti description is usually an approximation of a nonlinear relation. We are really assuming ℓti relations with the above uncertainty form, in order to be able to rigorously use Laplace transforms and frequency response methods. However, it has been rigorously proven [16] that uncertain linear time-varying plant problems are reducible to the above ℓti uncertainty form, and even uncertain nonlinear time-varying plant to a certain extent [15], can be so reduced. Hence the above modelling is highly justifiable. Finally, one must begin somewhere with the development of a scientific synthesis theory for uncertain systems, and the ℓti case is obviously where to start.

The objective is to achieve certain apriori specified performance objectives $\forall\, p \in \mathcal{P}$. Since the overall system is to be ℓti , it can be characterized by its response to any input, and the

step response is very popular because it combines within it both the fastest kind of input (an abrupt change) and the slowest (no change). Time domain specifications are reasonable in many cases, as in Figure 1.2a, the step response is to be inside the bounds b_1 , b_2 $\forall$ P $\in$ $\mathcal{P}$, with additional bounds of similar nature on the

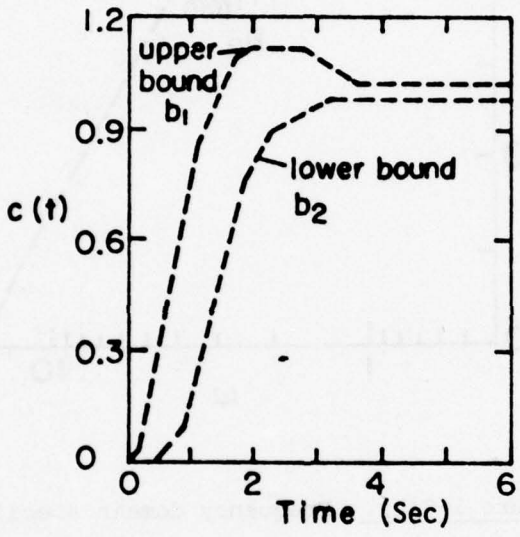

Figure 1-2(a). Time domain step response specification.

first and perhaps higher derivatives. Our design technique is in the frequency-domain, so we must translate such t-domain bounds into "equivalent" ω-domain bounds on the system frequency response $T(j\omega)$. If the system is minimum-phase [2], $|T(j\omega)|$ suffices and we restrict ourselves here to such systems. This translation is, as of this date, an engineering art rather than a science. Advice on how to translate is scattered in the literature [2,6,14]. Very good results have been obtained with only moderate effort. We shall

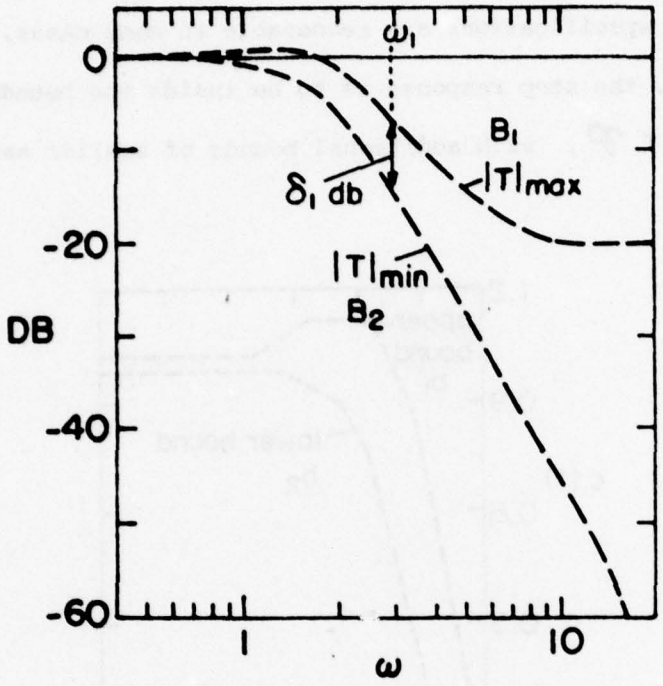

Figure 1-2(b). Frequency domain specification.

assume in this work this translation has already been done. It is worth noting that it has been shown [15] that for minimum-phase systems, time-domain specifications on the step response and on its derivative of the following nature

$$b_2^{(i)}(t) \leq c^{(i)}(t) \leq b_1^{(i)}(t) \ , \ i = 0,1,\ldots,n \qquad (1.1\text{-}2)$$

can always be satisfied by means of ω-domain bounds of the following nature

$$B_2(\omega) \leq |C(j\omega)/R(j\omega)| \leq B_1(\omega) \ . \qquad (1.1\text{-}3)$$

In our work, the bounds on system performance will have this form.

1.1.1. Previous work

The quantitative aspect of our work cannot be over-emphasized. The sensitivity reduction capability of feedback is very well-known. Hundreds of books and thousands of papers have been written on the subject, but the number of these which are quantitative in nature is extremely small, i.e., with uncertainty bounds and performance bounds explicitly included in the problem statement. It is as if the mere use of a feedback configuration around the uncertain plant, suffices to scare it into docile behavior. In the vast majority of the techniques the uncertainty is completely ignored, and there are no or extremely crude performance specifications. One presumably emerges with the same design whether the parameter uncertainty is x% or 1000x%, and irrespective of whether the bounds B_1 , B_2 in Figure 1-2(b) are narrow or wide apart. There is no concern with the 'cost of feedback' - which, aside from the sensors, lies in the bandwidth of the loop transfer function, and little concern with the extremely important matter of sensor noise [see Sec. 1.2]. These points have been emphasized in [5].

Our work follows closely in the tradition of 'quantitative synthesis' recently established [2,5,8]. To appreciate the present work, it is important to be aware of the highlights of this previous work. Quantitative synthesis was first developed for a plant with only one variable, the plant output, $c(t)$ in Figure 1-3, available for feedback [2]. The system command input $r(t)$ was also assumed accessible, so the processing of these two signals provides two independent compensation functions to the designer. An infinitude of canonical two-degree-of-freedom

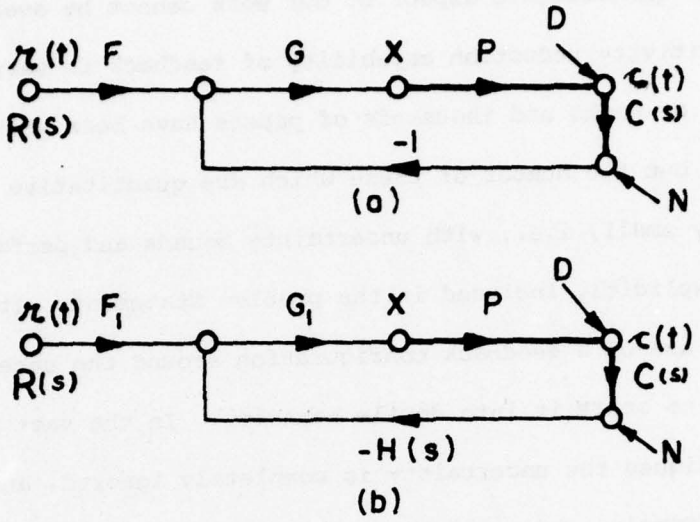

Figure 1-3. Structures of 2-D.O.F. system.

structure may be used [4]. The design procedure developed in [2] used Figure 1-3(a), but suppose the sensor transfer function is $H(s)$, then one can use Figure 1-3(b), letting G_1H (of Figure 1-3(b)) = G (of Figure 1-3(a)), in order to have the same loop transmission function $L(s) = GP = G_1PH$, and $F_1G_1 = FG$ in order to have the same system transfer function

$$T(s) = \frac{FGP}{1+GP} = \frac{F_1G_1P}{1+G_1PH} \quad . \tag{1.1-4}$$

1.1.2. A 2-degree-of-freedom structure with 2-loop implementation

Suppose large loop feedback bandwidth is needed and it is found that an independent sensor measuring $\dot{c}(t)$ (e.g., a tachometer in a position servo) gives less noise than the differentiation

of a position sensor, so both sensors are used, as in Figure 1-4, with the two sensor transfer functions H_1 , H_2 , and say the structure in Figure 1-4 is used. This is a two-loop structure

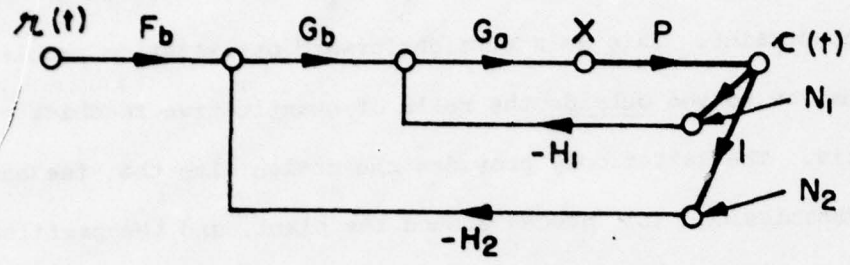

Figure 1-4. 2-loop, 2-D.O.F. structure.

physically, but in terms of fundamental feedback design it is a two-degree-of-freedom system, so the quantitative design theory of Figure 1-3(a) is used, giving G and F . It is required that the loop transmission around P , be the same in both cases, i.e.,

$$L = PG \text{ (Fig.1-3(a))} = P\, G_a(H_1+G_bH_2) \tag{1.1-5}$$

and

$$T = F\,\frac{GP}{1+GP} \text{ (Fig.1-3(a))} = F_b\,\frac{G_bG_aP}{1+P[G_a(H_1+G_bH_2)]} \tag{1.1-6}$$

so

$$G = G_a(H_1+G_bH_2) \ , \quad FG = F_bG_bG_a \ . \tag{1.1-7}$$

H_1, H_2 are known, so one must decide how to split $G = G_a(H_1+G_bH_2)$ between G_a and G_b . This is done by considering the effect of sensor noise N_1 , N_2 at the plant input,

$$-X_N(j\omega) = \frac{G_a(H_1N_1+H_2G_bN_2)}{1+P[G_a(H_1+G_bH_2)]} \tag{1.1-8}$$

given that

$$G = \frac{L}{P}(j\omega) = G_a(H_1+H_2G_b) \qquad (1.1\text{-}9)$$

is fixed by the quantitative design technique of [2].

The objective is to minimize $\int_0^\infty |X_N|^2 \, d\omega$, subject to the above constraint. This is a straightforward optimization problem which can be solved outside the realm of quantitative feedback synthesis. The latter only provides the design with the feedback loop transmission (L) needed around the plant, and the prefilter (F) needed to process the command input r(t) . The state-of-the-art in sensors and in filter synthesis determines how L and F are to be realized. In fact, in the above context one might consider use of an accelerometer in a 3-loop feedback structure. But from our point of view the structure remains that of a two-degree-of-freedom system and we shall continue to associate the latter with a single-loop system.

1.2 Review of Two-Degree-of-Freedom Quantitative Design Theory

Figure 1-3(a) is used with $T = F\,\frac{GP}{1+GP}$. It is assumed that the compensation network, whose power level can be very low (as the plant contains the power elements), can be constructed with negligible uncertainty in their transfer functions. Hence, due to the uncertainty in P ,

$$\Delta \ln T = \Delta \ln \frac{GP}{1+GP} = \Delta \ln \frac{L}{1+L} , \quad L = GP \qquad (1.2\text{-}1)$$

and

$$\Delta \ln |T(j\omega)| = \Delta \ln \left|\frac{L(j\omega)}{1+L(j\omega)}\right| . \qquad (1.2\text{-}2)$$

Given that $\Delta \ln |T(j\omega)| \lesssim \delta_1$ db for example at ω_1 in Figure 1-2(b), what are the resulting constraints on $L(j\omega)$? It is convenient to pick a "nominal" plant $P_o(s)$, and derive the bounds on the resulting "nominal" loop function $L_o = P_o G$. These bounds can be found by means of a digital computer, but it is very useful for insight to see it done on the Nichols' chart (logarithmic complex plane with abscissa in degrees, ordinate in decibels = 20 $\log_{10}$). The procedure is illustrated for the case

$$P(s) = \frac{ka}{s(s+a)} \quad ; \quad 1 \lesssim k \lesssim 10 \; ; \quad 1 \lesssim a \lesssim 10 \quad . \tag{1.2-3}$$

At $\omega = 2$ rps , $P(j2)$ lies within the boundaries given by ABCD in Figure 1-5. Since $\ln L = \ln G + \ln P$, the pattern outlined by

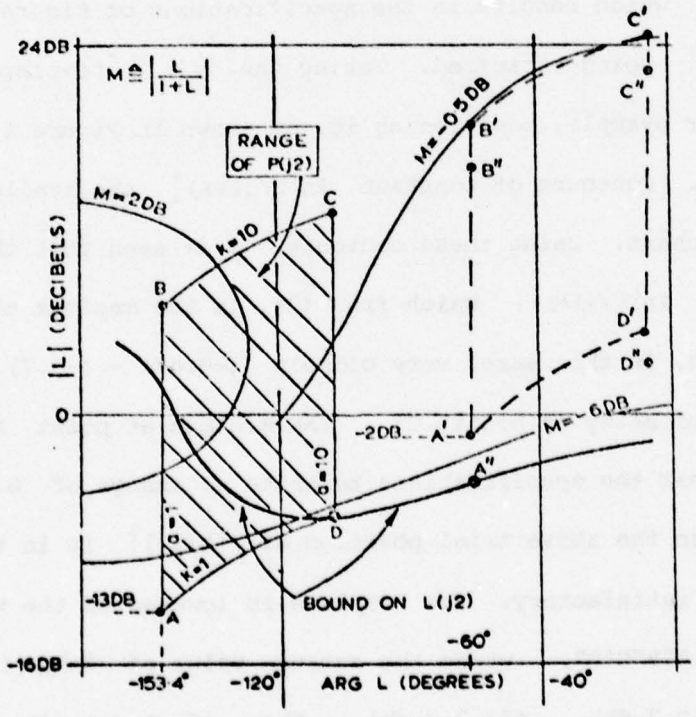

Figure 1-5. Derivation of bounds on $L(j\omega)$ on Nichols chart.

ABCD may be translated, but not rotated, on the Nichols' chart, the amount of translation being given by the value of $\ell n\ G(j2)$. For example, if a trial design of $L(j2)$ corresponds to the template $P(j2)$ at A'B'C'D' in Figure 1-5, then

$$|G(j2)|_{db} = |L(j2)|_{db} - |P(j2)|_{db}$$
$$= (-2.0) - (-13.0) = 11.0 \text{ db} \qquad (1.2\text{-}4)$$

$$\text{Arg } G(j2) = \text{Arg } L(j2) - \text{Arg } P(j2)$$
$$= (-60°) - (-153.4°) = 93.4° \ . \qquad (1.2\text{-}5)$$

1.2.1. Bounds on $L(j\omega)$ in the Nichols' chart.

The templates of $P(j\omega)$ are manipulated to find the position of $L(j\omega)$ which results in the specifications of Figure 1-2(b) on $\ell n\ |T(j\omega)|$ being satisfied. Taking the $\omega = 2$ template, one tries, for example, positioning it, as shown in Figure 1-5, at A'B'C'D' . Contours of constant $\ell n|L/(1+L)|$ are available on the Nichols' chart. Using these contours, it is seen that the maximum change in $\ell n|L/(1+L)|$ which from (2), is the maximum change in $\ell n\ |T|$ is, in this case, very closely (-0.49) - (-5.7) = 5.2 db , the maximum being at point C' , the minimum at point A' . Suppose that the specifications tolerate a change of 6.5 db at $\omega = 2$, so the above trial position of $|L(j2)|$ is in this case more than satisfactory. The template is lowered on the Nichols' chart to A"B"C"D", where the extreme value of $\ell n|L/(1+L)|$ are at C" (-0.7 db) , A"(-7.2 db) . Thus, if $\text{Arg } L_A(j2) = -60°$, then -4.2 db is the smallest magnitude of $L_A(j2)$ which satis-

fies the 6.5 db specification for Δ ℓn $|T|$. Any larger magnitude is satisfactory but represents over-design at that frequency. The manipulation of the $\omega = 2$ template is repeated along a new vertical line, and a corresponding new minimum of $|L_A(j2)|$ found. Sufficient points are obtained in this manner to permit drawing a continuous curve of the bound on $L_A(j2)$, as shown in Figure 1-5. The above is repeated at other frequencies, resulting in a family of boundaries on $L_A(j2)$.

1.2.2. Nature of the bounds on $L(j\omega)$.

A typical set of bounds is shown in Figure 1-6. The bounds

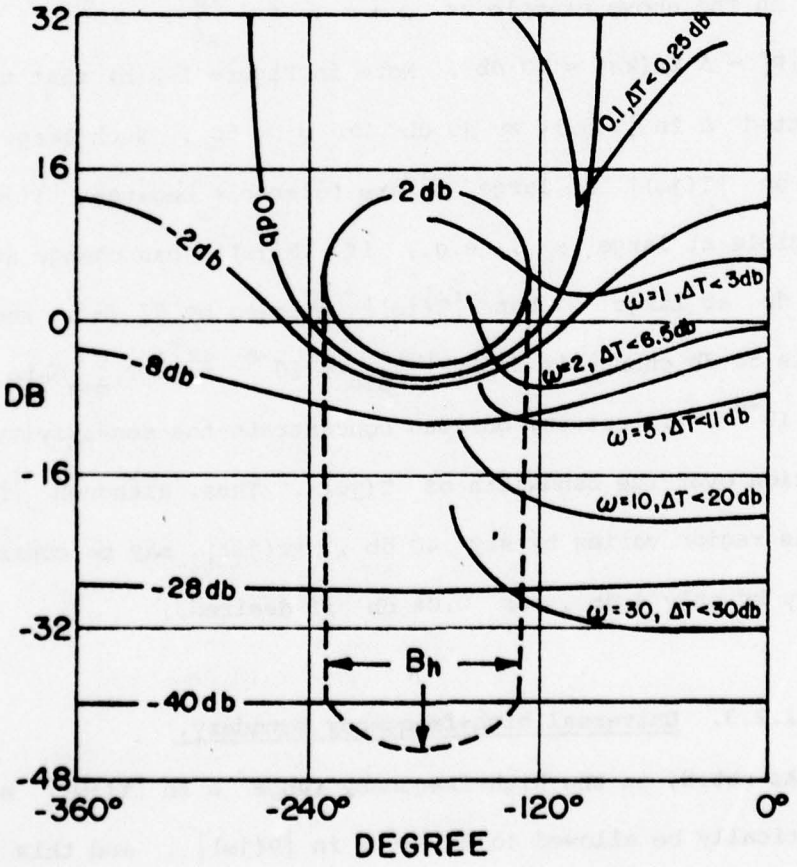

Figure 1-6. Typical bounds of L in Nichols' chart.

tend to move down in the Nichols' chart (become less onerous), obviously because as ω increases, greater change in $|T(j\omega)|$ is permitted, as in Figure 1-2(b). It is in fact essential that at large enough ω, the uncertainty in $|T(j\omega)|$ (i.e., the bounds on $|T(j\omega)|$) be greater than the uncertainty in $P(j\omega)$, because the net sensitivity reduction is always zero in any practical system as was long ago [1] shown by Bode,

$$\int_0^\infty \ell n \, |S_P^T(j\omega)| \, d\omega = - \int_0^\infty \ell n \, |1+L(j\omega)| \, d\omega = 0 \qquad (1.2\text{-}6)$$

where $S_P^T = \frac{\partial T/T}{\partial P/P}$ is the sensitivity function.

In the above example as $\omega \to \infty$, $P \to \frac{ka}{s^2}$, so $\Delta \ell n \, |P| \to \Delta \ell n(ka) = 40$ db. Note in Figure 1-2(b) that the permitted $\Delta \ell n \, |T(j\omega)| \gg 40$ db for $\omega > 50$. Such large tolerances on $|T(j\omega)|$ at large ω are tolerable because $|T(j\omega)|$ is negligible at large ω, e.g., if $|P(j\omega)|$ can change at most by 40 db at large ω but $|T(j\omega)|$ changes by 52 db, who cares if this 52 db change is from $|T|_{min} = 10^{-6}$ to $|T|_{max}$ to 400×10^{-6}. In return, one can concentrate the sensitivity reduction over the bandwidth of $T(j\omega)$. Thus, although $|P(j\omega)|$ in this region varies by say 40 db, $|T(j\omega)|$ may be controlled to vary by only 4 db, or 0.04 db if desired.

1.2.3. Universal high-frequency boundary.

As noted, in the high-frequency range $\Delta \ell n \, |T(j\omega)|$ must realistically be allowed to be $\gg \Delta \ell n \, |P(j\omega)|$, and this is reflected in the bounds on $L_o(j\omega)$ tending to a very narrow pencil.

In Figure 1-7, B_ν^p is drawn for the case $\Delta \ln L = \Delta \ln k = 20$ db, $\Delta \ln |T(j\omega)| = \Delta \ln |L/(1+L)| \leq 23$ db at ω_ν. However, the resulting peak value of $|L/(1+L)|$ is 23 db = 14.1 arithmetic at $k = k_{max}$, indicating a highly under-damped pole pair at the corresponding frequency with damping ratio $\xi = 0.034$, when $k = k_{max}$. This tremendous peaking does not appear in the system response to the command inputs R, because it is filtered out by the pre-filter F in Figure 1-3(a). But the system response to a disturbance D is given by $T_d = \frac{C}{D} = (1+L)^{-1}$. Disturbance attenuation generates its own requirements on L, which may lead to more stringent bounds on L than those due to $T(j\omega)$. The

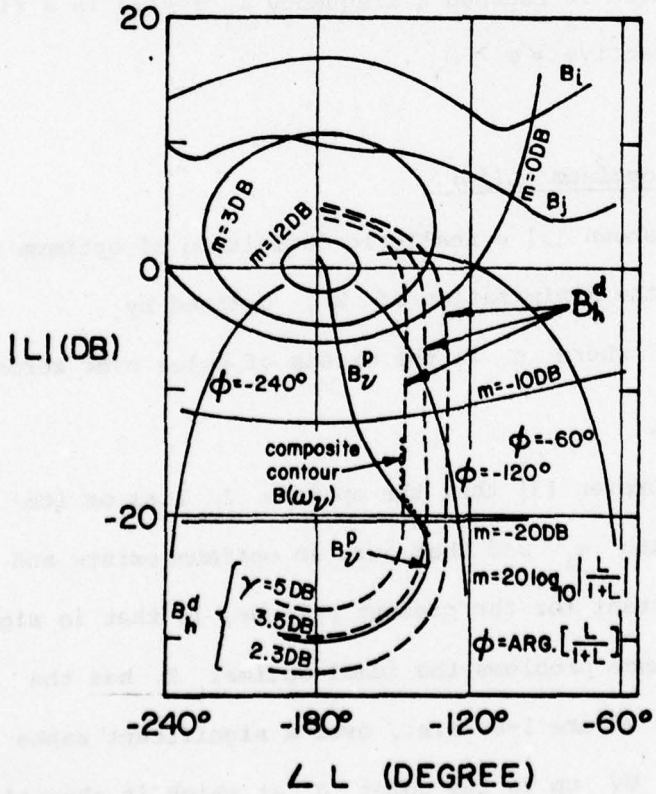

Figure 1-7 Bounds on $L(j\omega)$ on Nichols' chart

final contours used in the design [2] must be the most stringent composite of the two. However, even if D is very small, it is usually certain that a peak $|T_d|$ of 14.1 is intolerable. It is reasonable to add a requirement $|T_d| \leq \gamma$ some constant, for all ω and over the whole range of P parameter values. The resulting constraining contours denoted by B_h^d are shown in Figure 1-7 for the case $\Delta \ell n\, k = 20$ db , and for $\gamma = 2.3, 3.5, 5$ db (all these contours are symmetrical with respect to the vertical line Arg $L = -180°$ on the Nichols' chart). If $\gamma = 5$ db is used, then $B(\omega_\nu)$ indicates the composite contour shown in Figure 1-7. For $\omega > \omega_\nu$, $|\Delta T(j\omega)|$ increase while γ remains the same, so that sooner or later there is reached a frequency $\omega_\gamma \ni B(\omega)$ *is a fixed* boundary B_h^d , effective $\forall\, \omega > \omega_\gamma$.

1.2.4. The optimum $L(j\omega)$.

It has been shown [3] a realistic definition of optimum in the ℓti system is the minimization of k , defined by $\lim_{s\to\infty} L(s) = k\, s^{-e}$, where e is the excess of poles over zeros assigned to $L(s)$.

It has been proven [3] that the optimum L lies on its boundary B_i at each ω_i and that such an optimum exists and is unique. Most important for the present purpose, is that in significant plant ignorance problems the ideal optimal L has the properties shown in Figure 1-8, i.e., over a significant range it follows B_h along UV up to the point J at which it abruptly jumps to infinity along $WW'W''$ and returns on the vertical line

YZ , whose phase is $(-90°)\cdot e$. Such an ideal $L(j\omega)$ is, of course, impractical. A practical suboptimum L is shown in Figure 1-8.

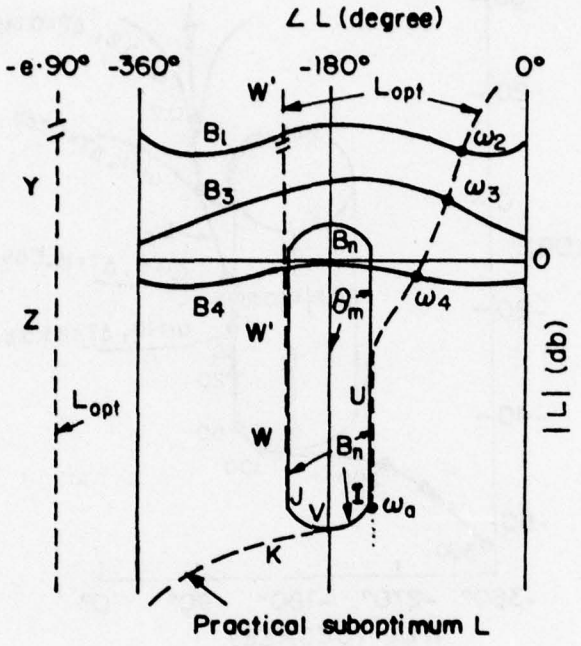

Figure 1-8. Bounds on L and Optimum L on Nichols' Chart.

Some results of a numerical design example are shown in Figure 1-9. They were derived for the following problem.

1.2.5. Numerical example. (Figure 1-3(a)).

Plant: $P = P_1 P_2$

Plant ignorance: $P_1 = k_1/s$, $\sqrt{2} \leq k_1 \leq 10\sqrt{2}$

$P_2 = k_2/s$, $\sqrt{2} \leq k_2 \leq 10\sqrt{2}$

Performance Specification: Shown in Figure 1-2(b) were originally derived from time domain bounds of Figure 1-2(a).

Disturbance response: $\gamma \leq 2.0$ db .

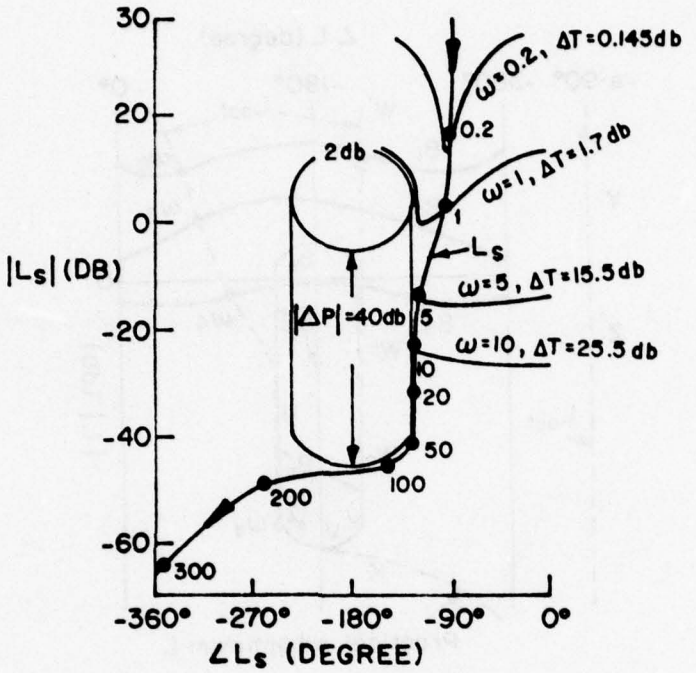

Figure 1-9. Single loop L_s and bounds of a numerical example.

This example is used later in Chapter 2 as a vehicle for presenting the plant-modification design technique.

1.3 Cost of Feedback and Effect of Sensor Noise

In significant plant ignorance problems, there is a strong tendency for the design to be such that N , in Figure 1-3(a), is so highly amplified as to saturate the plant input at X . The noise response function is (see Figure 1-3(a))

$$T_N \triangleq \frac{X}{N} = \frac{-G}{1+GP} = \frac{-L/P}{1+L}$$

$$\approx -L/P \quad \text{in h.f. range.} \qquad (1.3\text{-}1)$$

The noise response of the numerical design example of the last section is shown in Figure 1-10. Notice that the noise component at x , in Figure 1-3(a), is most important in the high-frequency range where the useful command and disturbance components due to D , are relatively small, rather than in the low frequency range where the latter are relatively large. This is further enhanced by the fact that arithmetic scales, shown in Figure 1-11, must be used to find

$$(x_N)_{rms} = \sqrt{\int_0^\infty (|T_N|^2 \cdot \Phi_N)\, d\omega} \quad , \quad \Phi_n = \text{noise power spectrum} \qquad (1.3\text{-}2)$$

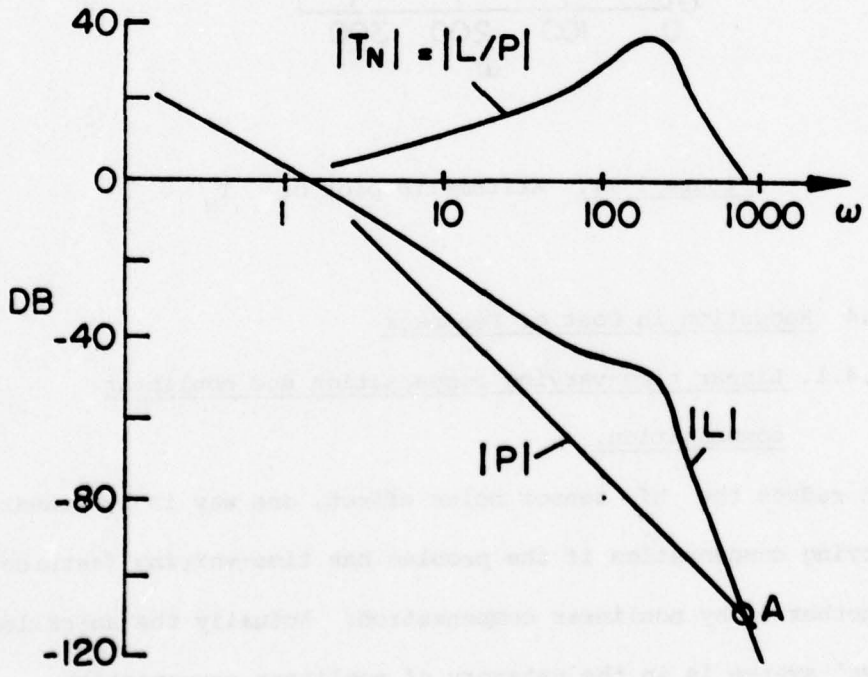

Figure 1-10. The noise response and |L| , |P| .

Hence, it is desirable to decrease $|L|$ vs ω, as fast as possible in the high frequency range. Even a saving which is small in the logarithmic scale near A in Figure 1-10, can be significant in rms sensor noise effect.

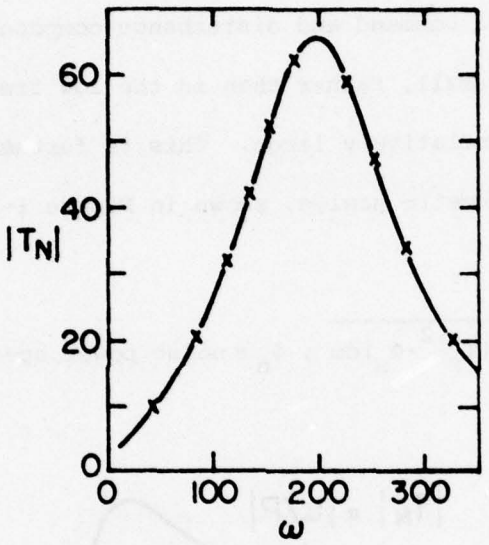

Figure 1-11. Arithmetic plot of T_N.

1.4 Reduction in Cost of Feedback

1.4.1. Linear time-varying compensation and nonlinear compensation.

To reduce the hf sensor noise effect, one way is by linear time-varying compensation if the problem has time-varying features [7]. Another is by nonlinear compensation. Actually the so-called "adaptive' system is in the category of nonlinear compensation. They may or may not be better than lti compensation in reducing the 'cost of feedback'. It is noteworthy and scandalous that in

the vast literature on adaptive systems, there is hardly ever any quantitative comparison between the adaptive design promoted and a proper ℓti design accomplishing the same design objectives. One could excuse this not being done in a general manner, because there is hardly any 'adaptive' method permitting quantitative design in the sense here defined. However, it could at least be done experimentally. Occasionally one sees a comparison, with an 'ordinary' or so-called 'classical' design. But the comparison is usually greatly biased, because generally some very naive ℓti design is used, and there is no statement of specifications - even made up after the fact. There is not recalled a single comparison, on the part of the proponents of adaptive systems, with the ℓti quantiative design technique [2] discussed here. Some nonlinear compensation techniques for which a quantitative design theory exists to a greater or lesser extent have appeared in the literature [8,9,10,11] for which such comparisons are possible. It is noteworthy that these were expressly motivated by the desire to reduce the 'cost of feedback', so that such comparisons were a natural by-product.

1.4.2. Multiple-loop feedback.

Another method of 'cost of feedback' reduction, in the context of ℓti design, is by means of multiple-loop feedback, restricted to those cases where additional plant variables (besides the plant output) are available for feedback purposes. Such a multiple loop design technique was first developed [5] for the cascaded structure of Figure 1-12.

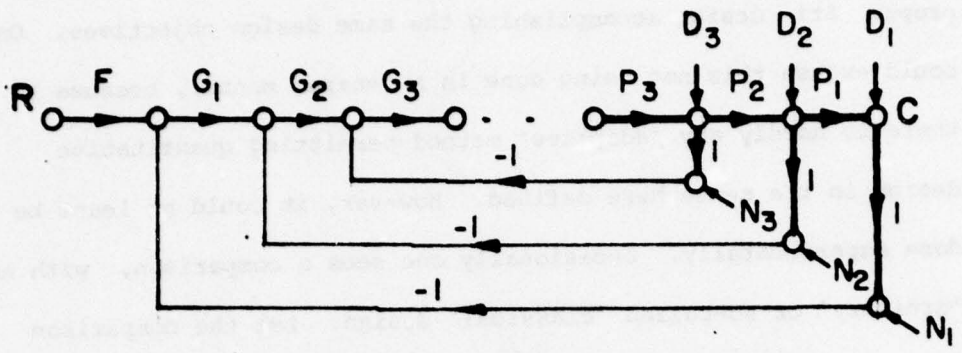

Figure 1-12. Cascaded multiple-loop system with (n+1) D.O.F. structure.

Then the technique was extended [12] to the parallel structure of Figure 1-13.

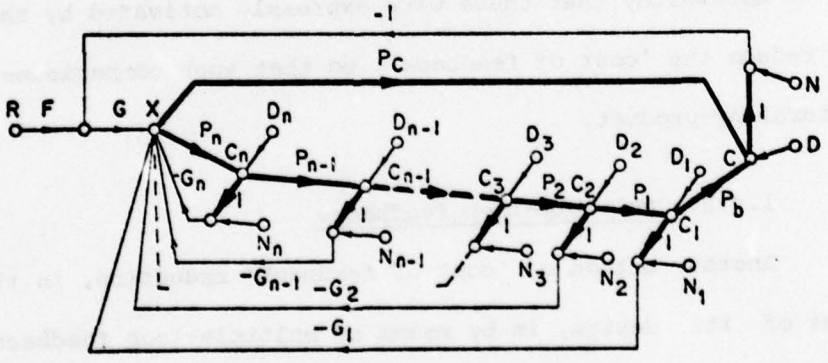

Figure 1-13. Parallel multiple-loop system with n+2 degree of freedom structure.

Finally, it is currently [13] being extended to the parallel-cascaded structure of Figure 1-14, where the number of cascaded

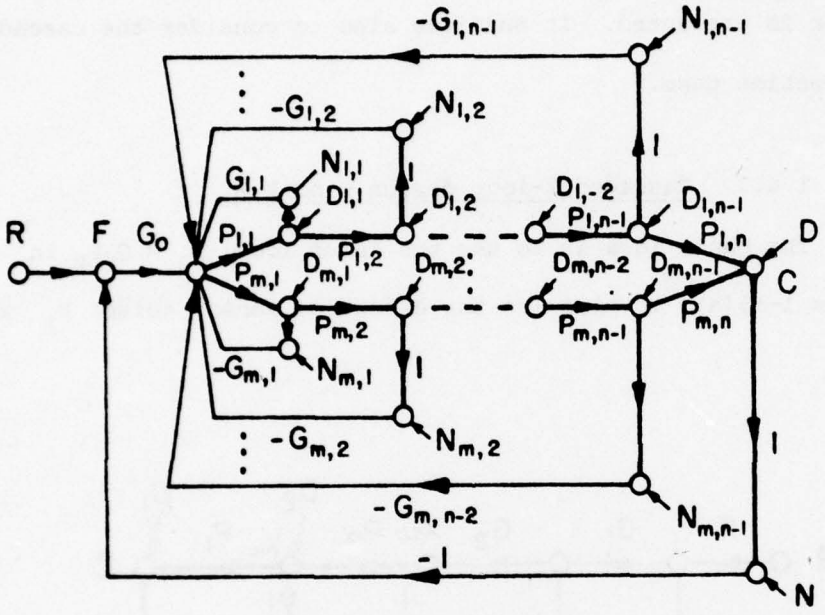

Figure 1-14. Parallel-cascaded multiple-loop structure with m(n-1)+2 D.O.F. structure.

element in each of the parallel path need not be the same. But note that in all three cases, there is no plant modification (P.M.) because each feedback loop is returned to the plant input, with none deliberately returned by the feedback designer (not the plant designer) to internal plant variables (see Section 1.6.2 for detailed discussion).

The multiple-loop plant modification synthesis theory developed here, is based to a large extent on the design theory

for the above non P.M. multiple loop designs. Hence, it is very important to first thoroughly understand the essentials of the above design philosophy, which is therefore next presented. Since this present work is confined to the cascaded plant, only the latter is presented. It suffices also to consider the cascaded two-section case.

1.4.3. Cascaded 2-loop design — no P.M.

The basic idea is to use the inner loop $L_2 = G_2P_2$ in Figure 1-15(a), to minimize the effect of sensor noise N_1 at the

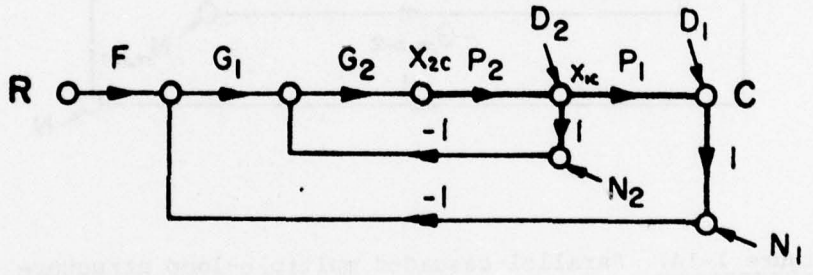

Figure 1-15(a). Cascaded 2-loop system — no P.M.

plant input X_{2C}. This effect is

$$T_{N_1} \triangleq \frac{X_{2C}}{N_1} = \frac{-G_1G_2}{1+G_2P_2+G_1G_2P_1P_2} \tag{1.4-1}$$

$$= \frac{-G_1G_2/(1+G_2P_2)}{1+\dfrac{P_1P_2G_1G_2}{1+G_2P_2}} \tag{1.4-2}$$

$$= \frac{-\frac{G_1}{P_2} \cdot P_{2e}}{1 + P_1 G_1 P_{2e}} \quad \text{where} \quad P_{2e} = \frac{G_2 P_2}{1+G_2 P_2} \tag{1.4-3}$$

$$= -\frac{L_1/(P_1 P_2)}{1 + L_1} \qquad L_1 = P_1 G_1 P_{2e} \tag{1.4-5}$$

$$\approx -\frac{L_1}{P_1 P_2} \quad \text{in the hf range where} \quad |L_1| \ll 1 \ . \tag{1.4-6}$$

Hence to reduce $\frac{X_{2C}}{N_1}$ in the hf range, one must try to reduce L_1. But L_1 must cope with the uncertainty in $P_1 P_{2e} = P_1(P_2G_2/1+P_2G_2))$. Assuming the worst case of uncorrelated uncertainties in P_1 and P_2, the best that can be done by the inner loop P_2G_2 is to wipe out the uncertainty of P_{2e}, so that L_1 need only cope with the uncertainty on P_1. Physically, this makes sense - for obviously the inner loop cannot take care of the uncertainty in P_1. There is then left the single-loop system of Figure 1-15(b) and L_1 can be designed to handle the ignorance of P_1 only. The resulting L_1 is therefore more economical in bandwidth than its

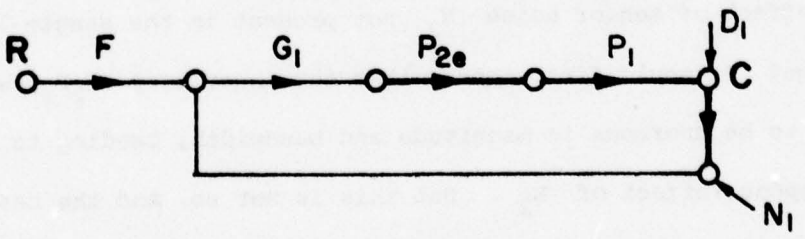

Figure 1-15(b). Equivalent single-loop structure of a cascaded 2-loop system.

counterpart in the single loop system, for the realization of the same C/R specifications. For example, compare the appropriate T_{N_i} in Figure 1-16(a) (logarithmic scale) and in Figure 1-16(b) (arithmetic scale) of the numerical example in Section 1.2-5.

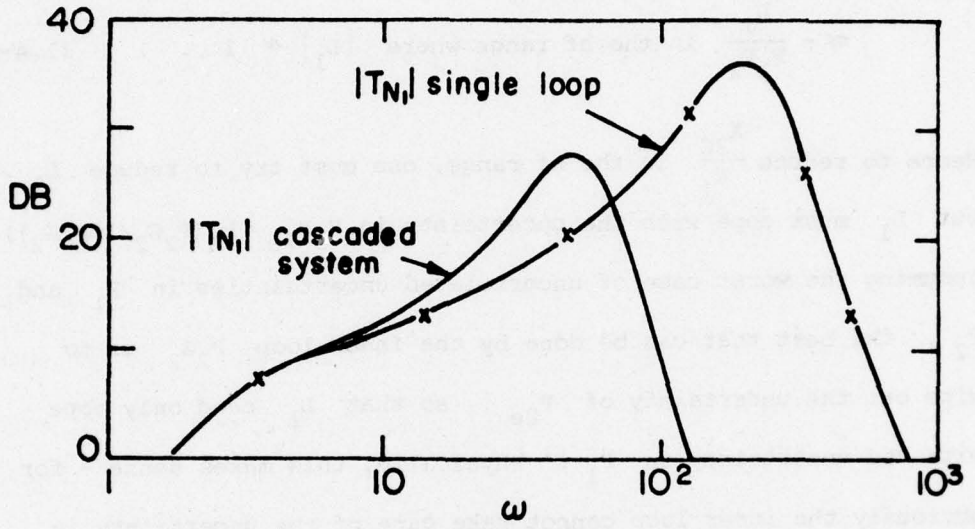

Figure 1-16(a). Comparison of noise response $|T_{N_1}|$ on Bode diagram.

This looks very good, but the obvious question is: What of the effect of sensor noise N_2 not present in the single loop design? It would first appear that the inner loop G_2P_2 would have to be enormous in magnitude and bandwidth, leading to tremendous effect of N_2. But this is not so. And the basic reason is available if one studies the mechanics of sensitivity reduction by frequency response methods. The reason is that design of the outer loop to handle a certain definite amount of uncertainty, even though designed optimally, is nevertheless able

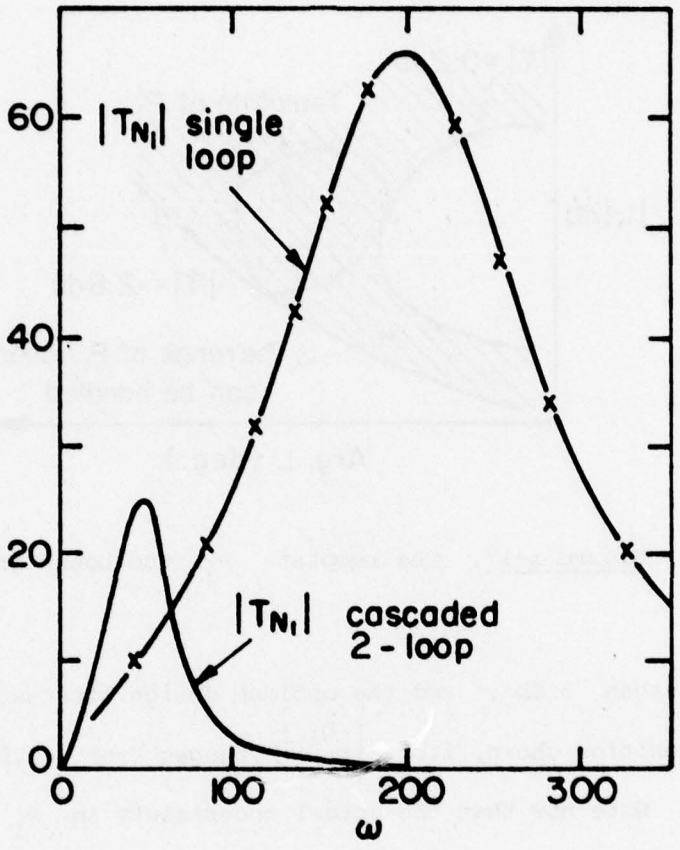

Figure 1-16(b). Comparison of noise response $|T_{N_1}|$ on arithmetical scale plot.

to handle a "much larger" amount of uncertainty. This is nicely seen in the Nichols' chart in Figure 1-17.

Thus, in Figure 1-17, suppose the uncertainty in $P_1(j\omega)$ is given by the template shown of P_1 which is not a point (it would be a point if there was no uncertainty) but a region. Suppose the specifications require the closed loop response uncertainty to be

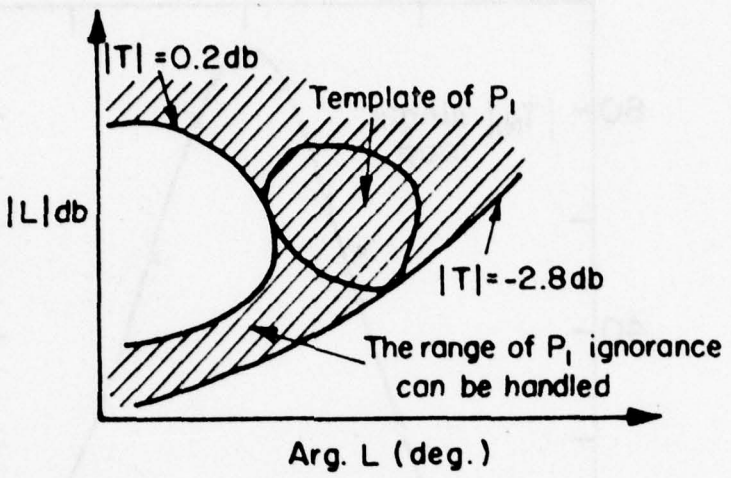

Figure 1-17. The template P_1 and bound on L_1 .

not more than 3 db , and the optimum design locates $L_1 = G_1P_1$ in the position shown, i.e. $\left|\frac{L_1}{1+L_1}\right|$ ranges from -2.8 db to 0.2 db . Note now that the actual uncertainty in P_1 , could be the entire shaded region lying in between the loci of $|T| = .2$ db and $|T| = -2.8$ db .

Thus P_{2e} can in practice have significant uncertainty, even though the outer loop was designed on the basis of no P_{2e} uncertainty. This is the secret of multiple-loop design – to understand the nature of the "free" uncertainty available in the various frequency ranges.

Thus, after L_1 has been designed, one finds what ignorance of P_{2e} can actually be tolerated in the above design of L_1 . It is found that in only one frequency range it is important to com-

promise (overdesign) the outer loop L_1 , in order to ease the L_2 design problem. This is in the range IVK in Figure 1-8, where trade-off between the two should be made.

Since $P_{2e} = \frac{L_2}{1+L_2}$ in Figure 1-15(a), with $L_2 = G_2P_2$, the final step is to determine the L_2 needed so that the resulting P_{2e} does indeed stay within the bounds found by the previous step. This is precisely a single loop design problem with P_{2e} and its tolerances replacing the T function. It was demonstrated [5] that the resulting two-loop design could be highly superior to a single loop design, in the sense of achieving the same quantitative sensitivity specifications, but with considerably less effect of sensor noise.

The numerical single loop design example of Section 1.2 was also done by a 2-loop cascaded design. The outer loop L_1 with its bounds is shown in Figure 1-18 and the inner loop L_2 with its bounds in Figure 1-19.

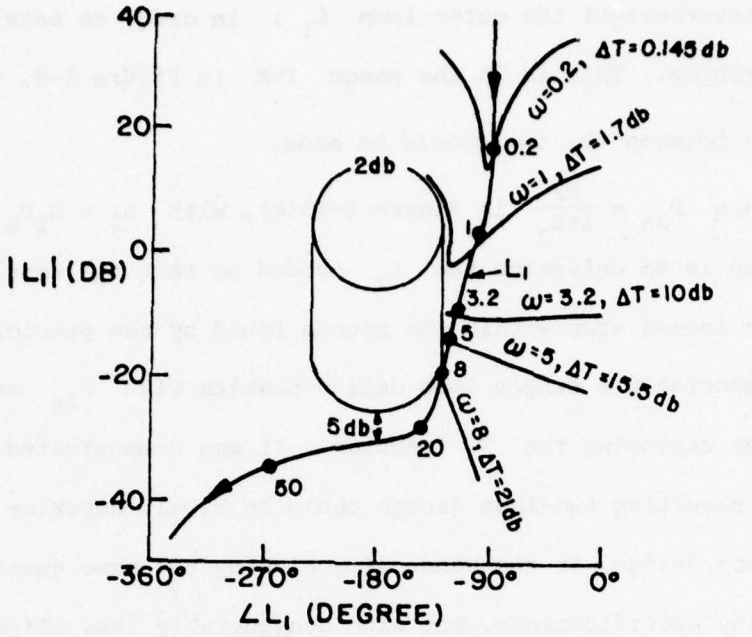

Figure 1-18. The outer loop L_1 and bounds in cascaded 2-loop system of a numerical example.

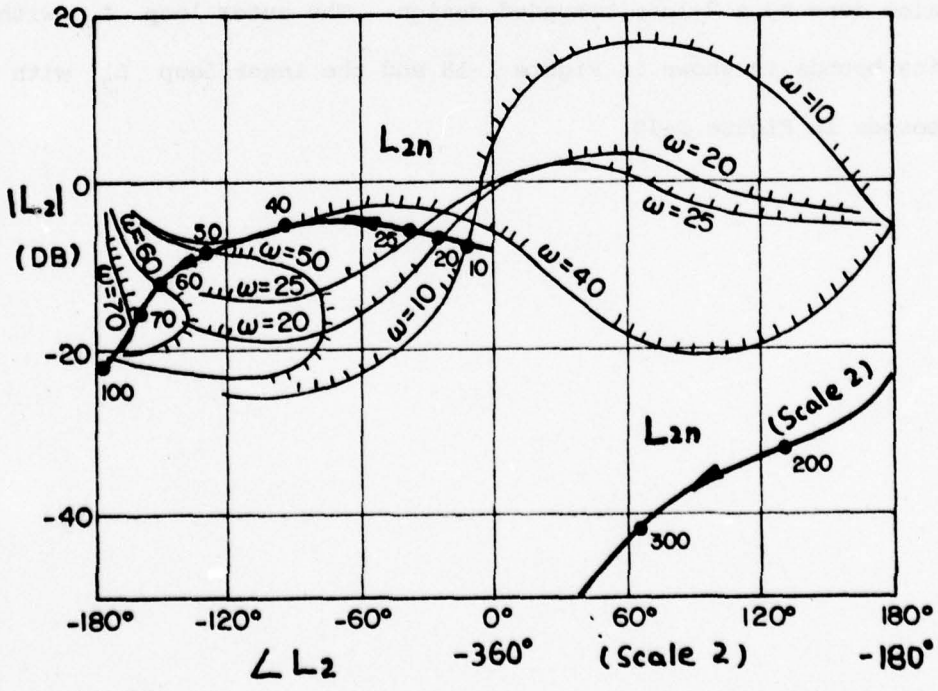

Figure 1-19. The inner loop L_2 and its bounds in cascaded 2-loop system of a numerical example.

1.5 A Simple Fast Technique for Multiple-Loop (no P.M.) Design Perspective

The cascaded synthesis procedure has a highly interesting property. One can achieve excellent design perspective by means of the following straightforward construction, which only requires an initial single-loop design in some detail.

Step. 1. Make a single-loop design L_{sn} to handle the entire problem and plot $|L_{sn}|$ on a Bode-diagram as in Figure 1-20.

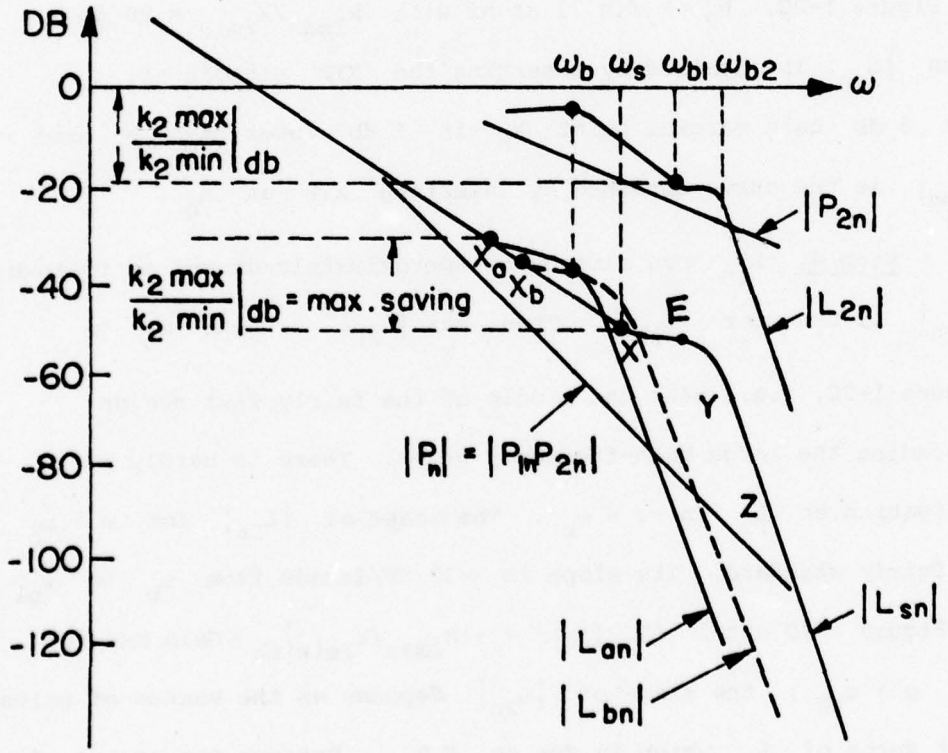

Figure 1-20. Bode plot significant loop and plant functions giving design perspective.

Step 2. Plot $|P_n| = |P_{1n}P_{2n}|$. The difference between $|L_{sn}|$ and $|P_n|$ in the region where $|L_{sn}| < 1$, is the N_1 sensor noise amplification (for its effect at the plant input).

Step 3. Note the hf uncertainty of P_2 . This is the maximum amount that can be saved in the hf range, giving $|L_{an}|$ in Figure 1-20. It is always worth having a few db overdesign of L_{an} , giving L_{bn} in Figure 1-20. Note that L_{an} is obtained by simply introducing the high frequency characteristic XYZ of L_{sn} , at point X_a which is 20 db higher than point X . For example, in Figure 1-20, $P_2 = k_2/(s^{e_2})$ at hf with $k_{2max}/k_{2min} = 20$ db , then $|L_{an}|$ is obtained by inserting the XYZ pattern at X_a . For 5 db gain margin, point X_b is 5 db lower than X_a and $|L_{bn}|$ is the curve obtained by inserting XYZ at X_b .

Step 4. L_{2n} can already be approximately drawn, as follows. $|L_{bn}|$ is used for $|L_{1n}|$. Then $\max_{\omega} |L_{2n}|$ is near ω_b in Figure 1-20, i.e., near the middle of the fairly flat region preceding the large high-frequency slope. There is hardly any obligation on L_2 in $\omega < \omega_b$. The shape of $|L_{2n}|$ for $\omega > \omega_b$ is fairly standard. Its slope is $\sim$30 db/decade from ω_b to ω_{b1} in Figure 1-20 until $|L_{2n}(j\omega)| = -[k_{2max}/k_{2min}|_{db} + \text{Gain Margin}]$. For $\omega > \omega_{b2}$, the shape of $|L_{2n}|$ depends on the excess of poles over zeros of L_2 which is due to G_2P_2 . Because the excess of poles over zeros of L_1 is due to $L_1 = G_1G_2P_2P_1$, the magnitude of the negative slope of $|L_2|$ is less than that of $|L_1|$.

Step 5. Sketch $|P_{2n}|$. The difference between $|L_{2n}|$ and

$|P_{2n}|$ is N_2 sensor noise amplification because in Figure 1-15(a)

$$|T_{N2}|_n \triangleq \left(\frac{x}{N_2}\right)_n = \frac{-G_2}{1+G_2P_{2n}+G_1G_2P_{1n}P_{2n}} \tag{1.5-1}$$

$$= \frac{-G_2/(1+G_2P_{2n})}{1+G_1G_2P_{1n}P_{2n}/(1+G_2P_{2n})} \tag{1.5-2}$$

$$= \frac{-L_{2n}/P_{2n}}{(1+L_{1n})(1+L_{2n})}\ ,\ L_{2n} \triangleq G_2P_{2n}\ ,$$

$$L_{1n} \triangleq G_1P_{1n}P_{2en}\ , \tag{1.5-3}$$

$$P_{2en} = \frac{P_{2n}}{1+L_{2n}}$$

$$\approx -\frac{L_{2n}}{P_{2n}} \text{ in the hf range where } |L_{1n}| \ll 1 \tag{1.5-4}$$

$$|L_{2n}| \ll 1\ .$$

Step 6. One can now decide whether to use L_{bn}, or to compromise further. Suppose that more compromise is wanted - e.g. x more db overdesign giving L_c for outer loop. Then the inner loop $|L_{2c}|$ maximum level can be reduced by x db relative to $|L_{2b}|_{max}$, as shown in Figure 1-21.

It is important to note that the above is based on $P_1, P_2 \to k_i/s^{e_i}$ in the ω-range at which L_1 is at B_h of Figure 1-8. This is reasonable in large hf uncertainty problems, because these require slow decrease of $|L|$ over large ω range. It is in these problems that the complexity of multiple loop design is warranted.

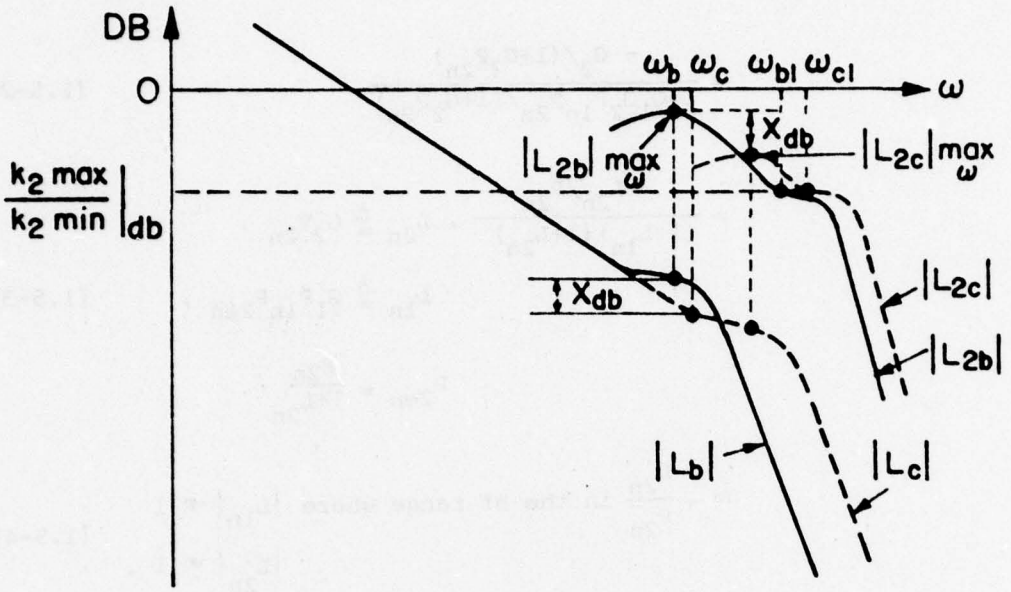

Figure 1-21. Trade off between inner loop and outer loop of a cascaded no-P.M., 2-loop system.

1.6 Plant Modification System Synthesis

1.6.1. Plant modification (P.M.) structure.

It is again emphasized that all the multiple-loop systems discussed above [5,12,13] are restricted to non-P.M. structures. In this case, the degree-of-freedom available for the design is limited. For a n cascaded plant system, (n plant variables available for measurement), there are n independent feedback loops which may be used — if no-P.M. is allowed, i.e., if the output of all the feedback processors are allowed only to the plant input. Together with the prefilter, this gives a (n+1) degree of freedom

system, as shown in Figure 1-11. If feedback to internal plant variables is allowed, then the number of independent feedback loops can be greatly increased. In a cascaded plant with $n-1$ internal variables and one output variable the number is $\sum_{o}^{n} (n-i) = (n+1)\cdot n/2$. Now the total numbers of freedom available is $(n+1)n/2 + 1$, including the prefilter as shown in Figure 1-22.

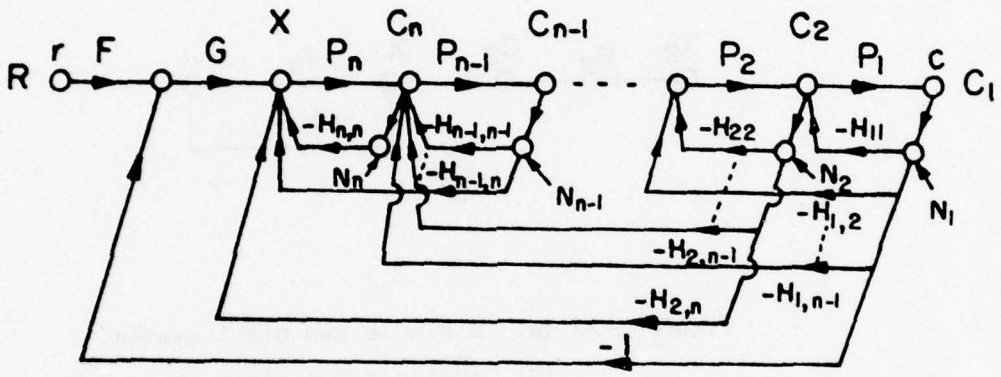

Figure 1-22. The P.M. multiple-loop with $n(n+1)/2 + 1$ D.O.F. structure.

1.6.2. The plant modification problem.

Consider a plant consisting of two cascaded sections, as in Figure 1-23(a) and suppose a certain maximum output signal level is required, with Laplace transform $C_1(s)$. The signal level at the input of P_1 is then $X_1 = C_1/P_1 = C_2$ (out of P_2) . This remains true in the cascaded feedback structure (no-P.M.). Thus, the feedback designer does not affect the signal level in the plant,

needed to obtain a specific output level. This is true for any feedback structure in which all the feedback paths return to the plant input. If a feedback loop is put around plant P_1, by means of H_1 in Figure 1-23(b), then the signal at X_1 is still

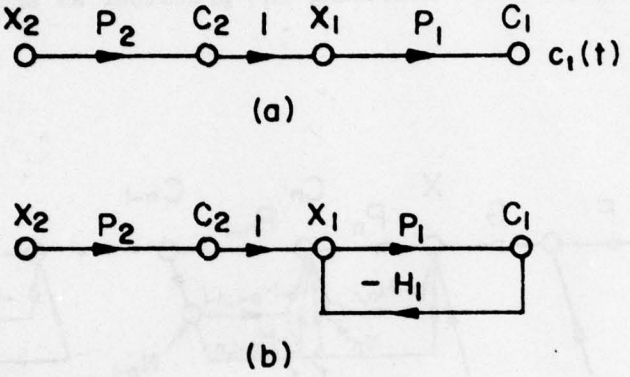

Figure 1-23 (a) A simple two plant system.
(b) Adding a P.M. loop $L_i = P_1H_1$.

C_1/P_1. But

$$C_2 = X_1+H_1C_1 = C_1P_1+H_1C_1 \qquad (1.6\text{-}1)$$

$$= (1+H_1P_1)\cdot C_1/P_1 = (1+H_1P_1)\cdot X_1 \qquad (1.6\text{-}2)$$

For the same signal level of C_1 and therefore of X_1, the signal level at C_2 is now multiplied by $(1+P_1H_1)$, which constitutes a modification of the plant. It is concievable that this new level of C_2 may be so much larger than the old one, that P_2 may have to be rebuilt to be able to handle this larger signal level.

If the 'feedback expert' is working together with the 'plant expert' in the design of the plant itself, then the trade-offs in such significant plant modification may be seriously considered. But in many cases this is not so. It is advisable to find a design method which uses the P.M. loop to improve the sensor noise problem, but keeps the increase in the signal level in the plant within a tolerable range. Recall that the noise problem is significant in the hf range (high relative the bandwidth of the useful control signals). This gives us a very good opportunity to achieve significant improvement in sensor noise effects with only small or moderate signal level increase. In addition, the insight obtained from such a synthesis procedure is very useful for those cases where the feedback expert is called in to help the plant expert in the actual plant design stage.

1.6.3. Reduction in cost of feedback by P.M. structure.

The cost of feedback can be tremendously reduced by a P.M. system. This is illustrated by the simple 2-plant, 3-loop P.M. system shown in Figure 1-24. The noise effect at X_1 and X_2 due

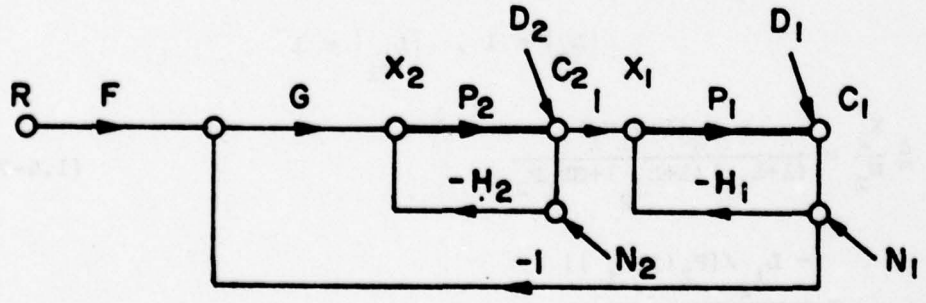

Figure 1-24. A P.M. 2-plant, 3-loop system structure with unit feedforward element between plant section.

to N_1 and N_2 are

$$T^2_{N_1} \triangleq \frac{X_2}{N_1} = \frac{-G}{1+P_1H_1+P_2H_2+GP_1P_2+P_1P_2H_1H_2} \tag{1.6-3}$$

$$= \frac{-G}{(1+L_{i_1})(1+L_{i_2})+P_1P_2G}, \quad L_{i_1} = P_1H_1, \quad L_{i_2} = P_2H_2$$

$$= \frac{-G/[(1+L_{i_1})\cdot(1+L_{i_2})]}{1+\frac{GP_1P_2}{(1+L_{i_1})(1+L_{i_2})}}$$

$$= \frac{-L_o/(P_1P_2)}{1+L_o}, \quad L_o \approx \frac{P_1P_2G}{(1+L_{i_1})(1+L_{i_2})}$$

$$\approx -L_o/(P_1P_2) \quad \text{in hf range where} \quad |L_o| \ll 1. \tag{1.6-4}$$

$$T^1_{N_1} \triangleq \frac{X_1}{N_1} = \frac{-[H_1(1+P_2H_2)+GP_2]}{(1+L_{i_1})(1+L_{i_2})+P_1P_2G} \tag{1.6-5}$$

$$= \frac{-[L_{i_1}/(1+L_{i_1})+L_o]/P_1}{1+L_o}$$

$$\approx -[L_{i_1}+L_o]/P_1 \quad \text{in hf range where} \tag{1.6-6}$$

$$|L_o| \ll 1, \quad |L_{i_1}| \ll 1$$

$$T^2_{N_2} \triangleq \frac{X_2}{N_2} = \frac{-H_2[1+P_1H_1)}{(1+L_{i_1})(1+L_{i_2})+GP_1P_2} \tag{1.6-7}$$

$$= \frac{-L_{i_2}/[P_2(1+L_{i_2})]}{1+L_o}$$

$$\approx -L_{i_2}/P_2 \quad \text{in hf range where}$$

$$|L_o| \ll 1 \ , \ |L_{i_2}| \ll 1 \tag{1.6-8}$$

$$T^1_{N_2} \triangleq \frac{X_1}{N_2} = \frac{-P_2H_2}{(1+L_{i_1})(1+L_{i_2})+GP_1P_2} \tag{1.6-9}$$

$$= \frac{-L_{i_2}/[(1+L_{i_1})(1+L_{i_2})]}{1+L_o}$$

$$\approx -L_{i_2} \quad \text{in hf range where} \quad |L_o| \ll 1 \ ,$$

$$|L_{i_1}| \ll 1 \ , \quad |L_{i_2}| \ll 1 \tag{1.6-10}$$

Following the same design philosophy as in a non-P.M. cascaded system design, let L_{i_2} cope with the uncertainty in P_2. But, for the sake of the significant signal level variation due to L_{i_1}, it is impractical to let L_{i_1} cope completely with the uncertainty in P_1. Let L_{i_1} cope with P_1 uncertainty in the high frequency range where sensor noise is significant, while the uncertainty in the low frequency range, where the control signals dominate, is taken care of by the outer loop L_o. Then, L_o can be designed as a highly economical loop, in terms of bandwidth. So the sensor noise effect at X_2 due to N_1 in (4) becomes very small compared to the single loop design.

The results of a numerical example, taken from Chapter 4, are shown here to illustrate the huge improvement in sensor noise effect, i.e., excellent saving in the cost of feedback. Figure 1-25(a) shows the Bode plots of noise response and the

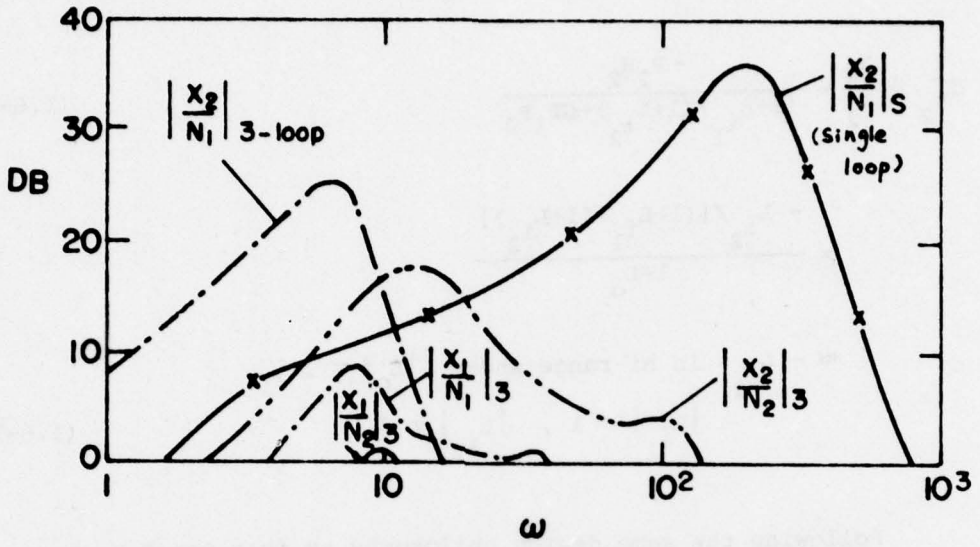

Figure 1-25(a). Sensor noise effect at X_1 and X_2 in single-loop system and P.M. 3-loop system.

arithmetical plots are in Figure 1-25(b). The effects of introducing a new sensor noise source N_2, i.e., $T^2_{N_2}$ and $T^1_{N_2}$ in (8), (10) and the effect at X_1, input to P_1, by introducing a new feedback loop H_1, i.e., $T^1_{N_1}$ in (6) are all shown in Figures 1-25(a), (b). It is known that, by a moderate trade-off between inner loops L_{i_1}, L_{i_2} and outer loop L_o, the effects of $T^2_{N_2}$, $T^1_{N_2}$ and $T^1_{N_1}$ are reasonable small, although they are bigger than their counter parts in a single-loop system. Note, $T^1_{N_1}$ is bigger here than the single loop, even though L_o bandwidth $\ll$ L_s bandwidth in single loop system. The reason is that, in the 3-loop P.M. system, there is an extra path $-H_1$ from N_1

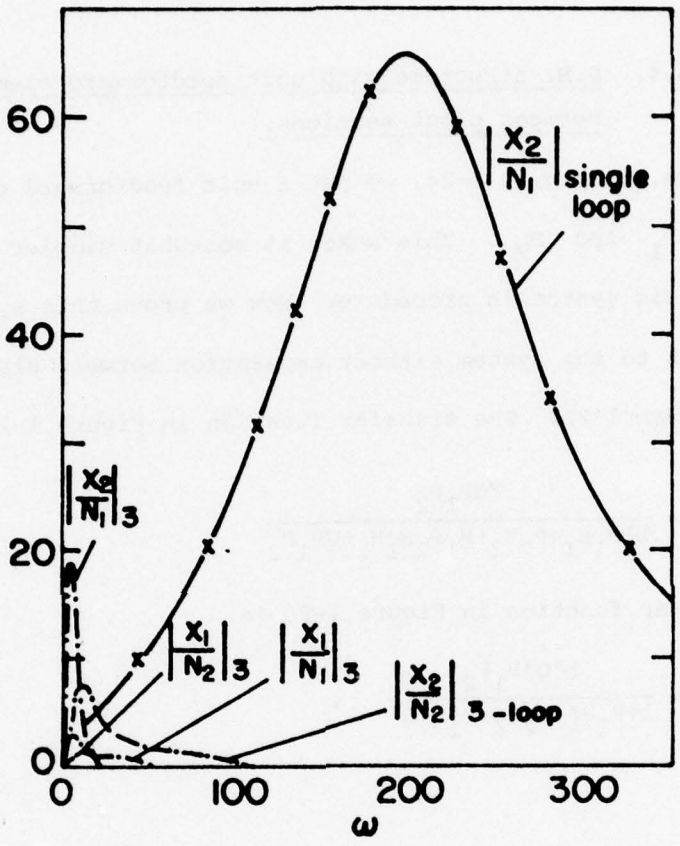

Figure 1-25(b). Sensor noise effect at X_1 and X_2 in single-loop system and P.M. 3-loop system — arithmetical scale.

to X_1. This is also seen in (6), as the $|L_{i_1}|$ bandwidth is not small compared with that of $|L_s|$, even though the $|L_o|$ bandwidth is relatively small.

It appears that the P.M. structure is very good in decreasing sensor noise effects. However, the signal levels in the plant to achieve a specific output are affected by the introduction of the

P.M. feedback loop, so that no longer does one really have a fixed, constrained plant. This is the plant modification problem.

1.6.4. P.M. structure with unit feedforward elements between plant sections.

Note, in Figure 1-24, we put a unit feedforward element between P_1 and P_2. This makes it somewhat simpler to develop a systematic synthesis procedure. Now we prove this system is equivalent to the system without separation between plant sections, as in Figure 1-26. The transfer function in Figure 1-24 is

$$T \triangleq \frac{C_1}{R} = \frac{FGP_1P_2}{1+P_1H_1+P_2H_2+P_1P_2H_1H_2+GP_1P_2} \quad . \tag{1.6-11}$$

The transfer function in Figure 1-26 is

$$T \triangleq \frac{C_1}{R} = \frac{F^*G^*P_1P_2}{1+P_1H_1^*+P_2H_2^*+P_1P_2G^*} \quad . \tag{1.6-12}$$

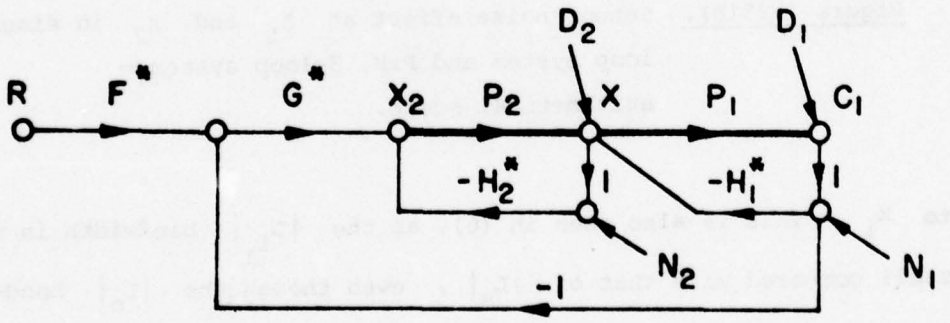

Figure 1-26. A P.M. 2-plant, 3-loop system structure — without separation between plants.

Compare (11) and (12). Let

$$H_1^* = H_1 \tag{1.6-13}$$

$$H_2^* = H_2 \tag{1.6-14}$$

$$G^* = G+H_1H_2 \tag{1.6-15}$$

$$F^* = FG/(G+H_1H_2) \tag{1.6-16}$$

and then the two systems are equivalent with respect to T and the effects of P_1, P_2 uncertainty on T. Note also that the actual output of P_2 is not $X_1 = C_1/P_1$ but is $X_1(1+P_1H_1^*) = \frac{C_1}{P_1}(1+P_1H_1^*)$ which is the same as that of $X_1(1+P_1H_1) = \frac{C_1}{P_1}(1+P_1H_1)$ in Figure 1-24. And the noise responses in Figure 1-26 are

$$T^2_{N_1} \triangleq \frac{X_2}{N_1} = \frac{-G^*+H_1^*H_2^*}{1+G^*P_1P_2+P_1H_1^*+P_2H_2^*} \tag{1.6-17}$$

$$T^1_{N_1} \triangleq \frac{X_1}{N_1} = \frac{-H_1^*-G^*P_2}{1+G^*P_1P_2+P_1H_1^*+P_2H_2^*} \tag{1.6-18}$$

$$T^2_{N_2} \triangleq \frac{X_2}{N_2} = \frac{-H_2^*(1+P_1H_1^*)}{1+G^*P_1P_2+P_1H_1^*+P_2H_2^*} \tag{1.6-19}$$

$$T^1_{N_2} \triangleq \frac{X_1}{N_2} = \frac{-H^*P_2}{1+G^*P_1P_2+P_1H_1^*+P_2H_2^*} \quad . \tag{1.6-20}$$

Substitute (13),...,(16) into (17),...,(20)

$$T^2_{N_1} = \frac{-(G+H_1H_2)+H_1H_2}{1+(G+H_1H_2)P_1P_2+P_1H_1+P_2H_2}$$

$$= \frac{-G}{1+P_1H_1+P_2H_2+GP_1P_2+P_1P_2H_1H_2} \tag{1.6-21}$$

$$T^1_{N_1} = \frac{-H_1-(G+H_1H_2)P_2}{1+(G+H_1H_2)P_1P_2+P_1H_1+P_2H_2}$$

$$= \frac{-[H_1(1+P_2H_2)+GP_2]}{(1+L_{i_1})(1+L_{i_2})+P_1P_2G} \qquad (1.6\text{-}22)$$

$$T^2_{N_2} = \frac{-H_2(1+P_1H_1)}{1+(G+H_1H_2)P_1P_2+P_1H_1+P_2H_2}$$

$$= \frac{-H_2(1+P_1H_1)}{(1+L_{i_1})(1+L_{i_2})+P_1P_2G} \qquad (1.6\text{-}23)$$

$$T^1_{N_2} = \frac{-H_2P_2}{1+(G+H_1H_2)P_1P_2+P_1H_1+P_2H_2}$$

$$= \frac{-P_2H_2}{(1+L_{i_1})(1+L_{i_2})+GP_1P_2} \quad . \qquad (1.6\text{-}24)$$

(21),...,(23) are exactly the same as in (3), (5), (7), (9) of Figure 1-24.

For simplicity, henceforth, we always choose the structure with unit element between plants, for development of the P.M. synthesis theory.

1.6.5. The RMS signal level problem.

The P.M. system synthesis theory in the present work is restricted to the RMS signal level problem — not to peak values. That is, this synthesis theory is based on the amount of signal level variation Q defined by

$$Q_i = \frac{\int_0^\infty |C_{i,m}(\omega)|^2_{max}\, d\omega}{\int_0^\infty |C_{i,s}(\omega)|^2_{max}\, d\omega}, \quad i = 2,\ldots,m \quad \text{for m-plant system} \qquad (1.6\text{-}25)$$

where $|C_{i,m}(\omega)|_{max}$ is the maximum signal level of P.M. multiple-loop system at stage $n-i$ such that there is at least one P.M. inner

loop in stage n-i+1 or in later stages; $|C_{i,s}(\omega)|_{max}$ is the maximum S.L. of the single-loop system at the corresponding n-i stage.

1.6.6. The P.M. synthesis philosophy.

P.M. design based on controlling the RMS value of the effect of plant modification, has the nice property that the individual contributions at each value of ω in $[0,\infty)$ add. Now the sensitivity reduction properties in the multiple-loop feedback system — the trade-offs between the loops, etc. — vary considerably in different parts of the frequency spectrum. This is evident from Sections 1.4, 1.5. This permits the designer to divide up the spectrum into significant portions and in each portion, concentrate on the crucial properties. Consider how complex the problem would be otherwise — quantitative design for significant parameter uncertainty, multiple loops, sensor noise effects and plant modification. Using frequency response, one can see the forest from the trees and obtain good engineering solutions. Modern control theory with its contempt for frequency response and non-analytic solutions, has not been able to cope quantitatively with the uncertainty problem, even in single-loop design, despite its vast number of competent researchers.

It is assumed that the design specifications dictate the permissible Q_{i+1} in RMS signal level at the outputs of $P_2,\ldots,P_n$ in Figure 1-22, which is allowed in the P.M. design. The design technique exploits this permitted increase so as to simultaneously decrease the net effects of the various sensor noise sources.

In the very low frequency range, the control signals are generally large, so even a small increase percentage-wise can have a significant effect on the signal level change. Fortunately, the outer loop (as is evident from Sections 1.4, 1.5) can do the sensitivity reduction job in this range, with little help. Therefore, the P.M. loop P_1H_1 is designed in this range to be as small as possible, in order to guarantee that the relative increase in signal level (of P_2, at C_2 in Figure 1-24) is very small. In the middle frequency range, the signal level is allowed to increase by amounts related to Q_{i+1}. And the P.M. loop is assigned to participate to some extent in the uncertainty problem. In the high frequency range, the signal level problem is relatively unimportant, so the P.M. loop is designed to minimize the cost of feedback, i.e., to minimize the effect of sensor noise without worrying over the S.L. effect.

CHAPTER 2

SIGNAL LEVEL

2.1 Introduction

The signal level (S.L.) problem is the basic one in plant modification (P.M.) system design. If there is no limitation on the output of each plant section, then P.M. is easy. In a practical system, the designer must understand the effect of the local feedback loop $P_i H_i$ on the signal level C_{i+1} of the preceding stage. This chapter presents a detailed analysis of this effect. The signal level variation ratio (SLVR) ρ is defined. Then the problem is simplified by dividing the frequency spectrum into distinct frequency ranges. A single simple factor $|1 + L_{in}|$, is shown to dominate ρ in each frequency region. A power increase tolerance level is assinged to any P.M. design and it is finally shown how to relate ρ and $|1 + L_{in}|$ to this tolerance level.

2.2 Definitions of Signal Level Variation Ratio (SLVR) and ρ

SLVR is defined with repsect to a single loop design for the same plant. Let $\mathcal{P} = \{P\}$ be the plant set due to uncertainty.

Single loop system (see Figure 2-1 for notation)

The maximum output signal level is

$$|C_s(j\omega)|_{\max_{\mathcal{P}}} = |RF_s(j\omega)| \cdot \left|\frac{L_s(j\omega)}{1 + L_s(j\omega)}\right|_{\max_{\mathcal{P}}} \qquad (2.2\text{-}1)$$

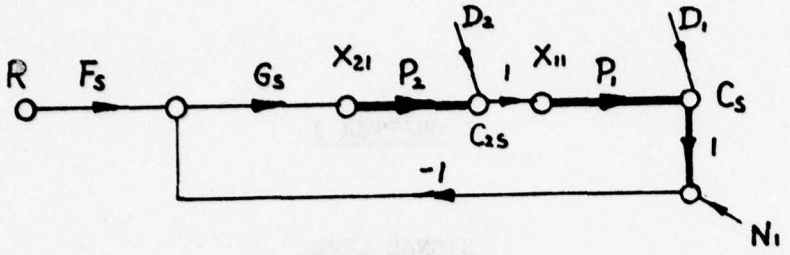

$$T \triangleq \frac{C_s}{R} = \frac{F_s L_s}{1+L_s} , \quad L_s \triangleq G_s P , \quad P \triangleq P_1 P_2$$

Figure 2-1 Canonic 2 section plant, single loop design.

and the maximum signal level at the output of P_2 is

$$|C_{2s}(j\omega)|_{\max_{\mathcal{P}}} = |RF_s(j\omega)| \cdot \left|\frac{L_s(j\omega)}{P_1(j\omega)\cdot(1+L_s(j\omega))}\right|_{\max_{\mathcal{P}}} \tag{2.2-2}$$

The ratio

$$\gamma_s(j\omega) \triangleq \frac{|C_{2s}(j\omega)|_{\max_{\mathcal{P}}}}{|C_s(j\omega)|_{\max_{\mathcal{P}}}} = \frac{|L_s(j\omega)/(P_1(j\omega)\cdot[1+L_s(j\omega)])|_{\max_{\mathcal{P}}}}{|L_s(j\omega)/[1+L_s(j\omega)]|_{\max_{\mathcal{P}}}} \tag{2.2-3}$$

$\mathcal{P}$ is dropped henceforth, i.e., maximization and minimization is always over $\mathcal{P}$ unless otherwise specified.

P.M. 2-loop system (see Figure 2-2 for notation)

Similarly,

$$|C_1(j\omega)|_{\max} = |RF(j\omega)| \cdot \left|\frac{L_0(j\omega)}{1+L_0(j\omega)}\right|_{\max} \tag{2.2-4}$$

$$|C_{22}(j\omega)|_{\max} = |RF(j\omega)| \cdot \left|\frac{L_0(j\omega)}{P_{1e}(j\omega)[1+L_0(j\omega)]}\right|_{\max} \tag{2.2-5}$$

$$\gamma_2(j\omega) \triangleq \frac{|C_{22}(j\omega)|_{\max}}{|C_1(j\omega)|_{\max}} = \frac{|L_0(j\omega)/(P_{1e}(j\omega)\cdot[1+L_0(j\omega)])|_{\max}}{|L_0(j\omega)/[1+L_0(j\omega)]|_{\max}} \tag{2.2-6}$$

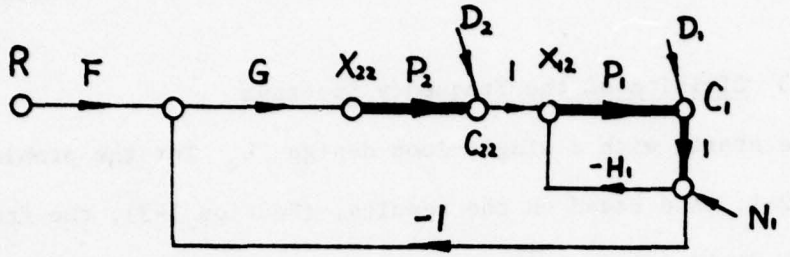

$$T \triangleq \frac{C_1}{R} = \frac{FL_o}{1+L_o}\ ,\quad L_o \triangleq GP_2P_{1e}\ ,\quad P_{1e} \triangleq \frac{P_1}{1+L_i}\ ,\quad L_i \triangleq P_1H_1$$

Figure 2-2 The P.M. 2-loop system structure

The signal level variation ratio (SLVR) ρ is defined to be $|C_{22}(j\omega)|_{max}/|C_{2s}(j\omega)|_{max}$

$$\rho(\omega) \triangleq \frac{|C_{22}|_{max}}{|C_{2s}|_{max}} = \frac{\gamma_2}{\gamma_s} \cdot \frac{|C_1|_{max}}{|C_s|_{max}}$$

$$= \frac{|L_s/(1+L_s)|_{max}}{|L_s/[P_1\cdot(1+L_s)]|_{max}} \cdot \frac{|L_0/[P_{1e}(1+L_0)]|_{max}}{|L_0/(1+L_0)|_{max}} \cdot \frac{|C_1|_{max}}{|C_s|_{max}} \qquad (2.2\text{-}7)$$

2.2.1 Nominal loop functions

In this and later sections, frequent references are made to "nominal" loop functions, which are the loop functions at some specific $P \in \mathcal{P}_i = \{P_i\}$. It is convenient to choose the nominal P such that $|P|_{min} = \min_{\mathcal{P}_i} \{|P_i|\}$. Often, one specific parameter combination gives $|P|_{min}$ for all ω, e.g. if $P = \frac{k}{s(s+a)}$, $k \in [k_1, k_2]$ and $a \in [a_1, a_2]$, $|P|_{min} = |\frac{k_1}{s(s+a_2)}|_{j\omega}$ for all ω. But this may not be so for more complex plant functions. In such a case we shall use at each ω, that parameter combination

which gives $|P|_{min}$ at that ω value. Note that at high frequencies $P_i \to k_i/s^{e_i}$ so $|P_i|_{min}$ corresponds to k_{imin}.

2.3 Division of the Frequency Spectrum

One starts with a single-loop design L_s for the problem of Figure 2-1. And based on the results, (Section 1-3), the frequency range is divided into 5 distinct parts, as in Figure 2-3. Let the

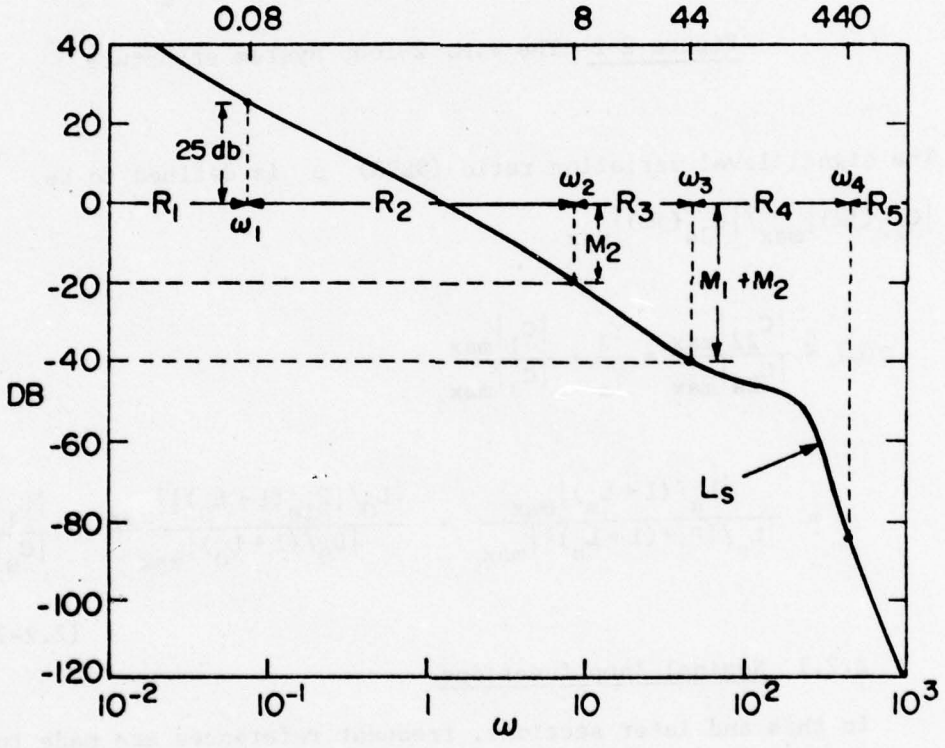

Figure 2-3 Division of the frequency spectrum

high-frequency (denoted by hf) uncertainty of P_1 be M_1 db (20 in our example) and that of P_2 be M_2 db (also 20 db in this example).

(1) The very low frequency range $R_1 = [0, \omega_1]$ is that in which $|L_s(j\omega)| \geq 25$ db over the entire plant parameter

space. In Figure 2-3, $\omega_1 = 0.08$, because L_s there is $|L_s|_{min}$. In this range in the multiple loop design (cascaded no modification, or P.M.) the inner loops are not used to help the outer loop L_0, i.e. in R_1, $L_{sn} \simeq L_{on}$, where L_{sn} and L_{on} designate the nominal loop transmissions.

(2) Middle frequency range $R_2 = (\omega_1, \omega_2]$ defined by $25 \text{ db} > |L_{sn}(j\omega)| \geq -M_2 \text{ db}$ where M_2 is the hf uncertainty of P_2, which is 20 db in this example. In Figure 2-3, $\omega_2 = 8$.

(3) High frequency range 1, $R_3 = (\omega_2, \omega_3]$ defined by $-M_2 \text{ db} > |L_{sn}(j\omega)| \geq -(M_1 + M_2)\text{db}$ where $(M_1 + M_2)$ is the hf uncertainty of $P = P_1P_2$. In Figure 2-3, $\omega_3 = 44$.

(4) High frequency range 2, $R_4 = (\omega_3, \omega_4]$ where $\omega_4 = 10\,\omega_3$. In Figure 2-3, $\omega_4 = 440$.

(5) The very high frequency range $R_5 = (\omega_4, \infty)$.

It is helpful, for interpretation of SLVR, to point out here orders of magnitude of the P.M. inner loop L_{in} (nominal value at $|P|_{min}$), before going into detail. Two numerical examples (from Chapter 3) of typical P.M. 2-loop designs are given in Figure 2-4. In R_1, $|L_{in}|$ is very small in general, though the actural values depend on the specific problem. Thus, in Figure 2-4, Design A has $|L_{in}(j\omega)| \leq -30 \text{ db}$ and in Design B, $|L_{in}(j\omega)| \leq -22 \text{ db}$ for $\omega \in R_1$. In R_2, the SLVR is allowed to increase and $|L_{in}|$ becomes bigger. In Figure 2-4, $-30 \text{ db} < |L_{in}(j\omega)| \leq -7 \text{ db}$ in Design A

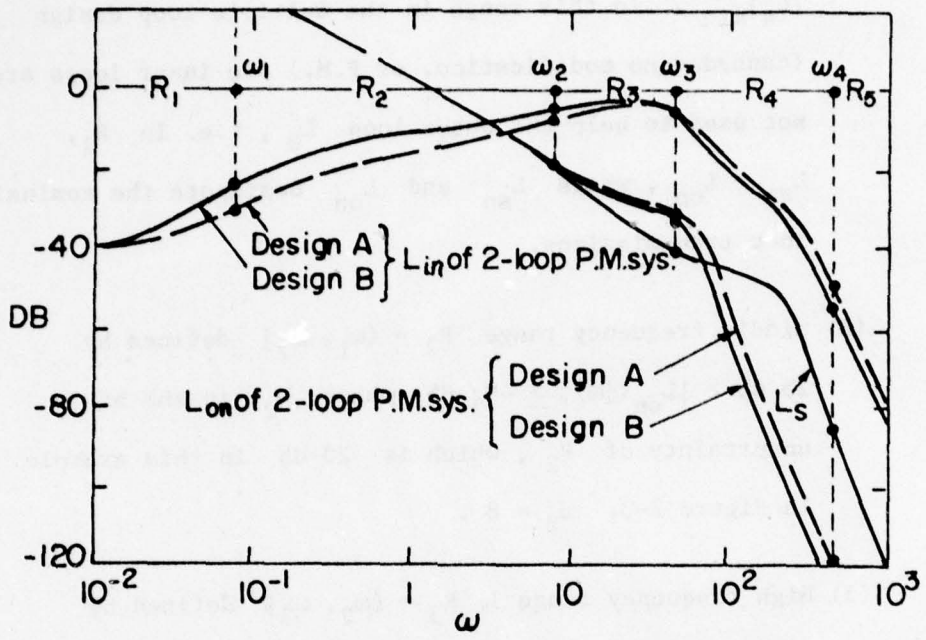

Figure 2-4 Division of frequency spectrum and corresponding L_{sn}, L_{on} and L_{in} of design examples.

and $-20 \text{ db} < |L_{in}(j\omega)| \leq -5 \text{ db}$ in Design B, for $\omega \in R_2$. In R_3, L_{in} is used to cope with the parameter uncertainty of P_1, so $|L_{in}(j\omega)|$ cannot be very small and actually tends ~ 0 db. In Figure 2-4, $-7 \text{ db} < |L_{in}(j\omega)| \leq -2.5 \text{ db}$ in Design A and $-5 \text{ db} < |L_{in}(j\omega)| \leq -2 \text{ db}$ in Design B, for $\omega \in R_3$. Note that here $|L_{in}(j\omega)|$ is much bigger than the corresponding $|L_{on}(j\omega)|$ and $|L_{sn}(j\omega)|$ - see Figure 2-4. In R_4, in which L_{on} design was based on no uncertainty in P_{le}, is nevertheless satisfactory for large P_{le} uncertainty (cf section 1.4.3), so $|L_{in}|$ can be small. In Figure 2-4, $-6 \text{ db} > |L_{in}(j\omega)| \geq -50 \text{ db}$ in Design B and $-4 \text{ db} > |L_{in}(j\omega)| \geq -44 \text{ db}$ in Design A, for $\omega \in R_4$. And the last range R_5 is the very high frequency range where both L_{sn}, L_{on}, L_{in} are very small. In Figure 2-4, $|L_{sn}(j\omega)| < -84 \text{ db}$;

$|L_{on}(j\omega)| < -120$ db , $|L_{in}(j\omega)| < -50$ db in Design A and

$|L_{on}(j\omega)| < -130$ db , $|L_{in}(j\omega)| < -54$ db in Design B.

2.4 Relation between SLVR ρ and $|1+L_{in}|$

The precise expression for $\rho(\omega)$ in (2.2-7) is too complex for practical engineering synthesis. But good simplifying approximations are possible.

In Figures 2-1, 2,

$$C_{2s} = C_s/P_1 \tag{2.4-1}$$

$$C_{22} = X_{12} \cdot (1+P_1H_1) = \frac{C_1}{P_1}(1+P_1H_1) \tag{2.4-2}$$

In a fair comparison of the two designs, the maximum outputs over $\mathcal{P}$ should be the same, i.e. $|C_1|_{max} = |C_s|_{max}$. so $(1+P_1H_1)$ is an important factor and it is useful to relate loci of constant $|1+P_1H_1|$ to P_1H_1 on the Nichol's chart.

Let $L_i = P_1H_1$, $\ell = 1/L_i$ and $\mathcal{L} = 1/(1+L_i)$, then

$$\mathcal{L} = \frac{1}{1+1/\ell} = \frac{\ell}{1+\ell} \tag{2.4-3}$$

The relation between $\mathcal{L}$ and ℓ gives the conventional loci of constant $\mathcal{L}$ magnitude on the Nichol's chart. So the relation of $|1+L_i|$ with respect to L_i is the reversed Nichol's plot, obtained by changing the sign of constant magnitude curves (see Figure 2-5). These loci will be very useful in P.M. design.

The simplification of (2.2-7) for SLVR ρ, follows.

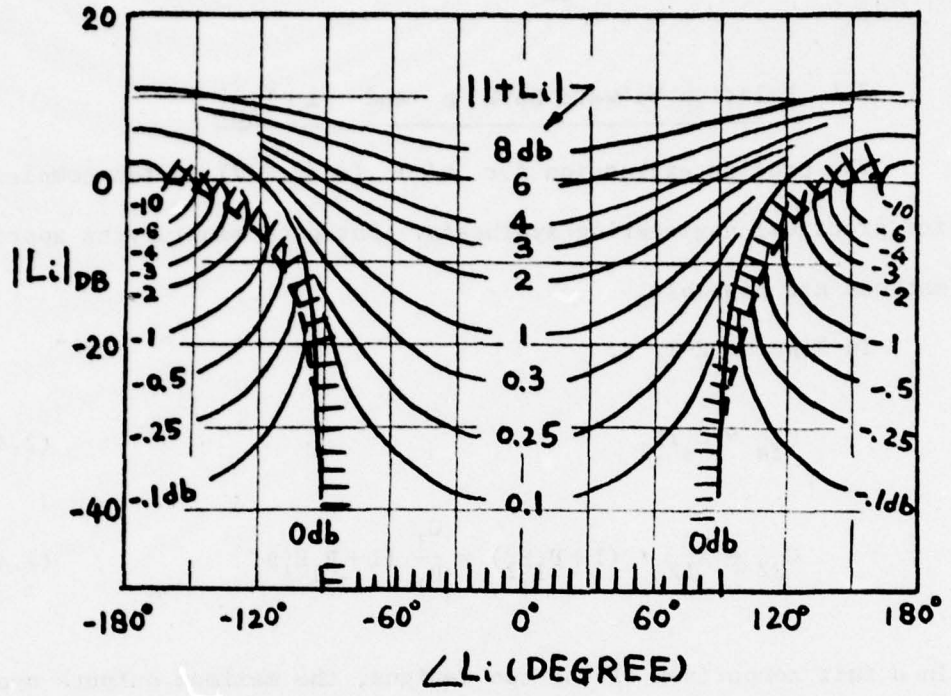

Figure 2-5 Loci of constant $|1+L_i|$ on the L_i Nichol's chart

2.4.1 $R_1 = [0, \omega_1]$

In this range, the single loop, unmodified cascade and P.M. designs are almost identical, so $|L_{sn}|$, $|L_{on}| \geq 25$ db (see Section 2.3 and Figures 2-4,6). Thus, the inner loop L_i is not used in R_1 to help the outer loop, and it is therefore small with typical maximum (over ω) values of the nominal L_{in} (chosen as the smallest over $\mathcal{P}_1$) $\sim$ -30 db (see Figure 2-7 which is a typical numerical example from Chapter 3). So $|L_o/(1+L_o)| \doteq 1$ over the range of plant uncertain, and in (2.2-7)

$$\left|\frac{L_o}{P_{1e}(1+L_o)}\right|_{\max} \doteq \left|\frac{L_o}{1+L_o}\right|_{\text{near max}} / |P_{1e}|_{\min_{\mathcal{P}_1}} \qquad (2.4\text{-}4)$$

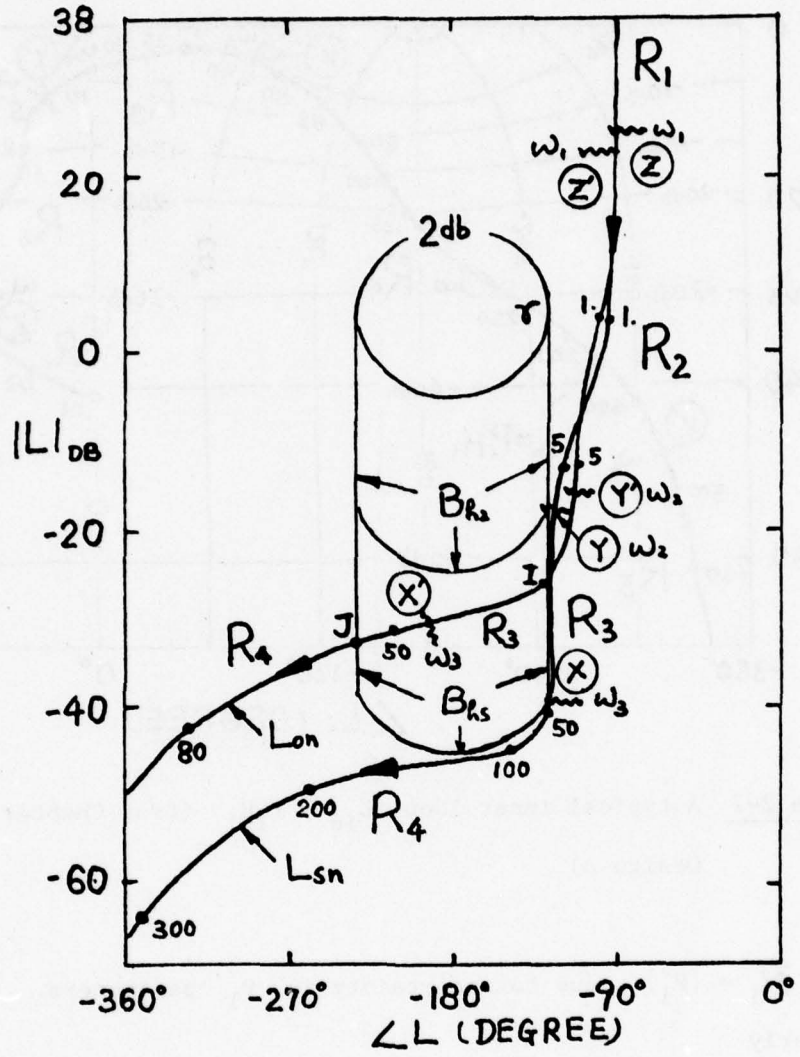

Figure 2-6 Typical L_{sn} and L_{on} (from Chapter 3, Design A)

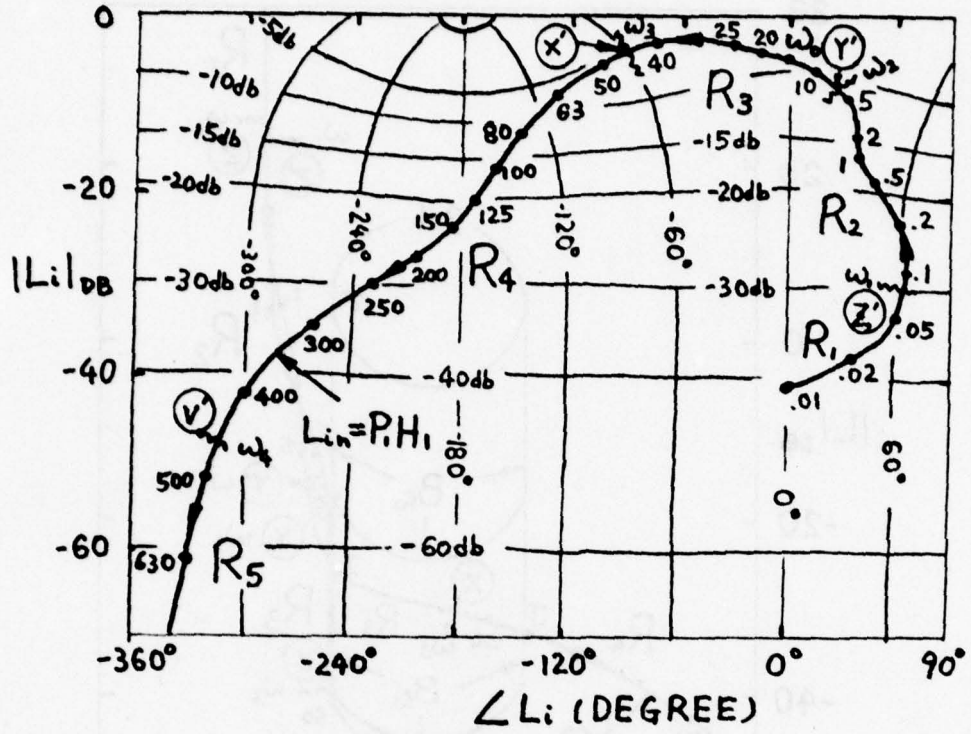

Figure 2-7 A typical inner loop $L_{in} = P_1 H_1$ (from Chapter 3, Design A)

where $\mathcal{P}_1 = \{P_1\}$, due to uncertainty in P_1 parameters.

Similarly

$$\left|\frac{L_s}{P_1(1+L_s)}\right|_{\max} \doteq \left|\frac{L_s}{1+L_s}\right|_{\text{near max}} / |P_1|_{\min_{\mathcal{P}_1}} \qquad (2.4\text{-}5)$$

With this, (2.2-7) becomes

$$\rho \doteq \left(\frac{\left| \frac{L_s}{1+L_s} \right|}{\left| \frac{L_s}{1+L_s} \right|_{s\ max}} \right) \cdot \left(\frac{\left| \frac{L_o}{1+L_o} \right|}{\left| \frac{L_o}{1+L_o} \right|_{o\ near\ max}} \right) \cdot \left(\frac{|P_1|_{min}}{|P_{le}|_{min}} \right)_{\mathcal{P}_1} \cdot \left(\frac{|C_1|_{max}}{|C_s|_{max}} \right) \tag{2.4-6}$$

$$\triangleq \delta_1 \left(\frac{|P_1|_{min}}{|P_{le}|_{min}} \right)_{\mathcal{P}_1} \cdot \left(\frac{|C_1|_{max}}{|C_s|_{max}} \right) \tag{2.4-7}$$

$$\doteq \left(\frac{|P_1|_{min}}{|P_{le}|_{min}} \right)_{\mathcal{P}_1} \cdot \left(\frac{|C_1|_{max}}{|C_s|_{max}} \right) \tag{2.4-8}$$

Consider the error introduced in letting $\delta_1 \doteq 1$ in (7,8). For example, let L_{sn} have its minimum value at 25 db $\angle -90°$ with gain uncertainty of P_1, 1 to 10. $|L_s/(1+L_s)| = |j17.8/(j+j17.8)| \doteq 0.99842$ at $|P_1|_{min}$, and $|j178/(1+j178)| \doteq$ 0.99998 at $|P_1|_{max}$. So the percentage error in cancelling the first factor of (6) is $(0.99998 - 0.99842)/0.99842 = 0.157\%$. Similarly, the second factor in (6) has the same error due to cancellation. But note that in the cancellation, the second factor in (6) has an error opposite to that of the first factor. So due to both cancellations, the total maximum error $<< 0.157\%$.

So in (7), $\delta \doteq 1$. Note again that we choose the nominal plant to be at the minimum value over $\mathcal{P}$.

Consider $|P_1|_{\min_{\mathcal{P}_1}} / |P_{1e}|_{\min_{\mathcal{P}_1}} = |P_1|_{\min_{\mathcal{P}_1}} / |P_1/(1+L_i)|_{\min_{\mathcal{P}_1}}$ in (8).

We want to justify (with $L_i = P_1 H_1$),

$$\left|\frac{P_1}{1+L_i}\right|_{\min_{\mathcal{P}_1}} \doteq \frac{|P_1|_{\min_{\mathcal{P}_1}}}{|1+(L_i)_{\min_{\mathcal{P}_1}}|} = \frac{1}{H_1} \cdot \frac{|L_i|_{\min_{\mathcal{P}_1}}}{|1+(L_i)_{\min_{\mathcal{P}_1}}|} \qquad (2.4\text{-}9)$$

from Figure 2-5 as follows. Recall that in R_1, in the P.M. design philosophy, the inner loop is not used to help the outer loop, so $|L_{sn}| \doteq |L_{on}|$ and L_i is rather small. For example, in the design in Figure 2-7, the biggest $|L_{in}|$ over $\omega \in R_1$ is -30 db $\angle 61°$ at $\omega = 0.08$. This values is $|L_{in}|_{\min}$ over $\mathcal{P}_1 = \{P_1\}$. A typical template of L_i due to P_1 uncertainty is ABCD in Figure 2-8 in which the loci are of constant $|L_i/(1+L_i)|$. It is obvious that both $|L_i/(1+L_i)|_{\min_{\mathcal{P}_1}}$ and $|L_i|_{\min_{\mathcal{P}_1}}$ are at A, so $|L_i/(1+L_i)|_{\min_{\mathcal{P}_1}} = |L_i|_{\min_{\mathcal{P}_1}} / |1+(L_i)_{\min_{\mathcal{P}_1}}| = -20.73$ db. Even if the template of L_i is AB'C'D instead of ABCD in Fig. 2-8, $|L_i/(1+L_i)|_{\min_{\mathcal{P}_1}} \doteq |L_i|_{\min_{\mathcal{P}_1}} / |1+(L_i)_{\min_{\mathcal{P}_1}}|$, e.g. $|L_i/(1+L_i)_{\min_{\mathcal{P}_1}} =$ -20.8124 db at A, $|L_i|_{\min_{\mathcal{P}_1}}$ can be any point along $\overline{AB'}$. Let us take B', the furthest from A, with $|L_i|_{B'} / |1+(L_i)_{B'}| =$ -20.5636 db. So $\delta_2 = |\{|L_i/(1+L_i)|_{\min_{\mathcal{P}_1}}\} - \{|L_i|_{\min_{\mathcal{P}_1}} / |1+(L_i)_{\min_{\mathcal{P}_1}}|\}|_{\max_{\overline{AB'}}} =$ $|20.8124 - 20.5635| = 0.2488$ db. Note that δ_2 depends on the

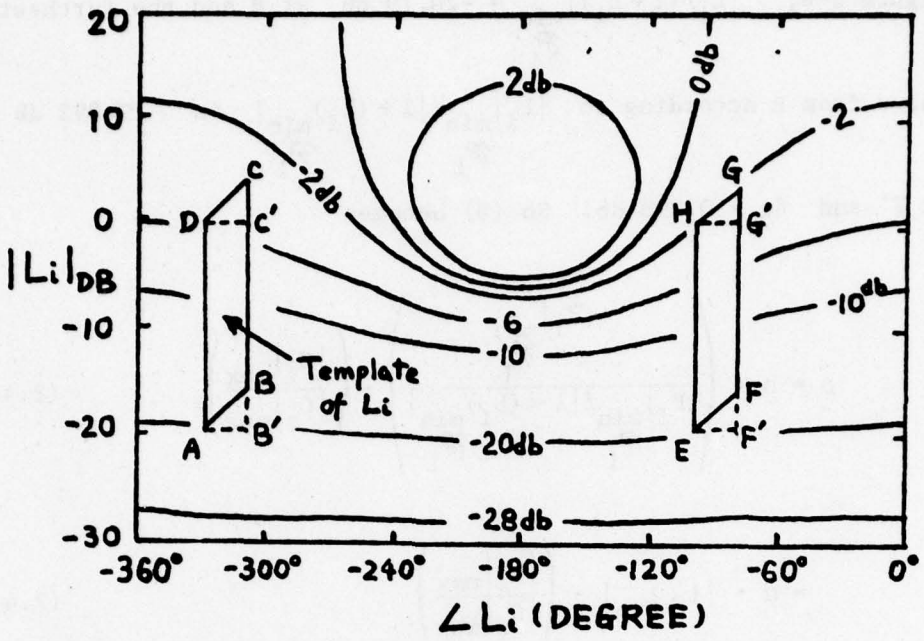

Figure 2-8 Templates of L_i in Nichol's chart in R_1

position of template L_i . Thus, if A in Fig. 2-8 is at -30 db $\angle 30°$ instead of $-20 \angle 30°$, then $\delta_2 = 0.058$ db and when A is at -10 db $\angle 30°$, $\delta_2 = 0.382$ db. Our design philosophy is to make L_i as small as possible in R_1 , in order that the minimum signal level of C_{22} be very closely equal to that of C_{2s} . This is because the control signal level is highest in this low frequency range, so that even small percent changes could lead to large absolute differences. So δ_2 is small in R_1 . Here we took $\angle L_i \sim 0°$, because R_1 is the low frequency range. Even if the system is type 1, it is the outer loop which is preferably made type 1, as the primary function of the inner loop, L_i , is to help relieve the burden on the outer loop in the hf range. But even if $\angle L_i$ in $R_1 \sim -90°$, the error δ_2 , in place of

0.2488 db for A at -20 db $\angle$ 30° is still not great, e.g. in Figure 2-8, $|L_i/(1+L_i)|_{\min_{\mathcal{P}_1}} = -20.19$ db at E and the furthest value from E according to $|L_i|_{\min_{\mathcal{P}_1}} / |1+(L_i)_{\min_{\mathcal{P}_1}}|$ is -19.892 db at F' and $\delta_2 = 0.298$ db. So (8) becomes

$$\rho = \alpha \cdot \left(\frac{|P_1|_{\min_{\mathcal{P}_1}}}{|P_1|_{\min_{\mathcal{P}_1}} / |1+(L_i)_{\min_{\mathcal{P}_1}}|} \right) \cdot \left(\frac{|C_1|_{\max}}{|C_s|_{\max}} \right) \tag{2.4-10}$$

$$= \alpha \cdot |1+L_{in}| \cdot \left(\frac{|C_1|_{\max}}{|C_s|_{\max}} \right) \tag{2.4-11}$$

where $\alpha \doteq 1$ in R_1.

Note again that L_{in} is the nominal value of L_i defined as the minimum of $|L_i|$ over $\mathcal{P}_1$.

At worst, in (11), a very slight adjustment can be made in $|C_1|_{\max}$ with respect to $|C_s|_{\max}$ to make $\alpha = 1$ exactly or even < 1. Curves of α for two numerical examples from Chapter 3, are shown in Figure 2-9.

The conclusion is that in R_1, the SLVR $\rho \doteq |1+L_{in}| \cdot (|C_1|_{\max}/|C_s|_{\max})$ with very good accuracy.

2.4.2 $R_2 = (\omega_1, \omega_2]$ (Figures 2-3,4,6,7)

Recall R_2 is the middle ω range in which the signal level is allowed to increase, $\rho > 1$, and with larger $|L_{in}|$ than in R_1.

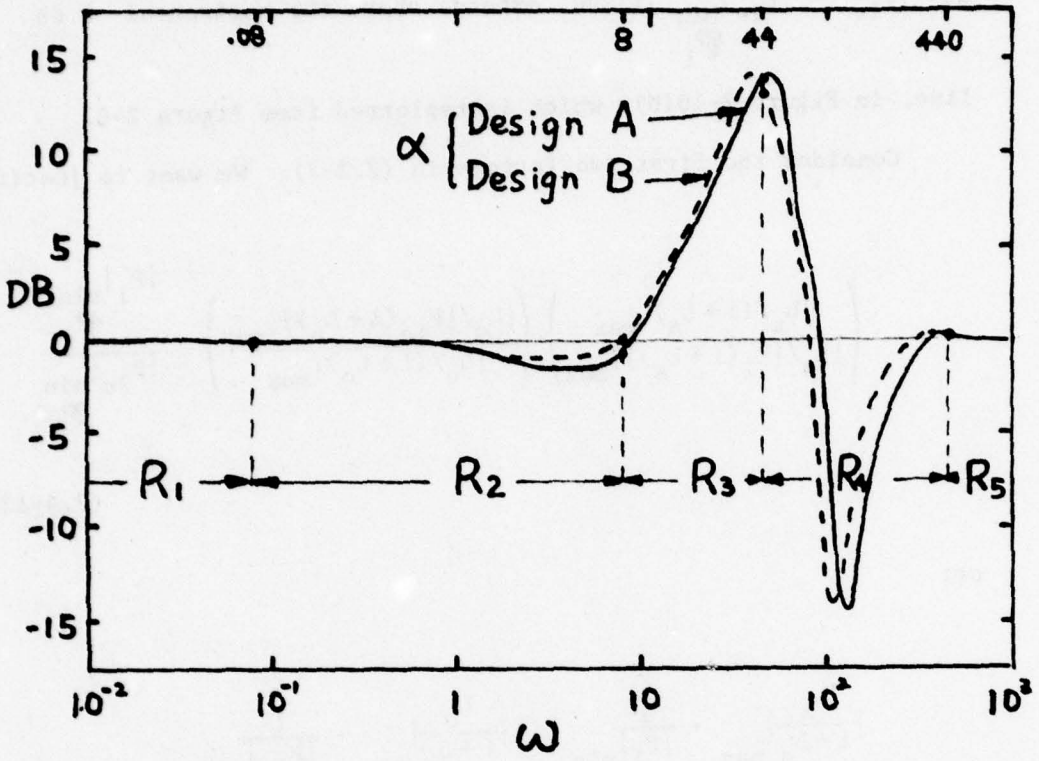

Figure 2-9 Nature of α - from examples in Chapter 3

From section 2.3, $R_2 = \{\omega | 25 \text{ db} > |L_{sn}(j\omega)| \geq -M_2 \text{ db}\}$ where M_2 is the h.f. uncertainty of P_2, i.e. $P_2 = k_2 P_{h2}$, $\lim_{s\to\infty} P_{h2} = 1/s^{e_2}$, e_2 = the excess of poles over zeros of P_2, $M_2 = 20 \log [k_{2max}/k_{2min}]$. Note that the M_2 uncertainty is handled by the outer loop L_o in the P.M. 2-loop design. If P_2 has significant uncertainty, R_2 covers a rather big range, e.g. (0.08, 8.] in Figure 2-10(a), which is replotted from Figure 2-6. It is important to note that even at ω_2 (=8), at the end of R_2, the template of $L_s = G_s P_1 P_2$ at $|P_1| = |P_1|_{\min_{\mathcal{P}_1}}$ fixed, extends above the horizontal 0 db line, in the Nichol's chart of

Figure 2-10(a). Similarly, in P.M. 2-loop system, $L_o = GP_{1e}P_2$ at $|P_{1e}| = |P_{1e}|_{\substack{\min \\ \mathcal{P}_1}}$ fixed, extends above the horizontal 0 db line, in Figure 2-10(b), which is replotted from Figure 2-6.

Consider the first two factors in (2.2-7). We want to justify

$$\left(\frac{|L_s/(1+L_s)|_{\max}}{|L_s/[P_1(1+L_s)]|_{\max}}\right)\cdot\left(\frac{|L_o/[P_{1e}(1+L_o)]|_{\max}}{|L_o/(1+L_o)|_{\max}}\right) \leq \frac{|P_1|_{\substack{\min \\ \mathcal{P}_1}}}{|P_{1e}|_{\substack{\min \\ \mathcal{P}_1}}} \tag{2.4-12}$$

or:

$$\frac{|\frac{L_s}{1+L_s}|_{\max}\cdot\frac{1}{|P_1|_{\substack{\min \\ \mathcal{P}_1}}}}{|\frac{L_s}{P_1(1+L_s)}|_{\max}} \leq \frac{|\frac{L_o}{1+L_o}|_{\max}\cdot\frac{1}{|P_{1e}|_{\substack{\min \\ \mathcal{P}_1}}}}{|\frac{L_o}{P_{1e}(1+L_o)}|_{\max}} \tag{2.4-13}$$

This is done by illustrating typical templates of single-loop and 2-loop P.M. designs, in each part of R_2.

It is concluded from Appendix I that there are three kinds of P_1, P_2 patterns, shown in Figure 2-11. In the first kind, the template extends upward and to the right from the nominal point P_{in} (see section 2.2.1), as in Figure 2-11(a). The second kind extends upward and to the left from P_{in}, Figure 2-11(b). The third extends both to the right and to the left from P_{in}, as in Figure 2-11(c).

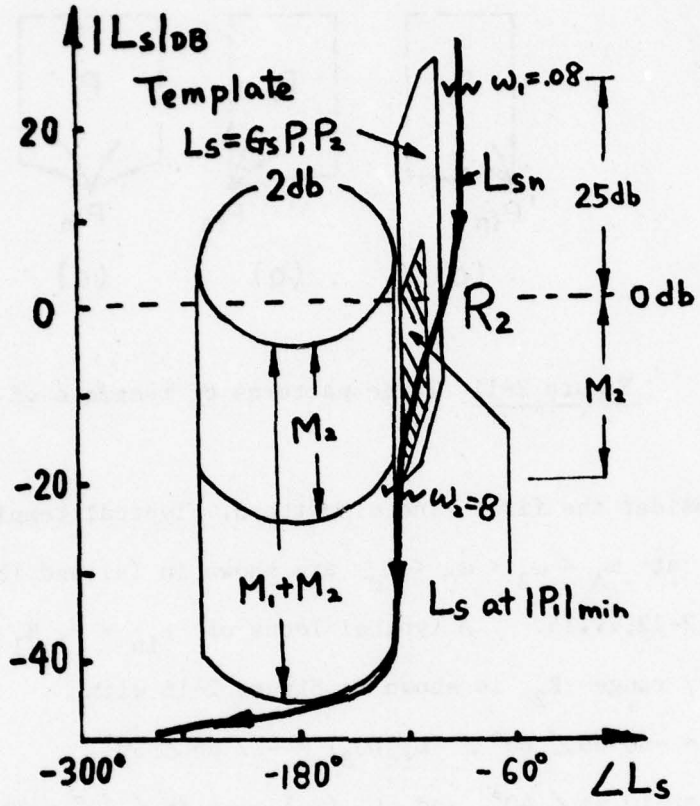

Figure 2-10(a) Typical L_s and template of L_s in R_2

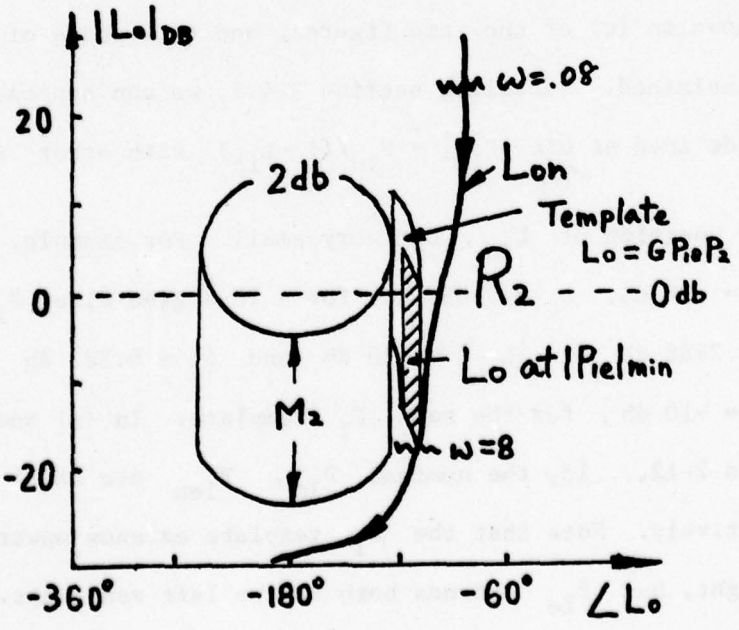

Figure 2-10(b) Typical L_o and template of L_o in R_2

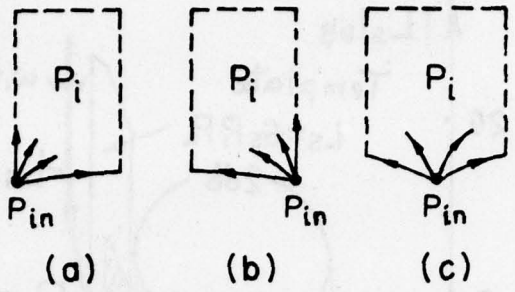

Figure 2-11 Three patterns of template of P_i

Consider the first kind of pattern. Typical templates of P_1, P_2 at $\omega_A < \omega_B < \omega_C < \omega_D$ are shown in (a) and (b) of Figures 2-12,...15. A typical locus of $L_{in} = P_{1n}H_1$ in the frequency range R_2 is shown in Figure 2-16 with $L_{in}(\omega_A) = -30$ db $\angle 60°$, $L_{in}(\omega_B) = -22$ db $\angle 50°$, $L_{in}(\omega_C) = -10$ db $\angle 40°$ and $L_{in}(\omega_D) = -4$ db $\angle 30°$. The resulting templates of $P_{1e} = P_1/(1+L_i)$, for P_1 in (a) of Figures 2-12,...15, are shown in (c) of the same figures, and this shape of P_{1e} is next explained. Recalling section 2.4.1, we can suppose P_{1en} (defined as $\min_{\mathcal{P}_1} |P_{1e}| \doteq P_{1n}/(1+L_{in})$ with error δ_2 depending on the position of L_{in}, but very small. For example, if $|L_{in}| = -30$ db, $\delta_2 = 0.058$ db for a 20 degree wide P_1 template, $\delta_2 = 0.2488$ db at $|L_{in}| = -20$ db and $\delta_2 = 0.382$ db if $|L_{in}| = -10$ db, for the same P_1 template. In (a) and (c) of Figures 2-12,...15, the nominal P_{1n}, P_{1en} are at A' and A" respectively. Note that the P_1 template extends upward and to the right, but P_{1e} extends both to the left and right. This can be explained by Figure 2-17 where A,B,C,D, correspond to A', B',

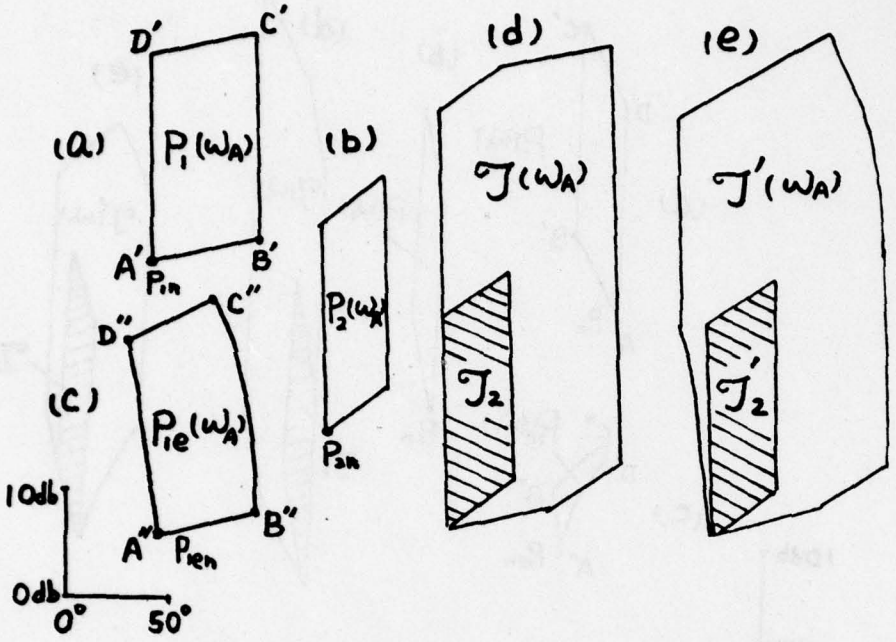

Figure 2-12 Templates at ω_A

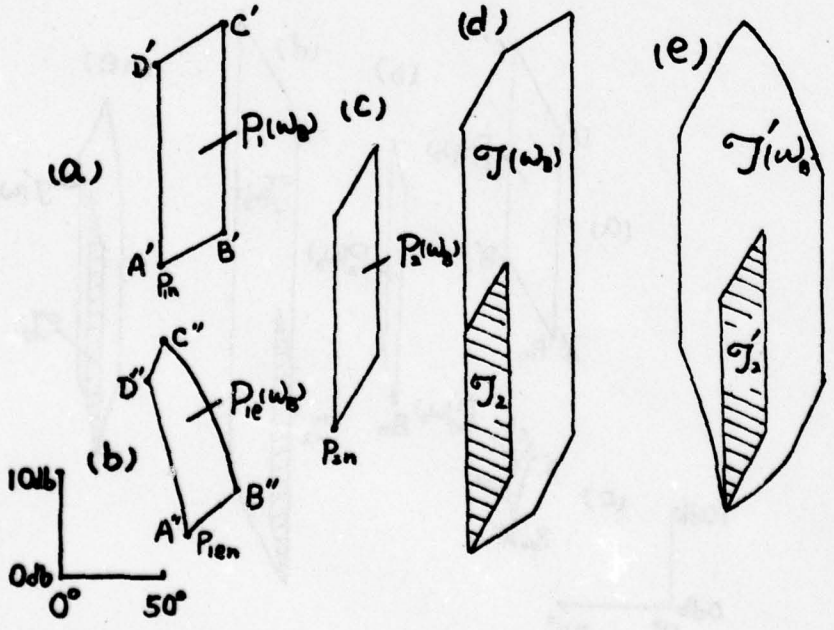

Figure 2-13 Templates at ω_B

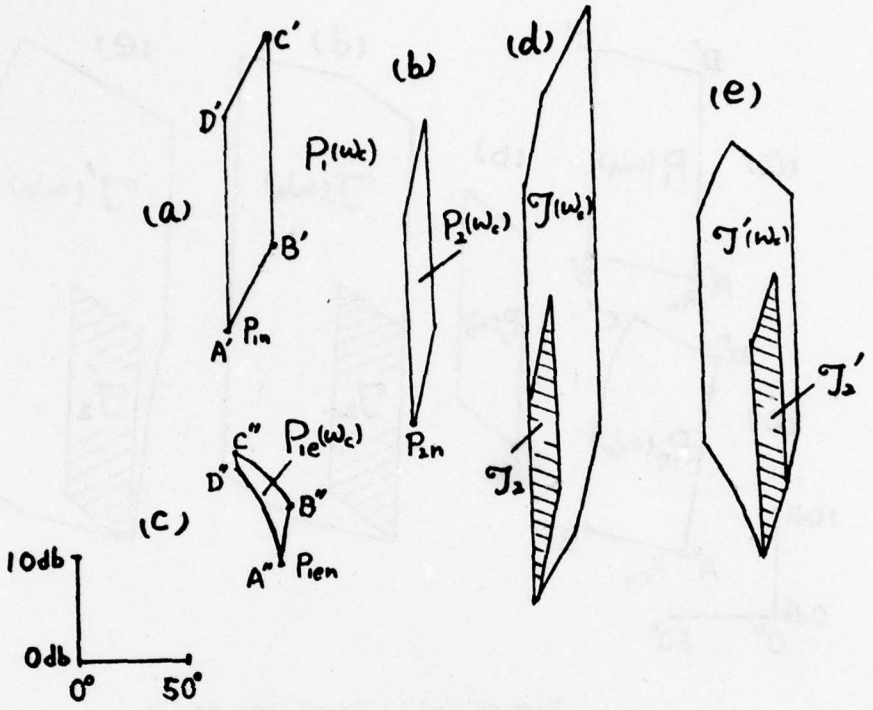

Figure 2-14 Templates at ω_C

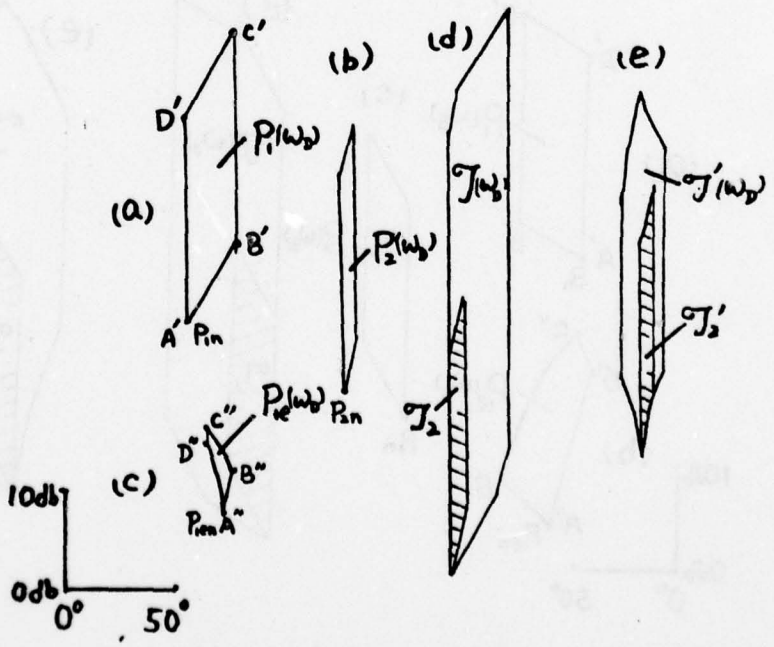

Figure 2-15 Templates at ω_D

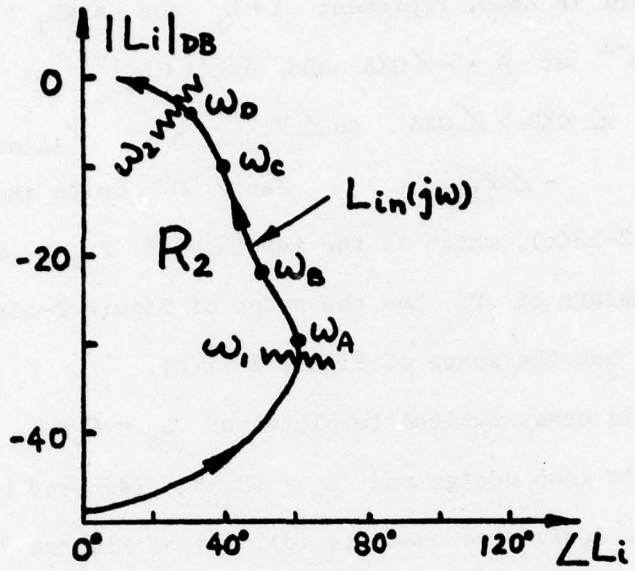

Figure 2-16 Typical $L_{in} = P_{1n}H_1$ in R_2

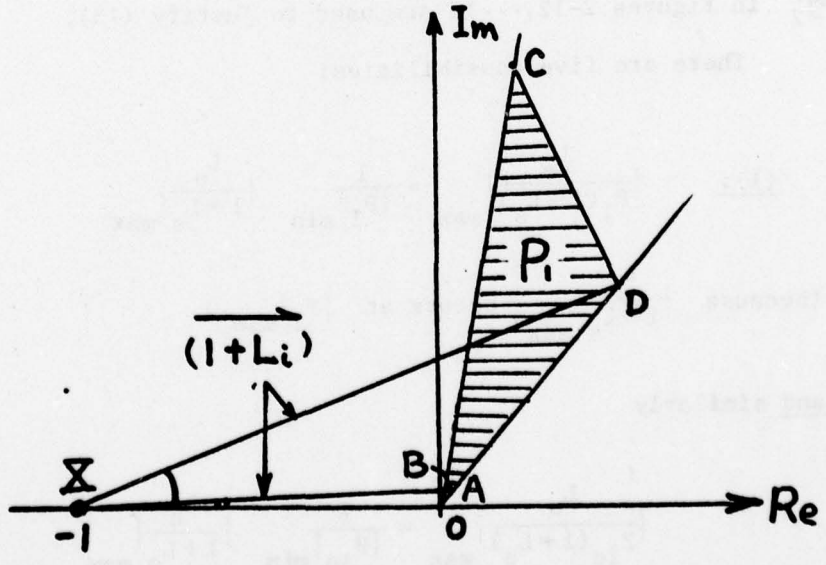

Figure 2-17 Relation between P_1 and P_{1e}

C', D' in Figure 2-13(a). Note $\overrightarrow{XO} = 1$, so the vector from X to any point in ABCD, represent $1+L_i$ and $\arg L_i > 0$ in R_2. $\text{Arg}(1+L_i)^{-1}$ at A $= -\angle OXA$ and $\text{Arg}(1+L_i)^{-1}$ at D $= -\angle OXD$. Obviously, $\angle OXD > \angle OXA$, so $\angle P_{1e}|_{\text{at D}} - P_{1e}|_{\text{at A}} > \angle P_1|_{\text{at D}} - \angle P_1|_{\text{at A}}$. Hence D" is to the left of A" in Figure 2-13(c), which is the template if P_{1e}. Summarizing, if the template of P_1 has the shape of Figure 2-11(a) in R_2, then P_{1e} has the shape of Figure 2-11(c).

In this case, typical templates of $L_s = G_s P_1 P_2$ (denoted by $\mathcal{T}$) in single loop design and $L_o = GP_{1e}P_2$ (denoted by $\mathcal{T}'$) in 2-loop P.M. design are shown in (d), (e) of Figures 2-12,...15. These are constituted from the corresponding P_1, P_2 and P_{1e} in each figure. The shaded regions in $\mathcal{T}$ and $\mathcal{T}'$ represent $\mathcal{T}$ at $|P_1|_{\min}$ due to $\mathcal{P}_2$ (denoted by $\mathcal{T}_2$) and $\mathcal{T}'$ at $|P_{1e}|_{\min}$ due to $\mathcal{P}_2$ (denoted by $\mathcal{T}_2'$) respectively. These templates $\mathcal{T}$, $\mathcal{T}'$, $\mathcal{T}_2$ and $\mathcal{T}_2'$ in Figures 2-12,...15 are used to justify (13).

There are five possibilities:

(1): $$\left|\frac{L_s}{P_1(1+L_s)}\right|_{\max} = \frac{1}{|P_1|_{\min}} \left|\frac{L_s}{1+L_s}\right|_{\max} \qquad (2.4\text{-}14)$$

(because $\left|\frac{L_s}{1+L_s}\right|_{\max}$ occurs at $|P_1|_{\min}$),

and similarly

$$\left|\frac{L_o}{P_{1e}(1+L_o)}\right|_{\max} = \frac{1}{|P_{1e}|_{\min}} \left|\frac{L_o}{1+L_o}\right|_{\max} \qquad (2.4\text{-}15)$$

Then both sides of (13) equal 1 and (13) is satisfied with '=' sign. The situation is shown in Figures 2-18,19.

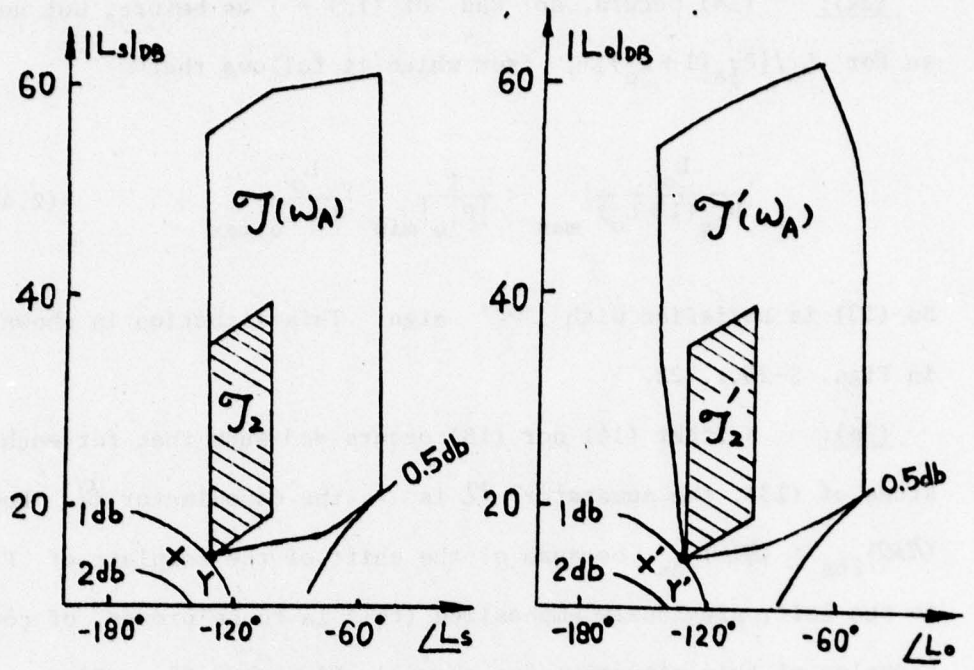

Figure 2-18 $\mathcal{T}(\omega_A)$, $\mathcal{T}'(\omega_A)$ at $|\Delta T(j\omega)| = 1.5$ db

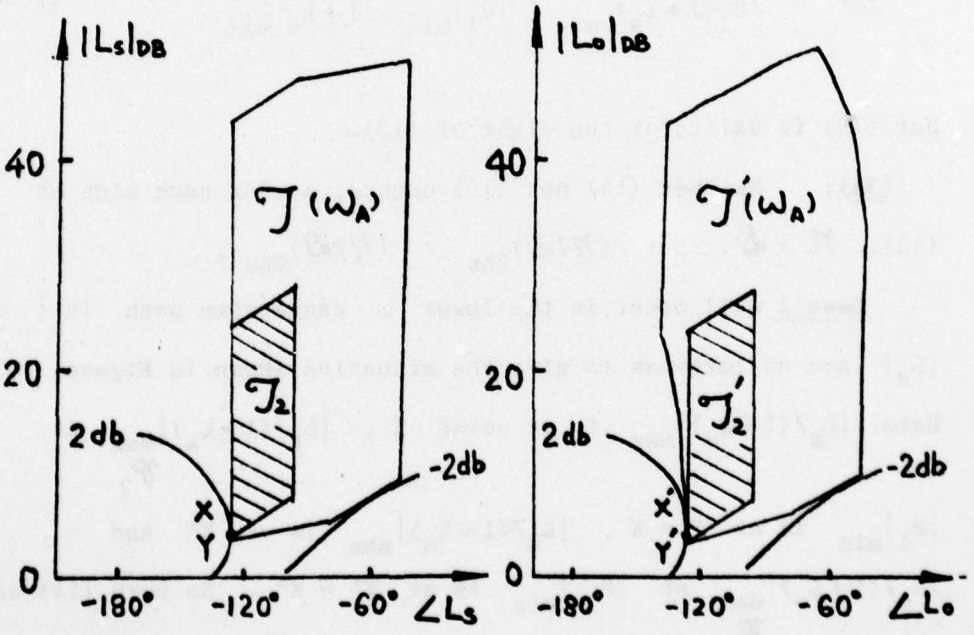

Figure 2-19 $\mathcal{T}(\omega_A)$, $\mathcal{T}'(\omega_A)$ at $|\Delta T(j\omega)| = 4$ db

(2a): (14) occurs, so lhs of (13) = 1 as before, but not so for $L_o/[P_{le}(1+L_o)]$, from which it follows that

$$\left|\frac{L_o}{P_{le}(1+L_o)}\right|_{max} < \frac{1}{|P_{le}|_{min}} \left|\frac{L_o}{1+L_o}\right|_{max} \qquad (2.4\text{-}16)$$

So (13) is satisfied with '<' sign. This situation is shown in Figs. 2-20,...22.

(3a): Neither (14) nor (15) occurs and such that for each sides of (13), the numerator $\mathcal{N}$ is > the denominator $\mathcal{D}$. However $(\mathcal{N}/\mathcal{D})_{lhs} \leq (\mathcal{N}/\mathcal{D})_{rhs}$, because of the shift of the template of P_{le} to the left, previously emphasized (this is to be proven, of course). Examples of this situation are shown in Figures 2-23,...25.

We also have to prove that cases (2b,3b) below do not occur.

(2b): $$\left|\frac{L_s}{P_1(1+L_s)}\right|_{max} \neq \frac{1}{|P_1|_{min}} \left|\frac{L_s}{1+L_s}\right|_{max} \qquad (2.4\text{-}17)$$

but (15) is valid for the right of (13).

(3b): Neither (14) nor (15) occurs, so for each side of (13), $\mathcal{N} > \mathcal{D}$. But $(\mathcal{N}/\mathcal{D})_{lhs} > (\mathcal{N}/\mathcal{D})_{lhs}$.

Case 1 will occur in the lower ω range when both $|L_o|$ and $|L_s|$ are so large as to give the situation shown in Figures 2-18,19. Here $|L_s/(1+L_s)|_{max}$ is at point X, $|L_s/(1+L_s)|_{max}$ at $\mathcal{P}_2$ $|P_1|_{min}$ is at Y = X, $|L_o/(1+L_o)|_{max}$ is at X' and $|L_o/(1+L_o)|_{max}$ at $\mathcal{P}_2$ $|P_{le}|_{min}$ is at Y' = X'. So both (14) and (15) occur and '=' sign in (13) is valid.

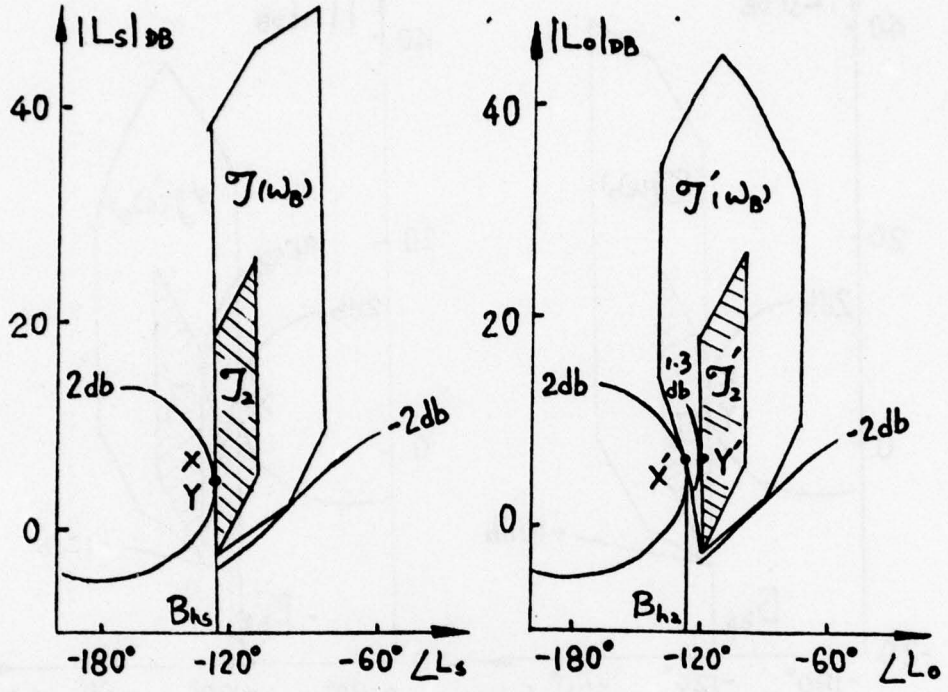

Figure 2-20 $\mathcal{T}(\omega_B)$, $\mathcal{T}'(\omega_B)$ at $|\Delta T(j\omega)| = 4$ db

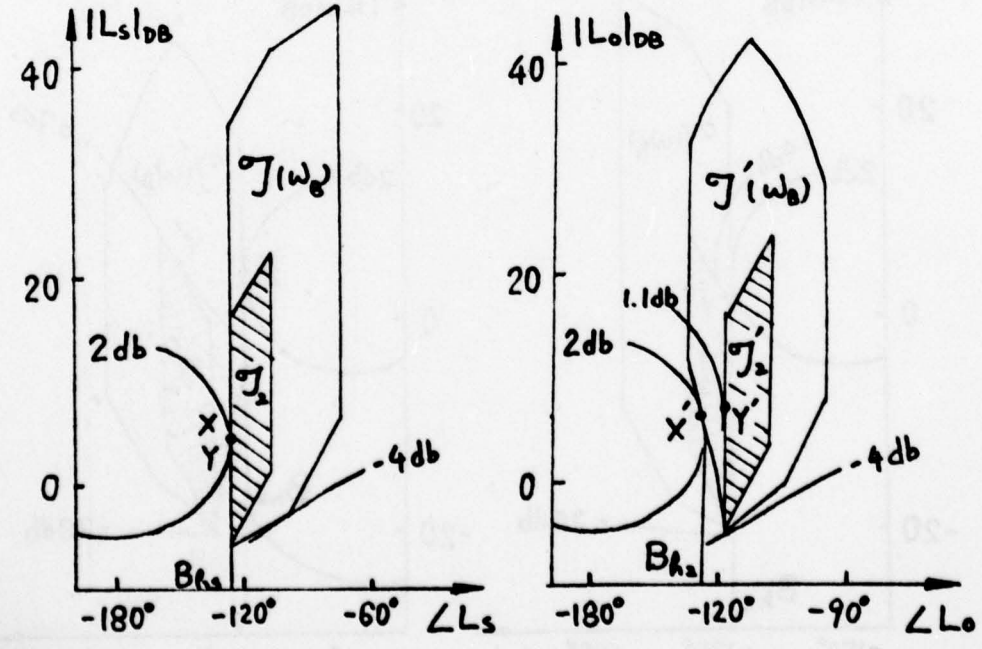

Figure 2-21 $\mathcal{T}(\omega_B)$, $\mathcal{T}'(\omega_B)$ at $|\Delta T(j\omega)| = 6$ db

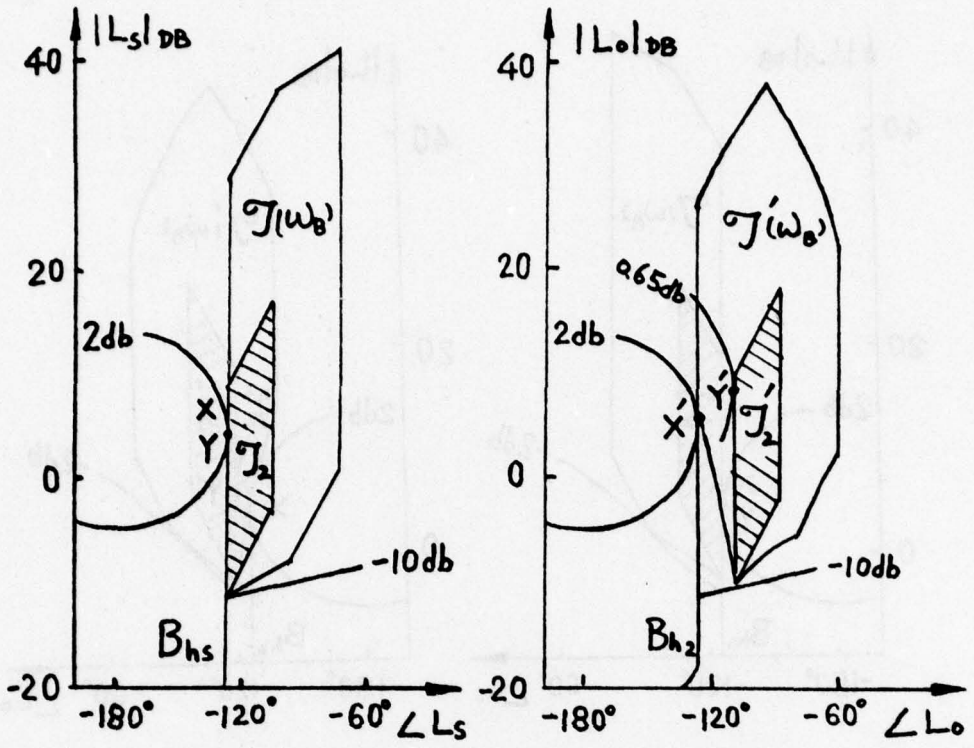

Figure 2-22 $\mathcal{J}(\omega_B)$, $\mathcal{J}'(\omega_B)$ at $|\Delta T(j\omega)|$ = 12 db

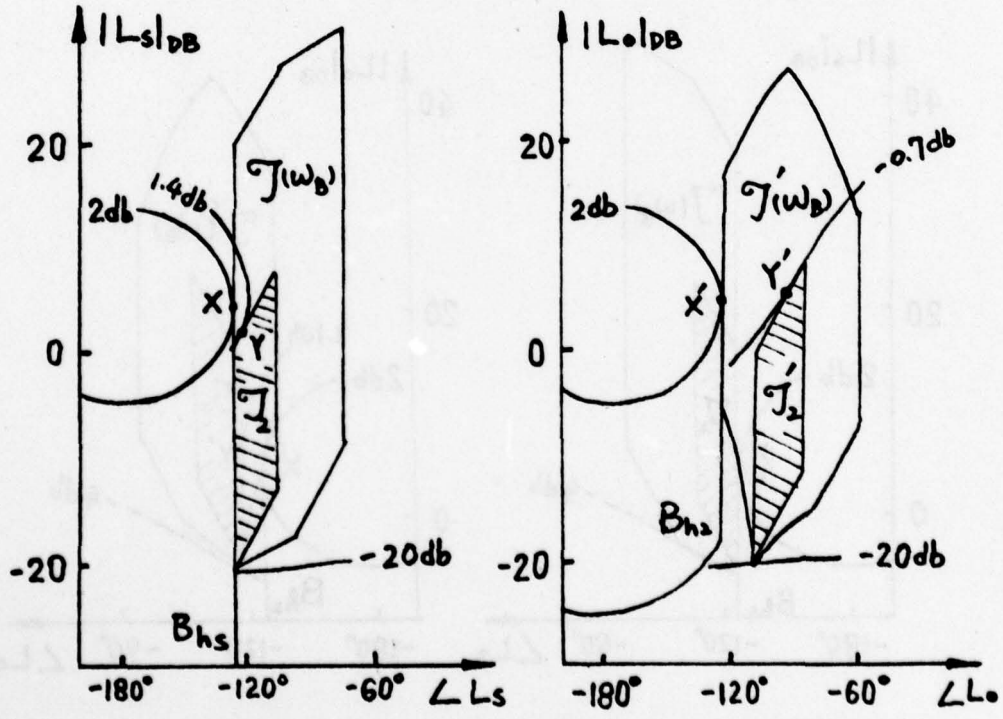

Figure 2-23 $\mathcal{J}(\omega_B)$, $\mathcal{J}'(\omega_B)$ at $|\Delta T(j\omega)|$ = 22 db

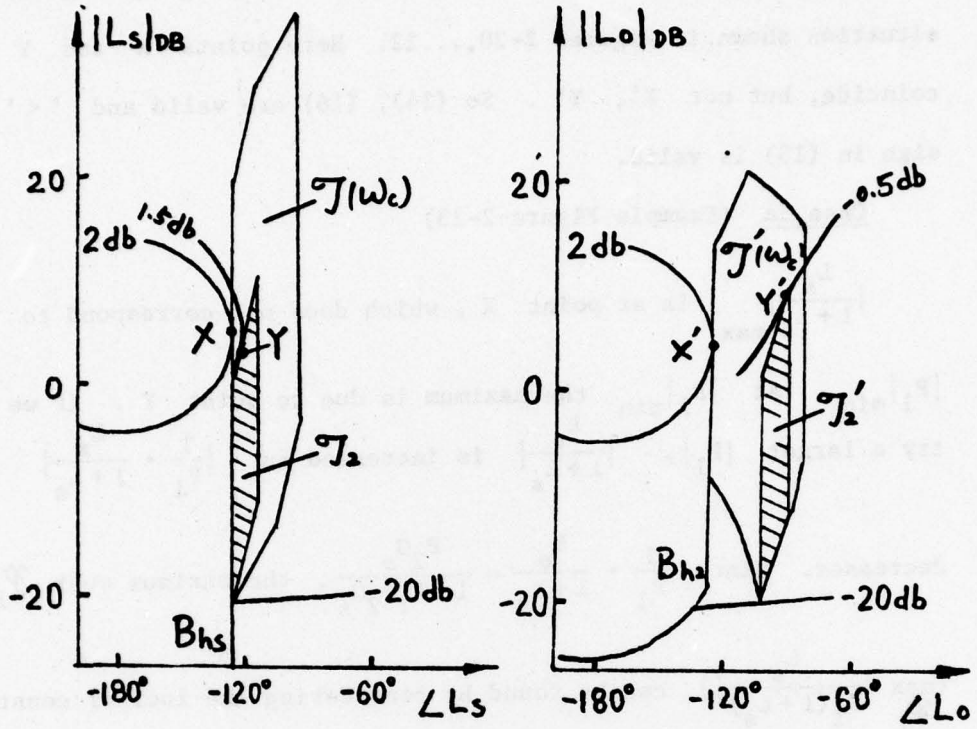

Figure 2-24 $\mathcal{T}(\omega_C)$, $\mathcal{T}'(\omega_C)$ at $|\Delta T(j\omega)|$ = 22 db

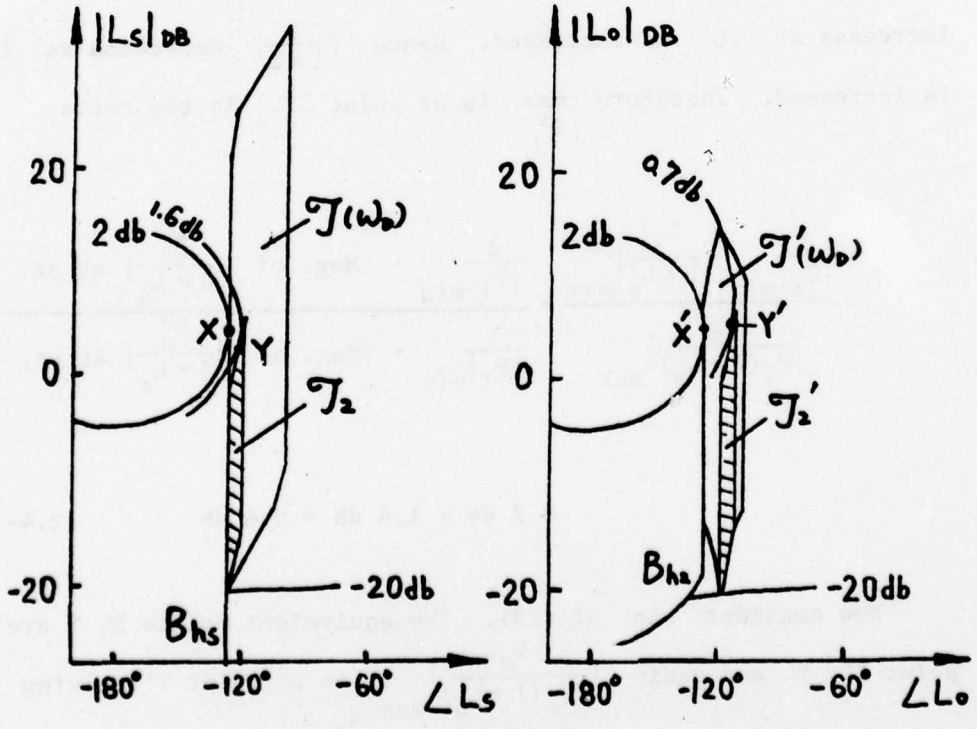

Figure 2-25 $\mathcal{T}(\omega_D)$, $\mathcal{T}'(\omega_D)$ at $|\Delta T(j\omega)|$ = 22 db

Case 2a tends to occur in the middle ω range giving the situation shown in Figures 2-20,...22. Here points X and Y coincide, but not X', Y' . So (14), (16) are valid and '<' sign in (13) is valid.

Case 3a (Example Figure 2-23)

$|\frac{L_s}{1+L_s}|_{s\ max}$ is at point X , which does not correspond to $|P_1|_{min}$. At $|P_1|_{min}$ the maximum is due to point Y . If we try a larger $|P_1|$, $|\frac{L_s}{1+L_s}|$ is increased but $|\frac{1}{P_1} \cdot \frac{L_s}{1+L_s}|$ decreases. Since $\frac{1}{P_1} \cdot \frac{L_s}{1+L_s} = \frac{P_2 G_s}{1+P_1 P_2 G_s}$, the maximum over $\mathcal{P}_1$ of $\{\max_{\mathcal{P}_2} |\frac{L_s}{P_1(1+L_s)}|\}$ can be found by considering the loci of constant $|1+L|$ in Figure 2-5. In the entire shaded region, $|1+L|$ increases as $|L|$ is increased. Hence $|\frac{1}{1+L}|$ decreases as $|L|$ is increased. Therefore $\max_{\mathcal{P}_1}$ is at point Y. So the ratio

$$\frac{\frac{1}{|P_1|_{min}} |\frac{L_s}{1+L_s}|_{s\ max}}{|\frac{L_s}{P_1(1+L_s)}|_{max}} = \frac{\frac{1}{|P_1|_{min}} \cdot \{\text{Mag. of } |\frac{L_s}{1+L_s}| \text{ at pt. X}\}}{\frac{1}{|P_1|_{min}} \cdot \{\text{Mag. of } |\frac{L_s}{1+L_s}| \text{ at pt. Y}\}}$$

$$= 2 \text{ db} - 1.4 \text{ db} = 0.6 \text{ db} \qquad (2.4\text{-}18)$$

Now consider rhs of (13). The equivalent points X, Y are point X', Y' and again $|\frac{L_o}{P_{1e}(1+L_o)}|_{max}$ is at point Y', giving

$$\frac{\frac{1}{|P_{1e}|_{min}} \cdot |\frac{L_o}{1+L_o}|_{max}}{|\frac{L_o}{P_{1e}(1+L_o)}|_{max}} = \frac{\frac{1}{|P_{1e}|_{min}} \cdot \{\text{Mag. of } |\frac{L_o}{1+L_o}| \text{ at pt X'}\}}{\frac{1}{|P_{1e}|_{min}} \cdot \{\text{Mag. of } |\frac{L_o}{1+L_o}| \text{ at pt Y'}\}}$$

$$= 2 \text{ db} - (-0.7 \text{ db}) = 2.7 \text{ db} \quad (2.4\text{-}19)$$

Note this value of 2.7 db > 0.6 db in (18), and the reason is due to the leftward shift of $\mathcal{J}'$ previously emphasized. This creates a bigger "effective" separation between X', Y' than between X, Y . This case also occurs in Figures 2-24,25 and it will be seen later that this is so in general in R_2 , when the template of P_1 has the shape of Figure 2-11(b).

Cases 2b,3b do not occur for exactly the same reason as in case 3a, due to the leftward shift of $\mathcal{J}'$ creating a bigger "effective" separation between X', Y' than between X, Y.

Consider the second kind of pattern of template P_i (Figure 2-11b). Typical templates of P_1, P_2 at $\omega_A < \omega_B < \omega_C < \omega_D$ are shown in (a) and (b) of Figures 2-26,...,29. With the same typical locus of $L_{in} = P_{1n}H_1$ in the frequency range R_2 in Figure 2-16, the resulting templates of $P_{1e} = P_1/(1+L_i)$, for P_1 in (a) of Figures 2-26,...29 are shown in (c) of the same figures and this shape of P_{1e} is next explained. Again, we can suppose $P_{1en} \doteq P_{1n}/(1+L_{in})$ with error δ_2 very small. In (a) and (c) of Figures 2-26,...29 the nominal P_{1n} , P_{1en} are at A' and A" respectively. Note that both templates P_1, P_{1e} extend upward and to the left, but P_{1e} bends more to the left than that of P_1 in Figures 2-26,...28. But P_{1e} bends less to the left than that of P_1 in Fig. 2-29. This can be explained by

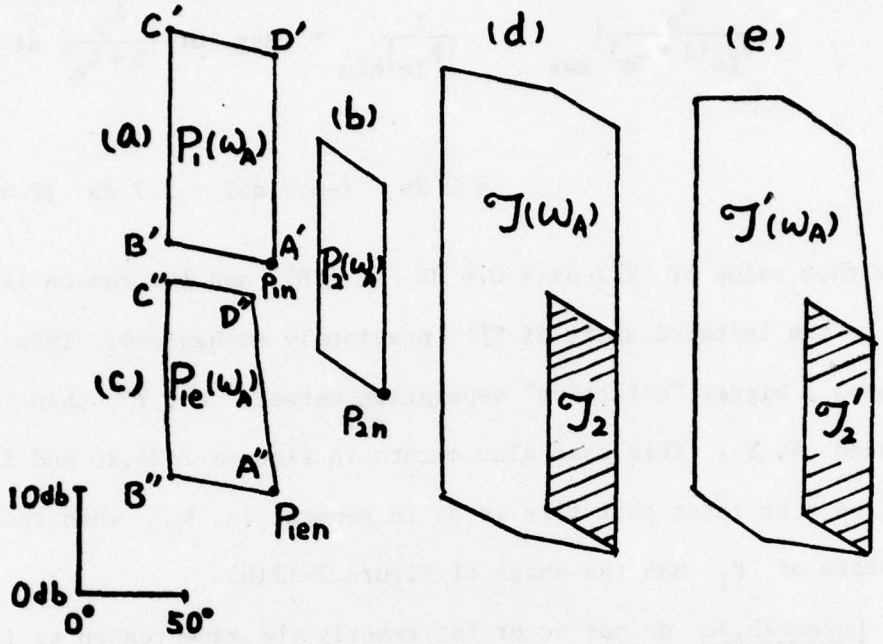

Figure 2-26 Templates at ω_A

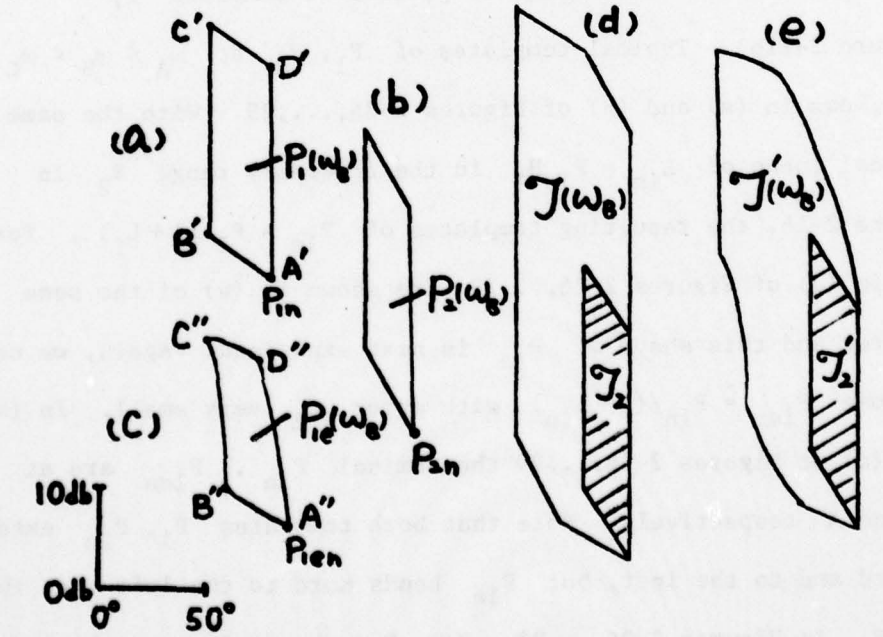

Figure 2-27 Templates at ω_B

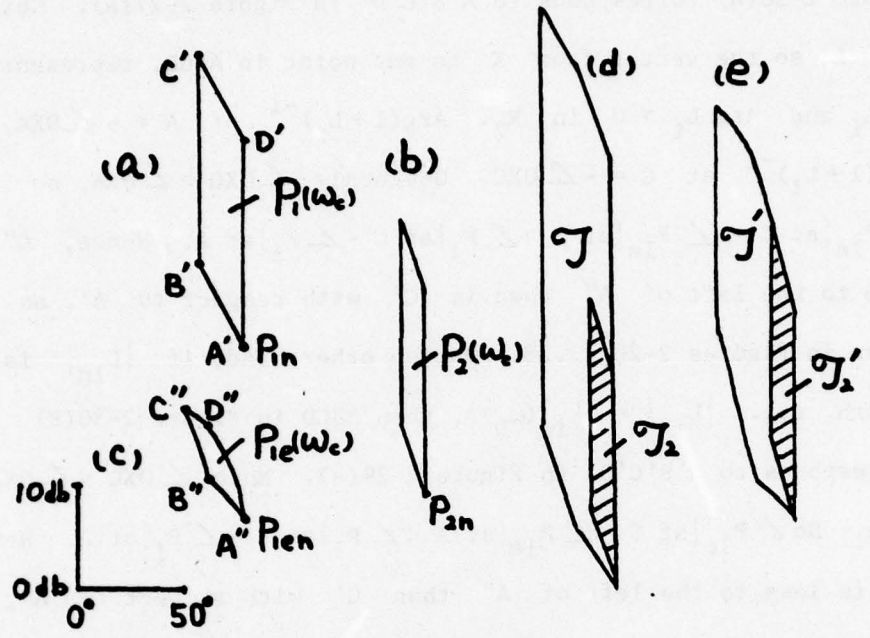

Figure 2-28 Templates at ω_C

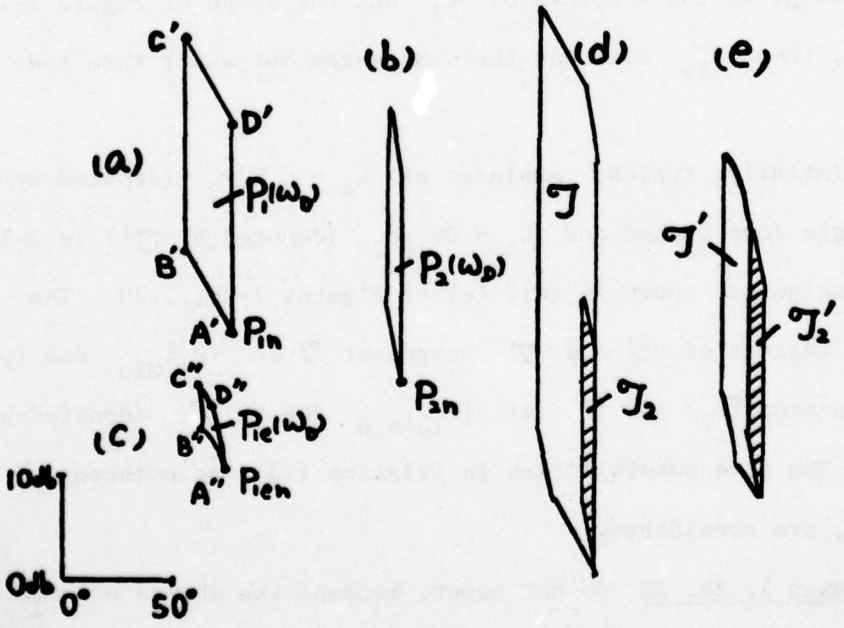

Figure 2-29 Templates at ω_D

Figures 2-30(a), (b). Very similar to Figure 2-17, ABCD in Figure 2-30(a) corresponds to A'B'C'D' in Figure 2-27(a). Note $\overrightarrow{XD} = 1$, so the vector from X to any point in ABCD, represents $1+L_i$ and $\text{Arg } L_i > 0$ in R_2. $\text{Arg}(1+L_i)^{-1}$ at $A = -\angle OXA$ and $\text{Arg}(1+L_i)^{-1}$ at $C = -\angle OXC$. Obviously, $\angle OXC > \angle OXA$, so $\angle P_{1e}|\text{at } C - \angle P_{1e}|\text{at } A > \angle P_1|\text{at } C - \angle P_1|\text{at } A$. Hence, C" is more to the left of A" than is C' with respect to A', as shown in Figures 2-26,...28. On the other hand, if $|L_{1n}|$ is big enough, e.g. $|L_{in}| = |L_{in}(\omega_D)|$, then ABCD in Figure 2-30(B) corresponds to A'B'C'D' in Figure 2-29(a). Note, $\angle OXC < \angle OXA$ here. So $\angle P_{1e}|\text{at } C - \angle P_{1e}|\text{at } A < \angle P_1|\text{at } C - \angle P_1|\text{at } A$. Hence C" is less to the left of A" than C' with respect to A', as in Figures 2-29(a),(c). Fortunately, this is the case with large $|L_{in}|$, in which ω is large. So if it does occur, it is only at the very end of R_2. In most cases, it will not occur in R_2. Concluding, if the template of P_1 has the shape of Figure 2-11(b) in R_2, then P_{1e} also has the same shape but wider than that of P_1.

Similarly, typical templates of $L_s = G_s P_1 P_2$ (denoted by $\mathcal{T}$) in single loop design and $L_o = GP_{1e}P_2$ (denoted by $\mathcal{T}'$) in 2-loop P.M. design are shown in (d), (e) of Figures 2-26,...29. The shaded regions of $\mathcal{T}$ and $\mathcal{T}'$ represent $\mathcal{T}$ at $|P_1|_{\min}$ due to $\mathcal{P}_2$ (denoted $\mathcal{T}_2$) and $\mathcal{T}'$ at $|P_{1e}|_{\min}$ due to $\mathcal{P}_2$ (denoted by $\mathcal{T}'_2$). The five possibilities in relation (13), as pointed out before, are considered.

<u>Cases 1, 2a, 2b</u> do not occur, because the shapes of P_1, P_2. P_{1e} are as in (a), (b), (c) of Figures 2-26,...29 and in (d), (e)

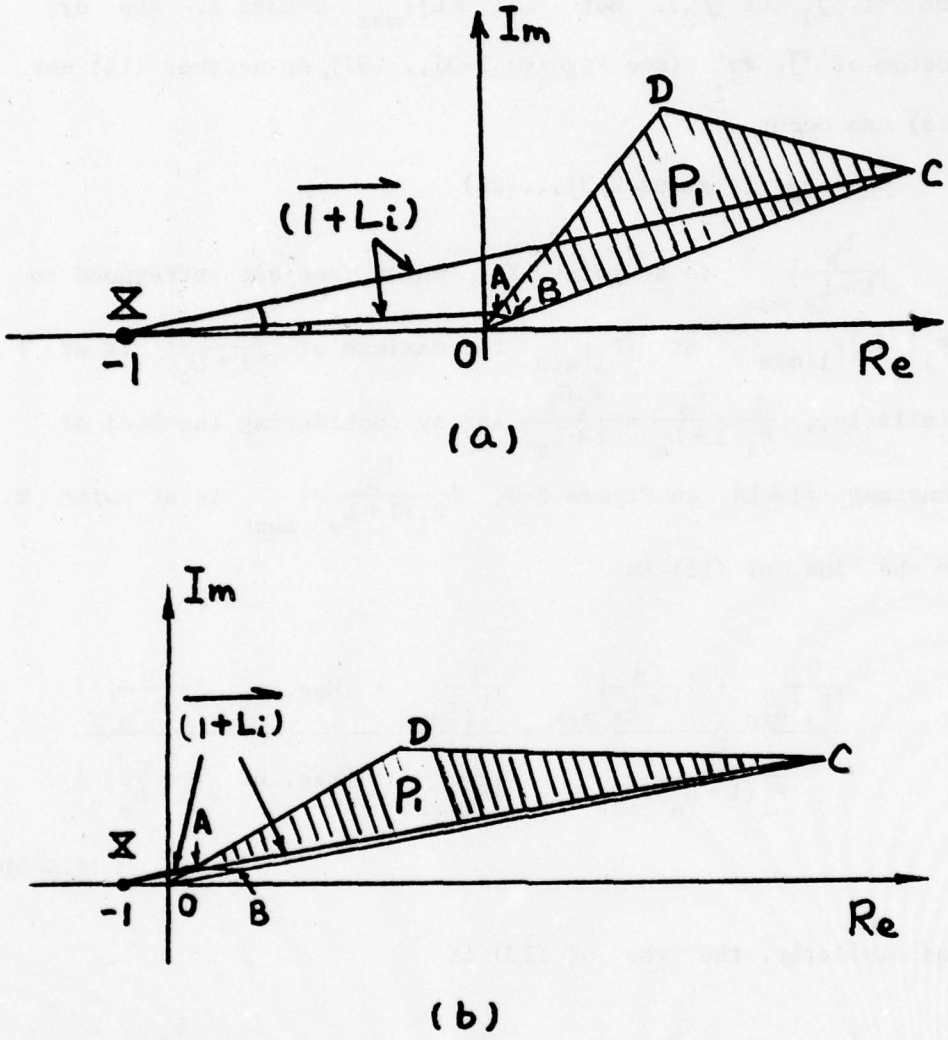

Figure 2-30 Relations between P_1 and $P_{1e} = P_1/(1+L_i)$

AD-A059 564 COLORADO UNIV BOULDER DEPT OF ELECTRICAL ENGINEERING F/G 12/2
SYNTHESIS OF MULTIPLE-LOOP FEEDBACK SYSTEMS WITH PLANT MODIFICA--ETC(U)
AUG 78 B WANG, I HOROWITZ AFOSR-76-2946
UNCLASSIFIED AFOSR-TR-78-1341 NL

2 OF 3
AD
A059 564

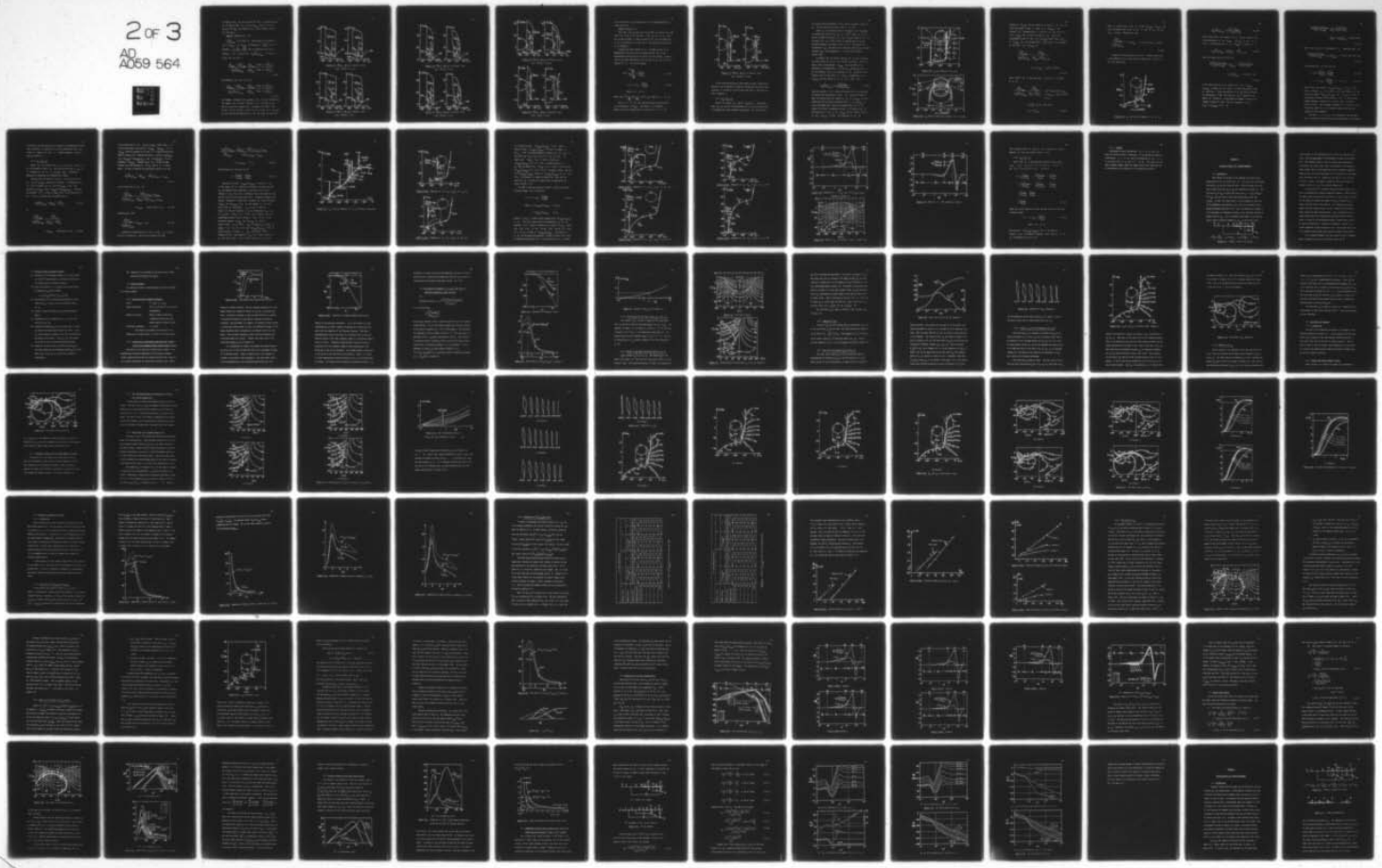

of Figures 2-26,...29; the rhs of $\mathcal{T}$ (or $\mathcal{T}'$) coincide with the rhs of $\mathcal{T}_2$ (or $\mathcal{T}_2'$). But $|L/(1+L)|_{max}$ occurs at lhs or bottom of $\mathcal{T}$, $\mathcal{T}_2'$ (see Figures 2-31,...37), so neither (14) nor (15) can occur.

Case 3a (Figures 2-31,...36)

$|\frac{L_s}{1+L_s}|_{max}$ is at point X, which does not correspond to $|P_1| = |P_1|_{min}$. At $|P_1|_{min}$ the maximum of $|\frac{L_s}{1+L_s}|$ is at Y. Similarly,, $\frac{1}{P_1}\frac{L_s}{1+L_s} = \frac{P_2G_2}{1+L_s}$ and by considering the loci of constant $|1+L|$ in Figure 2-5, $|\frac{L_s}{P_1(1+L_s)}|_{max}$ is at point Y. So the lhs of (13) is

$$\frac{\frac{1}{|P_1|_{min}} \cdot |\frac{L_s}{1+L_s}|_{s\ max}}{|\frac{L_s}{P_1(1+L_s)}|_{max}} = \frac{\frac{1}{|P_1|_{min}} \cdot \{\text{Mag. of } |\frac{L_s}{1+L_s}|_X\}}{\frac{1}{|P_1|_{min}} \cdot \{\text{Mag. of } |\frac{L_s}{1+L_s}|_Y\}} \qquad (2.4\text{-}20)$$

And similarly, the γhs of (13) is

$$\frac{\frac{1}{|P_{1e}|_{min}} \cdot |\frac{L_o}{1+L_o}|_{o\ max}}{|\frac{L_o}{P_{1e}(1+L_o)}|_{max}} = \frac{\frac{1}{|P_{1e}|_{min}} \cdot \{\text{Mag. of } |\frac{L_o}{1+L_o}|_{X'}\}}{\frac{1}{|P_{1e}|_{min}} \cdot \{\text{Mag. of } |\frac{L_o}{1+L_o}|_{Y'}\}} \qquad (2.4\text{-}21)$$

For example, in Figure 2-31, (20) gives 1 db - 0.32 db = 0.68 db and (21) gives 1 db - 0.32 db = 0.68 db, so '=' is valid in (13). And it is also so in Figure 2-32. In Figure 2-33, (20) → 2 db - 0.9 db = 1.1 db and (21) → 2 db - 0.7 db = 1.3 db, so '<' is true in (13), and also in Figures 2-33,...36. The reason is that $\mathcal{T}'$

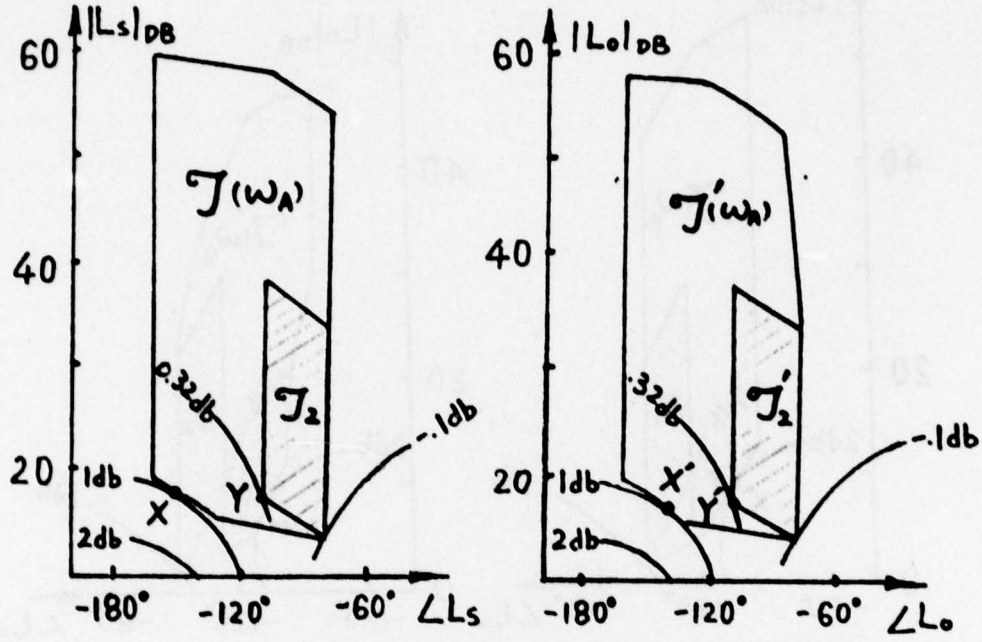

Figure 2-31 $\mathcal{T}(\omega_A)$, $\mathcal{T}'(\omega_A)$ in Nichols' chart with $|\Delta T(j\omega)| = 1.5$ db

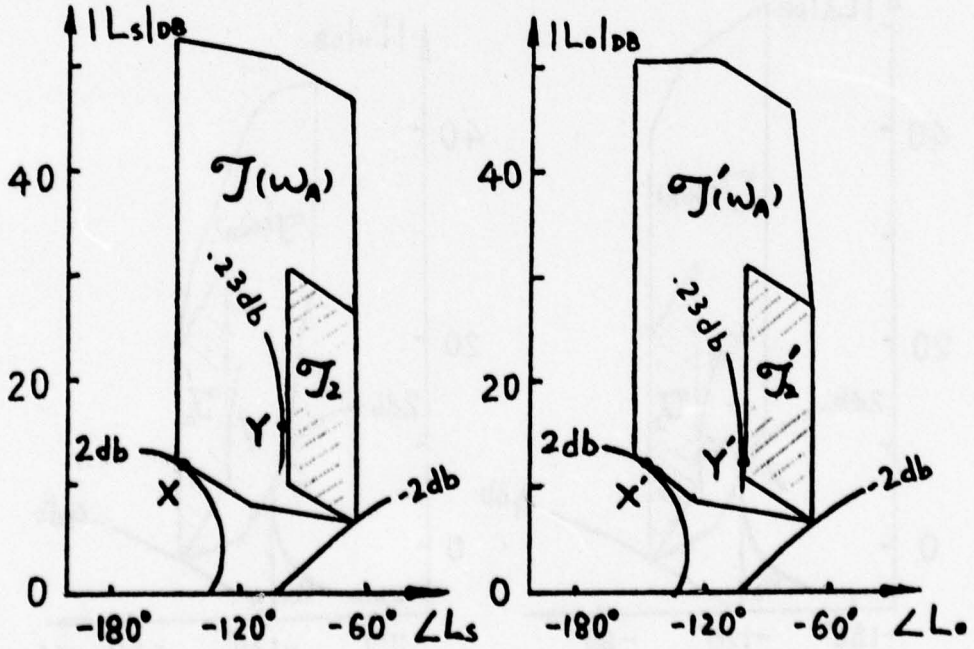

Figure 2-32 $\mathcal{T}(\omega_A)$, $\mathcal{T}'(\omega_A)$ in Nichols' chart with $|\Delta T(j\omega)| = 4$ db

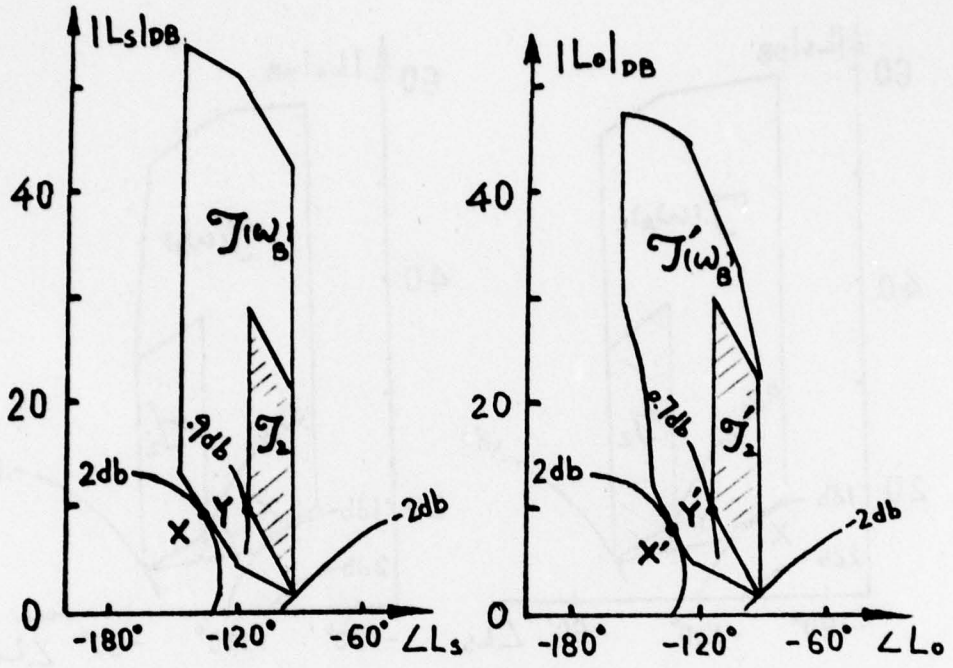

Figure 2-33 $\mathcal{T}(\omega_B)$, $\mathcal{T}'(\omega_B)$ in Nichols' chart with $|\Delta T(j\omega)| = 4$ db

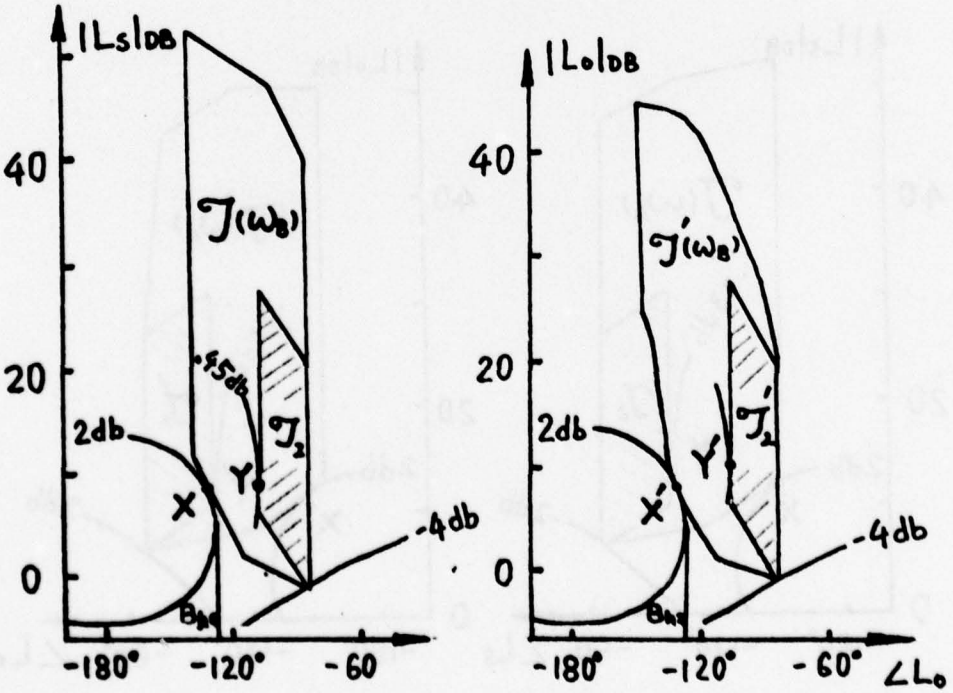

Figure 2-34 $\mathcal{T}(\omega_B)$, $\mathcal{T}'(\omega_B)$ in Nichols' chart with $|\Delta T(j\omega)| = 6$ db

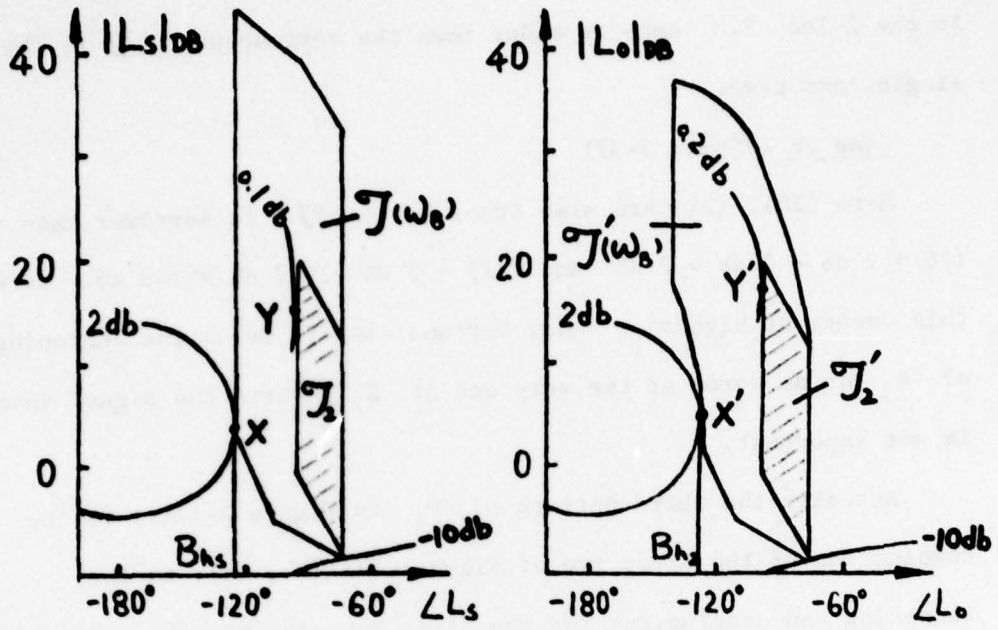

Figure 2-35 $\mathcal{J}(\omega_B)$, $\mathcal{J}'(\omega_B)$ in Nichol's chart with $|\Delta T(j\omega)|$ = 12 db

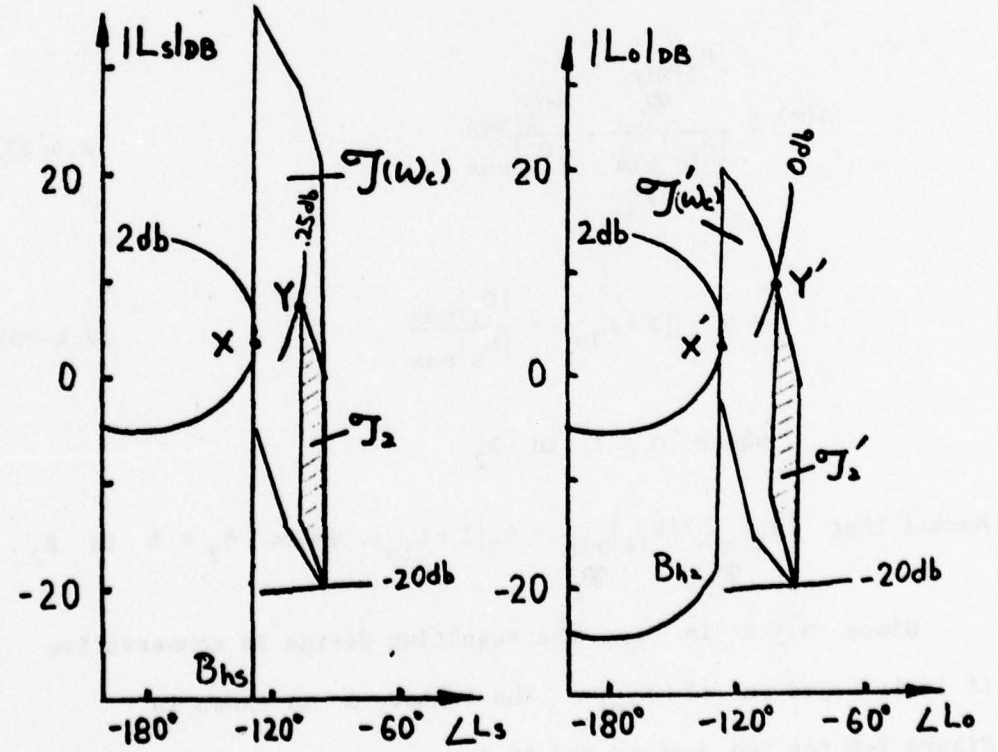

Figure 2-36 $\mathcal{J}(\omega_C)$, $\mathcal{J}'(\omega_C)$ in Nichols' chart with $|\Delta(j\omega)|$ = 22 db

in the 2-loop P.M. case is wider than the corresponding $\mathcal{T}$ in the single loop case.

Case 3b (Figure 3-37)

Here (20), (21) are also true, but as $\mathcal{T}'$ is narrower than $\mathcal{T}$, (20) → 2 db - 0 db = 2 db and (21) → 2 db - 0.7 db = 1.3 db. Note this occurs at higher ω and, fortunately, it is at the beginning of R_3 or at worst at the very end of R_2, where the signal level is not important.

Actually the third pattern of P_i in Figure 2-11(c) is the combination of the first two of Figures 2-11(a), (b), so the reasoning and conclusions for the first two also applies. Summarizing all the above discussions, (13) is true in R_2 for any kind of template of P_i. So (2.2-7) becomes

$$\rho(\omega) \leq \frac{|P_1|_{\min}}{|P_{1e}|_{\min}} \cdot \frac{|C_1|_{\max}}{|C_s|_{\max}} \qquad (2.4\text{-}22)$$

$$= \alpha \cdot |1+L_{in}| \cdot \frac{|C_1|_{\max}}{|C_s|_{\max}} \qquad (2.4\text{-}23)$$

where $\alpha \leq 1$ in R_2

Recall that $|P_1|_{\min}/|P_{1e}|_{\min} = \delta_2|1+L_{in}|$, where $\delta_2 \simeq 1$ in R_2.

Since $\alpha \leq 1$ in R_2, the resulting design is conservative if it is based on $|1+L_{in}|$. The factor α is shown in Figure 2-9 for two designs and it is seen that $\alpha < 1$ in R_2.

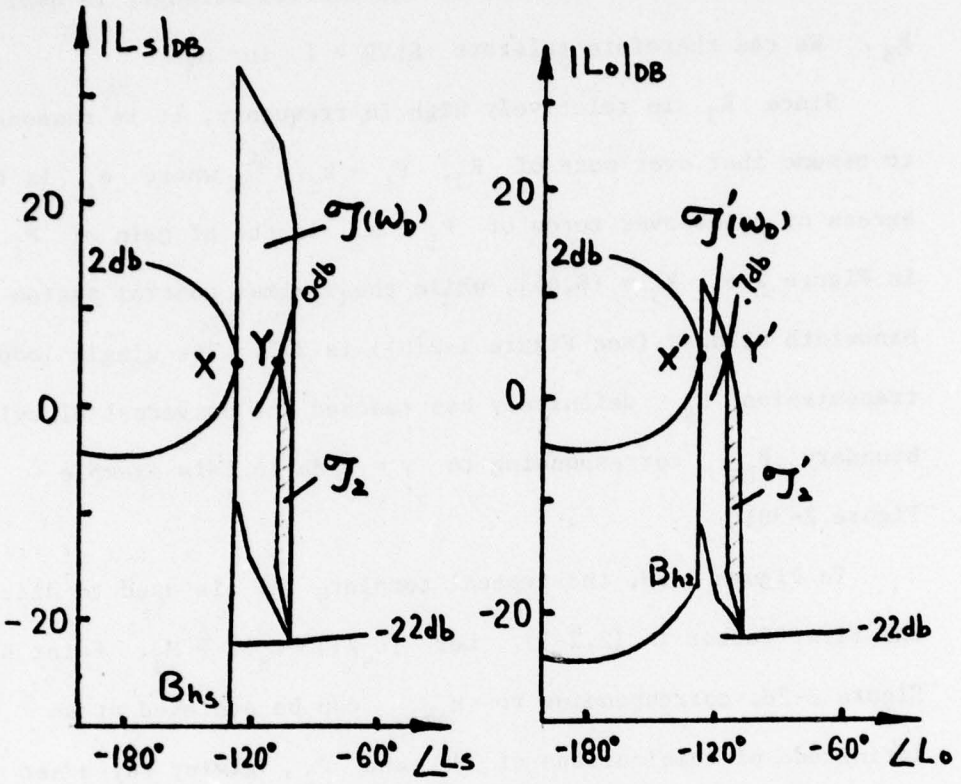

Figure 2-37 $\mathcal{J}(\omega_D)$, $\mathcal{J}'(\omega_D)$ in Nichols' chart with $|\Delta T(j\omega)| = 24$ db

A very interesting point is that based on such a conservative approach, one can design a 2-loop P.M. system with the signal level variation Q defined in (1.6-25) even less than 1. This will be seen in Chapter 3.

2.4.3 $R_3 = (\omega_2, \omega_3]$

Recall R_3 covers $\{\omega | -M_2 \text{ db} > |L_{sn}(j\omega)| \geq -(M_1 + M_2)\text{db}\}$ where M_1, M_2 are the hf uncertainties of P_1 and P_2 respectively. In problems with large parameter uncertainty, R_3 is well above

the control system bandwidth, so the control strength is small in R_3. We can therefore tolerate SLVR > 1 in R_3.

Since R_3 is relatively high in frequency, it is reasonable to assume that over most of R_3, $P_i \to k_i/s^{e_i}$, where e_i is the excess of poles over zeros of P_i, k_i is the hf gain of P_i, e.g. in Figure 2-6, $R_3 = (8,44]$, while the maximum control system bandwidth allowed (see Figure 1-2(b)) is 2.1. The single loop transmission L_{sn} definitely has reached the universal hf cylinder boundary B_{hs} (corresponding to $\gamma = 2$ db in this example - Figure 2-38).

In Figure 2-38, the typical template AF is used to discuss the first factor in (2.2-7). Let $|L_s/(1+L_s)| \triangleq M_s$. Point B in Figure 2-38, corresponding to M_{smax} can be achieved at an infinitude of combinations of P_1 and P_2, giving say a set S. Let the smallest $|P_1|$ in S be denoted by P_1^*. Obviously, from Figures 2-38, for any fixed P_1, M_s/P_1 is maximized at $P_2 = |P_2|_{max}$, and with respect to P_1 at $|P_1| \leq |P_1^*|$. Thus,

$$\left|\frac{L_s}{P_1(1+L_s)}\right|_{max} = \frac{G_s|P_2|_{max}}{|1+G_s P_{2max} P_1|_{min}} \qquad (2.4\text{-}24)$$

From the constant $|1+L|$ curves in Figure 2-39, it is seen that to minimize the denominator of (24), $|P_1|$ should be chosen as small as possible when the template of L_s at $|P_2|_{max}$ is in the shaded area and as large as possible when L_s at $|P_2|_{max}$ is below the shaded area. Hence the minimum point is at D in Figure 2-39, which corresponds to point D in Figure 2-38. In the early part of R_3, L_s at $|P_2|_{max}$ is on or above D $\forall$ P_1, so $|P_1| = |P_1|_{min}$ is used. But eventually in R_3, the

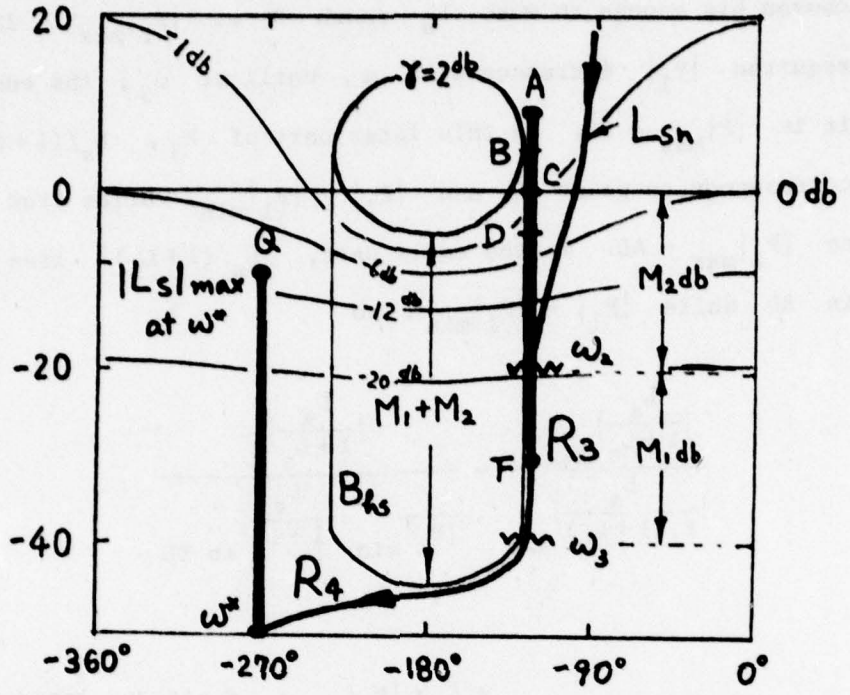

Figure 2-38 L_{sn} and template of L_s in R_3

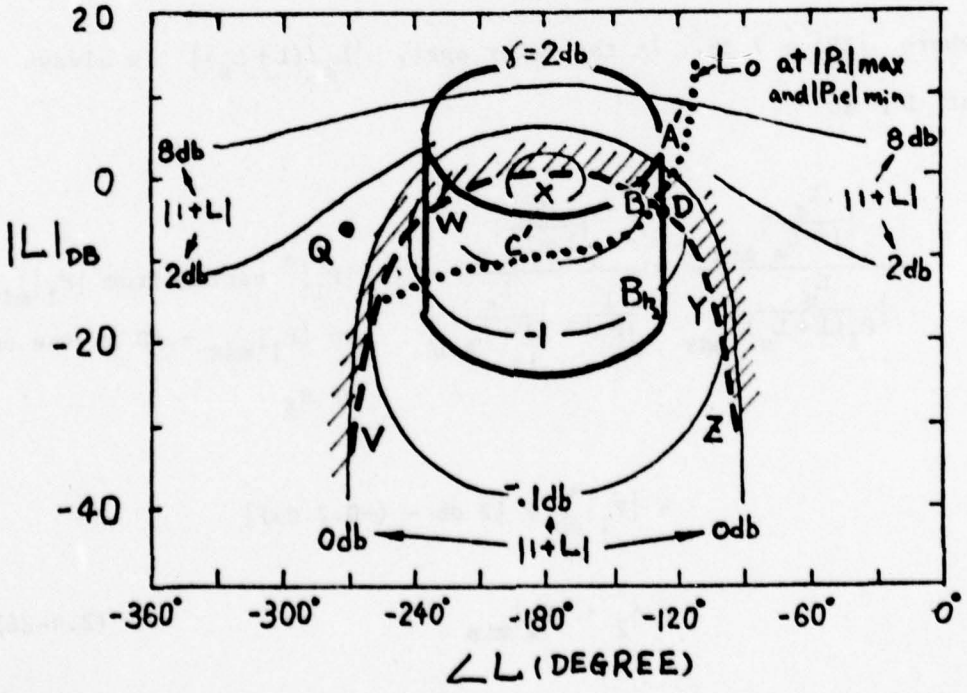

Figure 2-39 L_{on} Nichols' chart with constant $|1+L|$ curves

template at $|P_1|_{min}$ does not extend to or above D, so $|P_1|$ is chosen big enough to make L_s reach D at $|P_2|_{max}$. The required $|P_1|$ increases with ω, until at ω_3, the end of R_3, it is $|P|_{max}$ - AD. In this later part of R_3, $L_s/(1+L_s)$ corresponds to point D and $|P_1| \geq |P_1|_{min}$, varies from $|P_1|_{min}$ to $|P_1|_{max}$ - AD. In the early part, $|L_s/(1+L_s)|$ lies somewhere in BD while $|P_1| = |P_1|_{min}$, so

$$\frac{\left|\frac{L_s}{1+L_s}\right|_{s\ max}}{\left|\frac{L_s}{P_1(1+L_s)}\right|_{max}} = \frac{\left|\frac{L_s}{1+L_s}\right|_{s\ B}}{\frac{1}{|P_1|_{min}}\left|\frac{L_s}{1+L_s}\right|_{s\ in\ BD}}$$

$$= \delta_1 \cdot |P_1|_{min}\ ;\quad \delta_1 \varepsilon [0\ db,\ |BD|db]$$

(2.4-25)

where $|BD| \doteq 7$ db. In the later part, $|L_s/(1+L_s)|$ is always at D, so

$$\frac{\left|\frac{L_s}{1+L_s}\right|_{s\ max}}{\left|\frac{L_s}{P_1(1+L_s)}\right|_{max}} = \frac{\left|\frac{L_s}{1+L_s}\right|_{s\ B}}{\frac{1}{|P_1|^*}\left|\frac{L_s}{1+L_s}\right|_{s\ D}}$$

$|P_1|^*$ varies from $|P_1|_{min}$ to $|P_1|_{max}$ - AD at the end of R_3

$$= |P_1|^*_{db} + [2\ db - (-0.2\ db)]$$

$$= \delta_2 \cdot |P_1|_{min} \qquad (2.4\text{-}26)$$

where δ_2 varies from 2.2 db to 2.2 db + $|P_1|_{max} - |P_1|_{min}$ - AD, since the smallest AD, is at $\omega = \omega_3$, $\doteq$ 3 db. So $\delta_2 \in$ [2.2 db, $|\Delta P_1|$ - 0.8 db]. Combine (25), (26)

$$\frac{\left|\frac{L_s}{1+L_s}\right|_{max}}{\left|\frac{L_s}{P_1(1+L_s)}\right|_{max}} = \delta \cdot |P_1|_{min} \quad , \quad \delta = [0 \text{ db}, |\Delta P_1| - 0.8 \text{ db}]$$

(2.4-27)

Consider the second factor in (2.2-7). A typical outer loop L_o and template of L_o in R_3, is shown in Figure 2-40. Just as in the first factor (24).

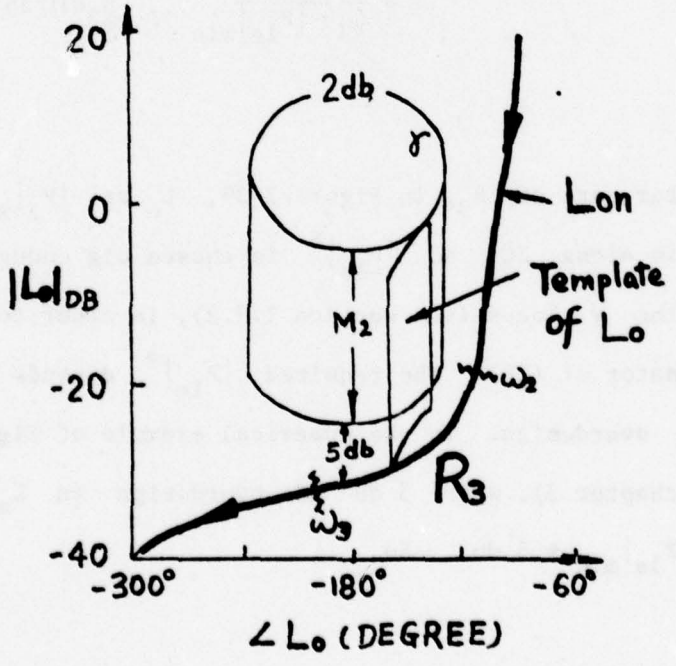

Figure 2-40 L_{on} and typical template of L_o in R_3

$$\left|\frac{L_o}{P_{le}(1+L_o)}\right|_{max} = \frac{|G| \cdot |P_2|_{max}}{|1+GP_{2max}P_{le}|_{min}} \qquad (2.4\text{-}28)$$

And by inspection of the constant $|1+L|$ curves of Figure 2-39, the corresponding L_o at $|P_2|_{max}$, $|P_{le}|_{min}$ in R_3, is in A'B'C'. In the early part of R_3, $GP_{2max}P_1$ is above B, so

$$\left|\frac{L_o}{P_{le}(1+L_o)}\right|_{max} = \frac{1}{|P_{le}|_{min}} \cdot \left|\frac{L_o}{1+L_o}\right|_{\text{in AB}} \qquad (2.4\text{-}29)$$

Thus, the second factor of (2.2-7) is

$$\frac{|L_o/[P_{le}(1+L_o)]|_{max}}{|L_o/(1+L_o)|_{max}} = \frac{1}{|P_{le}|_{min}} \cdot \frac{|L_o/(1+L_o)|_{\text{in AB}}}{|L_o/(1+L_o)|_{\gamma}}$$

$$= \frac{1}{\delta_3 \cdot |P_{le}|_{min}}, \quad \delta_3 \varepsilon [0\,\text{db},\ 3\,\text{db}] \qquad (2.4\text{-}30)$$

In the latter part of R_3, in Figure 2-39, L_o at $|P_2|_{max}$, $|P_{le}|_{min}$ is along BC, so $|P_{le}|^*$ is chosen big enough to make L_o reach the γ locus (see section 1.2.2), in order to minimize the denominator of (28). The required $|P_{le}|^*$ depends on the amount hf overdesign. In the numerical example of Figure 2-40 (Design A chapter 3), with 5 db hf overdesign on L_o, $|P_{le}|^* = |P_{le}|_{min} + 5$ db. So

$$\frac{|L_o/[P_{le}(1+L_o)]|_{max}}{|L_o/(1+L_o)|_{max}} = \frac{1}{|P_{le}|^*} \cdot \frac{|L_o/(1+L_o)|_\gamma}{|L_o/(1+L_o)|_\gamma}$$

$$= \frac{1}{|P_{le}|^*} = \frac{1}{\delta_4 |P_{le}|_{min}} , \quad \delta_4 \varepsilon [0 \text{ db}, \beta \text{ db}]$$

(2.4-31)

where β db is the hf overdesign of L_o. Combining (30), (31)

$$\frac{|L_o/[P_{le}(1+L_o)]|_{max}}{|L_o/(1+L_o)|_{max}} = \frac{1}{\delta' \cdot |P_{le}|_{min}} , \quad \delta' \varepsilon [0 \text{ db}, \max \{3 \text{ db}, \beta \text{ db}\}]$$

(2.4-32)

Substituting (27), (32) into (2.2-7),

$$\rho = \frac{\delta}{\delta'} \cdot \frac{|P_1|_{min}}{|P_{le}|_{min}} \cdot \frac{|C_1|_{max}}{|C_s|_{max}} \qquad (2.4\text{-}33)$$

$$= \alpha \cdot |1+L_{in}| \cdot \frac{|C_1|_{max}}{|C_s|_{max}} ; \quad \alpha > 1 \text{ in } R_3 \qquad (2.4\text{-}34)$$

From (33,34), the relation $|P_1|_{min}/|P_{le}|_{min} \simeq |1+L_{in}|$ still holds. Although L_{in} is not small in R_2 (see Figure 2-7), the difference between $|P_1|_{min}/|P_{le}|_{min}$ and $|1+L_{in}|$ ($\simeq 0.4$ db) is fairly small compared with the error in δ/δ'. In the previous example (Design A, chapter 3), $\alpha \varepsilon [0 \text{ db}, |\Delta P_1| - 5.5 \text{ db}] = [0 \text{ db}, 14.5 \text{ db}]$. And in Design B (chapter 3), $\alpha \varepsilon [0 \text{ db}, 14.5 \text{ db}]$. The actual results for α are shown in Figure 2-9, and they confirm the above argument.

Note that $\alpha > 1$ in R_3, but fortunately, the frequency here is relatively high where the design philosophy is to emphasize

the saving in sensor noise effect, instead of considering the signal level variation. In addition, if we use an additional inner loop around P_2 (Figure 2-2), the $\alpha > 1$ region disappears. This is shown in Chapter 4.

2.4.4 $R_4 = (\omega_3, \omega_4]$

Recall R_4 is the range from ω_3 to $\omega_4 \triangleq 10\,\omega_3$, where ω_3 is the frequency at which L_{sn} turns the bottom corner of B_{hs} at X in Figure 2-6. In R_4, L_s is under B_{hs}, decreasing moderately in magnitude and considerably in phase.

Consider the first factor of (2.2-7). In the early part of R_4, $|L_s/(1+L_s)|_{max}$ reaches the forbidden γ disturbance locus (γ = 2 db in Figure 2-6), so $|L_s/(1+L_s)|_{max} = \gamma$ db, and $|L_s/[P_1(1+L_s)]|_{max} = |G_s| \cdot |P_2|_{max}/|1+G_sP_{2max}P_1|_{min}$. Consider the constant $|1+L|$ curves of Figure 2-39. In the early part of R_4, $|1+L_s|$ is always under the VWXYZ line, so

$$\left|\frac{L_s}{P_1(1+L_s)}\right|_{max} = \frac{1}{|P_1|_{max}} \cdot \left|\frac{L_s}{1+L_s}\right|_{\gamma} \qquad (2.4\text{-}35)$$

so

$$\frac{\left|\frac{L_s}{1+L_s}\right|_{s\ max}}{\left|\frac{L_s}{P_1(1+L_s)}\right|_{max}} = \frac{\left|\frac{L_s}{1+L_s}\right|_{\gamma}}{\frac{1}{|P_1|_{max}} \cdot \left|\frac{L_s}{1+L_s}\right|_{\gamma}}$$

$$= |P_1|_{max} \qquad \text{(early part of } R_4\text{)} \qquad (2.4\text{-}36)$$

In the latter part of R_4, $|L_s/(1+L_s)|_{max}$ cannot reach γ in a practical design, but occurs at $|P_1|_{max}$, $|P_2|_{max}$, i.e. at $|L_s|_{max}$ which for example is at point Q in Figure 38 and above VWXYZ in Figure 2-39. Consider the factor $|L_s/[P_1(1+L_s)]|_{max} = |G_s| \cdot |P_2|_{max}/|1+G_sP_{2max}P_1|_{min}$, and $|1+G_sP_{2max}P_1|$ is not a minimum at $|P_1|_{max}$. However, since $|L_s|$ is small enough (Figure 2-6), the variation of $|1+L_s|$ due to P_1 is fairly small. In order to simplify the explanation later on, we take

$$\left|\frac{L_s}{P_1(1+L_s)}\right|_{max} \doteq \frac{1}{|P_1|_{max}} \cdot \left|\frac{L_s}{1+L_s}\right| |P_1|_{max},\ |P_2|_{max} \tag{2.4-37}$$

in the latter part of R_4. So

$$\frac{\left|\frac{L_s}{1+L_s}\right|_{max}}{\left|\frac{L_s}{P_1(1+L_s)}\right|_{max}} \doteq \frac{\left|\frac{L_s}{1+L_s}\right| |P_1|_{max},\ |P_2|_{max}}{\frac{1}{|P_1|_{max}} \left|\frac{L_s}{1+L_s}\right| |P_1|_{max},\ |P_2|_{max}}$$

$$= |P_1|_{max} \qquad \text{(latter part of } R_4\text{)} \tag{2.4-38}$$

Combining (36), (38)

$$\frac{\left|\frac{L_s}{1+L_s}\right|_{max}}{\left|\frac{L_s}{P_1(1+L_s)}\right|_{max}} \doteq |P_1|_{max}, \text{ in } R_4 \tag{2.4-39}$$

Consider the second factor of (2.2-7). In R_4, L_{on} is after point X' in Figure 2-6. Just as in the single loop case,

$$\frac{\left|\frac{L_o}{P_{1e}(1+L_s)}\right|_{max}}{\left|\frac{L_o}{1+L_o}\right|_{max}} \doteq \frac{\frac{1}{|P_{1e}|_{max}} \cdot \left|\frac{L_o}{1+L_o}\right| |P_{1e}|_{max}, |P_2|_{max}}{\left|\frac{L_o}{1+L_o}\right| |P_{1e}|_{max}, |P_2|_{max}}$$

$$= 1/|P_{1e}|_{max}, \quad \text{in } R_4 \tag{2.4-40}$$

Substituting (39), (40) into (2.2-7)

$$\rho = \frac{|P_1|_{max}}{|P_{1e}|_{max}} \cdot \frac{|C_1|_{max}}{|C_s|_{max}} \tag{2.4-41}$$

Consider the factor $|P_1|_{max}/|P_{1e}|_{max}$ at several $\omega \in R_4$. In this range, the P_1 template is certainly a vertical line and L_{in} has negative phase angle $\forall P_1$ (see Figure 2-7), so the template of $P_{1e} = P_1/(1+L_i)$ definitely looks like Figure 2-11(a), and this is so for our large plant class. A numerical example from Chapter 3 (Design A) is shown here to explain the relation between $|P_1|_{max}$ and $|P_{1e}|_{max}$ in R_4. In this example P_1, P_2 each have 20 db hf uncertainty. L_{in} in R_4 is shown in Figure 2-41 with the template P_1 at the frequencies $\omega_A, \ldots \omega_F$. At ω_A (=50), $|\Delta P_{1e}| = 0.2 - (-5.8) = 6$ db (Figure 2-41), is considerably smaller than the range of $|\Delta P_1| = 20$ db. So the difference between $|P_1|_{max}$ and $|P_{1e}|_{max}$ is 14 db - Figure 2-42(a). At ω_B (=80), $|L_{in}|$ is smaller, so $\Delta|P_{1e}|$ is larger = 5.5 - (-11.5) = 17 db and $|P_1|_{max}/|P_{1e}|_{max}$ = 3 db in Figure 2-42(b). At larger ω, L_{in} is close to -180° (Figures 2-7,41). The template of P_{1e} = 10 - (-16) = 26 db at ω_C = 100 and $\Delta|P_{1e}|$ = 15.5 - (-20) = 35.5 db at ω_D = 125.

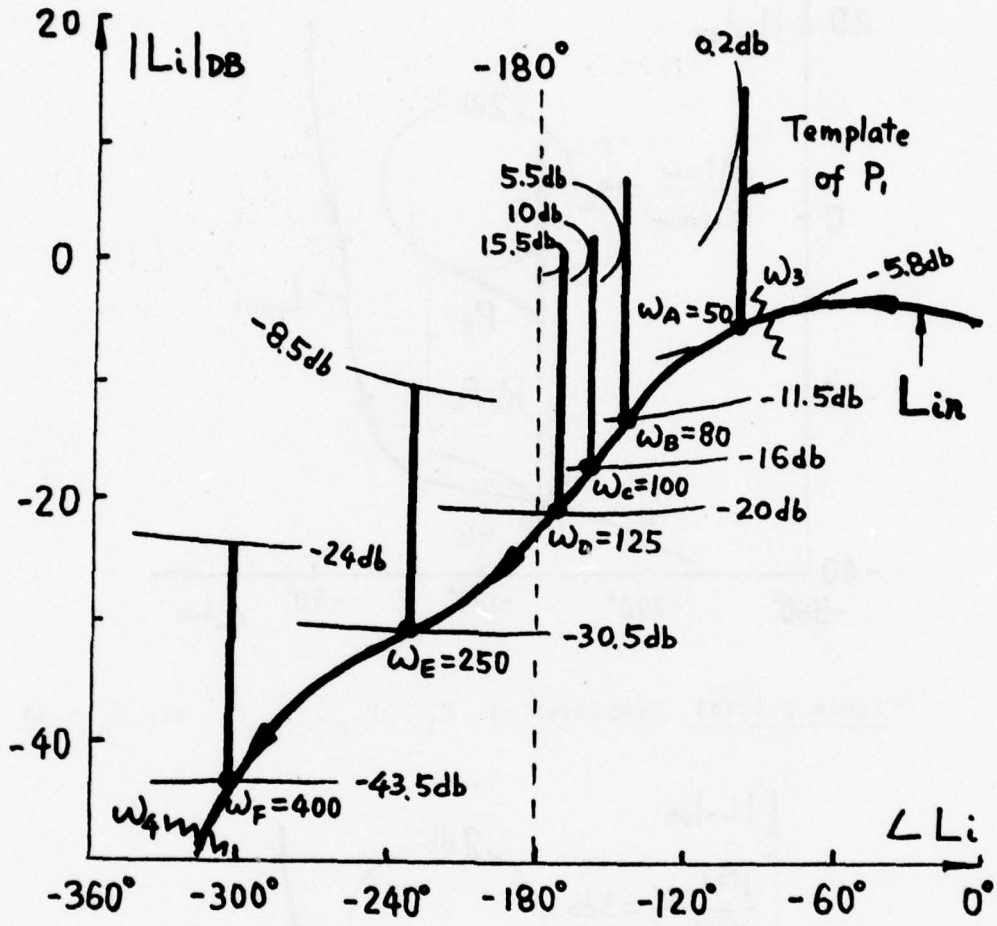

Figure 2-41 L_{in} in R_4 and templates of P_1 at different frequencies

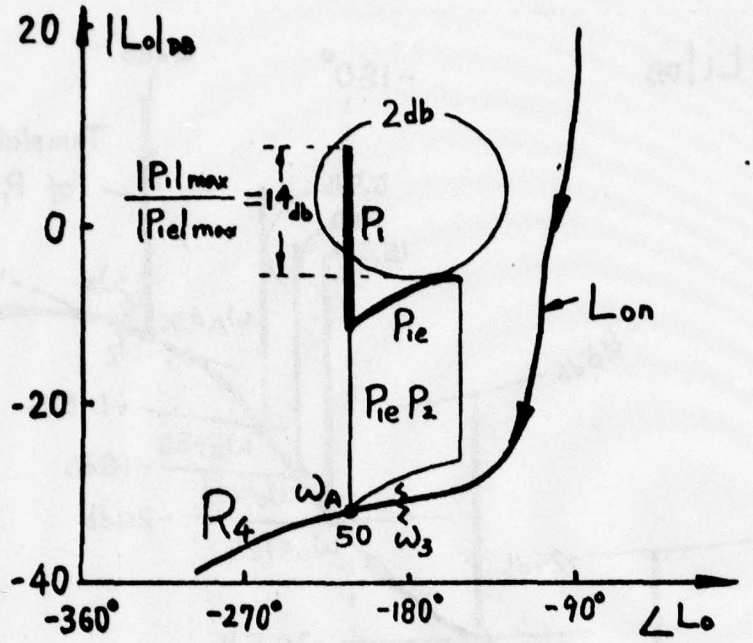

Figure 2-42(a) Templates of P_1, P_{1e}, $P_{1e}P_2$ at $\omega_A = 50$

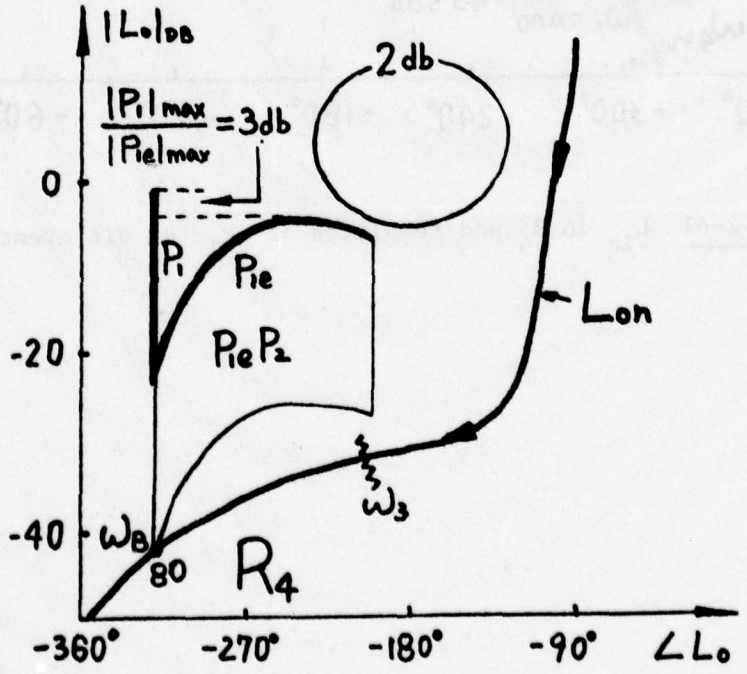

Figure 2-42(b) Templates of P_1, P_{1e}, $P_{1e}P_2$ at $\omega_B = 80$

So in Figure 2-42(c), $|P_1|_{max}/|P_{1e}|_{max} = -6$ db. And in Figure 2-42(d), $|P_1|_{max}/|P_{1e}|_{max} = -15.5$ db. At higher ω, $\angle L_{in} < -180°$ and moves downward in Figure 2-41. So $|L_{in}|$ is very small and $P_{1e} = P_1/(1+L_i) \doteq P_1$. At $\omega_E = 250$, in Figure 2-41, $\Delta|P_{1e}| = -8.5 - (-30.5) = 22$ db, and $|P_1|_{max}/|P_{1e}|_{max} = 20 - 22 = -2$ db in Figure 2-42(e). At $\omega_F = 500$, in Figure 2-41, $\Delta|P_{1e}| = -24 - (-43.5) = 19.5$ db, and $|P_1|_{max}/|P_{1e}|_{max} = 20 - 19.5 = 0.5$ db in Figure 2-42(f). The plot of $P/[|C_1|_{max}/|C_s|_{max}]$, (which is $|P_1|_{max}/|P_{1e}|_{max}$ in R_4 - see (41)), for Design A, is shown in Figure 2-43. Note that the results in R_4 of Figure 2-43 agree with the explanation and Figure 2-42(a),...(f).

In order to have an expression similar to that in the other frequency ranges, (41) is rewritten

$$\rho = \alpha \cdot |1+L_{in}| \cdot \frac{|C_1|_{max}}{|C_s|_{max}} \qquad (2.4\text{-}42)$$

where $\alpha = |P_1|_{max}/[|P_{1e}|_{max} \cdot |1+L_{in}|]$

$$\doteq |P_1|_{max}/|P_{1e}|_{max} \quad \text{in } R_4$$

because $|1+L_{in}|$ is fairly small compared with $|P_1|_{max}/|P_{1e}|_{max}$ in R_4. This can be seen from the corresponding L_{in} in the constant $|1+L|$ curves of Figure 2-44, in which $|1+L_{in}|$ varies from 1 db, 0 db, -1.7 db, -0.5 db, 0 db, 0.05 db to $\sim$ 0 db. So α in R_4 is close to $|P_1|_{max}/|P_{1e}|_{max}$. The nature of α in R_4 for two numerical examples, is shown in Figure 2-45, which is replotted from Figure 2-9. It is seen that in R_4, α varies

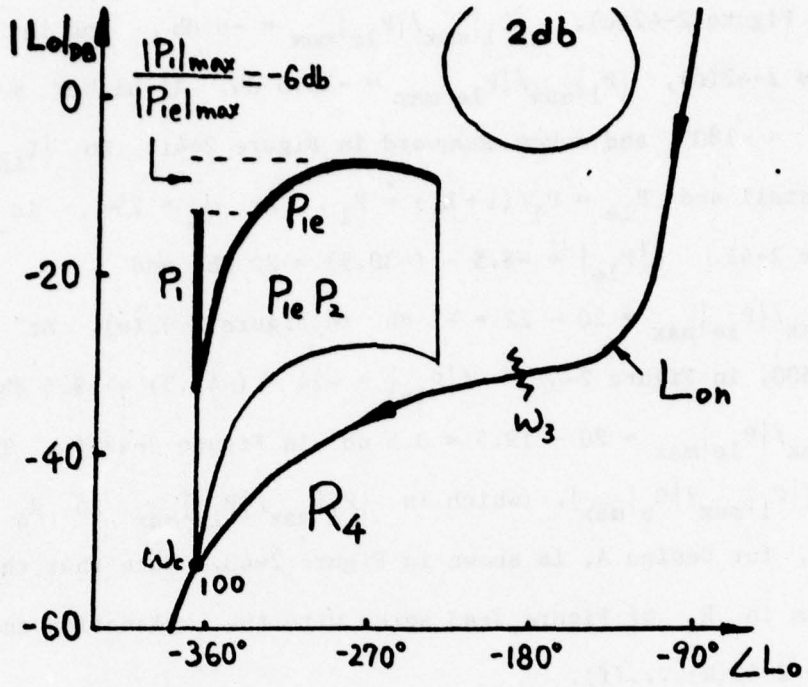

Figure 2-42(c) Templates of P_1, P_{1e}, $P_{1e}P_2$ at $\omega_C = 100$

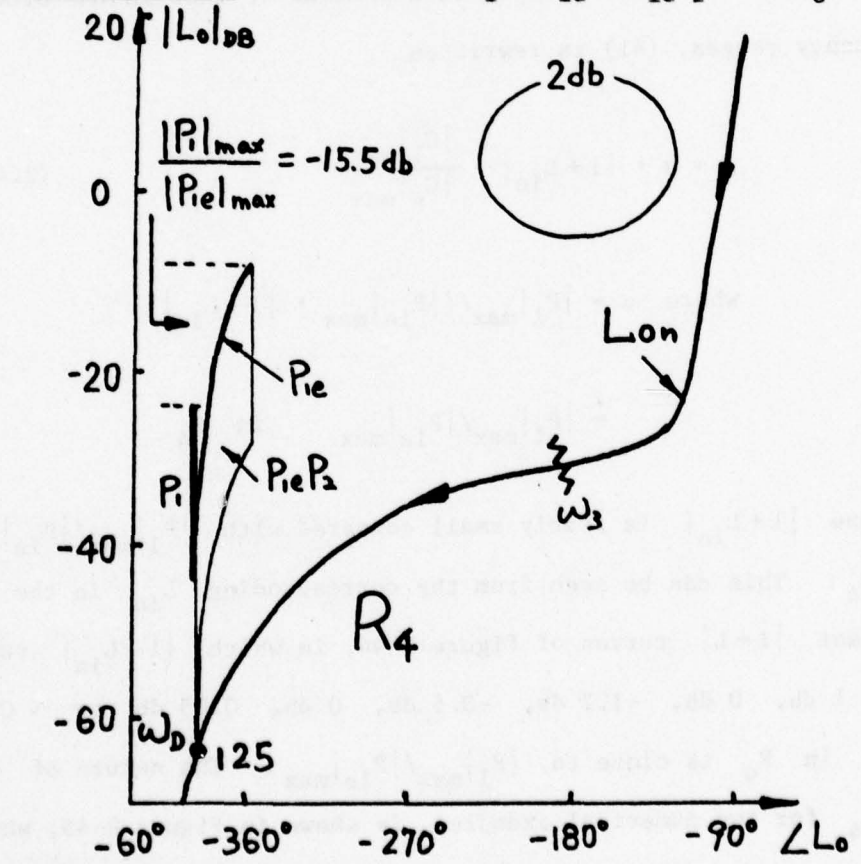

Figure 2-42(d) Templates of P_1, P_{1e}, $P_{1e}P_2$ at $\omega_D = 125$

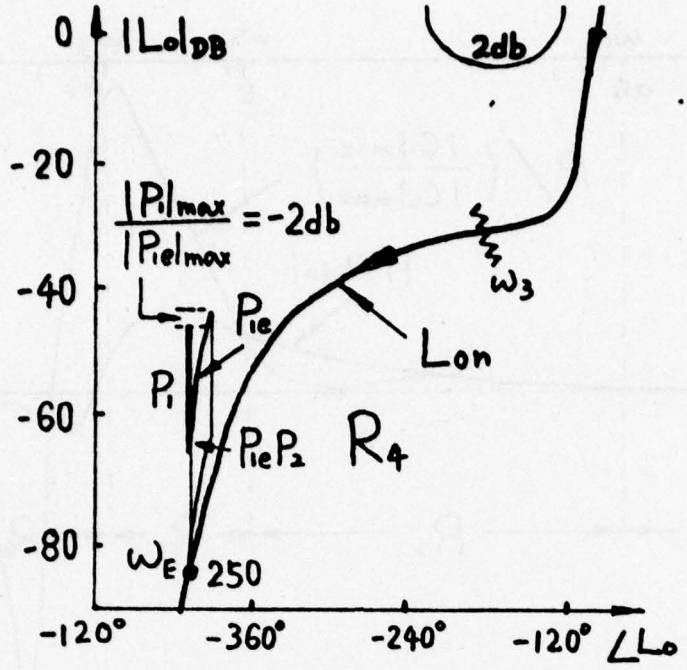

Figure 2-42(e) Templates of P_1, P_{1e}, $P_{1e}P_2$ at $\omega_E = 250$

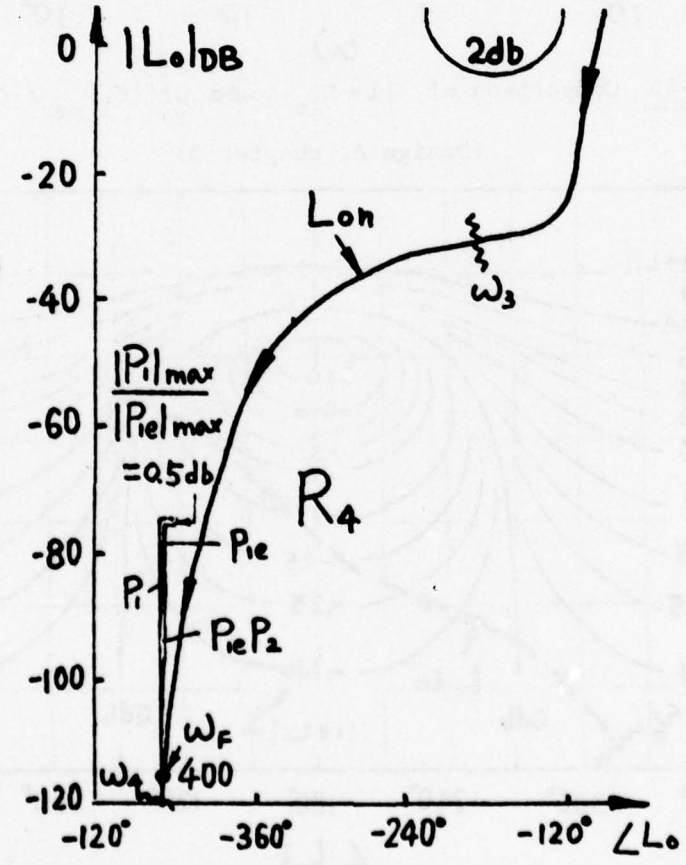

Figure 2-42(f) Templates of P_1, P_{1e}, $P_{1e}P_2$ at $\omega_F = 400$

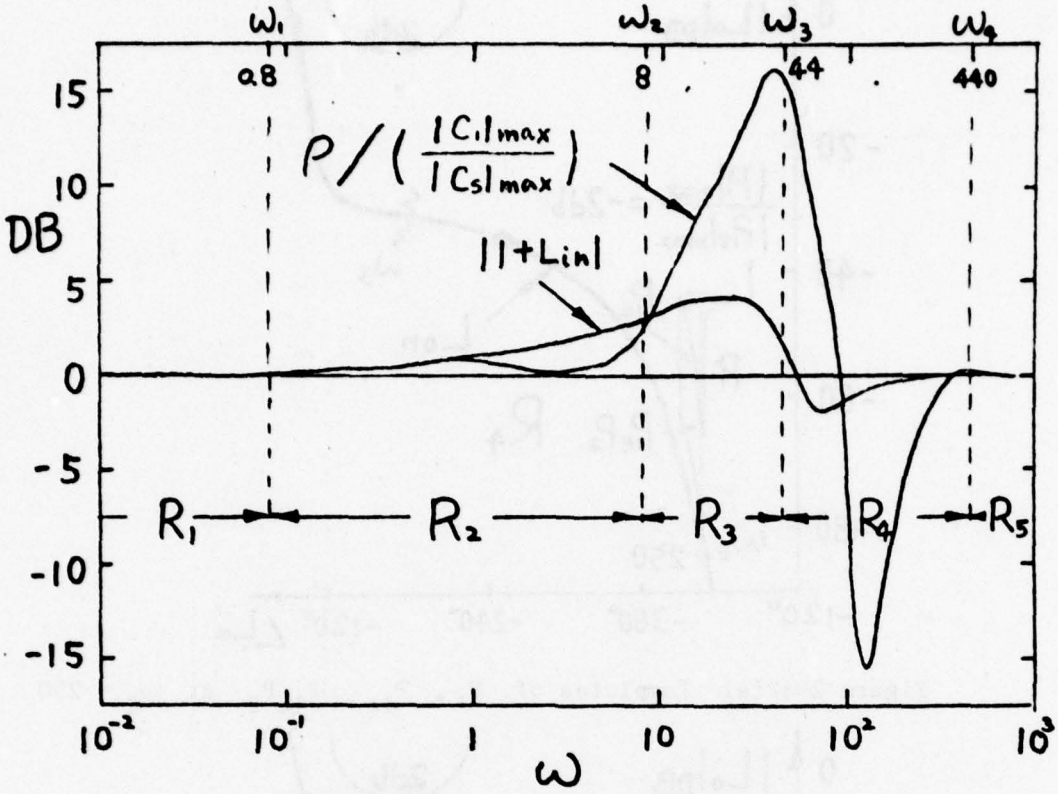

Figure 2-43 Comparison of $|1+L_{in}|$ and $\rho/[|C_1|_{max}/|C_s|_{max}]$

(Design A, chapter 3)

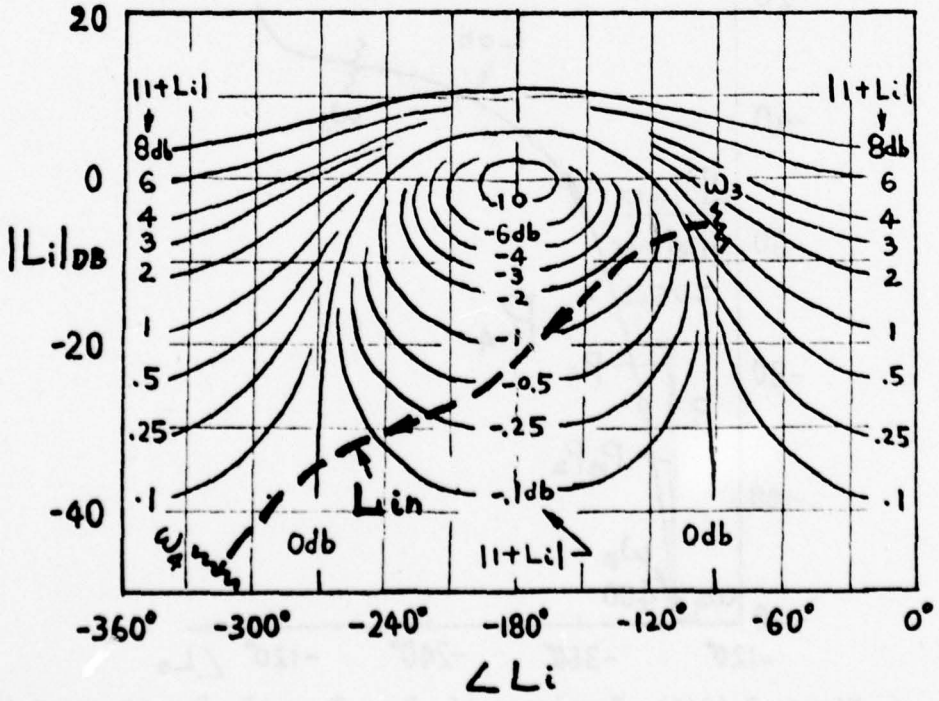

Figure 2-44 Typical L_{in} on constant $|1+L_i|$ curves in R_4

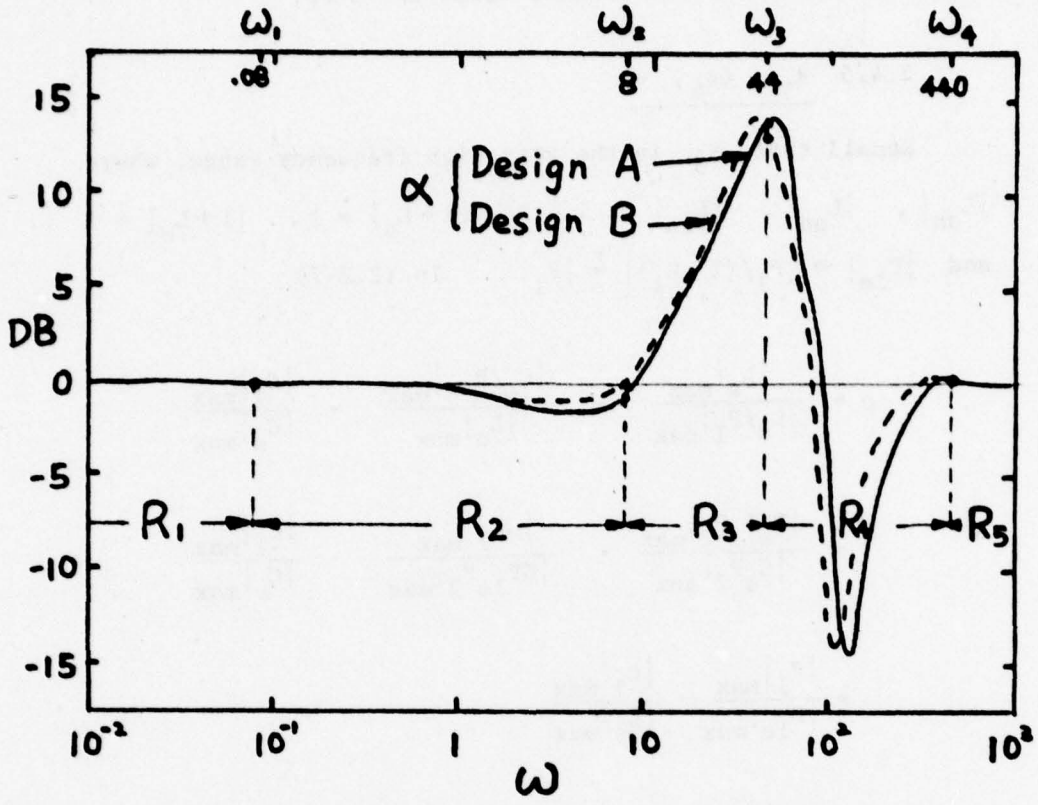

Figure 2-45 Nature of α - from examples in chapter 3

from a large positive db value to 0 db, and then to a large negative db value and finally tends to 0 db.

2.4.5 $R_5 = (\omega_4, \infty)$

Recall that R_5 is the very high frequency range, where $|L_{sn}|$, $|L_{on}|$, $|L_{in}| << 1$. So $|1+L_s| \doteq 1$, $|1+L_o| \doteq 1$ and $|P_{1e}| = |P_1/(1+L_i)| \doteq |P_1|$. In (2.2-7)

$$\rho \doteq \frac{|L_s|_{max}}{|L_s/P_1|_{max}} \cdot \frac{|L_o/P_{1e}|_{max}}{|L_o|_{max}} \cdot \frac{|C_1|_{max}}{|C_s|_{max}}$$

$$= \frac{|G_s P_1 P_2|_{max}}{|G_s P_2|_{max}} \cdot \frac{|GP_2|_{max}}{|GP_{1e} P_2|_{max}} \cdot \frac{|C_1|_{max}}{|C_s|_{max}}$$

$$= \frac{|P_1|_{max}}{|P_{1e}|_{max}} \cdot \frac{|C_1|_{max}}{|C_s|_{max}}$$

$$\doteq \frac{|C_1|_{max}}{|C_s|_{max}} \qquad (2.4\text{-}43)$$

Again (43) can be rewritten to have the same form as in the other frequency ranges

$$\rho = \alpha \cdot |1+L_{in}| \cdot \frac{|C_1|_{max}}{|C_s|_{max}} \qquad (2.4\text{-}44)$$

where $\alpha \doteq 1$ in R_5

The curves of $\rho/[|C_1|_{max}/|C_s|_{max}]$ and α are shown in Figures 2-43,9 for numerical examples. Note, both are $\doteq 1$ in R_5 in agreement with (43), (44).

2.4.6. Summary

Concluding the above discussions, $\alpha \leq 1$ in R_1 and R_2, where the control signal is important. So the design philosophy is conservative. $\alpha > 1$ in R_3 and in the beginning of R_4, $\alpha < 1$ in the latter part of R_4 and $\alpha \doteq 1$ in R_5. The latter are the high frequency ranges, where the signal level is not important and we concentrate on the reduction of the sensor noise effect.

CHAPTER 3

2-PLANT, 2-LOOP, P.M. SYSTEM SYNTHESIS

3.1 Introduction

This chapter is devoted to the simplest (two-loop) plant-modification (P.M.) structure--Fig. 3-1. The plant has two cascaded sections P_1, P_2 and two loops are used. (A more complex structure with a third loop from C_{22} to X_{22} is considered in chapter 4). The loop from C_1 to X_{22} is called the outer loop $L_o = G\,P_2P_1/(1+P_1H_1) \triangleq G\,P_2P_{1e}$ and the other is the plant modification inner loop $L_i = P_1H_1$. At best, the inner loop L_i can be designed to take care of all parameter uncertainties in P_1, as in the cascaded no P.M. design philosophy (section 1.4.3). But, as discussed in chapter 2, it is necessary to compromise, because of the resulting increase in signal level of C_{22}. $|L_i|$ is therefore made small in the low frequency control bandwidth regions R_1, R_2. So the inner loop L_i

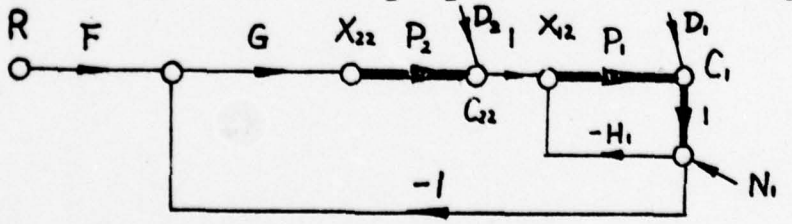

$$T \triangleq \frac{C_1}{R} = \frac{FL_o}{1+L_o}\,,\quad L_o \triangleq GP_2P_{1e}\,,\quad P_{1e} \triangleq \frac{P_1}{1+L_i}\,,\quad L_i \triangleq P_1H_1$$

Figure 3-1. 2-plant, 2-loop, P.M. system

cannot handle all the uncertainties of P_1 in R_1, R_2, and the outer loop L_o must in this sense be "overdesigned" to make up the difference. The important point is that in problems with significant uncertainty, the sensor noise effect is strongest in the high frequency range, which is well beyond the control frequency bandwidth. Based on this, the design philosophy is to concentrate on the signal level increase in the ℓ.f. ranges (R_1, R_2) and let L_i do its best in the h.f. range. The means of doing the former was prepared in chapter 2, with $(1 + L_{in})$ the principal design tool.

In this chapter, a systematic design procedure based on the above is presented with detailed numerical examples. Several values of signal level increase ratio are chosen, in order to get a feeling for the trade-off between the bounds on $|1+L_{in}|$, increase in C_{22} signal level and sensor noise effects. For comparison purposes, single loop and cascaded 2-loop, no P.M., designs are also given, which satisfy the same specifications. Also, a hypothetical P.M. design which ignores the signal-level-variation problem (ISLV) is given, in order to see the maximum savings in sensor noise effect, in case the permitted S.L. increase is unlimited. Finally, a detailed comparison is made between the P.M. 2-loop system and the no P.M. cascaded 2-loop system, with respect to sensor noise effects.

It is assumed throughout that each plant section is minimum-phase, although it need not be open-loop stable [2, 5].

3.2 Principle Steps in Design Procedure

(1) Translation of time-domain bounds on c(t) into bounds on $|T(j\omega)| \triangleq |C(j\omega)/R(j\omega)|$, if the specifications are not originallyin the frequency domain.

(2) Choice of bounds on $|1 + L_{in}(j\omega)|$ from a given value of permitted C_{22} power increase

$$Q = \int_o^\infty \{C_{22}(\omega)\}^2 d\omega / \int_o^\infty \{C_{2s}(\omega)\}^2 d\omega.$$

(3) Determination of the resulting bounds $B_{Li}^{\rho}(\omega)$ on the inner loop $L_{in} = P_{1n}H_1$ in the low frequency range, R_1, R_2.

(4) Design of inner loop L_{in}^{ρ} in R_1, R_2 which satisfies $B_{Li}^{\rho}(\omega)$.

(5) Determination of the template of $P_{1e} = P_1/(1 + L_i^{\rho})$ from L_i^{ρ}, in R_1, R_2.

(6) Finding the bounds $B_{Lo}(\omega)$ on the outer loop, in order to satisfy the design specification on $T(j\omega)$. In R_1, R_2, these bounds are chosen so that L_i^{ρ} is satisfactory and need not be altered. In R_3, R_4, R_5, the bounds are chosen as in the cascaded design philosophy.

(7) Design of the outer loop L_o from the bounds $B_{Lo}(\omega)$, and then finding the corresponding bounds $B_{Li}(\omega)$ on the inner loop, in R_3, R_4, R_5, such that L_o chosen is satisfactory.

(8) Completion of the design of the inner loop L_i which satisfies both $B^{o}_{Li}(\omega)$ and $B_{Li}(\omega)$.

3.3 Design Procedure

The design procedure is explained and illustrated by means of a design example.

3.3.1 Specifications on Numerical Example

Plant: $P = P_1P_2$, $P_i = k_i/s_i$

Plant uncertainty: $\sqrt{2} \leq k_1 \leq 10\sqrt{2}$, $\sqrt{2} \leq k_2 \leq 10\sqrt{2}$ independently

Bounds on $|T(j\omega)|$: shown in Figure 3-2(b) were originally derived from time domain bounds of Figure 3-2(a).

Disturbance response: $\gamma \leq 2.0$ db

(All above are the same as in Section 1.2.5)

Restriction on signal level: $Q \leq 1.05$ for unit step input.

3.3.2 Translation of time-domain specifications (Figure 3-2(a)) into frequency domain bounds (Figure 3-2(b))

This effort is as yet an art rather than a science. In a minimum-phase system the magnitude of the frequency response $|T(j\omega)|$ completely specifies the transfer function $T(s)$, which in turn uniquely determines the system step response $c_s(t)$. Hence,

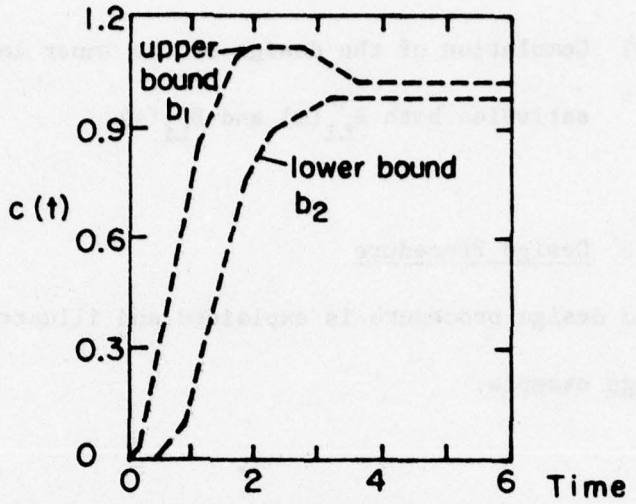

Figure 3-2(a). Time domain step response specification.

bounds on $\ell n|T(j\omega)|$ suffice. But the rigorous translation of time-domain bounds into bounds on $|T(j\omega)|$ is, as yet, an unsolved problem. In practice, however, it has not been difficult to achieve a translation suitable for any specific numerical problem encountered. One may begin, for example, by assuming a simple second- or third-order system model for T(s), and finding the bounds on the model parameters which correspond to the bounds on the time response. From the model parameter bounds, one then determines the resulting bounds on $\ell n|T(j\omega)|$. Suppose this steps leads to the solid-line bounds B_u, B_ℓ of Figure 3-3.

It is desirable, of course, to increase the spread between B_u and B_ℓ, but it will be seen that there is no advantage in doing so at isolated points. There is benefit only if the spread increases, on the whole, with increasing ω. One soon finds, with a little experimentation, that indicated modifications B_1, B_2 in

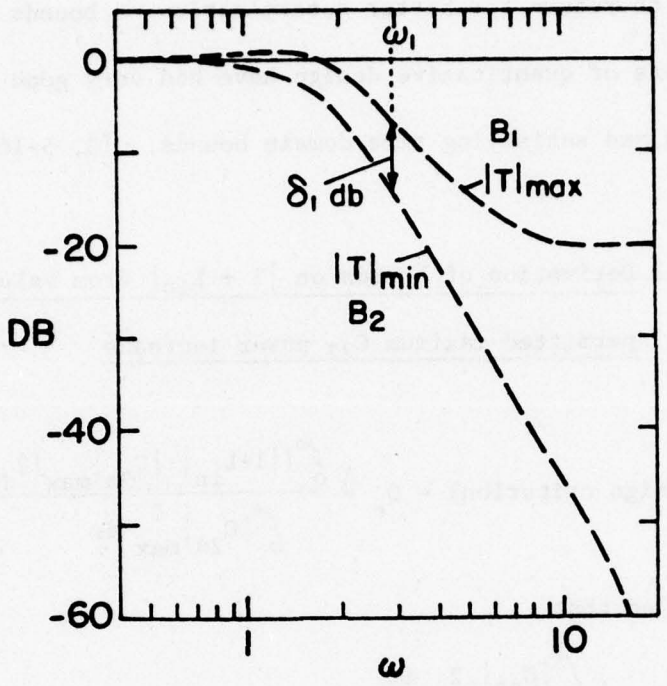

Figure 3-2(b). "Equivalent" frequency domain specification

Figure 3-3 are generally achievable. It is very helpful for such experimentation to have a computer programme for finding time response from the magnitude of the frequency response. Additional experimentation reveals that there is a definite limit to the permissible spread in the lower frequency range for a reasonably smooth curve of $|T(j\omega)|$. Subsequent design details provide one with an appreciation of the frequency ranges in which broadening of the bounds may or may not be important. Such ranges depend a great deal on the nature of the plant and its uncertainty. Hence, it is best to obtain comparatively quickly estimates of B_1, B_2 and proceed with the design. The designer will subsequently understand whether it is

worthwhile to return for better determination of bounds on $|T(j\omega)|$. Practitioners of quantitative design have had very good results in translating and satisfying time domain bounds. [2, 5-16].

3.3.3 Derivation of bounds on $|1 + L_{in}|$ from values of permitted maximum C_{22} power increase

Let

$$Q(\text{design criterion}) = Q_c \triangleq \frac{\int_0^\infty [|1+L_{in}| \cdot |C_{2s}|_{max}]^2 d\omega}{\int_0^\infty |C_{2s}|_{max}^2 \, d\omega}$$

It is recalled that

$$Q \triangleq \frac{\int_0^\infty |C_{22}|_{max}^2 \, d\omega}{\int_0^\infty |C_{2s}|_{max}^2 \, d\omega}$$

is the power increase, which is apriori given as part of the system specifications. For the time being, assume that from this given Q, we are able to determine $Q_c = 1.22$ in this example. The procedure for finding Q_c from Q is given in section 3.5. The next step is to determine the $|1 + L_{in}(j\omega)|$ specification from Q_c. The procedure for doing so and for finding Q_c from Q, will be much better appreciated after a few design examples, so it is postponed. In the meantime, we accept the curve shown in Figure 3-4 for $[|1 + L_{in}| \cdot |C_{2s}|_{max}]^2$ vs ω, from which there is obtained the bound on $|1 + L_{in}(j\omega)|$ in Figure 3-5.

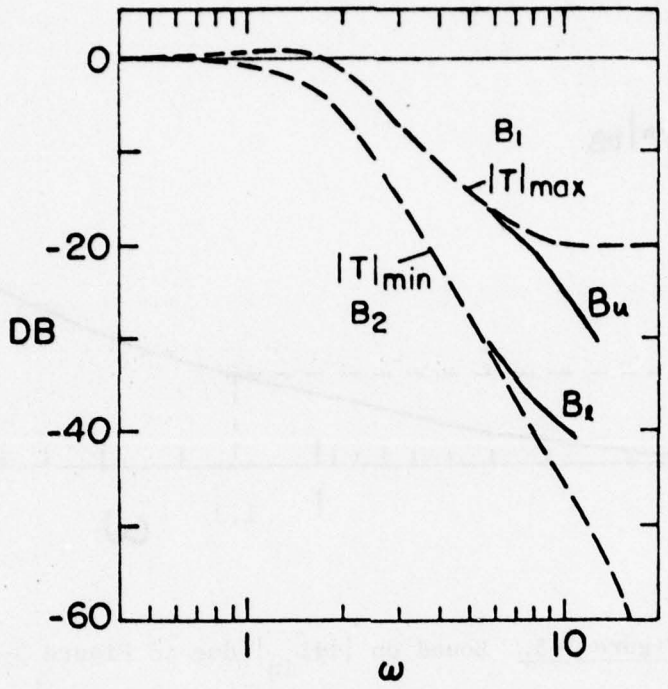

Figure 3-3. Derivation of bounds on $|T(j\omega)|$

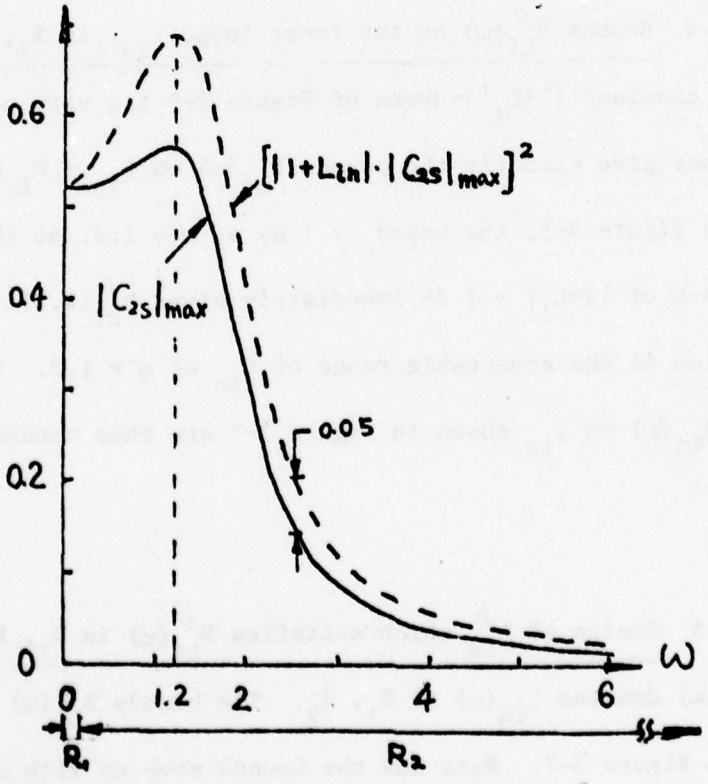

Figure 3-4. The choice of $(|1+L_{in}|\cdot|C_{2s}|)^2$ - Design C

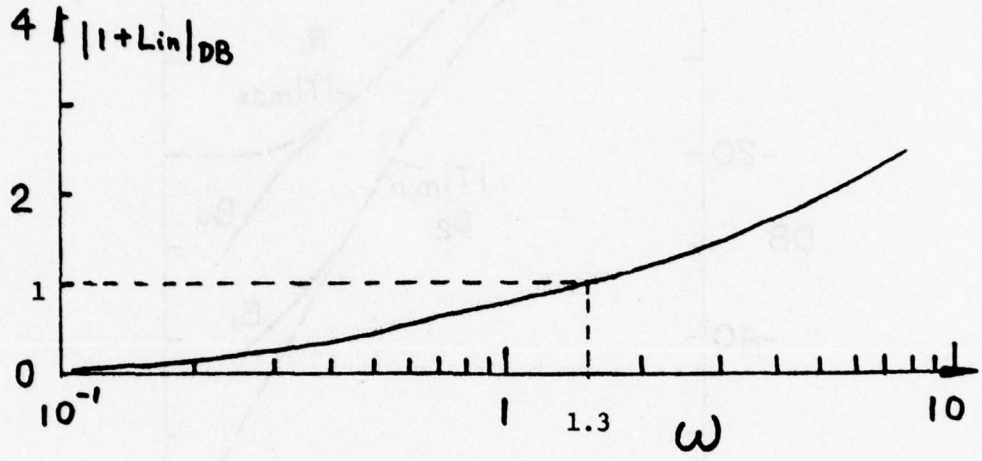

Figure 3-5. Bound on $|1+L_{in}|$ due to Figure 3-4

3.3.4 Bounds $B^{\rho}_{Li}(\omega)$ on the inner loop, L_{in}, in R_1, R_2

The constant $|1+L_i|$ curves of Figure 2-5 are very useful here, as they give directly the bounds $B_{Li}(\omega)$ on $L_{in} = P_{1n}H_1$. For example, in Figure 3-5, the bound is 1 db at $\omega = 1.3$, so the locus in Figure 3-6 of $|1+L_i| = 1$ db immediately gives $B^{\rho}_{Li}(1.3)$. The shaded region is the acceptable range of L_{in} at $\omega = 1.3$. The set of bounds $B_{Li}(\omega)$ on L_{in} shown in Figure 3-7 are thus obtained in R_1, R_2.

3.3.5 Design of L^{ρ}_{in} which satisfies $B^{\rho}_{Li}(\omega)$ in R_1, R_2

$L^{\rho}_{in}(\omega)$ denotes $L_{in}(\omega)$ in R_1, R_2. The bounds $B^{\rho}_{Li}(\omega)$ are shown in in Figure 3-7. Note how the bounds move up with ω in the Nichols' chart. The resulting increase in $|L^{\rho}_{in}|$ is accompanied by

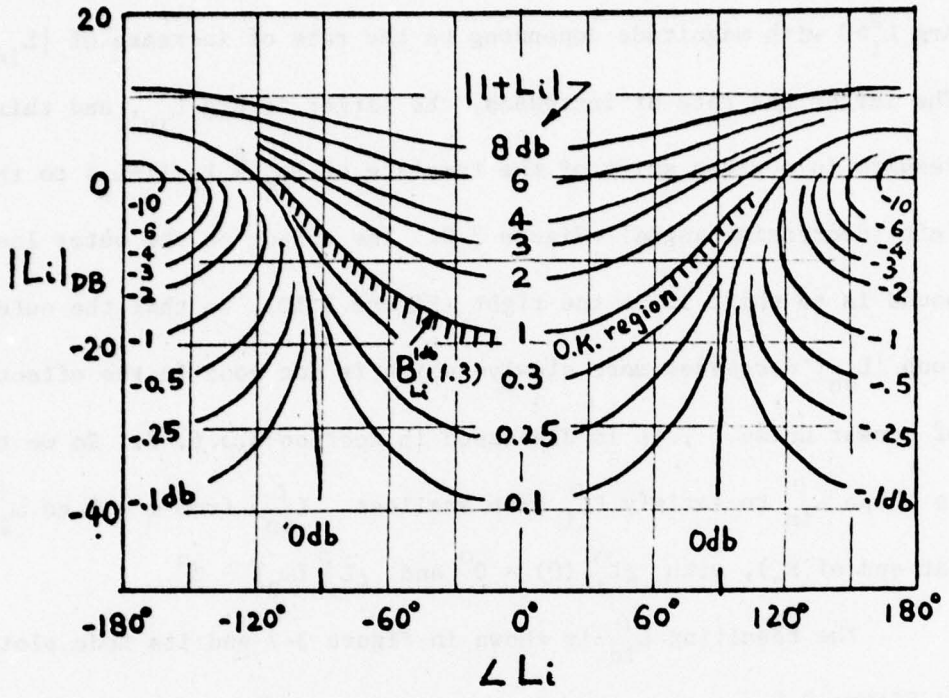

Figure 3-6. The bound of $B_{Li}^{\rho}(\omega)$

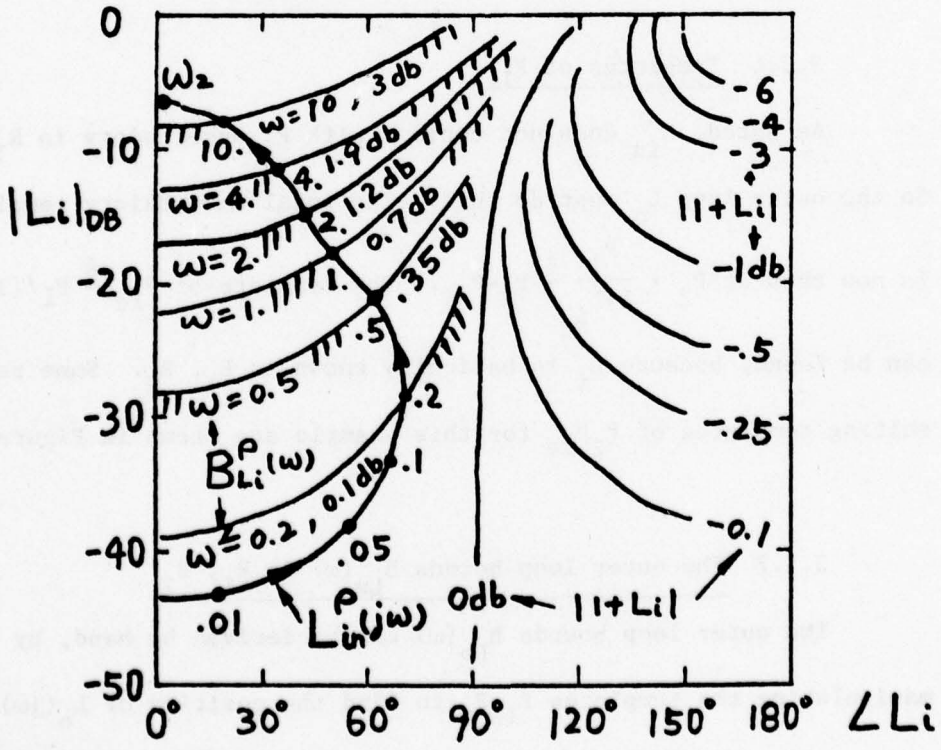

Figure 3-7. Bounds $B_{Li}^{\rho}(\omega)$ and resulting L_{in} in R_1, R_2 (Design C)

Arg $L_i^{\rho}>0$ with magnitude dependong on the rate of increase of $|L_{in}|$. The larger the rate of increases, the larger is Arg L_{in}^{ρ}, and this results in a wider shift of the template of $P_{1e} \triangleq P_1/(1+L_i)$ to the left (decreasing angle)--Figure 3-9. The effect on the outer loop bound is to shift it to the right (Figure 3-10), so that the outer loop $|L_{on}|$ decreases more slowly--which is not good in the effect of sensor noise. This is discussed in section 3.3.6, 7. So we try to shape L_{in}^{ρ} to satisfy B_{Li}^{ρ} with smallest $\angle L_{in}^{\rho}$, from $\omega = 0$ to ω_2 (at end of R_2), with $\angle L_{in}^{\rho}(0) = 0^o$ and $\angle L_{in}^{\rho}(\omega_2) \sim 0^o$.

The resulting L_{in}^{ρ} is shown in Figure 3-7 and its Bode plot in Figure 3-8.

3.3.6 Templates of P_{1e}

As noted, L_{in}^{ρ} does not contend with P_1 uncertainty in R_1, R_2. So the outer loop L_o must do this. The total uncertainty template is now that of $P_2 \cdot \frac{P_1}{1+L_i} \triangleq P_2 \cdot P_{1e}$. The template of $P_{1e} \triangleq P_1/(1+L_i)$, can be found, because L_i is basically known in R_1, R_2. Some resulting templates of $P_2 P_{1e}$ for this example are shown in Figure 3-9.

3.3.7 The outer loop bounds $B_{Lo}(\omega)$ in R_1, R_2

The outer loop bounds $B_{Lo}(\omega)$ can be derived by hand, by manipulating the templates $P_{1e}P_2$ to find the position of $L_o(j\omega)$ which results in the specifications of Figure 3-2(b) on $\ell n|T(j\omega)|$

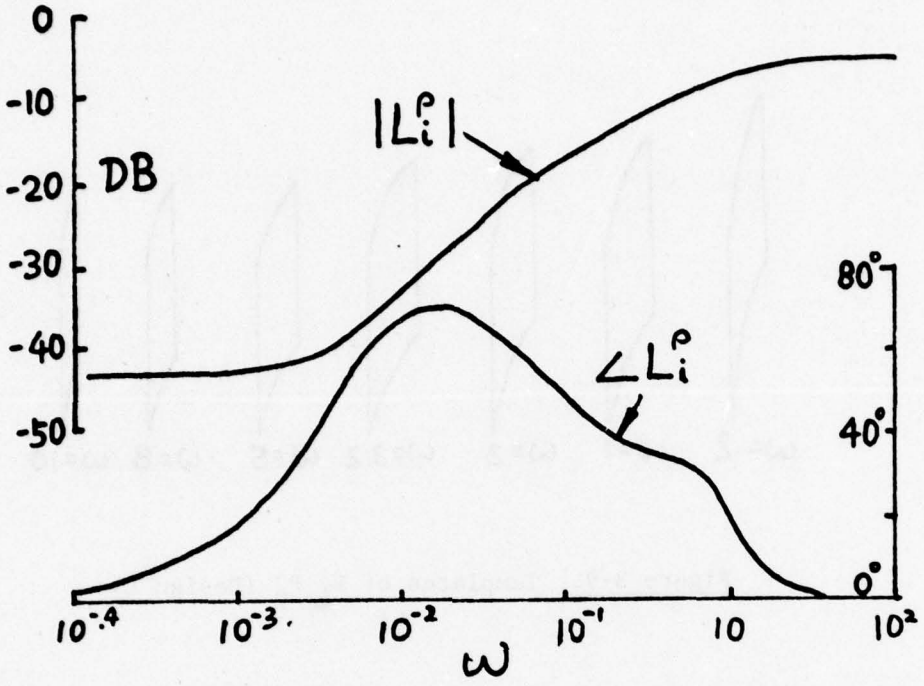

Figure 3-8. Bode plot of L_i^ρ in R_1, R_2 (Design C)

being satisfied. The details are the same as in the single loop system discussed in section 1.2.1, because it is an identical problem. This is pretty fast but it can, of course, be done entirely on the computer. The results in R_1, R_2, are shown in Figure 3-10. Note, in Figure 3-10, the left hand side of $B_{Lo}(\omega)$ do not reach the disturbance forbidden cylinder B_{h2} in R_1, R_2. This is because $\angle L_{in}^\rho > 0$ in R_1, R_2 in Figures 3-7, 8, so the templates of $P_{1e}P_2$ in Figure 3-9, all go upward and to the left from P_{1en} (the nominal point of P_{1e} as defined in section 2.2.1). Obviously, this kind of $B_{Lo}(\omega)$ forces L_{on} to be further to the right, i.e., with larger phase angle thereby decreasing the rate of decrease of $|L_{on}(j\omega)|$

Figure 3-9. Templates of $P_{le}P_2$ (Design C)

and increasing the sensor noise response in hf region. This is the price we must pay for restricting SLVR in R_1, R_2.

3.3.8. Design of L_{on} and determination of $B_{Li}(\omega)$

The outer loop L_{on} is designed to satisfy the $B_{Lo}(\omega)$ obtained in section 3.3.7 in R_1, R_2, and to be pretty much like in an ordinary no P.M. cascaded design, for R_3, R_4, R_5, i.e., with a safety margin--chosen as 5 db in this example--see Figure 3-10. It is important here to note that in R_3, R_4, R_5, L_{on} is designed (except for 5 db margin) as if there is no uncertainty in P_{le}--as in the no P.M. cascaded philosophy.

The resulting L_o design is final. The next step is to obtain the inner loop bounds $B_{Li}(\omega)$ in R_3, R_4, R_5, such that the L_{on}

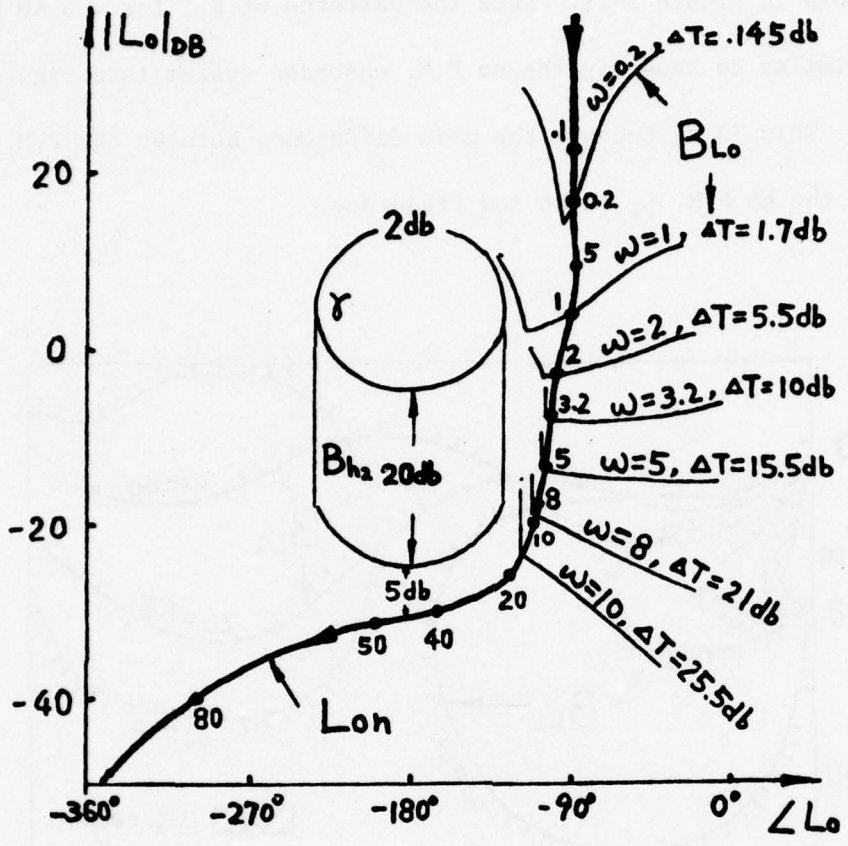

Figure 3-10. $B_{Lo}(\omega)$ and L_{on} in Nichols' Chart (Design C)

design is satisfactory, despite its neglect of P_{1e} uncertainty in R_3, R_4, R_5. (This part is the same as in no P.M. cascaded design.) Also, to be absolutely sure that the final design satisfies the frequency specification of Figure 3-2(b), this is also done in R_1, R_2. This precaution is worthwhile because L_{in} as originally designed for R_1, R_2, must be modified, albeit very little. The procedure is now exactly the same as in the cascaded multiple loop (no P.M.) system. It can be done either graphically as in [2] or by a computer search program. Some B_{Li} corresponding to L_o of Figure 3-10,

are shown in Figure 3-11. Note the patterns of B_{Li} for $\omega \geq 40$ is very similar to those in the no P.M. cascaded system (see Figure 1-19). This is so because the main difference between the P.M. L_i and the no P.M. L_i is at low frequency.

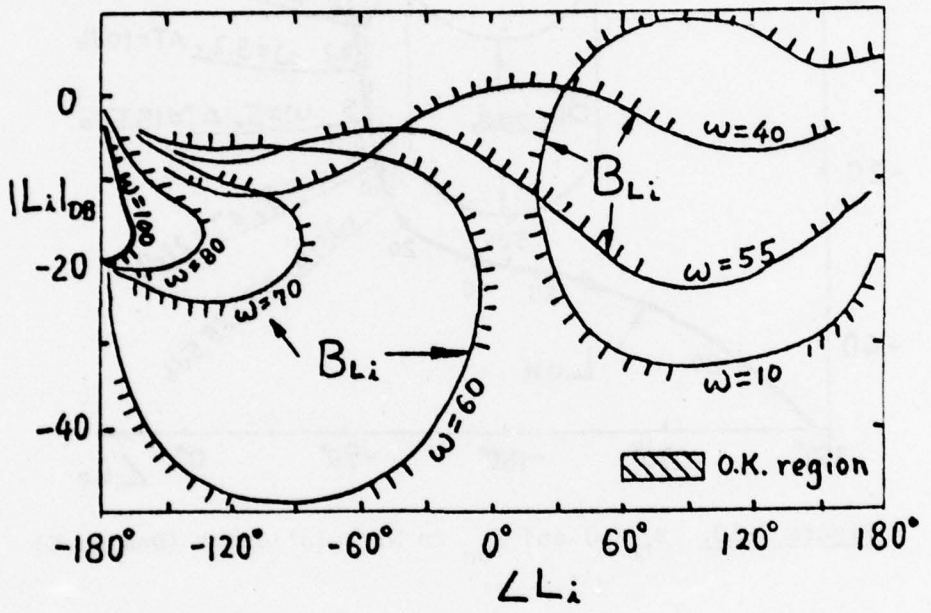

Figure 3-11. The bounds of B_{Li} (Design C)

3.3.9 Completion of L_{in}

Recall (section 3.3.5, Figures 3-7, 8) that L_{in}^{ρ} (from $\omega = 0$ to $\omega_2 = 10$), was obtained as the first step in design of L_{in}, i.e. in R_1, R_2. The final step is to complete L_{in} so as to satisfy the bounds B_{Li}, some of which are redrawn in Figure 3-12. Note that we have deliberately designed $|L_{in}(j\,\omega_2)|$ to be near the maximum value

needed by L_{in}--approximately 6 db at $W \approx 55$. So from $\omega = \omega_2 = 10$ to $\omega \approx 55$, L_{in} must be approximately horizontal. Since L_{in}^{ρ} was designed (see Figure 3-8) to be approximately horizontal for $\omega > \omega_2$, it is relatively easy to achieve a good fitting of L_{in}^{ρ} with an L_{in} which satisfies the bounds for all ω, i.e., the low-frequency poles and zeros used in L_{in}^{ρ} are retained in L_{in}, which, of course, has more poles and zeros in the higher range in order to achieve the shaping needed to satisfy the $B_{Li}(\omega)$.

The resulting L_{in} is shown in Figure 3-12. Comparison with other designs is done later--Figures 3-28,31. These other designs are next presented.

3.4 More Numerical Examples

3.4.1 Introduction

Sections 3.3.2-9 presented the details of a design for the problem presented in section 3.3.1. We now present with much less detail, more designs for the same problem, differing chiefly in the signal level ratio Q and also in system structure. This is done in order to give the reader a good perspective on the effect of Q and how the design results compare with those of single-loop and no P.M. cascade structures.

3.4.2 Single loop system (Figure 1-3(a))

Recall section 1.2.5, where the single loop transmission

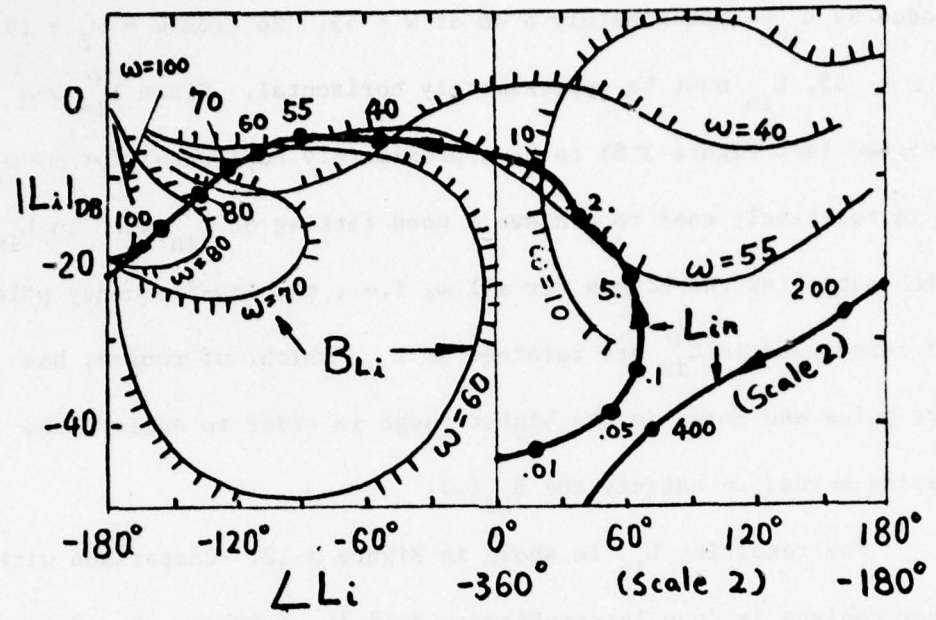

Figure 3-12. The inner loop L_{in} with B_{Li}

$L_{sn} = G_s P_{1n} P_2$ for this numerical problem was shown in Figure 1-9. Henceforth, L_{sn} is used for comparison with the P.M. 2-loop system, with respect to signal level, sensor noise effect, etc.

3.4.3 Cascaded, 2-loop, no P.M. system (Figure 1-15(a))

In section 1.4.3, the outer loop L_1 and inner loop $L_2 = P_2 H_2$ of the cascaded, 2-loop, no P.M. systems (Figures 1-18, 19) were presented for this numerical problem. These are used to compare the sensor noise effects at points X_1, X_2, with the 2-loop P.M. design (see Figures 1-15(a), 3-1) later in section 3.9.

3.4.4 ISLF (Ignoring-signal-level-variation), 2-loop, P.M. system (Figure 3-1)

In this system, we ignore the problem of signal level increase. The inner loop $L_i = P_1H_1$ is designed in precisely the same manner as L_2 (= P_2H_2 there) in the cascaded, no P.M. design of section 3.4.3, i.e., to relieve the burden on L_o as much as possible. The ISLV, 2-loop, P.M. system is compared with the other 2-loop, P.M. systems to see the sacrifice in sensor noise effect due to the problem of signal level variation in the P.M. design.

3.4.5 More 2-loop, P.M. designs (Figure 3-1)

Four more 2-loop, P.M. designs with different SLVR requirements, are presented here. These designs, denoted by B, D, A, E, were achieved trying different L_{in}^{ρ} in R_1, R_2, which resulted in different Q value. Based on these results, we derive a relation between Q and SLVR in section 3.5. This relationship enables us to choose SLVR from a specified Q value. Also, the sensor noise effects obtained from these designs gives us the trade-off between Q and sensor noise effect in a 2-loop, P.M. system--section 3.8.

The assumed L_{in}^{ρ} of designs B, D, A, E, are shown in Figures 3-13(a-d) and the corresponding $|1 + L_{in}|$ values in Figure 3-14. (Curve C represents a design done by deliberate synthesis, unlike A, B, D, E.) The templates $P_{1e}P_2$ are shown in Figures 3-15 (a,. . . d), and the B_{Lo} and L_{on} in Figures 3-16 (a, . . . d). Finally,

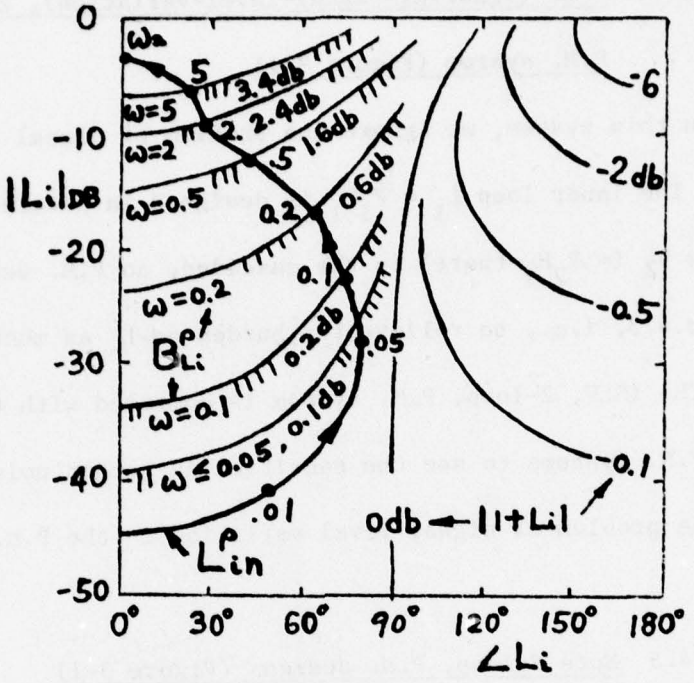

(a) Design B

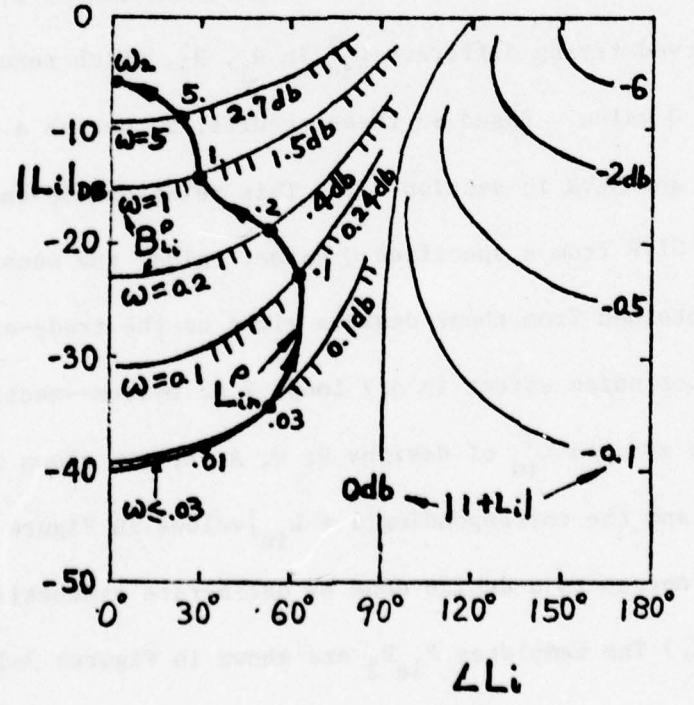

(b) Design D

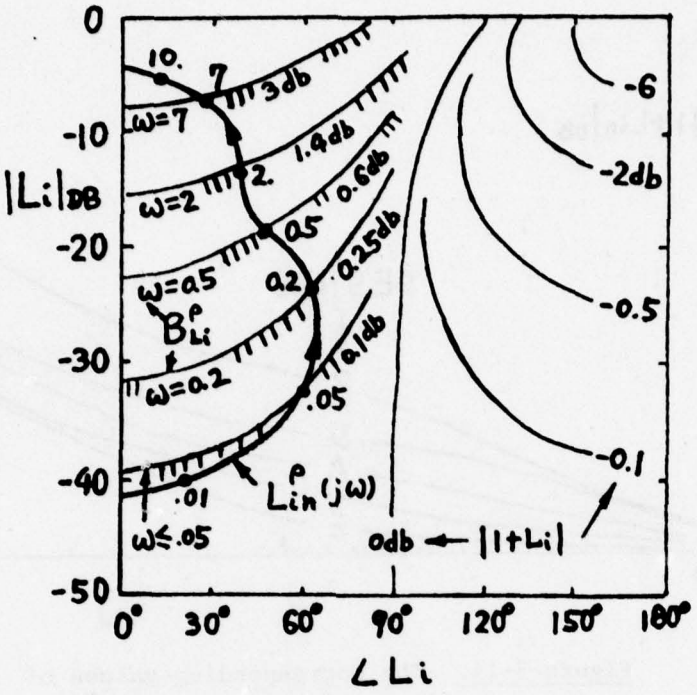

(c) Design A

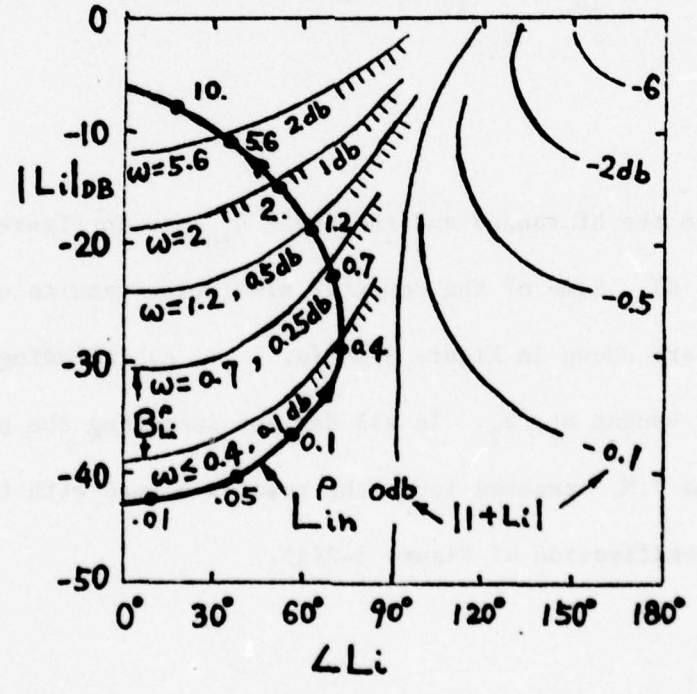

(d) Design E

Figure 3-13. Bounds $B_{Li}^{\rho}(\omega)$ and L_{in}^{ρ} with constant $|1+L_{in}|$ curves.

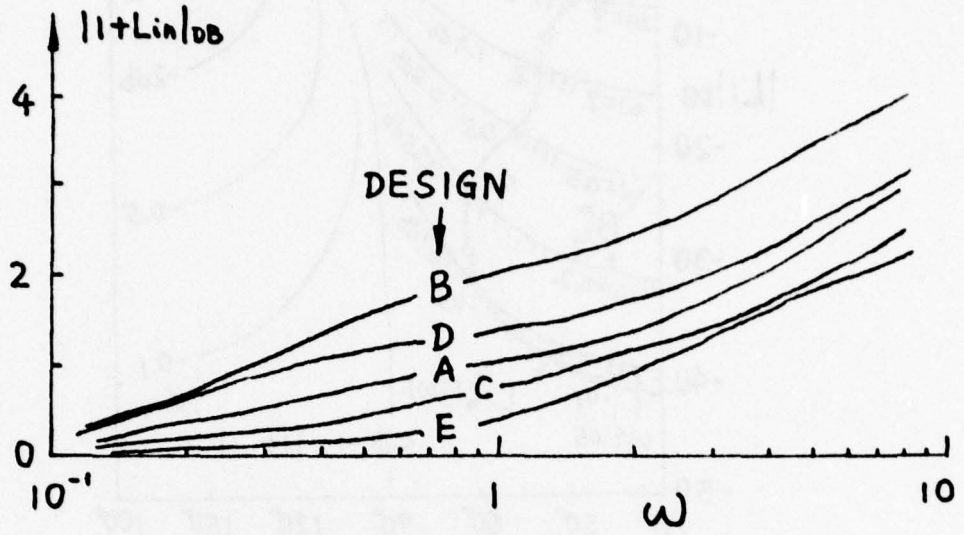

Figure 3-14. The corresponding values of $|1+L_{in}|$ for L_{in}^{ρ} in Figures 3-13 (a), . . . (d)

the B_{Li} in the hf ranges and the final L_{in} are in Figures 3-17 (a, . . . d). Some of the computer simulation results of unit step response are shown in Figure 3-18 (a, . . . c) including the upper and lower bounds b_1, b_2. In all designs including the single loop and the no P.M. cascaded loop, the results agreed with the time-domain specification of Figure 3-2(a).

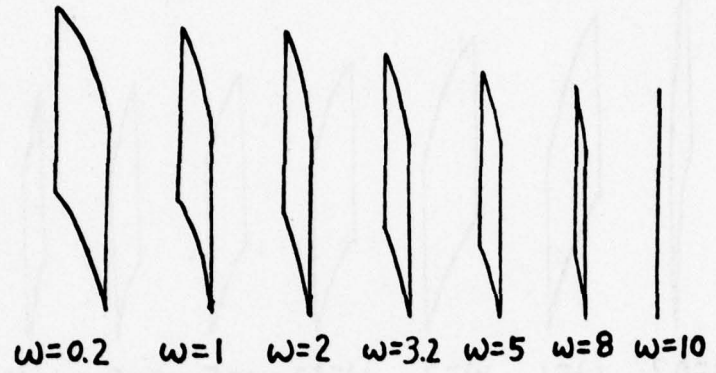

(a) Design B

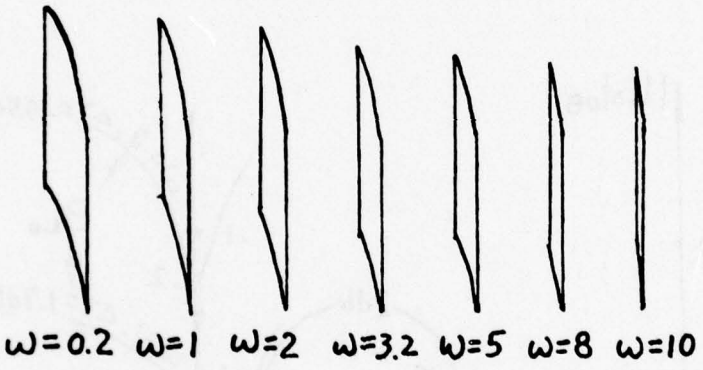

(b) Design D

(c) Design A

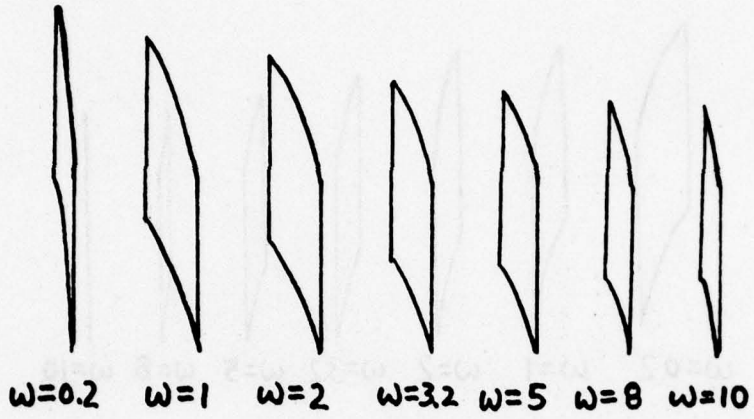

(d) Design E

Figure 3-15. Templates of $P_{1e}P_2$

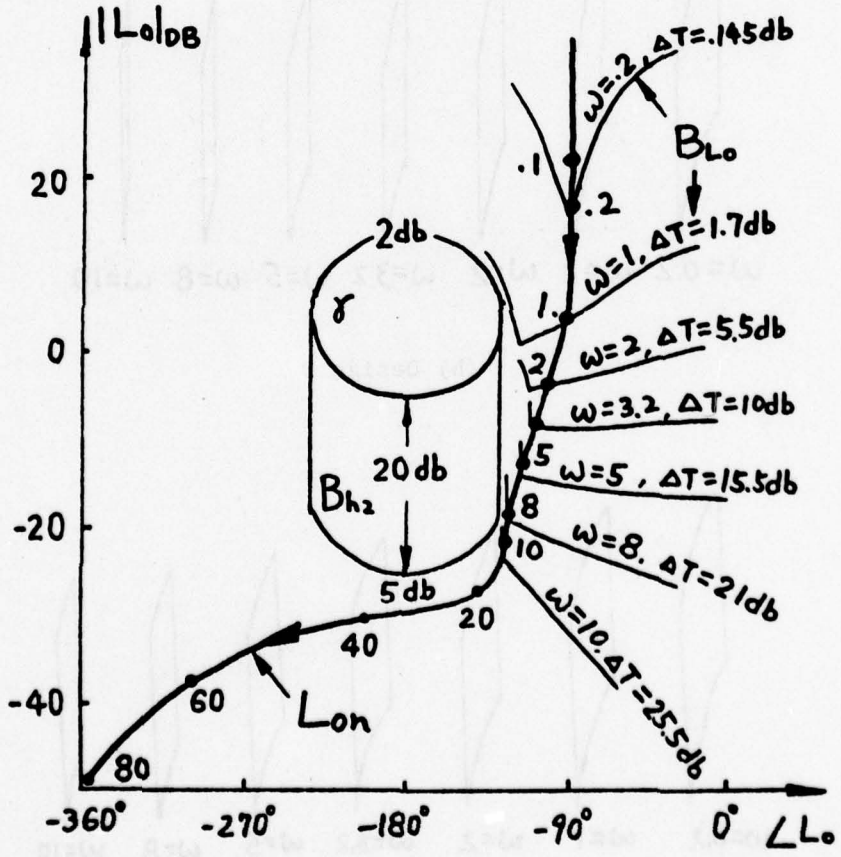

(a) Design B

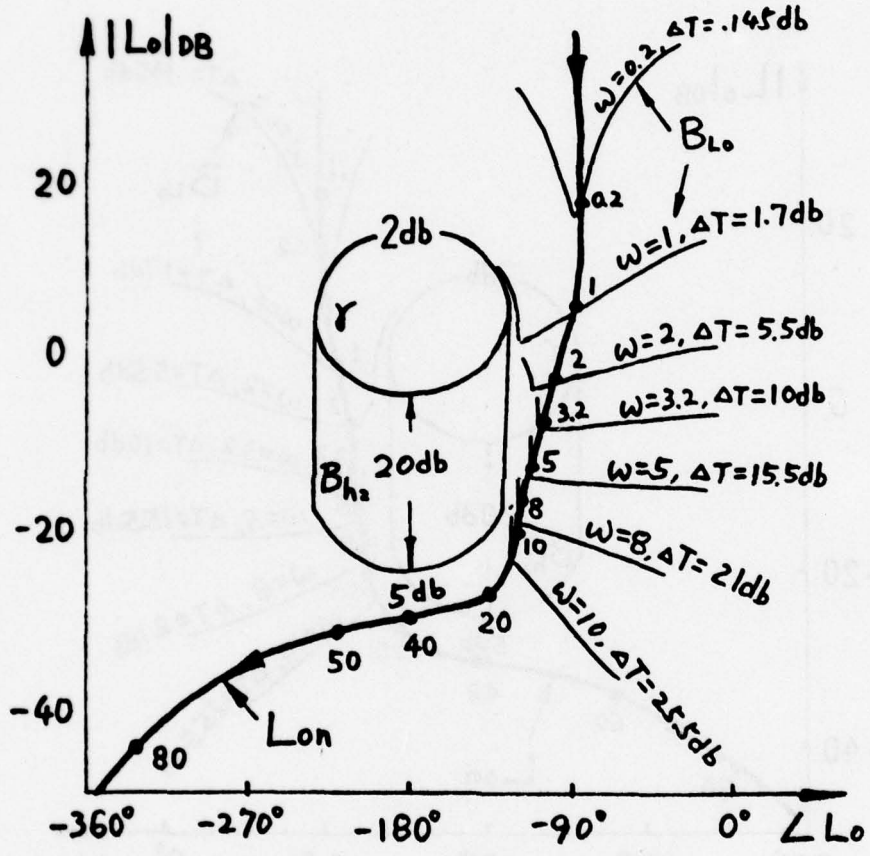
|Lo|DB
20
0
-20
-40
-360°
-270°
-180°
-90°
0°
∠Lo
ΔT=.145db
ω=0.2
BLo
0.2
ω=1, ΔT=1.7db
1
2db
γ
2
ω=2, ΔT=5.5db
3.2
ω=3.2, ΔT=10db
5
ω=5, ΔT=15.5db
8
ω=8, ΔT=21db
10
ω=10, ΔT=25.5db
Bh2
20db
5db
20
40
50
80
Lon

(b) Design D

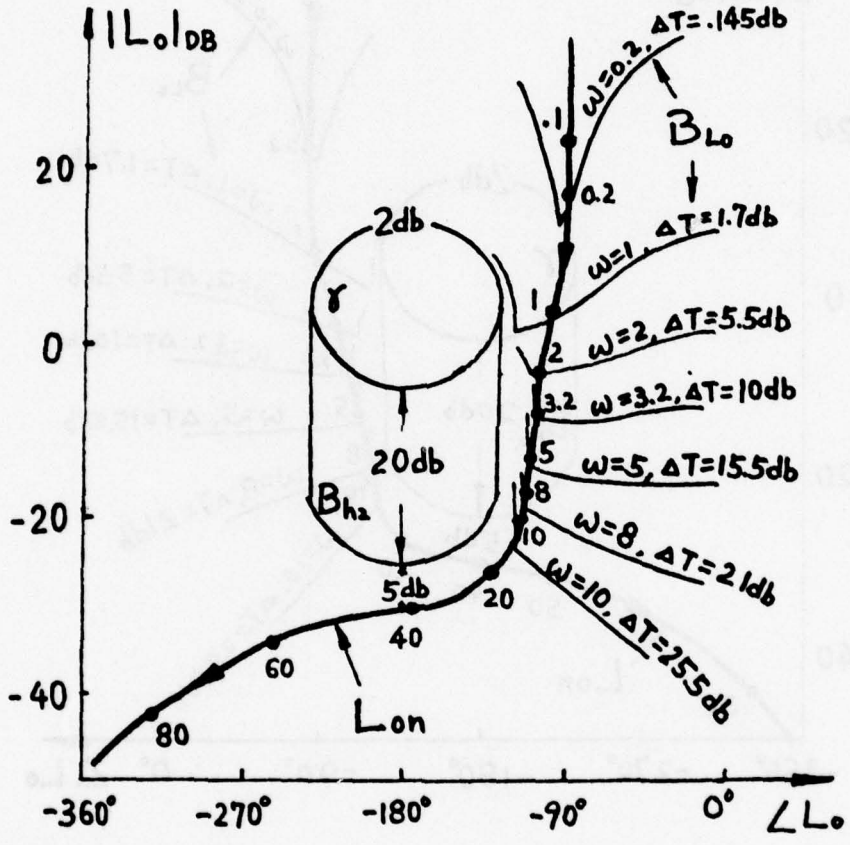
$|L_o|_{DB}$
20
0
-20
-40
-360°
-270°
-180°
-90°
0°
$\angle L_o$
ΔT=.145db
ω=0.2,
B_{Lo}
.1
0.2
ΔT=1.7db
ω=1,
2db
γ
1
2
ω=2, ΔT=5.5db
3.2
ω=3.2, ΔT=10db
5
ω=5, ΔT=15.5db
20db
B_{h2}
8
ω=8, ΔT=21db
10
ω=10, ΔT=25.5db
5db
20
40
60
80
L_{on}

(c) Design A

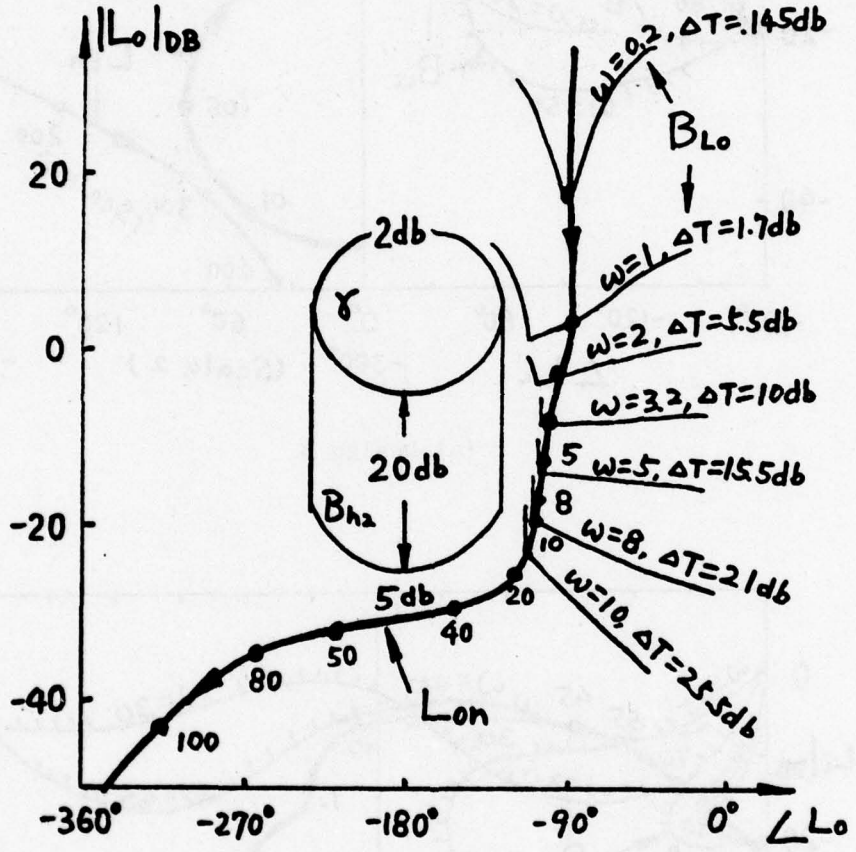

(d) Design E

Figure 3-16. B_{Lo} and L_{on} in the Nichols' chart.

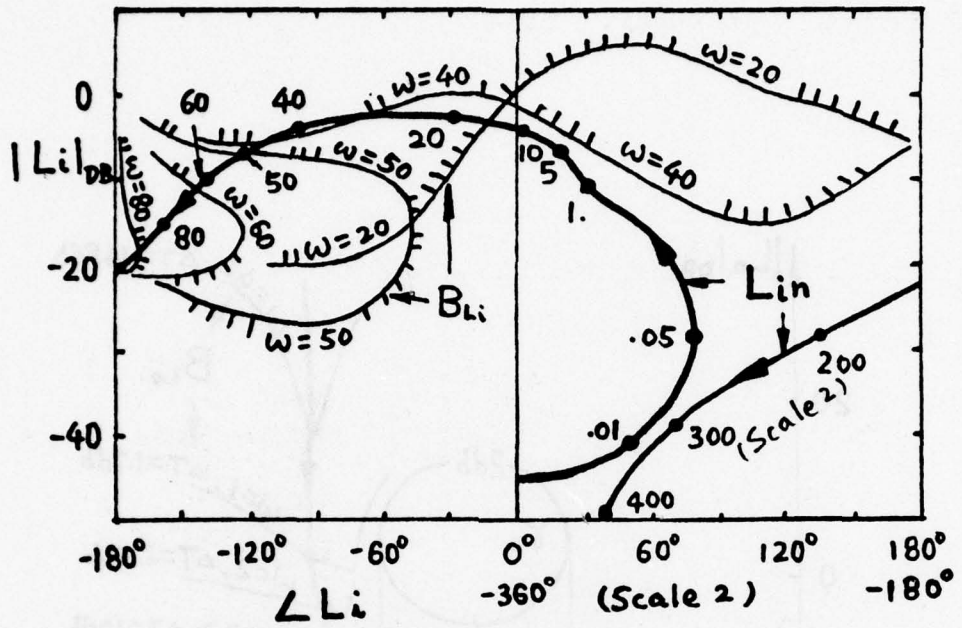

(a) Design B

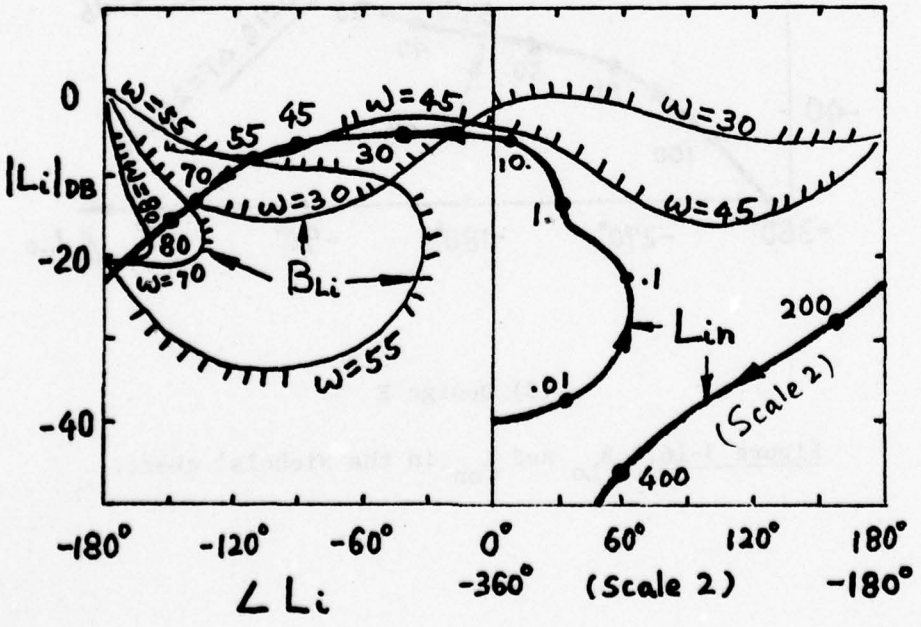

(b) Design D

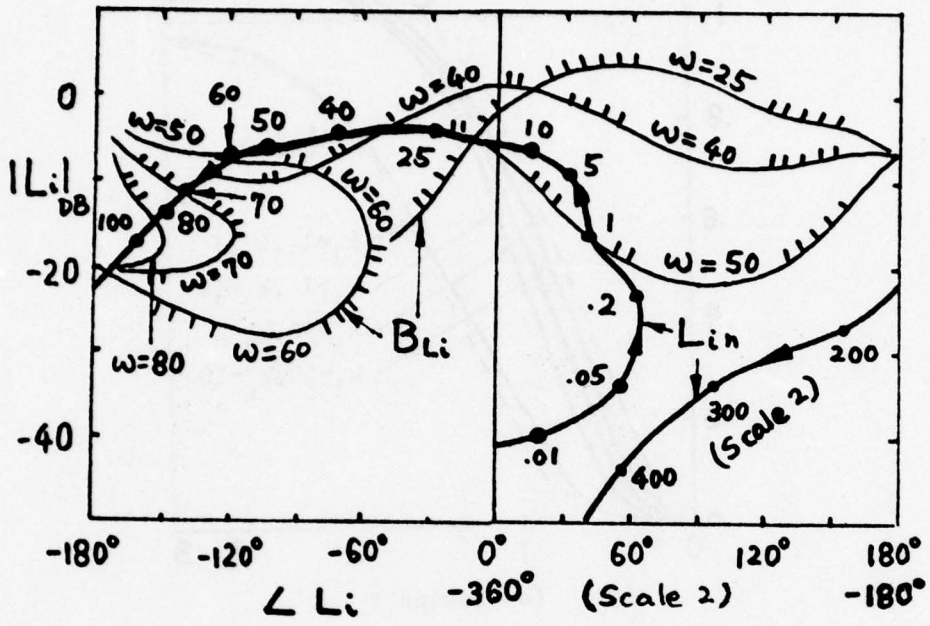

(c) Design A

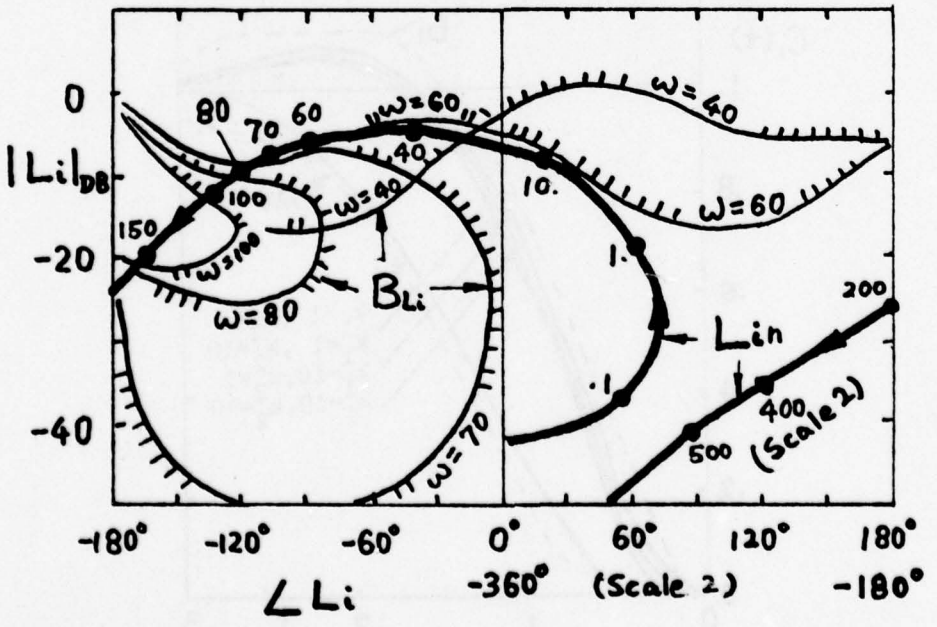

(d) Design E

Figure 3-17. The inner loop L_{in} with B_{Li}

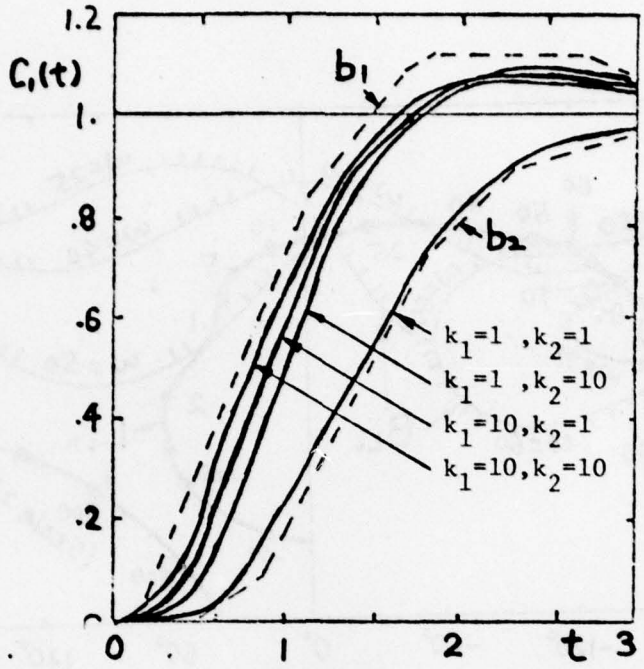

(a) Design B

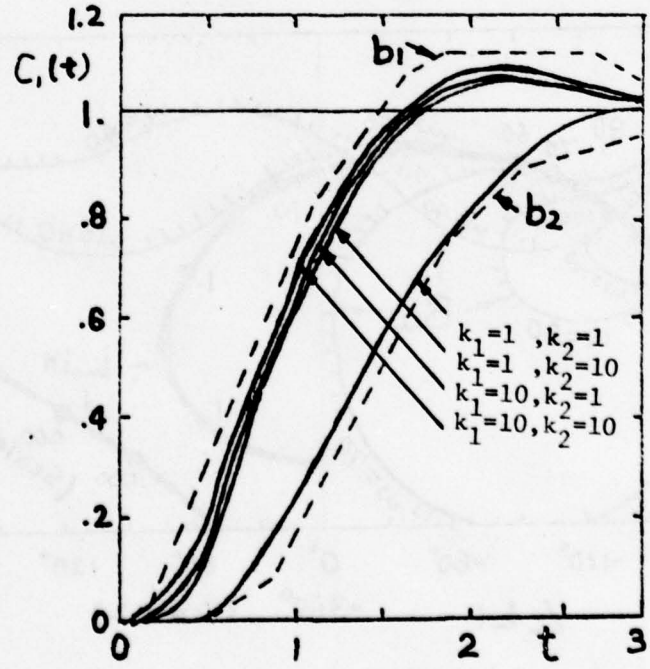

(b) Design A

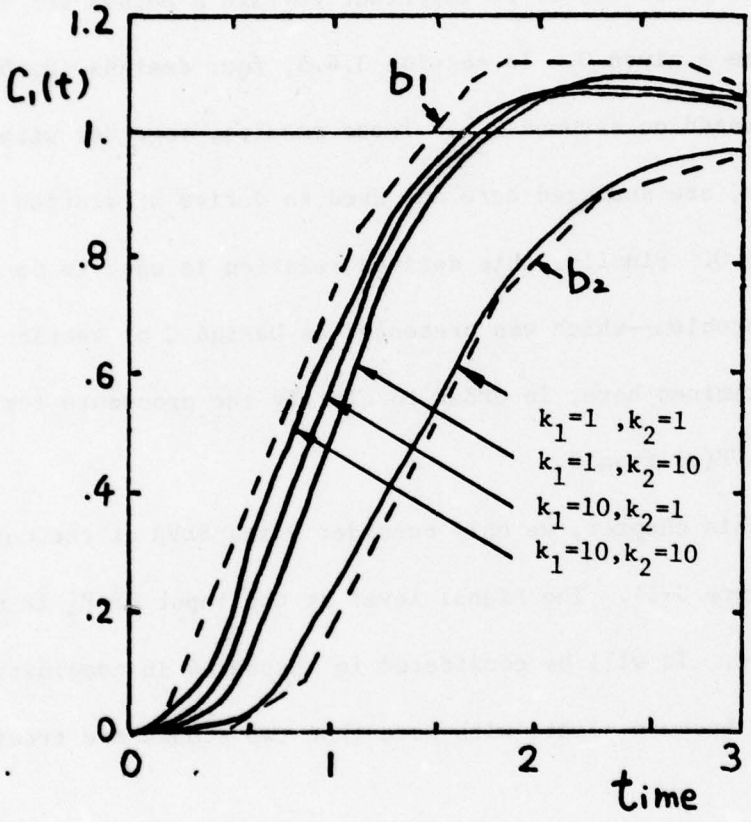

(c) Design E

Figure 3-18. The unit step response of a 2-loop, P.M. system

3.5 The Relation between Q and SLVR

3.5.1 Introduction

Recall (section 1.6.5) that this work is restricted to the RMS problem defined by Q. But the design criterion is based on SLVR (ω) (section 2.2). So it is important to have a method for choosing SLVR(ω) from a given Q. In section 3.4.5, four designs (B, D, A, E) were made based on assumed L_{in}^{ρ}. These results, together with the ISLV design, are analyzed here and used to derive a relation between SLVR(ω) and Q. Finally, this derived relation is used to do a synthesis problem--which was presented as Design C of section 3.3. It is re-examined here, in order to clarify the procedure for choosing SLVR(ω) from Q.

In this chapter, we only consider Q and SLVR at the output of P_2 (see Figure 3-1). The signal level at the input of P_2 is not considered here. It will be considered in chapter 4 in considerable generality, because plants with more than two stages are treated there.

3.5.2 The nature of $|C_{22}|_{max}$ and $|C_{2s}|_{max}$

In the single loop system of Figure 2-1, $|C_{2s}(j\omega)| = |R(j\omega) \cdot T_s(j\omega)/P_1(j\omega)|$, where $T_s(j\omega) \triangleq C_1(j\omega)/R(j\omega)$, is the system transfer function. Similarly, in 2-loop, P.M. system of Figure 3-1, $|C_{22}(j\omega)| = |R(j\omega)\ T(j\omega)/P_{1e}(j\omega)|$, where $P_{1e} \triangleq P_1/(1 + L_i)$, $L_i \triangleq P_1H_1$. $|C_{22}|_{max}^2$ of Design A is compared here for various conditions

with $|C_{2s}|^2_{max}$ of the same problem. Curves of $(|1+L_{in}|\cdot|C_{2s}|_{max})^2$ are also shown. Figure 3-19 is for R = unit step, P_1 = type 1. Figure 3-20 shows the results for R = unit step but P_1 = type 0. Figure 3-21 shows the case of R = unit impulse and P_1 = type 1. Finally, Figure 3-22 shows R = unit impulse and P_1 = type 0. Note that in Figures 3-19 -22, the region of strength of the signals changes with the input function and type number of P_1. For example, in Figure 3-19, the peak control signal is near 1.2 rad/sec, and in Figure 3-20, it is at $\omega = 0$. In section 1.6.5, the power

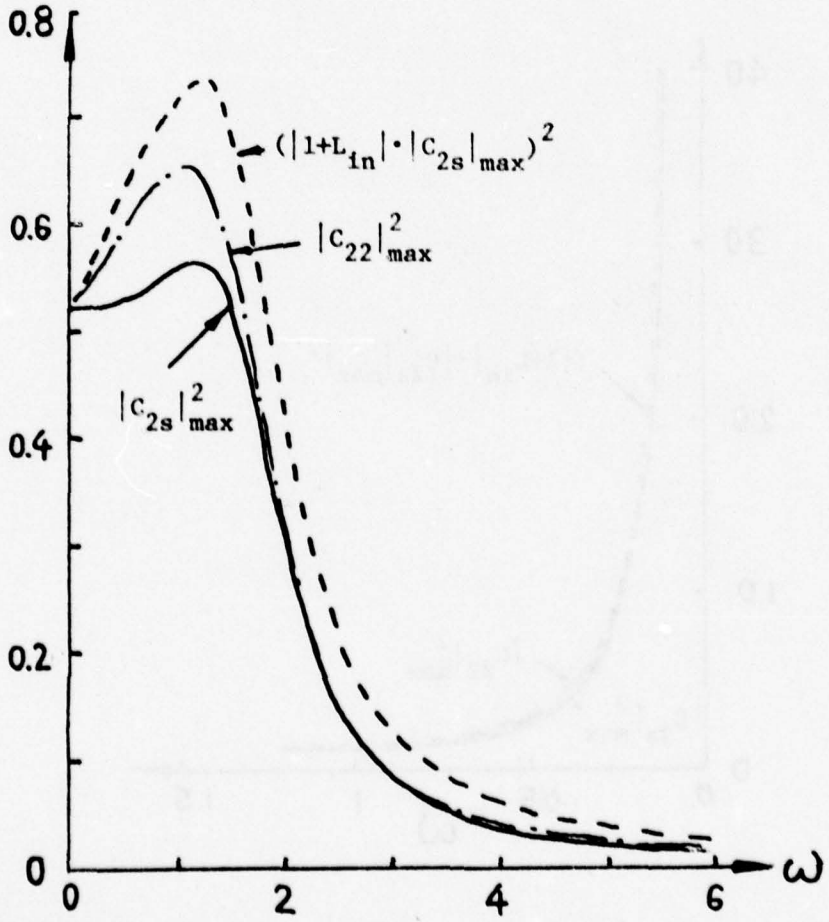

Figure 3-19. Comparison of signal levels R = unit step, P_1 = type 1

variation Q was defined to be the ratio of area under the curves $|C_{22}|^2_{max}$, $|C_{2s}|^2_{max}$. The designer knows $|C_{2s}(j\omega)|_{max}$ before commencing the P.M. design. He can use these figures to predict the resulting $|C_{22}(j\omega)|_{max}$.

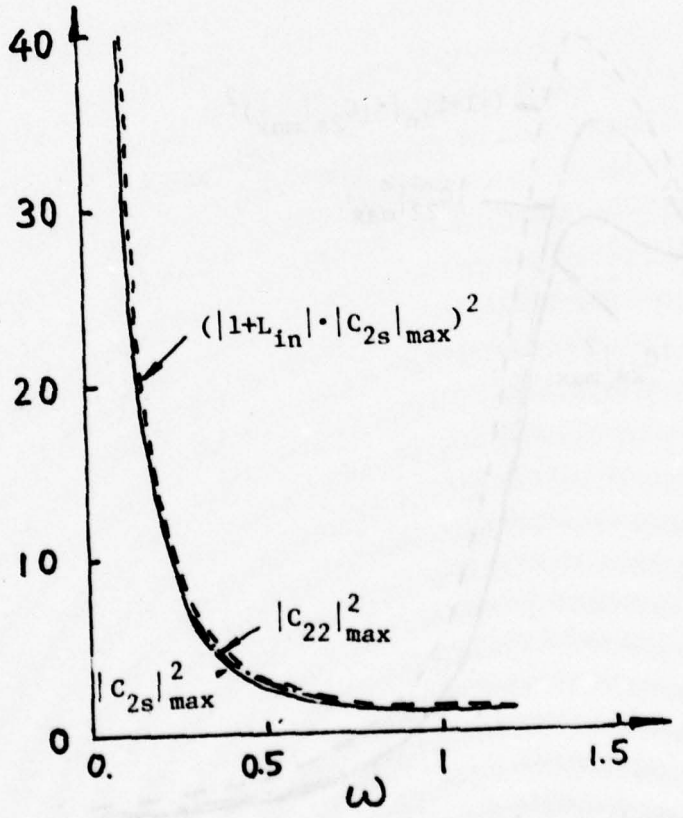

Figure 3-20. Comparison of signal levels R = unit step, P_1 = type 0

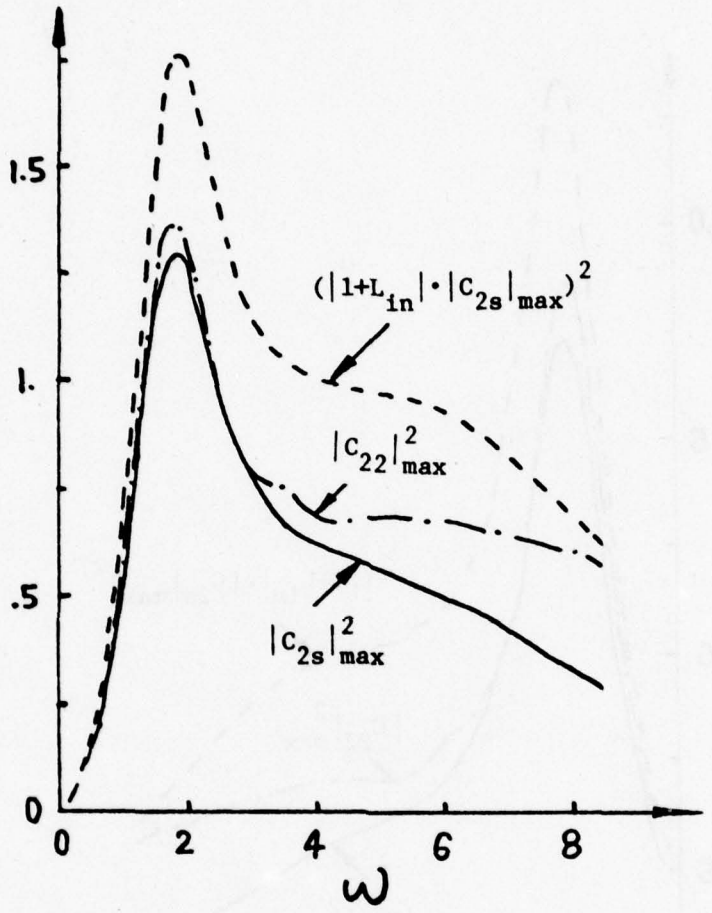

Figure 3-21. Comparison of signal levels R = impulse, P_1 = type 1

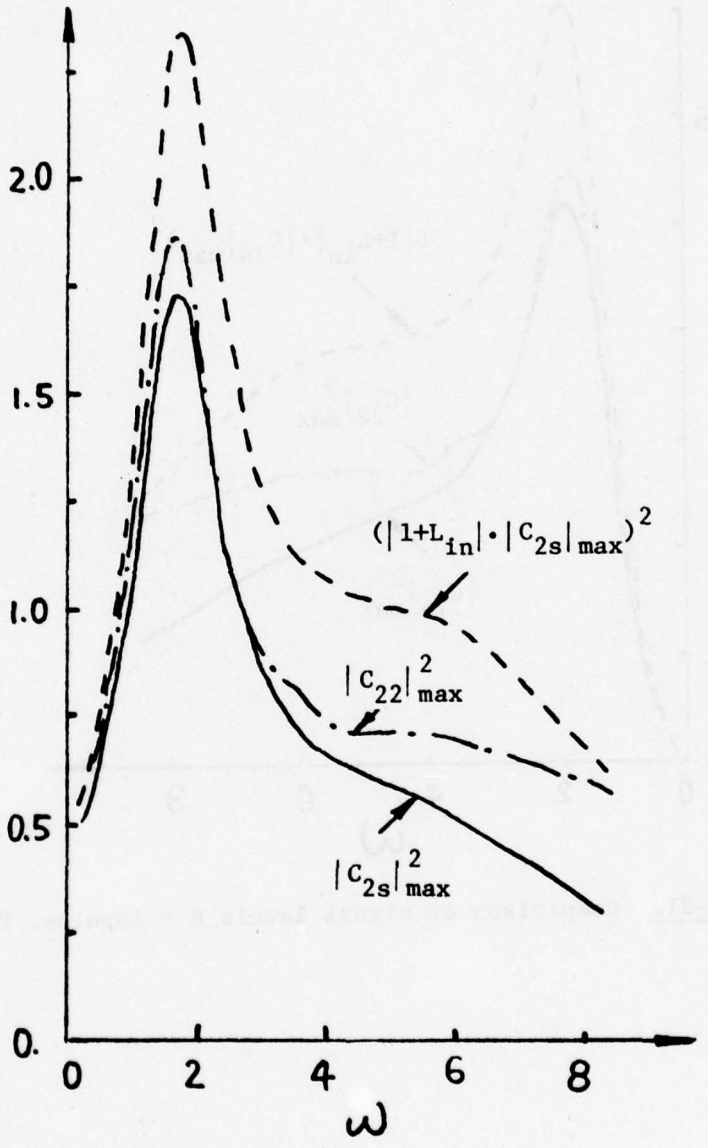

Figure 3-22. Comparison of signal levels R = impulse, P_1 = type 0.

3.5.3 Comparison of $\int_0^\infty |C_{22}|^2_{max} d\omega$ and Q

In order to understand the relation between $|1 + L_{in}|$ and Q for various conditions, the various 2-loop P.M. design are compared in Tables 3-1, 2. In these tables, 'criterion' means the data are calculated from $\int_0^\infty \{|1 + L_{in}| \cdot |C_{2s}|_{max}\}^2 d\omega$, and the 'result' column contain the actual $\int_0^\infty |C_{2s}|^2_{max} d\omega$ for the single loop and $\int_0^\infty |C_{22}|^2_{max} d\omega$ for the 2-loop, P.M. system. In the Q column, 'criterion' indicates $Q = \int_0^\infty \{|1 + L_{in}| \cdot |C_{2s}|_{max}\}^2 d\omega / \int_0^\infty |C_{25}|^2_{max} d\omega$, and 'result' gives $Q = \int_0^\infty |C_{22}|^2_{max} d\omega / \int_0^\infty |C_{2s}|^2_{max} d\omega$.

The ISLV design (ignoring-signal-level-variation) may be impractical, because the signal level problem is ignored and the only objective is the reduction of sensor noise effect. So in Tables 3-1, 2, its Q etc. values are the largest. But, it is useful to know that even in this extreme case $Q \simeq 2$. Design E for R a step input (Table 3-1) is excellent in terms of signal level variation because Q (result) = .98<1, although Q (criterion) = 1.17. This is because the design criteria are very conservative, as noted in section 2.4.2.

Next, the data of Q in Tables 3-1, 2 are plotted: Q (result) $\triangleq Q_r$ vs Q (criterion) $\triangleq Q_c$ in Figure 3-23. The very interesting point is that for each condition (e.g., P_1 = type 1, R = unit step), the data lie on a straight line. In Figure 3-23, a, b, there has

R = unit step function								
Type no. of P_1	1				0			
Kinds of data	$\int_0^\infty \lvert C_{22} \rvert_{max}^2 d\omega$		Q		$\int_0^\infty \lvert C_{22} \rvert_{max}^2 d\omega$		Q	
Kinds of value	Criterion	Result	Criterion	Result	Criterion	Result	Criterion	Result
Single-loop system		1.27				9.63		
2-loop P.M. sys. (E)	1.48	1.24	1.17	0.98	10.1	9.71	1.05	1.01
" (C)	1.55	1.33	1.22	1.047	10.3	9.89	1.07	1.03
" (A)	1.65	1.40	1.29	1.10	10.6	10.2	1.10	1.06
" (D)	1.78	1.58	1.40	1.24	11.3	10.9	1.17	1.13
" (B)	2.04	1.80	1.61	1.41	11.7	11.1	1.21	1.15
" (ISLV)		2.49		1.96		18.9		1.96

Table 3-1. Data of $\int_0^\infty \lvert C_{22} \rvert_{max}^2 d\omega$ and Q for unit step input

R = unit impulse function								
Type no. of P_1	1				0			
Kinds of data	$\int_0^\infty \lvert C_{22} \rvert^2_{max} d\omega$		Q		$\int_0^\infty \lvert C_{22} \rvert^2_{max} d\omega$		Q	
Kinds of value	Criterion	Results	Criterion	Results	Criterion	Results	Criterion	Results
Single-loop sys.		5.15				6.43		
2-loop P.M. sys. (E)	7.34	5.53	1.43	1.07	8.84	6.80	1.37	1.06
" (C)	7.52	5.79	1.46	1.12	9.11	7.15	1.42	1.11
" (A)	8.26	6.34	1.60	1.23	9.95	7.77	1.55	1.21
" (D)	8.65	7.27	1.68	1.41	10.5	8.89	1.63	1.38
" (B)	10.4	9.15	2.02	1.78	12.5	11.0	1.94	1.71
" (ISLV)		10.4		2.02		12.9		2.01

Table 3.2. Data of $\int_0^\infty \lvert C_{22} \rvert^2_{max} d\omega$ and Q for unit impulse input.

four straignt lines representing the four different cases--

(1) P_1 = type 0, R = unit step; (2) P_1 = type 0, R=unit impulse;

(3) P_1 = type 1, R = unit step; (4) P_1 = type 1, R = unit impulse. Also, the data for each of Designs A, B, C, D, E, give straight lines, as shown in Figures 3-23(c)(d). (The lines were obtained by linear regression). By means of these lines, the designer can find Q_c from his known required Q_r. With regards to C, in section 3.3.1, the specification on Q_r was 1.05, for R = unit step, P_1 = type 1. In Figures 3-23(b,d), the corresponding Q_c = 1.22, which was used in the design in section 3.3.3.

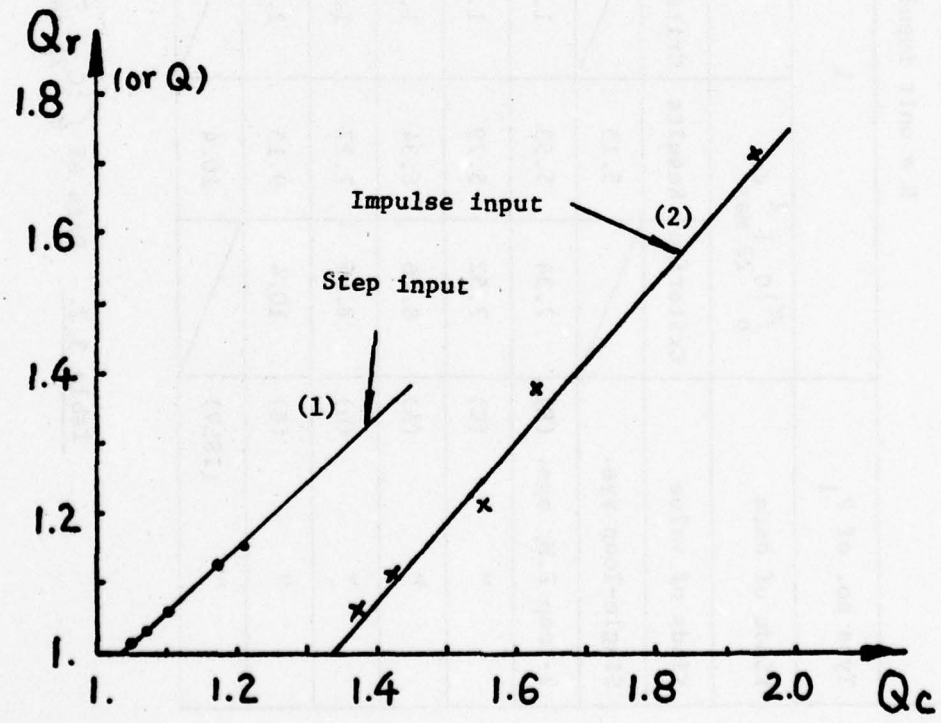

Figure 3-23(a). Relation between Q_r and Q_c--P_1 = type 0.

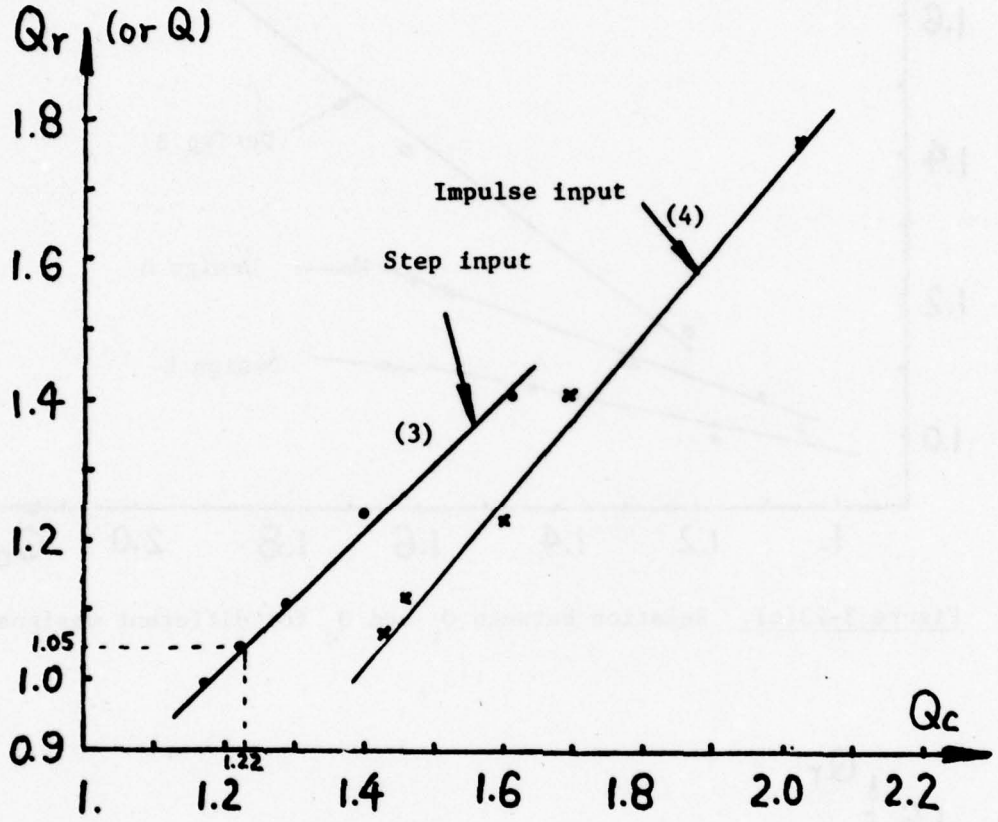

Figure 3-23(b). Relation between Q_r and Q_c--P_1 = type 1.

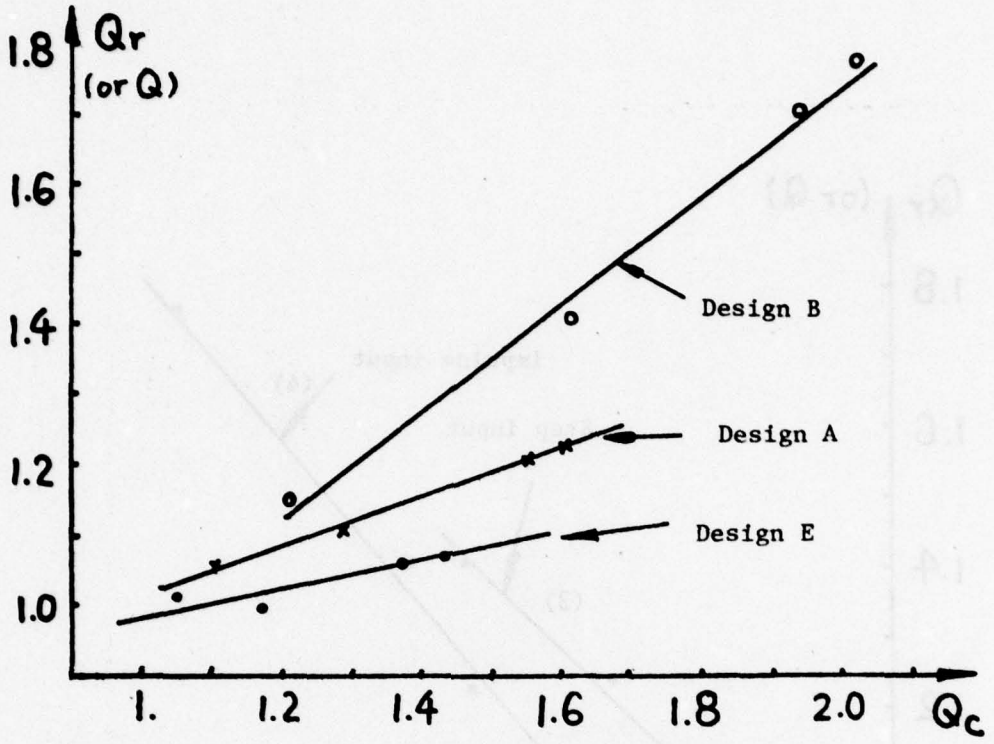

Figure 3-23(c). Relation between Q_r and Q_c for different designs.

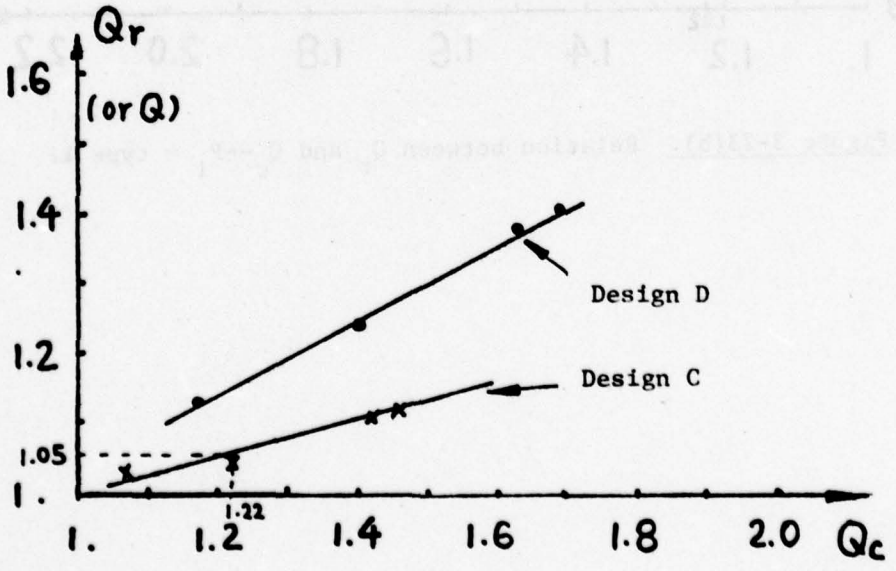

Figure 3-23(d). Relation between Q_r and Q_c for different designs.

3.5.4. The nature of L_{in}

For pedagogic reason, it is better to understand the nature of L_{in} in R_1, R_2 before considering how to derive $|1 + L_{in}(j\omega)|$ from Q_c. The nature of L_{in} is decisively influenced by the nature of non P.M. cascaded loop design [5], note previously in chapter 1. Recall that in the lf range (R_1, R_2) there is little demand on L_i; the bounds are upper ones, i.e., L_i must be below some boundary. Consider the loci of constant $|1 + L_i|$ in Figure 3-24, which is replotted from Figure 2-5. We want it to be small in R_1, R_2 because it is being used to determine SLVR, and in these ranges we want small SLVR. We also know from our experience in cascaded (no P.M.) design that at higher frequencies (R_3, R_4) the bounds change to lower bounds (L_i must be above the boundary) and the level of these lower bounds gradually increases to a maximum at ω_M in Figure 3-24, and then decreases along MNQ in Figure 3-24 (see Figure 3-12). In our P.M. problem, we want to retain and improve the nice property of the non P.M. design in its drastic reduction of sensor noise effect. The above properties of the bounds in the non P.M. design continue to exist in the P.M. design. The natural tendency for L_i is to reach ω_M, at $L_i \sim -90^\circ$ in Figure 3-24. And this is precisely the region in which $|1 + L_{in}|$ is large ~ 5db in Figure 3-24, giving a large SLVR value. However, it is not this large SLVR at ω_M which bothers us because ω_M is relatively large--in R_4, in which the signal level is small. It

is the fact that we must reach this region at ω_M starting from a small value of $|L_{in}|$ in R_1. (Recall that small $|1 + L_{in}|$ is required in R_1, R_2 because the signal level is largest in R_1, R_2). So we have to shape L_{in} in R_1, R_2 to join MNQ, but hopefully so as to achieve small $|1 + L_{in}|$. Also Arg $L_{in}(0)$ must be a multiple of $\frac{\pi}{2}$. Curve ABC in Figure 3-24 seems attractive but it gives a negative half encirclement of the -1 point, so $(1 + L_{in})$ has a rhp zero, unless L_{in} has a rhp pole. This is seen from the Nyquist criterion: no. of encirclements = $N = N_z - N_p$, where N_z = no. of $1 + L_{in}$ in the rhp and N_p = no. of poles of $1 + L_{in}$ in rhp. Consider the two alternatives:

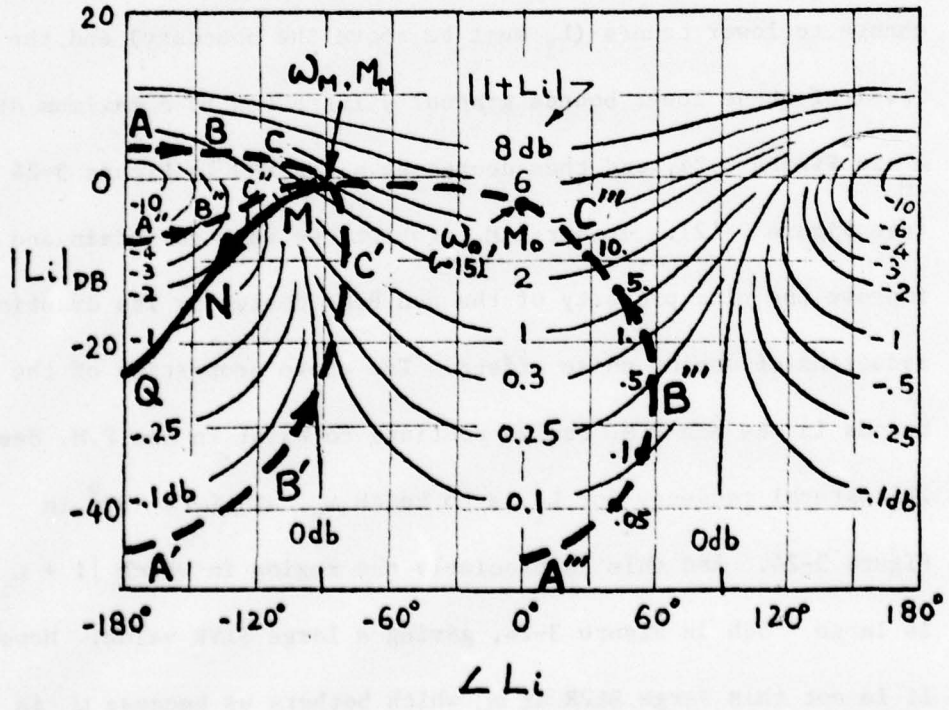

Figure 3-24. Constant |1+L| curves and possibility of L_i curves.

1. $L_{in} = P_{1n}H_1$ has a rhp pole. This pole must be due to H_1 and then it appears as a rhp zero of $L_{on} = GP_{2n}P_{1n}/(1+P_{1n}H_1)$, which is then nonminimum phase and is very limited in its feedback capabilities. So it is excluded.

2. L_{in} does not have a rhp pole. If so, it is impossible for such a stable L_{in} to achieve the encirclement shown in Figure 3-24, because in such a case $N = -1$, $N_p = 0$, so $N_z = -1$ which is impossible

A second attractive possibility for L_{in} in R_1, R_2 appears to be A'B'C' or A"B"C" in Figure 3-24, which was seriously attempted. The problem is achievability of such curves. Achievability of such curves has been discussed in detail in section 7.7 of [45] (Figure 7.7-4, etc.) and it was shown to be impossible to achieve the kinds of ratio $|M_1/M_2|$ generally needed here, where M_1 is the maximum $|L_{in}|$ needed and M_2 is = -20 db due to the hf uncertainty in P_1.

This leaves us only with the third possibility A"'B"' C"' . Here Arg $L_{in}(0) = 0$ and $|L_{in}(0)|$ should be small in order that $|1 + L_{in}|$ is small in this range where the signal level is large. But at higher ω, L_{in} must merge into MNQ in Figure 3-24. Hence, Arg L_{in} must be positive over much of R_1, R_2, in order that $|L_{in}|$ may increase from its low value at $\omega = 0$ to the value needed at M_o, denoted by ω_o .

We want to estimate the ω value at which L_{in} across the zero phase line on its way to MNQ. We know from our experience in cascaded design that $|L_{in}|_{max}$ (i.e., point M in Figure 3-24) occurs near J of L_{on} in Figure 3-25. Our experience is that a reasonable estimate of $\omega_J/\omega_o \sim 3$. This can also be approximately theoretically justified as follows. Arg L_{in} is by definition positive from 0 to ω_o and $|L_{in}|_{max}$ is at ω_M (pt J). Now M_M (magnitude of L_{in} at point M) cannot be much bigger than M_o, because Arg L_i in this range is < 0. So must of the increase in $|L_{in}|$ from its small $|L_{in}(0)|$ to $|L_{in}(M)|$ must be achieved in $(0, \omega_o)$. From ω_o to ω_M, $|L_{in}|$ will be fairly horizontal and cover a range of $\sim 90^o$ decrease in phase. This is somewhat similar to the situation from I to J in Figure 3-25, where $\sim 90^o$ is also covered and where the range $\omega_J/\omega_I \sim 3$. This gives ω_o near point I in Figure 3-25.

3.5.5 Choice of "criterion" $|1+L_{in}|$ from Q_c

Recall $Q_c = \int_o^\infty \{|1 + L_{in}| \cdot |C_{2s}|_{max}\}^2 d\omega / \int_o^\infty |C_{2s}|_{max}^2 d\omega$ (= 1.22 in design C). $|C_{2s}|_{max}^2$ is known by executing a single loop design and is shown in Figure 3-26 (which is replotted from Figure 3-4). So the area under the curve $\{|1 + L_{in}| \cdot |C_{2s}|_{max}\}^2 = \Psi(\omega)$ should be 1.22 times that under $|C_{2s}|_{max}^2$. This curve should be such that the resulting $L_{in}(j\omega)$ looks more or less like A''' B''' C''' (Figure 3-24) in the region R_1, R_2 which covers the significant range in

1. $L_{in} = P_{1n} H_1$ has a rhp pole. This pole must be due to H_1 and then it appears as a rhp zero of $L_{on} = GP_{2n} P_{1n} / (1+P_{1n} H_1)$, which is then nonminimum phase and is very limited in its feedback capabilities. So it is excluded.

2. L_{in} does not have a rhp pole. If so, it is impossible for such a stable L_{in} to achieve the encirclement shown in Figure 3-24, because in such a case $N = -1$, $N_p = 0$, so $N_z = -1$ which is impossible

A second attractive possibility for L_{in} in R_1, R_2 appears to be A'B'C' or A"B"C" in Figure 3-24, which was seriously attempted. The problem is achievability of such curves. Achievability of such curves has been discussed in detail in section 7.7 of [45] (Figure 7.7-4, etc.) and it was shown to be impossible to achieve the kinds of ratio $|M_1/M_2|$ generally needed here, where M_1 is the maximum $|L_{in}|$ needed and M_2 is = -20 db due to the hf uncertainty in P_1.

This leaves us only with the third possibility A"'B"'C"'. Here Arg $L_{in}(0) = 0$ and $|L_{in}(0)|$ should be small in order that $|1 + L_{in}|$ is small in this range where the signal level is large. But at higher ω, L_{in} must merge into MNQ in Figure 3-24. Hence, Arg L_{in} must be positive over much of R_1, R_2, in order that $|L_{in}|$ may increase from its low value at $\omega = 0$ to the value needed at M_o, denoted by ω_o.

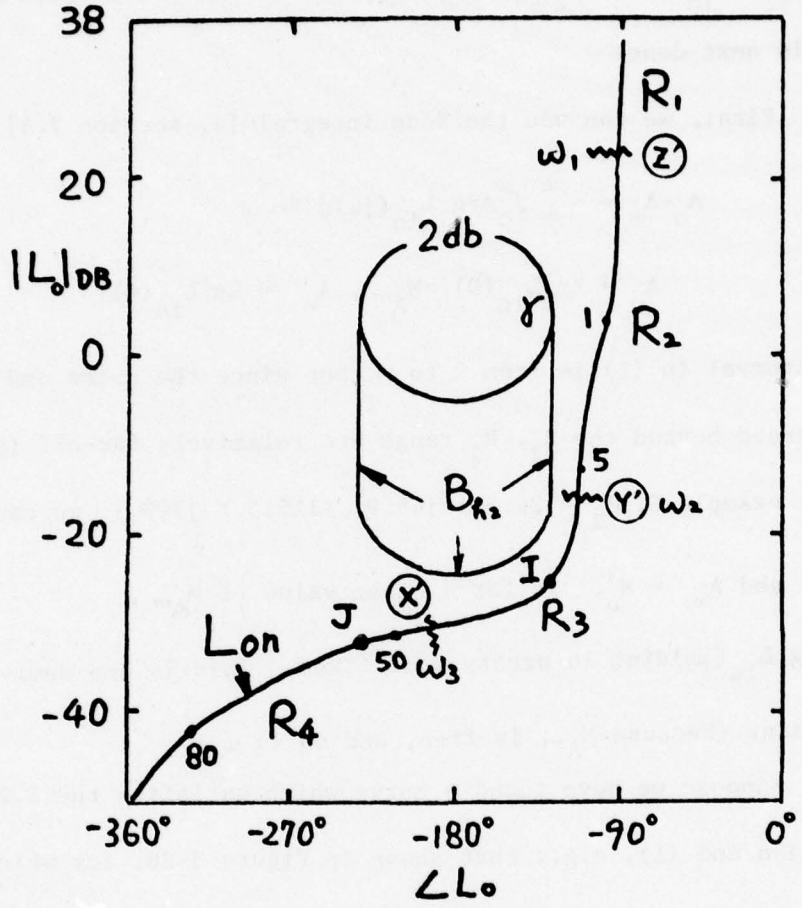

Figure 3-25. L_{on} in Nichols' chart.

Figure 3-26. This is necessary in order that a higher ω, (to achieve significant sensor noise reduction), L_{in} satisfy the bound M_M at ω_M and then follow a curve like MNQ in Figure 3-24. So the primary concern at this stage is to start L_{in} at $\omega = 0$ at a point like A''', and arrive at a point like M_o in Figure 3-24 (where $\omega_o \approx 15$). Obviously, there is no unique curve of $\Psi(\omega)$. What are the trade-offs and constraints? It is easier to see the

effect of $L_{in}(j\omega)$ shaping on $\Psi(\omega)$, rather than vice versa and this is next done.

First, we can use the Bode integral [4, section 7.5]

$$A_o - A_\infty = -\frac{4}{\pi}\int_0^\infty \text{Arg } L_{in}(j\omega)\, d\,\ell n\,\omega \qquad (3.5\text{-}1)$$

$$A_o = \ell n|L_{in}(0)| = M_{A'''}\,,\quad A_\infty = \ell n|L_{in}(\infty)|$$

The interval in (1) is from 0 to ∞, but since the poles and zeros introduced beyond the R_1, R_2 range are relatively far-off (e.g., in our example C, $P_i = 26.5 \pm j45.9, -115.5 \pm j309.$), we can take $\int_0^{\omega_o}$, and $A_\infty = M_o$. So far a given value of $M_{A'''}$, $\int_0^{\omega_o} \text{Arg } L_{in}(j\omega)d\ell n\omega$ is pretty well fixed. This is one semi-constraint (because $M_{A'''}$ is free, and so is ω_o).

Suppose we have found a curve which satisfies the 1.22 condition and (1), e.g., that shown in Figure 3-26, for which the resulting L_{in} in R_1, R_2 is shown in Figure 3-27. Consider keeping the same shape of L_{in} as in Figure 3-27, but shifting the pattern as a whole to the left, i.e., achieving the transfer from A''' to C''' in Figure 3-24 in a lower frequency range. Clearly, this would cause $\Psi(\omega)$ to be the same for $\omega > \omega_o$, but considerably larger in between 0 and ω_o, thereby violating the 1.22 condition. So, if we want to "start $|L_{in}(j\omega)|$ off" sooner, we must flatten somewhat the curve of Arg $L_{in}(j\omega)$ in Figure 3-27--lower its peak and spread it out over a larger range, so that its area remains the same, as shown by dashed line in Figure 3-27. This will increase

Ψ at lower ω and decrease it at higher ω. Note that lifting A''' higher, i.e., increasing $|L_{in}(0)|$, means $\int_o^{\omega_o}$ can be less, and so peak Arg $L_{in}(j\omega)$ can be smaller. However, in Figure 3-24, it is seen that this tends to increase $|1 + L_{in}|$ and therefore Ψ. However, reduction of Arg $L_{in}(j\omega)$ is good, especially in latter part of R_2--because the bound on the outer loop L_{on} is shifted less to the right (Recall section 3.3.7 and Figure 3-10). So this kind of effort (starting $L_{in}(j\omega)$ up sooner and raising A''') is good and one should do this as much as possible. But the 1.22 limit on $\int_o^{\infty} \Psi d\omega$ limits how much can be done and that is basically the optimum, which is seen by considering the opposite kind of variation.

Suppose the pattern in Figure 3-27 is pushed to the right. $\Psi(\omega)$ is thereby decreased but the peak in Arg $L_{in}(j\omega)$ occurs at a higher ω, which is more harmful to $L_{on}(j\omega)$ in the sense of sensor noise effect (see section 3.3.7, Figure 3-10). Thus, one wants to move in the opposite direction--to the left--as previously seen.

The above presents the trade-offs. The optimum $\Psi(\omega)$ curve would require some cut and try. Our experience has been that a good way to start is to take the peak of $[\Psi(\omega)]_{max} \triangleq M_X$ in Figure 3-26 at the same ω value as the peak of $|C_{25}|_{max}$, take $\Psi(0) = |C_{2s}|_{max}$ at zero, allow a value $\sim .05$ larger than $|C_{2s}|_{max}$ in the higher ω range (see Figure 3-26) and draw a fairly smooth

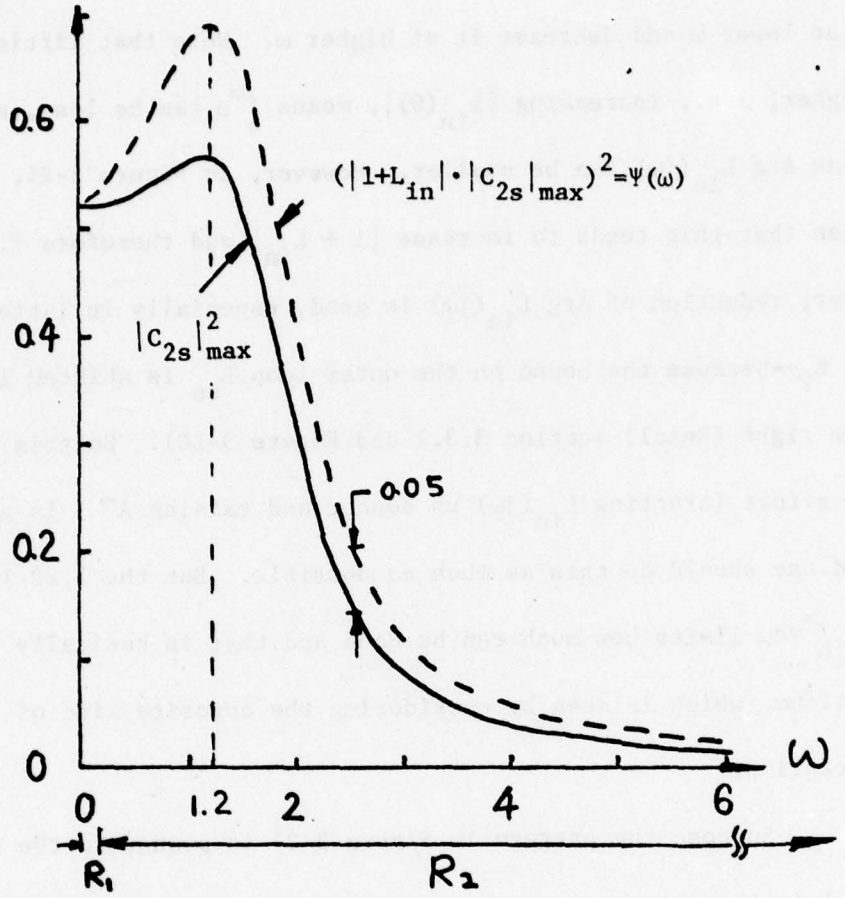

Figure 3-26. The choice of $(|1+L_{in}|\cdot|C_{25}|_{max})^2$ (Design C)

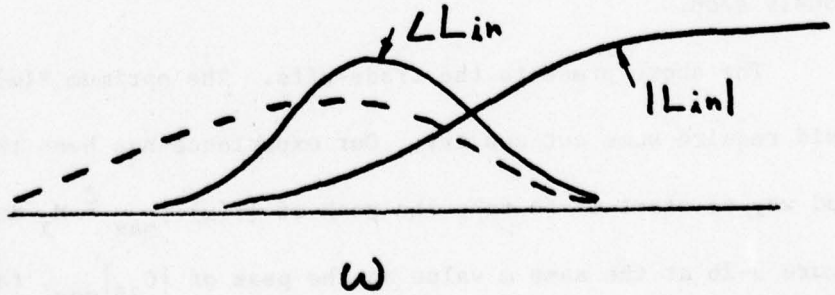

Figure 3-27. L_{in} and $|L_{in}|$

curve satisfying the above. Try different M_X values until the 1.22 condition is satisfied. So now a trial $\Psi(\omega)$ is available. Use it to determine the bounds on $|1 + L_{in}^{\rho}|$ and find the resulting L_{in}^{ρ} (i.e., L_{in} in R_1, R_2) wilch will look like that in Figure 3-24. Use this as a starter. Now work from L_{in}^{ρ}, rather than from $\Psi(\omega)$. Push the $|L_{in}|$ increase toward lower frequency as previously indicated and modify Arg L_{in}^{ρ} and possibly the A''' point in this quest. We have found this to be a good approach.

3.6 Comparison of the Loop Transmissions

Bode plots of the inner loop L_{in} and the outer loop L_{on} for the five different P.M. 2-loop designs are given in Figure 3-28, as well as the single loop transmission L_{sn}. Recall section 2.3, $R_1 = (0., \omega_1]$, $|L_{sn}(j\omega_1)| = 25$ db; $R_2 = (\omega_1, \omega_2]$, $|L_{sn}(j\omega_2)| = -M_2$, M_2 = hf uncertainty of P_2; $R_3 = (\omega_2, \omega_3]$, $|L_{sn}(j\omega_3)| = -(M_1 + M_2)$, M_1 = hf uncertainty of P_1; $R_4 = (\omega_3, \omega_4]$, $\omega_4 = 10\omega_3$; $R_5 = (\omega_4, \infty)$.

$|L_{in}|$ in R_1, R_2, in Figure 3-28 is closely related to SLVR and Q. The larger $|L_{in}|$, the large are SLVR and Q. Note, when L_{in} in R_2 is lower than some limit, say Design E, then, although the criterion on SLVR, $|1 + L_{in}|$, >1 the actual $\rho/(|C_1|_{max}/|C_s|_{max})$ <1 in Figure 2-29(e) in most of R_2. So Q < 1, because of the conservative character of the design philosophy. It is reemphasized that the signal level in R_3, R_4, R_5 is not important, so

even large SLVR (ρ)--there poses no problem. The curves of $|1+L_{in}|$ and $\rho/(|C_1|_{max}/|C_s|_{max})$ for Design B, D, A, C, E are shown in Figure 3-29 (a), . . ., (e). Note the values of $\rho/\{|C_1|_{max}/|C_s|_{max}\}$ in Figure 3-29 in R_1, R_2, are directly related to the value of $|L_{in}|$ in Figure 3-28. For example, Design B in Figure 3-28 is the largest in R_1, R_2, so the value of $\rho/\{|C_1|_{max}/|C_s|_{max}\}$ of Figure 3-29(a) is the largest. The comparison of $\rho/\{|C_1|_{max}/|C_s|_{max}\}$ are shown in Figure 3-29(f).

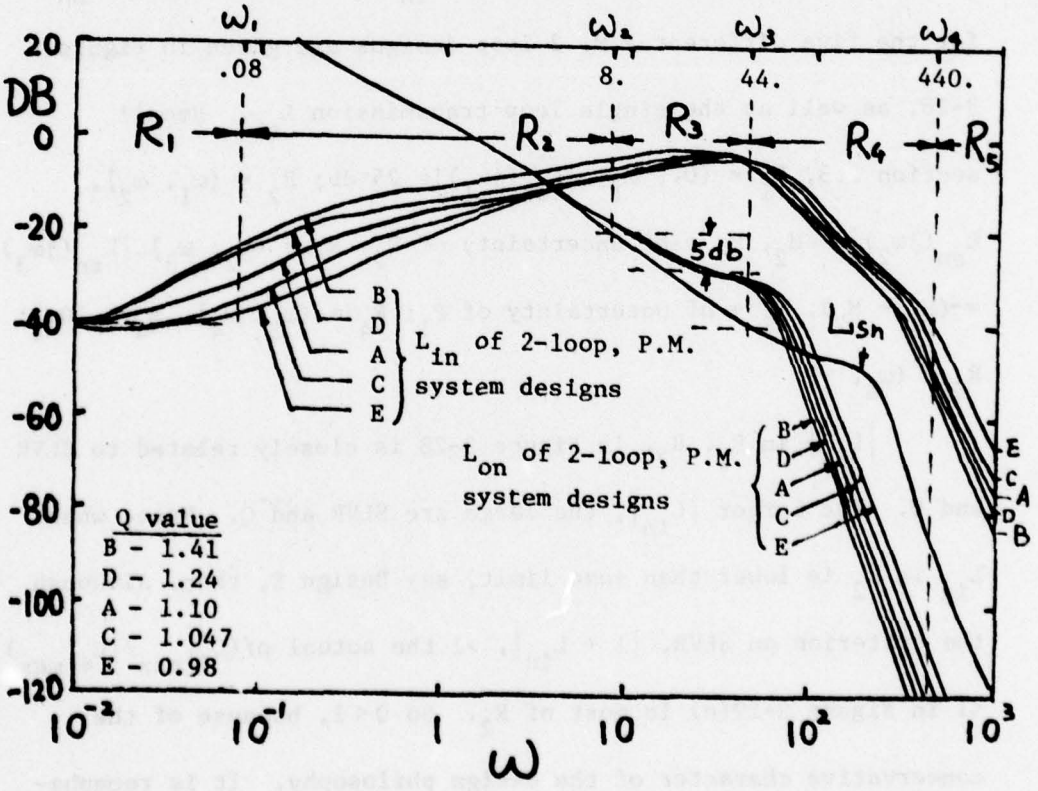

Figure 3-28. Loop transmissions of L_{sn}, L_{on}, L_{in}

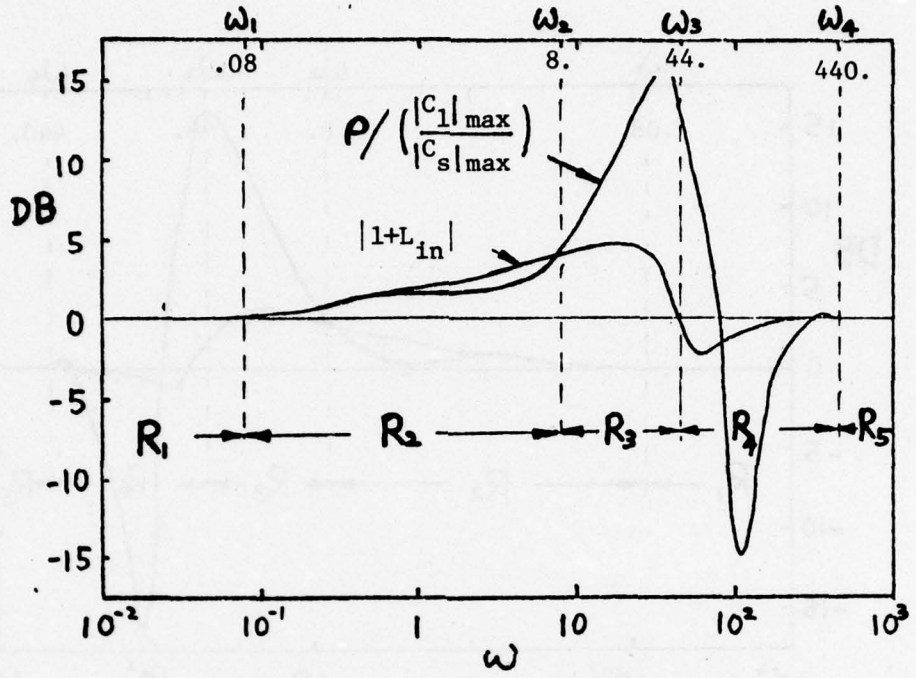

Figure 3-29(a). Design B

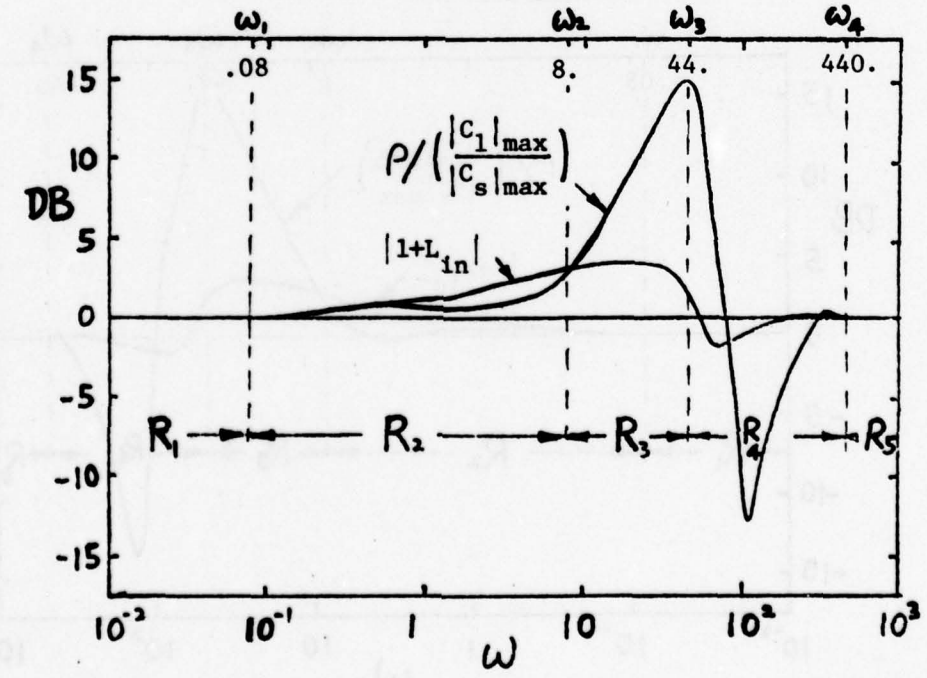

Figure 3-29(b). Design D

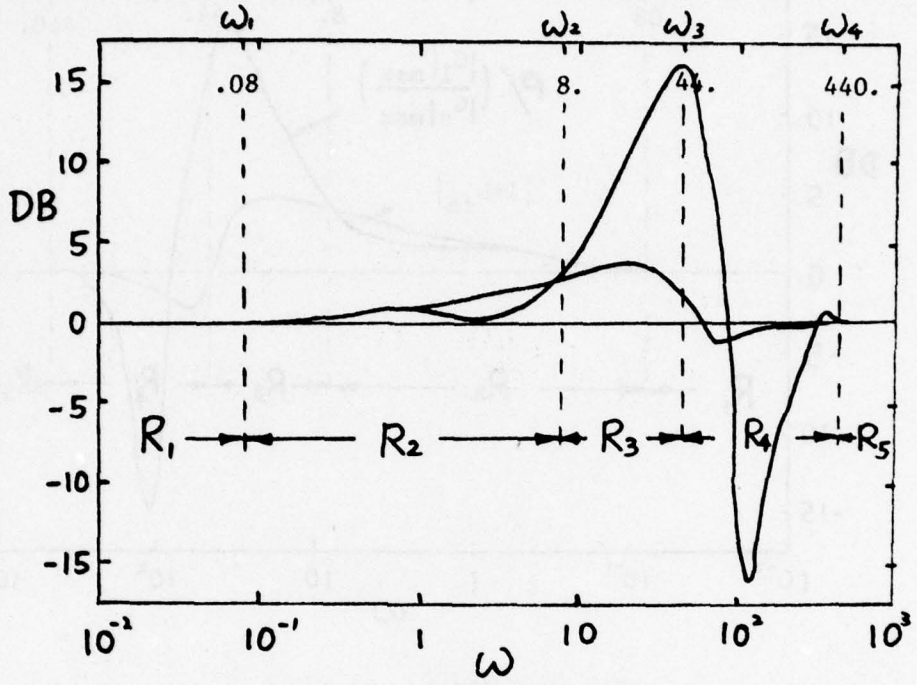

Figure 3-29(c). Design A

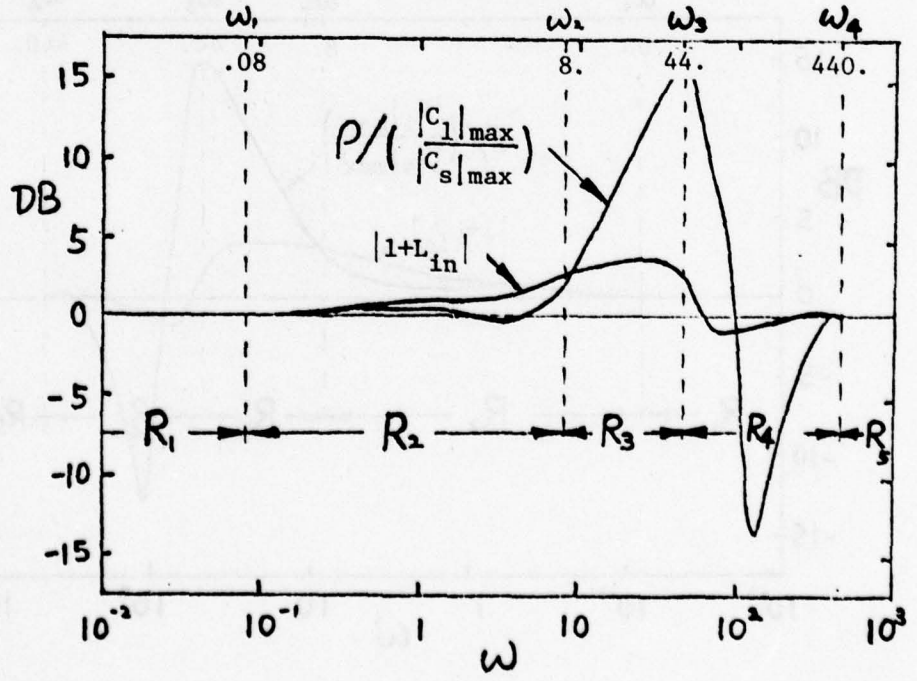

Figure 3-29(d). Design C

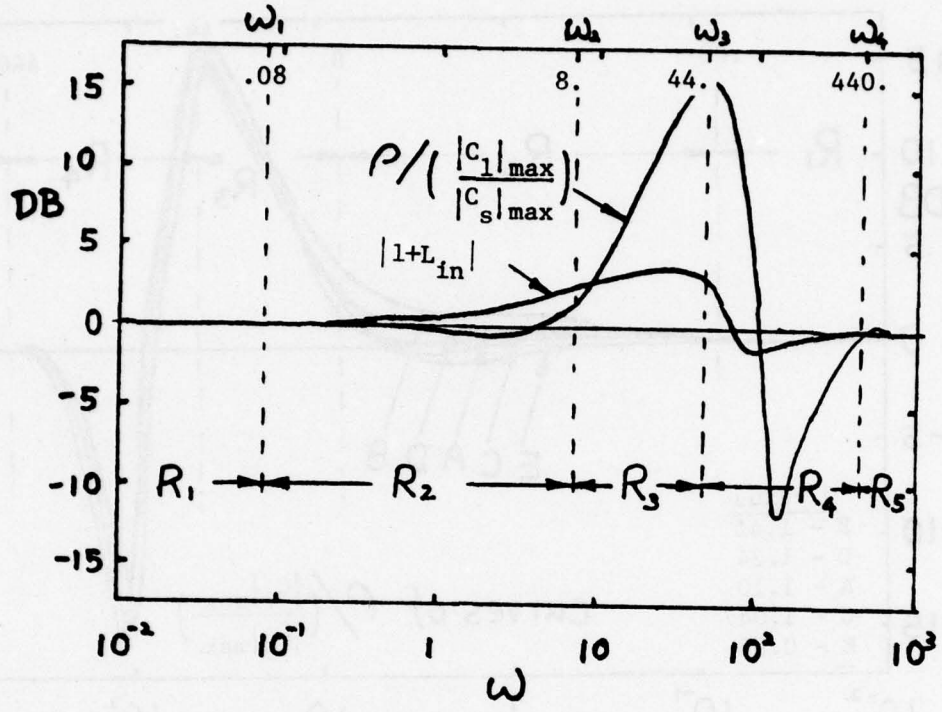

Figure 3-29(e). Design E

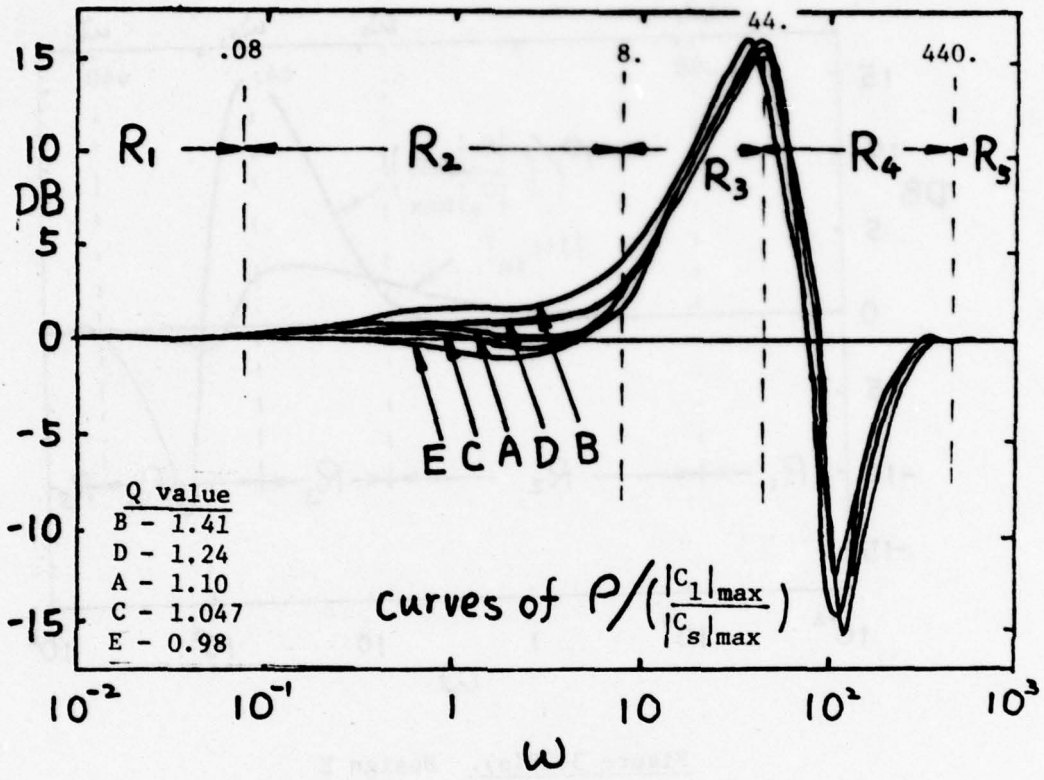

(f) Comparison of $\rho/(|C_1|_{max}/|C_s|_{max})$

Figure 3-29. Bode plots of $|1+L_{in}|$ and $\rho/(|C_1|_{max}/|C_s|_{max})$

The levels of L_{on} and L_{in} in R_3, R_4, R_5 in Figure 3-28, determine the sensor noise effect. The overall tendency of the effect of sensor noise depends on the levels of $|L_{on}|$, $|L_{in}|$ in R_3, R_4, R_5 relative to the corresponding value of $1./|P_1P_2|$ and $1./|P_2|$. The equations are derived in (3.7-3, 4) in section 3.7. The layer Q, the smaller the price that must be paid in $|L_{on}|$ in R_4, R_5. Obviously, the smaller L_{on}, L_{in} in R_3, R_4, R_5, the smaller is the sensor noise effect.

Note, in Figure 3-28, all L_{on} have 5 db hf overdesign. It is known that in the cascaded (no P.M.) design, some overdesign of L_{on} in this range, makes the design of L_{in} much easier. This is basically because $|L_{in}|_{max}$ can be thereby reduced. In a P.M. system, this is equivalent to shift L_{in} from AB'C'D'E in Figure 3-30 (with $|L_{in}|_{max}$ at $M_X' \approx 0$ db) to ABCDE. In our example, the design is 5 db, so $|L_{in}|_{max}$ is at $M_X \approx -5$ db. Note the corresponding $|1+L_{in}|$ value in Figure 3-30, is much smaller along ABC than AB'C'. Recalling section 3.5.5, one wants to start $L_{in}(j\omega)$ up sooner and raise A''' (see Figure 3-24), to achieve $|L_{in}|_{max}$ in a shorter ω range. Obviously, curve ABC in Figure 3-30 is better for this purpose than AB'C'.

3.7 Sensor Noise Effects

Recall the sensor noise effect is evident in hf range where the signal level and disturbance response are usually small. The noise transfer functions are as follows:

A. The single loop system--Figure 2-1, sensor N_1

$$T_{N_1}^2 \triangleq \frac{X_{21}}{N_1} = \frac{-G_s}{1+G_sP_1P_2} = \frac{L_s/P_1P_2}{1+L_s} \quad , \quad L_s \triangleq G_sP_1P_2$$

$$\approx -L_s/P_1P_2, \text{ in the hf range where } |L_s| << | \qquad (3.7\text{-}1)$$

$$T_{N_1}^1 \triangleq \frac{X_{11}}{N_1} = \frac{-G_sP_2}{1+G_sP_1P_2} = \frac{-L_s/P_1}{1+L_s}$$

$$\approx -L_s/P_1, \text{ in the hf range where } |L_s| << | \qquad (3.7\text{-}2)$$

The curve of $T_{N_1}^{2}$ is shown in Figure 3-32. And $T_{N_1}^{1} < 0$ db for all .

(B) The 2-loop, P.M. system--Figure 3-1 sensor N_1

$$T_{N_1}^{2} \triangleq \frac{X_{22}}{N_1} = \frac{-G}{1+P_1H_1+P_1P_2G}$$

$$= \frac{-G}{(1+L_i)(1+L_o)}, \quad L_i = P_1H_1, \; L_o = GP_2\frac{P_1}{1+L_i}$$

$$= \frac{-L_o/P_1P_2}{(1+L_o)}$$

$$\approx L_o/P_1P_2, \text{ in the hf range where } |L_o| << | \qquad (3.7\text{-}3)$$

$$T_{N_1}^{1} \triangleq \frac{X_{12}}{N_1} = \frac{-(GP_2+H_1)}{1+P_1H_1+GP_1P_2}$$

$$= \frac{-[L_o(1+L_i)/P_1+L_i/P_1]}{(1+L_i)(1+L_o)}$$

$$\approx (L_o/P_1+L_i/P_1) \text{ in the hf range where}$$

$$|L_i| << |, \; |L_o| << |$$

$$\approx L_i/P_1, \text{ in the hf range where } |L_o| << |L_i| \qquad (3.7\text{-}4)$$

The curves of $|T_{N_1}^{1}|$ and $|T_{N_2}^{2}|$ for the five different 2-loop, P.M. design are shown in Figure 3-31(a) in DB vs log ω and in Figure 3-31(b) in arithematical scale. In these figures Design E is the worst and B the best case, which is as it should be as the SLVR constraint in Design E is the toughest. This also can be seen directly from (3), (4) and Figure 3-28. In (3), (4), $|T_{N_1}^{1}|$ and $|T_{N_2}^{2}|$ depends on $|L_o|$, $|L_i|$ and $|P_1P_2|$, $|P_1|$. Since $|P_1P_2|$ and $|P_1|$

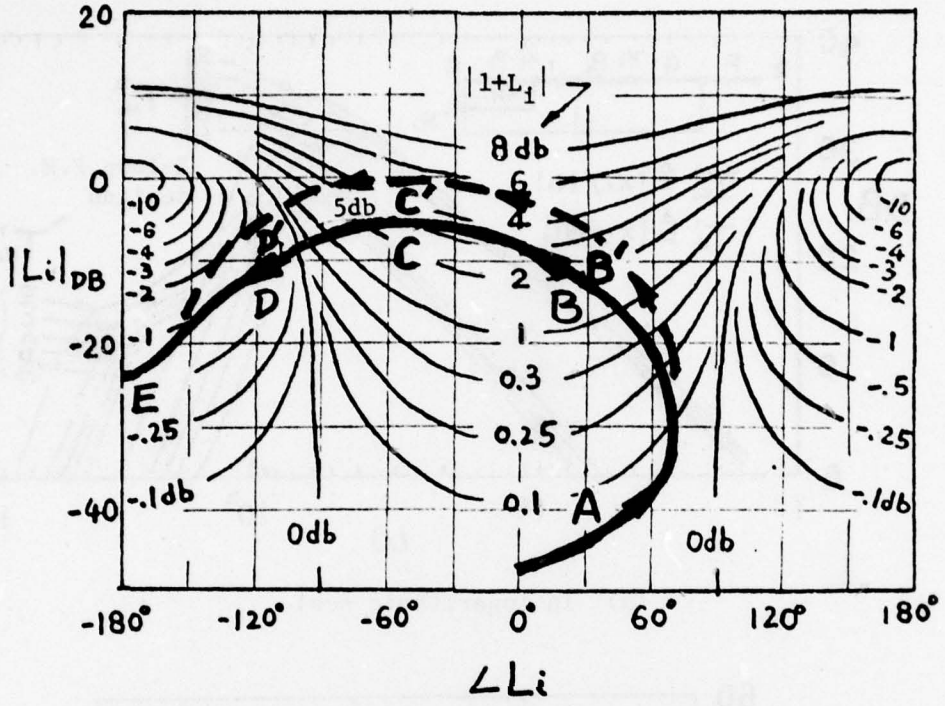

Figure 3-30. The result of hf overdesign on L_o

are the same in all designs, the values of $|L_o|$, $|L_i|$ determine $|T_{N_1}^1|$ and $|T_{N_1}^2|$.

Compare Design E with the single loop design in Figure 3-32 (a), (b). $T_{N_1}^1$ of signal loop <0 db for all ω, so it is not shown in Figures 3-32(a, b), but $T_{N_1}^1$ of Design E >0 db as shown in Figure 3-32(a, b). The single loop design is better than the 2-loop, P.M. design with respect to sensor noise effect at the input of P_1. However, with respect to the overall effect sensor noise, the two-loop system is better.

The principal reason is that it is the actual sensor noise effects at the inputs to P_2, P_1 which are important, not the

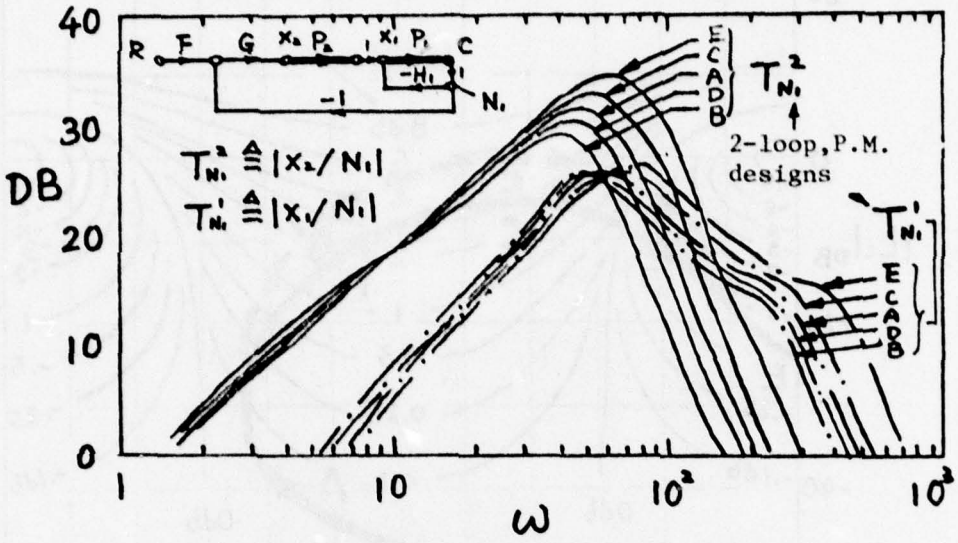

(a) In logarithmic scale

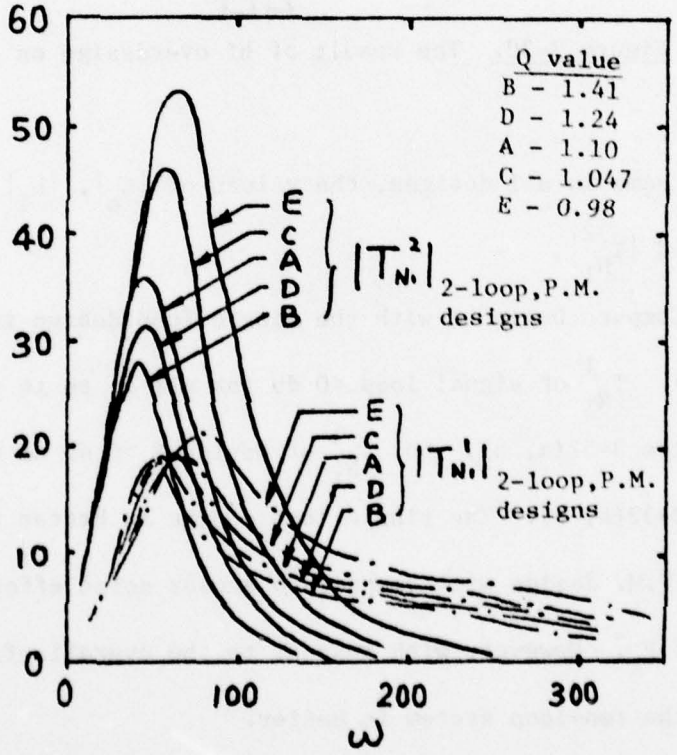

(b) In arithematical scale

Figure 3-31. Comparison of $T_{N_1}^1$, $T_{N_1}^2$ of 2-loop, P.M. system.

comparison between noise effect at X_{12} in the single two-loop designs. To illustrate this point, suppose that in the single-loop design, the effect at X_{22} (Figure 3-1) is given by a number 10, and at X_{12} it is .1, whereas the signal level capacity of X_{12} is of the same order of magnitude or even larger than that of X_{22}. Hence, it is the noise at X_{22} which may render the design impractical. The noise effect at X_{12} is insignificant. Now, in the two-loop design, suppose the effect of X_{22} is 2 and at X_{12} it is .5 (five times that in the single-loop design). The two-loop design is obviously considerably superior. Thus, the two important ratios are $\frac{T_{N_1}^{2}\ (2\text{-loop})}{T_{N_1}^{2}\ (1\text{-loop})}$ and $\frac{T_{N_1}^{1}\ (2\text{-loop})}{T_{N_1}^{2}\ (1\text{-loop})}$. $\frac{T_{N_1}^{1}\ (2\text{-loop})}{T_{N_1}^{1}\ (1\text{-loop})}$ is not important.

The above is precisely the situation here. $C_{22} = X_{22}P_2$ and in the relatively low control signal frequency range, $|P_2|>1$ generally in this range, or at least ~1, so $|C_{22}|\geq|X_{22}|$. Hence, the signal level capacity (i.e., which the output stage there can comfortably handle) at C_{22} must be $\geq$ that at X_{22}. In the single-loop design $|T_{N_1}^{2}|$ is enormous (see Figure 3-32) while $|T_{N_1}^{1}|<1$. In the two-loop design $|T_{N_1}^{2}|$ is considerably reduced, while $|T_{N_1}^{1}|>1$ but still small relative to $|T_{N_1}^{2}|_{2\text{-loop}}$ and certainly very small compared to $|T_{N_1}^{2}|$. Hence, the 2-loop design is decidedly better in terms of overall system performance. It will be seen in

chapter 4 that this superiority is considerably increased if another loop is added around P_2.

3.8 Trade-off between Q and Sensor Noise Effect

The results of six different 2-loop P.M. designs, ISLV, B, D, A, C, E are shown in Figure 3-33. The total noise effects at X_{12} and X_{22} (in Figure 3-1) are calculated by means of $\int_0^\infty |T_{N_1}^1|^2 (\Phi_{N_1})^2] d\omega$ and $\int_0^\infty |T_{N_1}^2|^2 (\Phi_{N_1})^2] d\omega$ respectively, where $T_{N_1}^1$, $T_{N_1}^2$ are defined in (3.7-3, 4) and Φ_{N_1} is the noise spectrum of sensor N_1, taken as a uniform distribution ($\Phi_{N_1} = 0.001$). In Figure 3-33, the two curves give the relations between Q and sensor noise power response at X_{12}, X_{22}. These are useful for giving the designer a feeling for the trade-off between signal level and

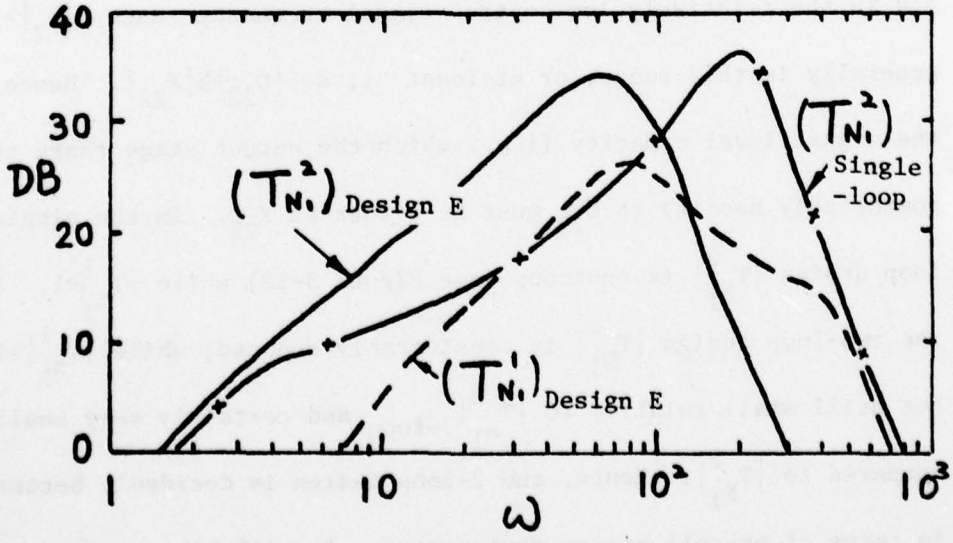

(a) In logarithmic scale

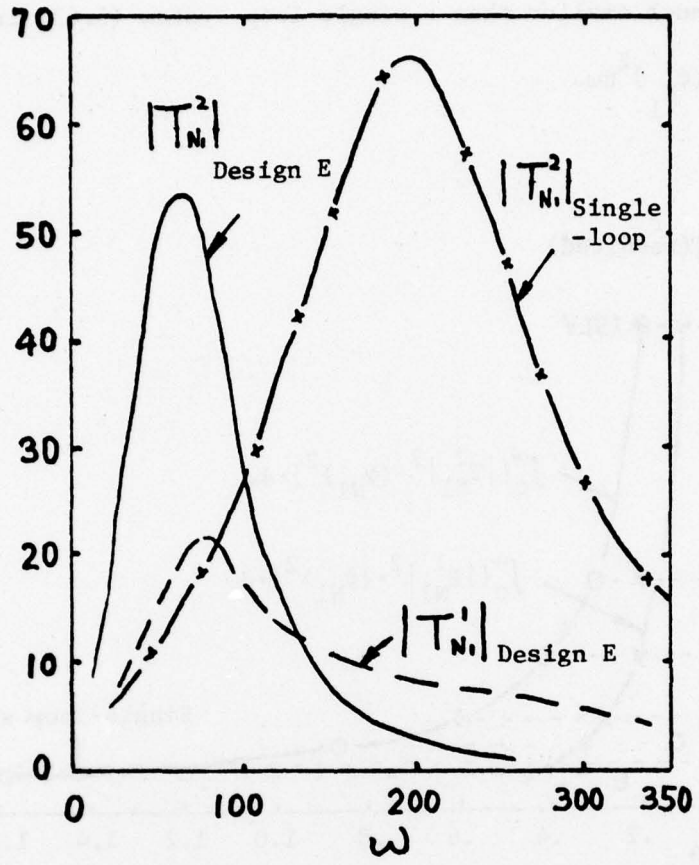

(b) In arithematical scale

Figure 3-32. Comparison of $|T_{N_1}^1|$, $|T_{N_1}^2|$ between single-loop system and 2-loop, P.M. system, Design E.

noise effect. Of course, Design ISLV is the best one in sensor noise effect, but Q is rather high (=1.96). In Design B, the noise is a little larger than in ISLV but the improvement in Q is fairly large. In Design E, Q is excellent (=0.98) but the noise is significantly more than in Design C with its Q = 1.047. It is again emphasized that even in Design E with Q<1, the noise response (1.59)

is still much smaller than a single loop system (5.63) in

$\int_0^\infty [|T_{N_1}^2|^2 (\Phi_{N_1})^2 d\omega$.

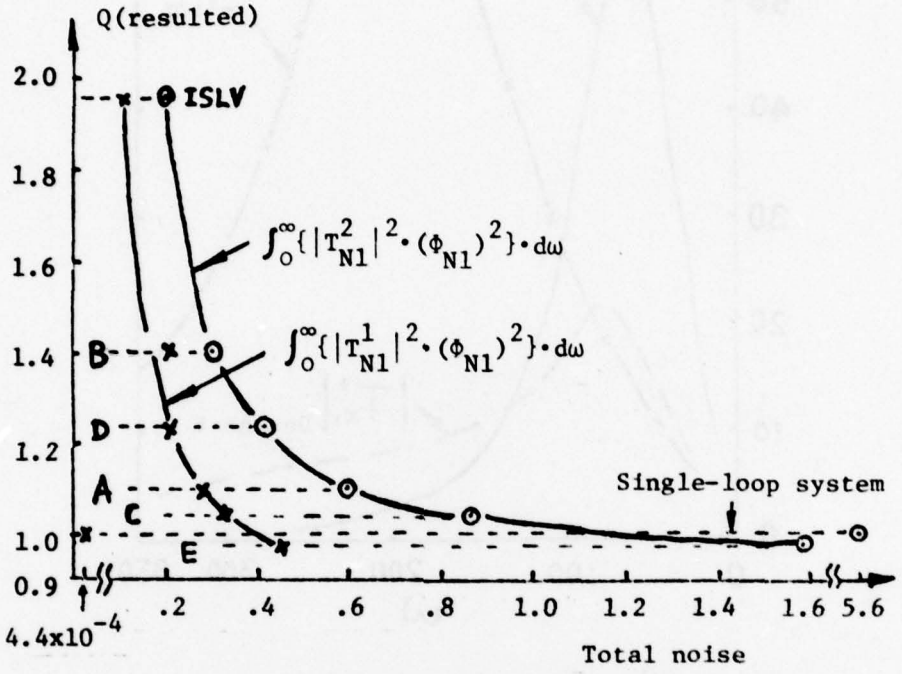

Figure 3-33. Trade-off between Q and sensor noise effect.

3.9 Comparison of Noise Effect between the 2-loop, P.M. System and the Cascaded, 2-loop, no P.M. System.

For a system with 2 plant sections, if the design is restricted to 2 loops, there are two options: One is the cascaded, 2-loop, no P.M. system (Figure 3-34(b)), the other one is the 2-loop, P.M. system (Figure 3-34(a)). Suppose the choice of structure is dependent on the savings of sensor noise effect which

means ignoring the fact that the 2-loop no P.M. design requires two sensors instead of one. A fairer comparison is therefore the 3-loop P.M. design in chapter 4 which uses two sensors of the 2-loop no P.M. design.

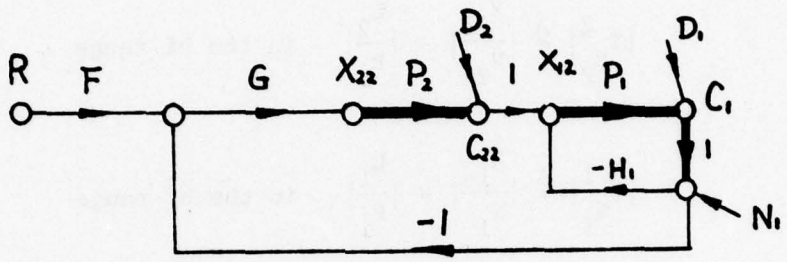

(a) 2-loop, P.M. system

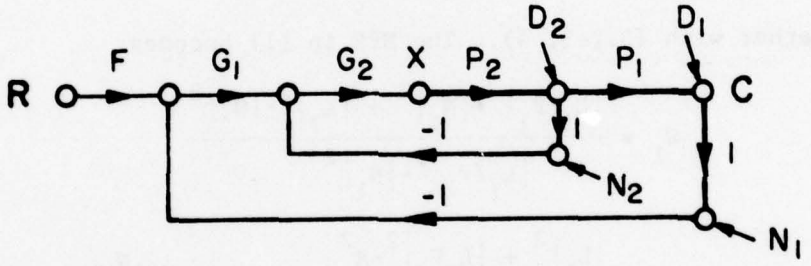

(b) Cascaded, 2-loop, no P.M. system

Figure 3-34. 2-loop systems.

The noise power ratio (N.P.R.) W_i is defined as the ratio of total noise power in the cascaded, 2-loop, no P.M. system to that of the 2-loop, P.M. system,

$$W_i = \frac{|X_{ic}/N_1|^2 \cdot |N_1|^2 + |X_{ic}/N_2|^2 \cdot |N_2|^2}{|X_{12}/N_1|^2 \cdot |N_1|^2} \qquad (3.9\text{-}1)$$

Since the noise response of a cascaded, 2-loop, no P.M. system is (see Figure 1-15(a) and (1.4-6))

$$|T_{N_1}^{2}| \triangleq |\frac{X_{2c}}{N_1}| \approx |\frac{L_1}{P_1 P_2}| \text{ in the hf range} \tag{3.9-2}$$

$$|T_{N_2}^{2}| \triangleq |\frac{X_{2c}}{N_2}| \approx |\frac{L_2}{P_2}| \quad \text{in the hf range} \tag{3.9-3}$$

$$|T_{N_1}^{1}| \triangleq |\frac{X_{1c}}{N_1}| \approx |\frac{L_1}{P_1}| \quad \text{in the hf range} \tag{3.9-4}$$

$$|T_{N_2}^{1}| \triangleq |\frac{X_{1c}}{N_2}| \approx |L_2| \quad \text{in the hf range} \tag{3.9-5}$$

together with (3.7-3, 4). The NPR in (1) becomes

$$W_1 = \frac{|L_1/P_1|^2 \cdot |N_1|^2 + |L_2|^2 \cdot |N_2|^2}{|L_i/P_1|^2 \cdot |N_1|^2} \tag{3.9-6}$$

$$= \frac{|L_1|^2 + |L_2 P_1|^2 \cdot R^2}{|L_i|^2}, \text{ where } R \triangleq |\frac{N_2}{N_1}| \tag{3.9-7}$$

$$W_2 = \frac{|L_1/(P_1P_2)|^2 \cdot |N_1|^2 + |L_2/P_2|^2 \cdot |N_2|^2}{|L_o/(P_1P_2)|^2 \cdot |N_1|^2} \tag{3.9-8}$$

$$= \frac{|L_1|^2 + |L_2 P_1|^2 \cdot R^2}{|L_o|^2} \tag{3.9-9}$$

Figures 3-35, 36 give graphs $W_2(\omega)$, $W_1(\omega)$ for different values of R, $|P_1|$, using the design results of the cascaded, 2-loop system in section 3.4.3 and Design A for the 2-loop, P.M.

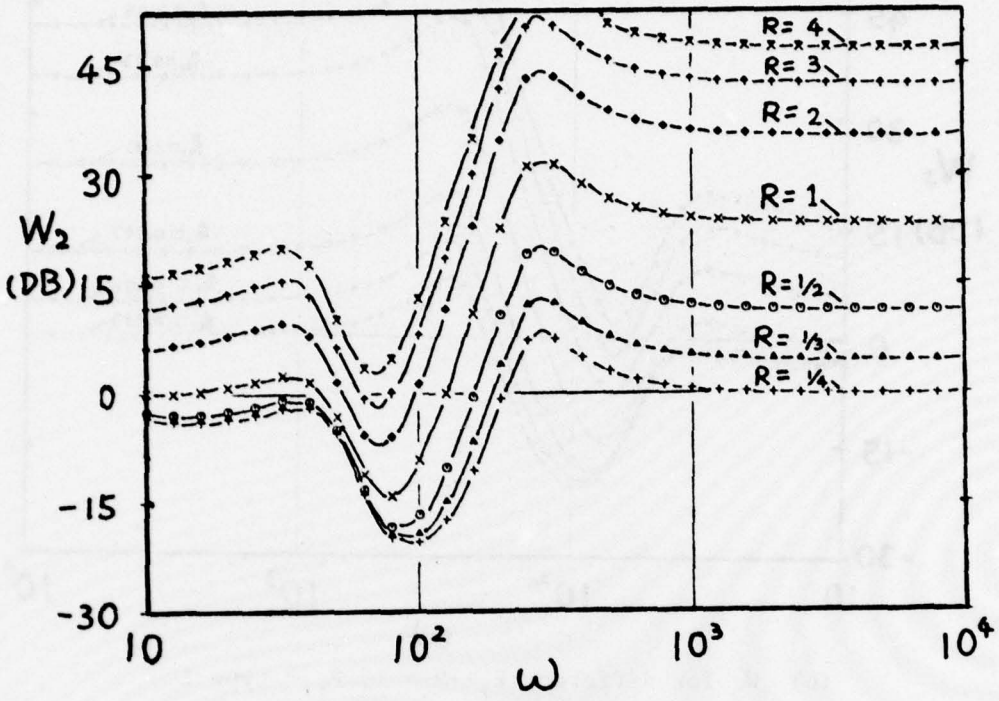

(a) W_2 for different R--P_1 = type I, k_1 = 1

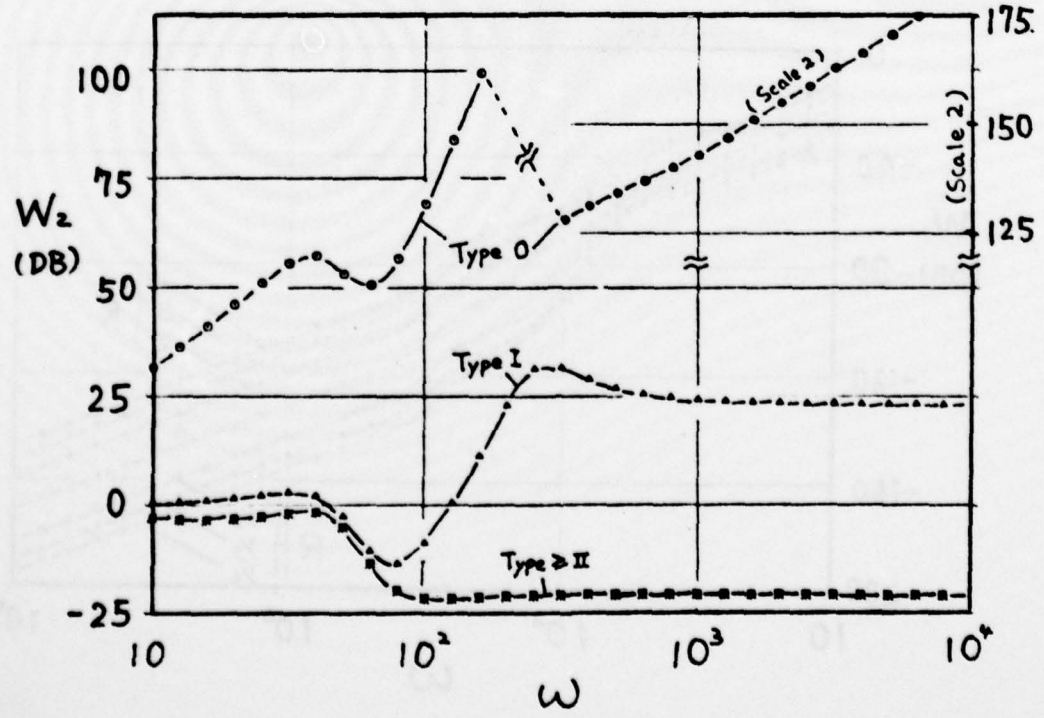

(b) W_2 for different type number of P_1--R = 1, k_1 = 1

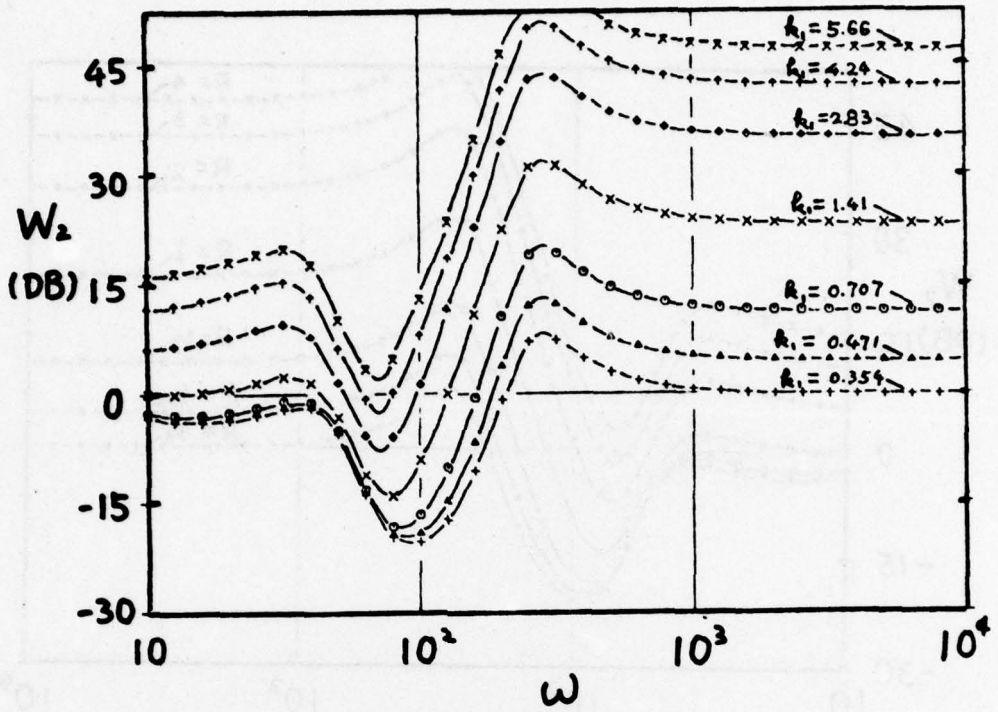

(c) W_2 for different k_1--R = 1, P_1 = type I

Figure 3-35. The noise power ratio at X_2

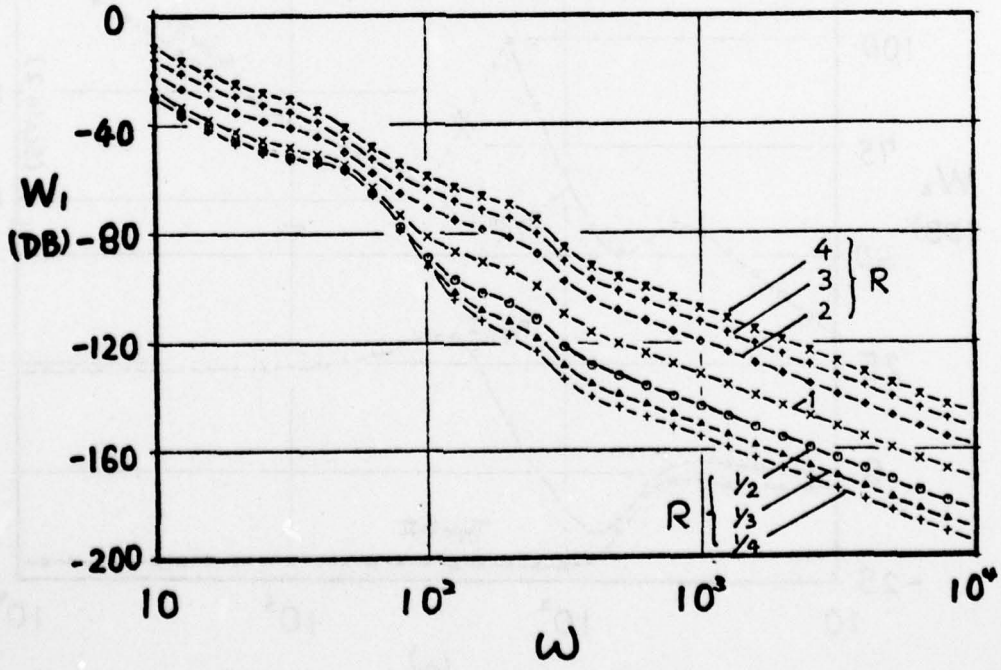

(a) W_1 for different R--P_1 = type I, k_i = 1

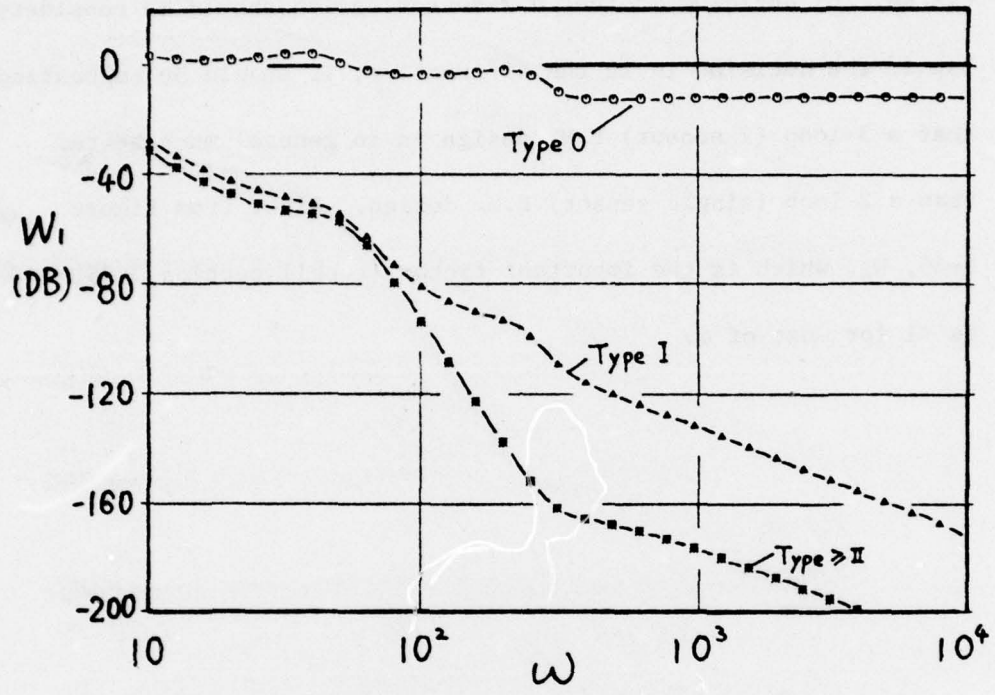

(b) W_1 for different type number of P_1--R = 1, k_1 = 1

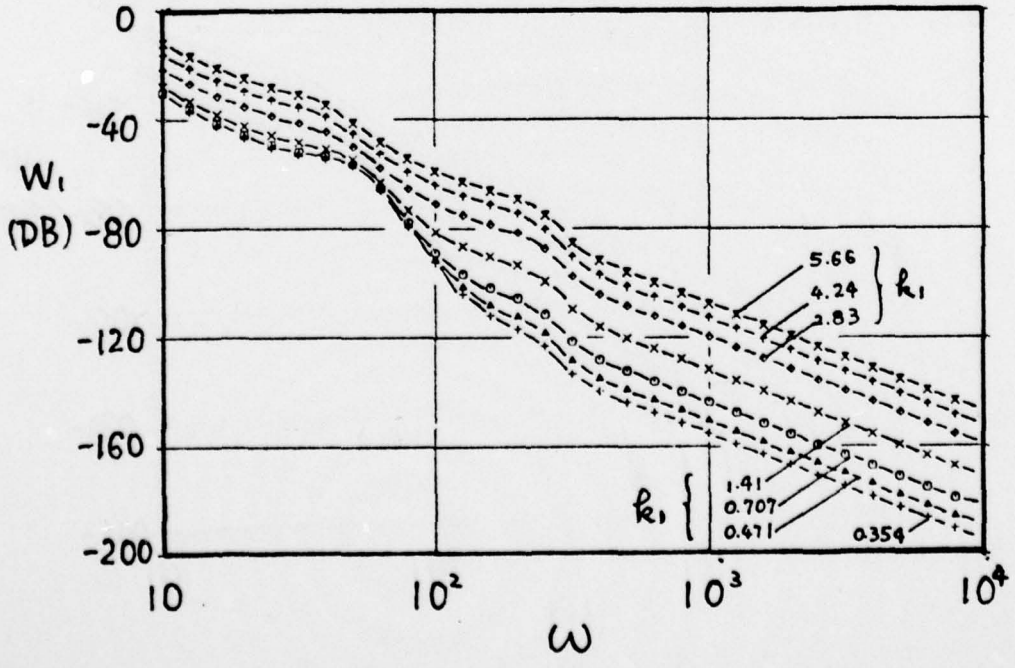

(c) W_1 for different k_1--P_1 = 1, P_1 = type I

Figure 3-36. The noise power ratio at X.

system, for deciding whether a 2-sensor design should be considered. But if the decision is in the affirmative, it should be emphasized that a 3-loop (2 sensor) P.M. design is in general much better than a 2-loop (single sensor) P.M. design. Also, from Figure 3-35, W_2, which is the important factor (recall section 3.7), is <1 for most of ω.

CHAPTER 4

MULTIPLE-LOOP P.M. SYSTEM SYNTHESIS

4.1 Introduction

Chapter 3 dealt with the simple P.M. structure for the two-section (P_1, P_2) cascade plant. A more general structure for this 2-section case admits three feedback loops--one from C_{23} to X_2 in Figure 4-1 may be added. To determine the most general feedback structure, observe that no feedforward loops are allowed (i to i+1 in Figure 4-2), other than in the original plant in Figure 4-2. In this research we consider only structures in which there are no crossings of lines when the feedback loops are all drawn below (or all above) the plant, e.g., in Figure 4-3(a) feedback from output of P_1 to input of P_2 is not allowed because such a line would cross the present one from P_2 output to P_4 input. How many different structures are possible? We shall assume that in each structure there is a local feedback loop around each plant section and one from n to 0 in Figure 4-2, as these do not prevent any other loops.

Let S_n be the number of structure for the n-section of Figure 4-2. Either there is a loop from node n to node 1, or there isn't. If there is one, the remainder on the right forms

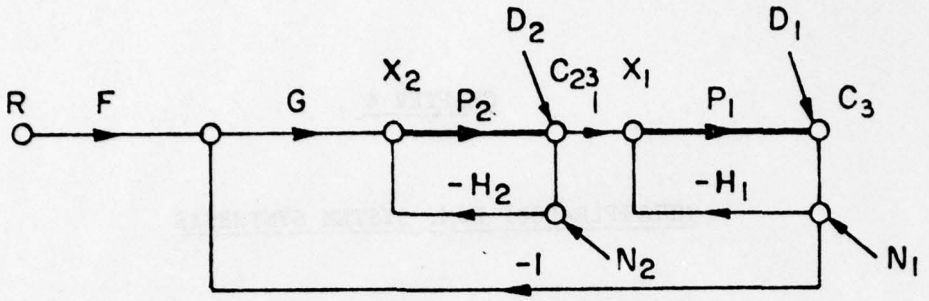

$$L_o \triangleq G\,P_{1e}P_{2e},\quad P_{1e} \triangleq \frac{P_1}{1+L_{i1}},\quad P_{2e} \triangleq \frac{P_2}{1+L_{i2}},\quad L_{i1} \triangleq P_1H_1,\quad L_{i2} \triangleq P_2H_2$$

Figure 4-1. 2-plant, 3-loop, P.M. system

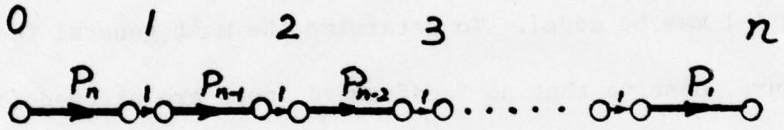

Figure 4-2. n stage cascaded-plant

an n-1 section with number S_{n-1}. The remainder on the left has only one section giving S_1 possibilities with a total of $S_{n-1} \times S_1$. If there isn't one from n to 1, there are two possibilities: Either there is one from n to 2, or there isn't. If there is one, then the remainder on the right is a n-2 section with S_{n-2} and on the left a 2-section giving S_2, with a total of $S_{n-2} \times S_2$. If there isn't one from n to 2, there are two possibilities: Either there is one from n to 3, or not. If there is one, the remainders on the right and left are respectively n-3 and 3, giving

AD-A059 564 COLORADO UNIV BOULDER DEPT OF ELECTRICAL ENGINEERING F/G 12/2
SYNTHESIS OF MULTIPLE-LOOP FEEDBACK SYSTEMS WITH PLANT MODIFICA--ETC(U)
AUG 78 B WANG, I HOROWITZ AFOSR-76-2946

UNCLASSIFIED AFOSR-TR-78-1341 NL

3 OF 3
AD
A059 564

END
DATE
FILMED
-12-78
DDC

$S_{n-3} \times S_3$, etc. Thus, in an n-section with no "feedback crossings," for n>2

$$S_n = S_{n-1} \times S_1 + S_{n-2} \times S_2 + \ldots + S_{n-2} \times S_2 + S_{n-1} \times S_1$$

with $S_1 \triangleq 1$, $S_2 \triangleq 1$. Hence, $S_3 = 2$, $S_4 = 5$, etc. The five cases of n=4 are shown in Figure 4-3.

Maximum number of loops

Each of the possible structures has a maximum of 2n-1 feedback loops, proven as follows. In every structure, local feedback loop (i to i-1) is possible for each section without interfering with any other feedback loop, so each structure has these n local loops. Consider the structure in which every section except the first in Figure 4-2 (for which is extraneous), also feeds back to the plant input 0, giving an additional n-1 loops, making a total of 2n-1 loops. Obviously, no more loops are possible without crossing.

Let us hypothesize that the maximum number of loops for a plant with n-1 cascaded sub-plants is independent of the specific structure used, so is a constant = 2(n-1)-1 and that this is true for each of n=1, 2, ... up to n-1. We will prove that it is true for a plant with n cascaded sub-sections. Take any sub-section structure whatsoever and give it its initial n local loops. Starting from the plant input 0, proceed to the right in Figure 4-4, until the first point, say n_1, is reached which has at least one

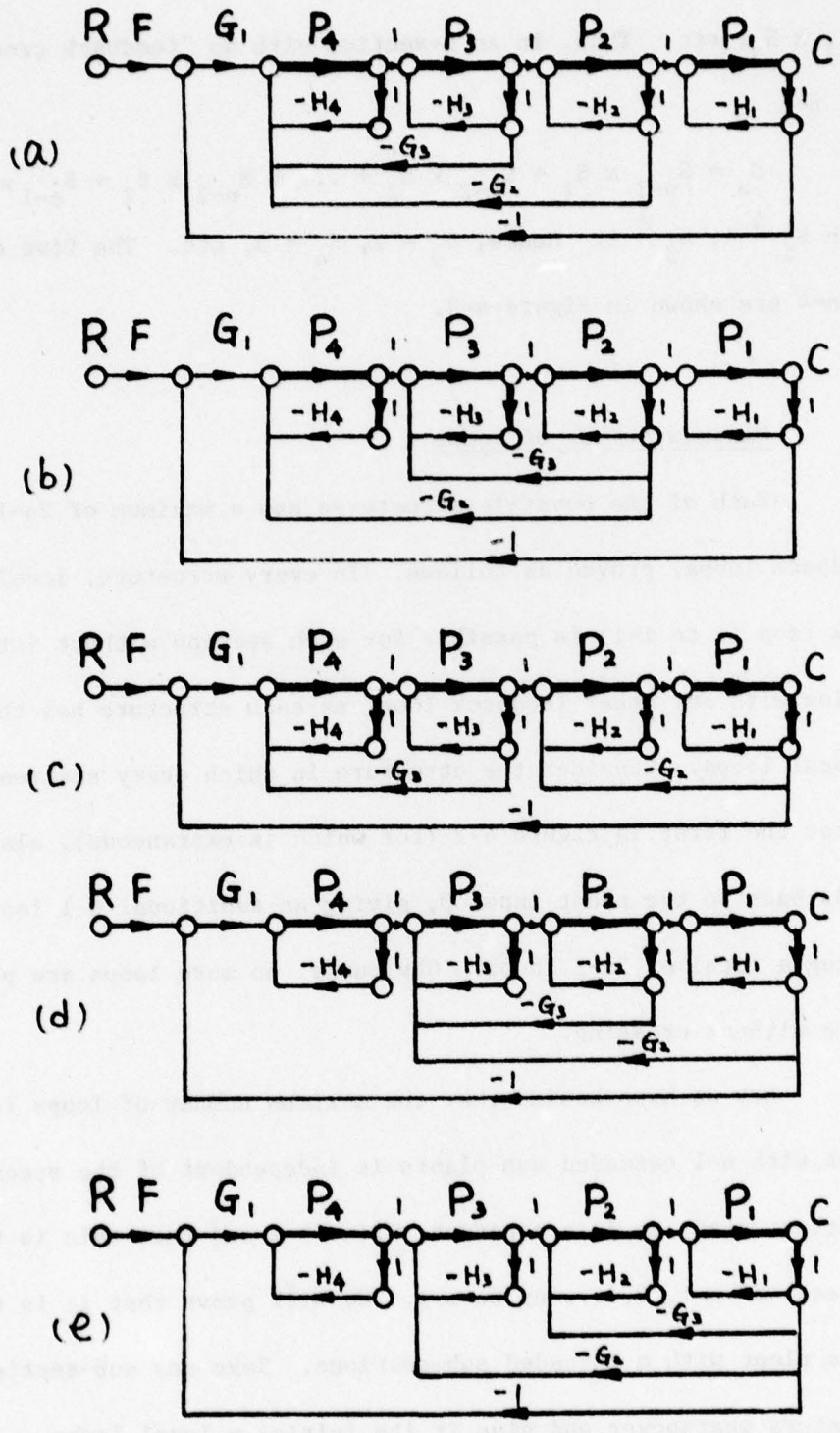

Figure 4-3. 5 different cases of 2n D.O.F., 4-plant, 7-loop, P.M. system

loop (other than from n+1) feeding into point n_1. There will be a loop from n_1 to 0 because there is nothing preventing it. Proceed forward (to the right) from n_1 until the last point is reached which has a feedback loop terminating on n_1. By hypothesis there must be at least one such point. Let this be point $n_2 > n_1$ (of course). The part from n_1 to n_2 can be considered as "semi-isolated" (n_2-n_1) structure with a maximum total of $\eta_{n_2-n_1}$ loops, because there can be no loop from any point inside reaching outside or vice versa without crossing the loop from n_2 to n_1.

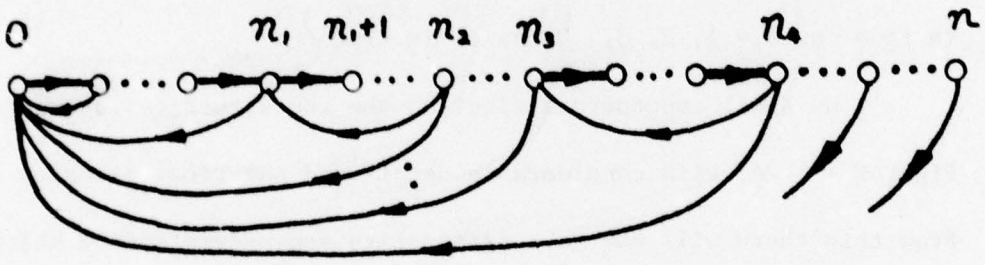

Figure 4-4. No crossing multiple loop system.

Now work backwards from the last point n until the first point n_4 (Figure 4-4) is reached which has at least one loop feeding back to some $n_3 \neq 0 (n_3 < n_4 - 1)$ in addition to 0. If n_4 has more than one, take that one furthest away (to the left) from n_4. Note that $n_3 > n_2$ by hypothesis because no crossing is allowed. The part from n_3 to n_4 also forms a "semi-isolated" multiple-loop system with

$\eta_{n_4-n_3}$ maximum loops. Let us now count the total loops. By hypothesis $\eta_{n_4-n_3} = 2(n_4-n_3)-1$, $\eta_{n_2-n_1} = 2(n_2-n_1)-1$. The number of loops from the first n_1 sub-plants (from 0 to n_1) is: n_1 local (i to i-1) and n_1-1 (2 to 0, 3 to 0, ..., n_1 to 0), giving a total of = $2n_1-1$. The number of loops from the part consisting of plant sections from n_2 to n_3 is: n_3-n_2 local and $n_3-n_2 + 1$ to 0 (i.e., from n_2, n_2+1, ..., n_3 each to 0), totalling $2(n_3-n_2)+1$. Finally the number from the sub-plants from n_4 to n is: $n-n_4$ local and $n-n_4+1$ (i.e., from n_4, n_4-1, ..., n to 0), totalling $2(n-n_4)+1$. Adding all of these gives 2n-1. It is easy to prove the hypothesis is true for n = 1, 2, 3. *Hence it is true* $\forall n$.

We shall concentrate first on the two structures shown in Figures 4-1,24, with considerable detail and numerical examples. From this there will emerge a perspective and understanding which will enable us to tackle any non-crossing structure. In fact it will be possible to know in advance, without a detailed design, a great deal about the design problem--just as in the cascade no P.M. design approach (recall section 1.5).

4.2 The 2-plant, 3-loop, P.M. system

4.2.1 Design perspective (Figure 4-1).

The important design factors are the increase in signal level of C_{23} and the effects of sensor noise sources N_1, N_2 at X_2

and X_1. As in chapter 3, the former is controlled by careful design of L_{i1}^{ρ} (i.e., L_{i1} in the lf range), although the actual relation between Q and Q_c (of Figure 3-23) is different in the 3-loop case (see section 4.3.9). Just as in chapter 3, L_{i1} can handle the P_1 uncertainty problem in the hf range, with the help of some safety margin in the IVJ region of Figure 1-8 (5 db was used in chapter 3; recall Figures 3-10, 16). But now $L_{i2} = P_2H_2$ is available to remove the burden of P_2 uncertainty from L_o. Thus, except for the (5 db) safety margin in the IVJ region of Figure 1-8, L_o need handle no hf uncertainty at all and only P_{1e} lf uncertainty. One more point, however, this safety margin can be divided between L_{i1} and L_{i2}. This relative strengths of N_1, N_2 and the dynamic ranges of the stages at X_2, C_{23} influence the way the division should be made. Our objective is to give the designer the perspective and understanding of the trade-offs to enable him to make an intelligent choice.

4.2.2 Specifications on numerical examples

Plant: $P = P_1P_2$, $P_i = k_i/s$

Plant uncertainty: $\sqrt{2} \leq k_1 \leq 10\sqrt{2}$, $\sqrt{2} \leq k_2 \leq 10\sqrt{2}$ independently

Bounds on $|T(j\omega)|$: shown in Figure 3-2(b) were originally derived from time domain bounds of Figure 3-2(a)

Disturbance Response: $\gamma \leq 2.0$ db

(All above are the same as in sections 1.2.5, 3.3.1)

System structure: as shown in Figure 4-1,

Restruction on signal level: $Q \leq 1.28$ for unit step input

(The rational function values of the compensation functions in Figure 4-1 are given in Appendix II)

4.2.3 Single and cascaded, 2-loop, no P.M. design

Since the first half of the specifications in section 4.4.1 are the same as in sections 1.2.5, 3.3.1, so the single loop and cascaded 2-loop, no P.M. designs of sections 3.4.2, 3, are valid here.

4.2.4 The P.M. inner loop $L_{i1} = P_1 H_1$

The choice of $|1+L_{i1n}|$ (for $Q = 1.28$) is made in accordance with the philosophy of chapter 3, section 3.5, resulting in Figure 4-5. The inner loop bounds $B^{\rho}_{Li1}(\omega)$ in the lf range and the resulting L_{i1n} are shown in Figure 4-6.

4.2.5 Design of L_{on}

Following section 3.3.8, templates of $P_{1e} \triangleq P_1/(1+L_{i1})$ in R_1, R_2 are obtained and shown in Figure 4-7. As the uncertainty in P_2 will be handled by $L_{i2} = P_2 H_2$, only P_{1e} uncertainty need be

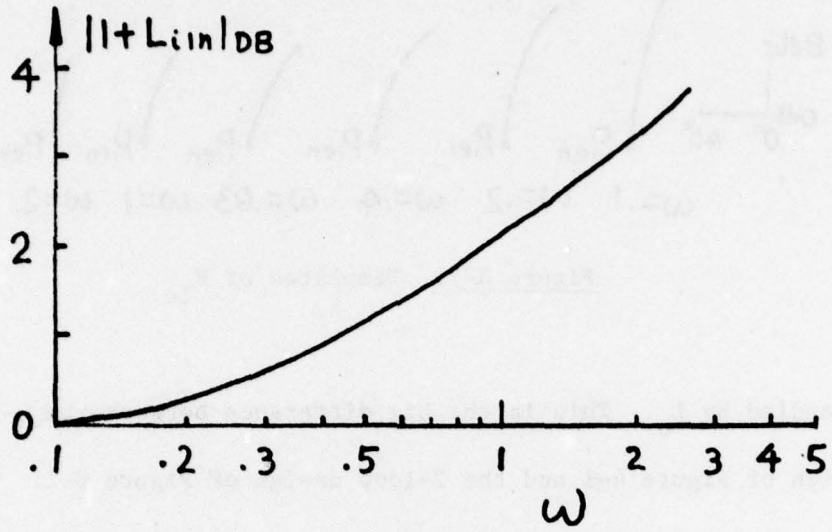

Figure 4-5. The criterion on $|1+L_{iln}|_{DB}$

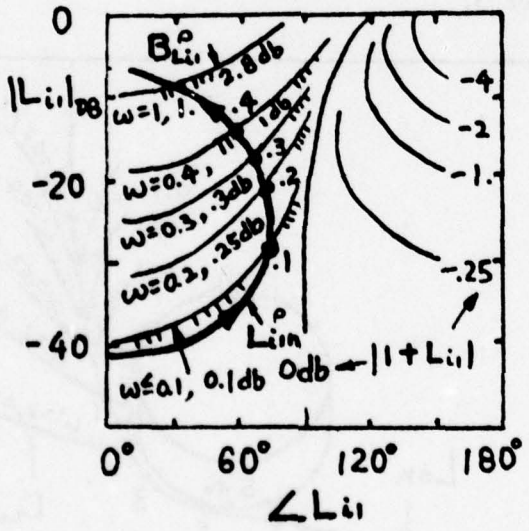

Figure 4-6. L_{iln}^{ρ} with bounds $B_{Lil}^{\rho}(\omega)$

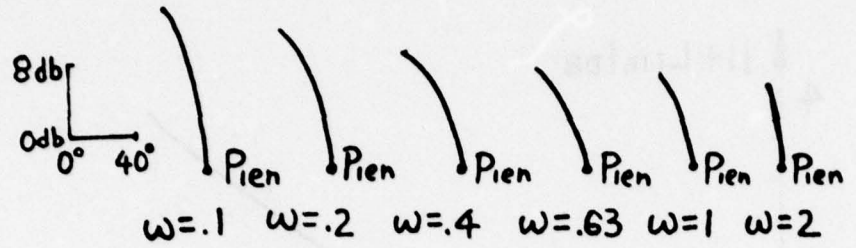

Figure 4-7. Templates of P_{1e}

handled by L_o. This is the big difference between the 3-loop design of Figure 4-1 and the 2-loop design of Figure 3-1. Bounds $B_{L_o}(\omega)$ due to P_{1e} in R_1, R_2, are shown in Figure 4-8. With 5 db hf overdesign, L_{on} is designed to satisfy $B_{L_o}(\omega)$ and is shown in Figure 4-8. All above procedures are the same as in 2-loop, P.M. design in chapter 3.

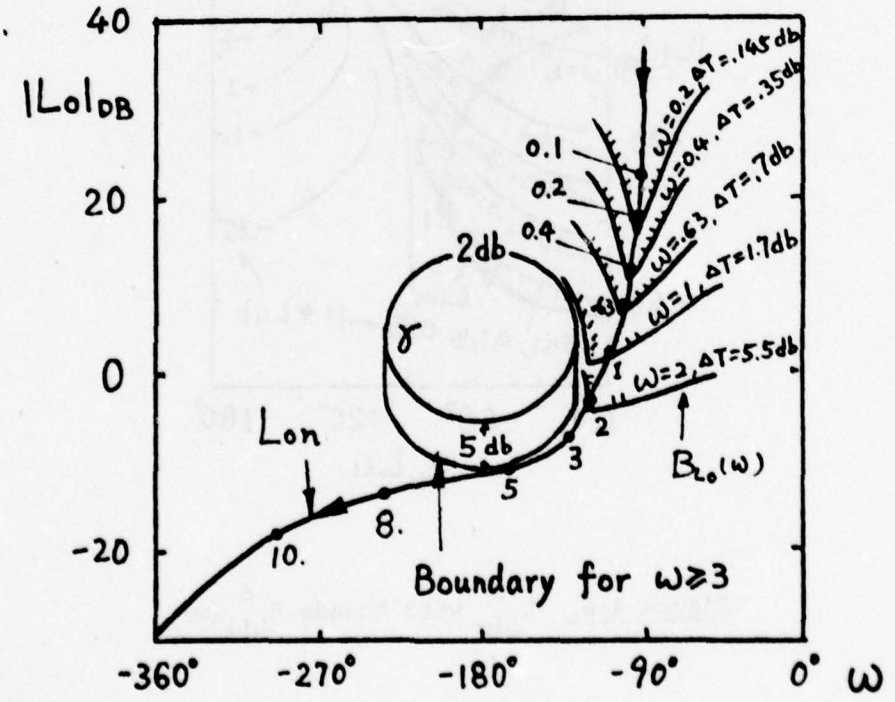

Figure 4-8. $B_{L_o}(\omega)$ and L_{on}

4.2.6 Determination of $B_{L_{i1}}(\omega)$ in R_3, R_4, R_5 and completion of L_{in}

If we follow section 3.3.8 precisely, we would find $B_{L_{i1}}(\omega)$ the bounds on L_{i1}, such that L_{on} remains satisfactory despite the hf uncertainty in P_{1e}. This is done in Figures 4-9(a, b). The next step would be design of L_{i1} followed by finding $B_{L_{i1}}(\omega)$ the bounds on L_{i2}, such that the design of L_o remains satisfactory despite the uncertainty in P_2. But in such a procedure, we do not consider L_{i2} when we design L_{i1}. This increases the burden on L_{i2}, especially for some frequency ranges.

Figure 4-10(a) shows L_{on} and $\mathcal{T}_{1e}$ which are templates of $L_o(j\omega)$ at several ω values due to P_{1e} uncertainty only, with P_2 fixed at P_{2n}, i.e., templates of $P_{2en} G P_{1e}$. In the "hf" range ($\omega \geq 4$), γ is the forbidden region for $L_o = G P_{1e} P_{2e}$. Suppose the template of P_{2e} is that shown in Figure 4-10(b)) (it is so because at this hf range $L_{i2} < 0$, specifically at $\omega = 18$, $L_{i2n} = -10\text{db}\ \underline{-150^o}$). At $\omega = 5$, the template of $L_o = G P_{1e} P_{2e}$ remains satisfactory. But at $\omega = 12$, it is definitely not satisfactory because it violates the bound $\gamma = 2$ db. Thus, for $\omega \in [6, 20]$ in Figure 4-10(a), there is not much margin of uncertainty left for P_{2e}. To remedy this, we restrict the range of the templates of $G P_{2en} P_2$ as shown in Figure 4-11, instead of that in Figure 4-10(a). This makes it harder, of course, on L_{i1} and easier on L_{i2} in this range. Thus,

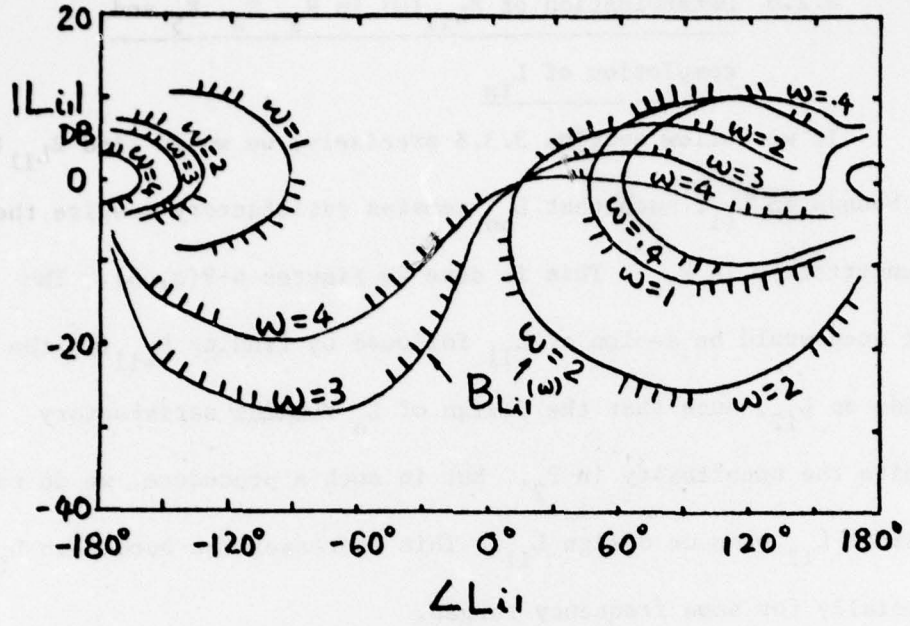

(a) Bounds for $\omega \leq 4$

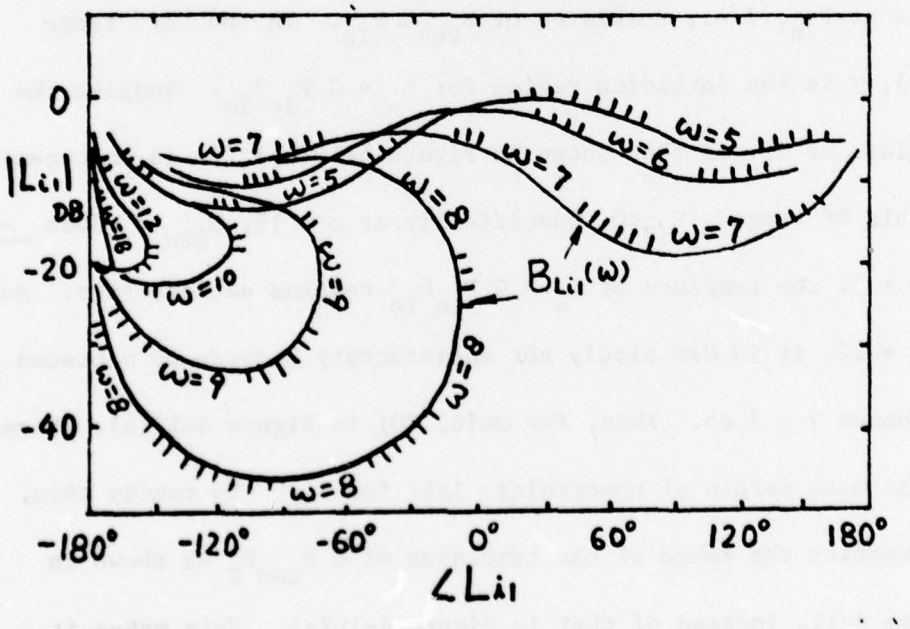

(b) Bounds for $\omega \geq 5$

Figure 4-9. Bounds on L_{il}

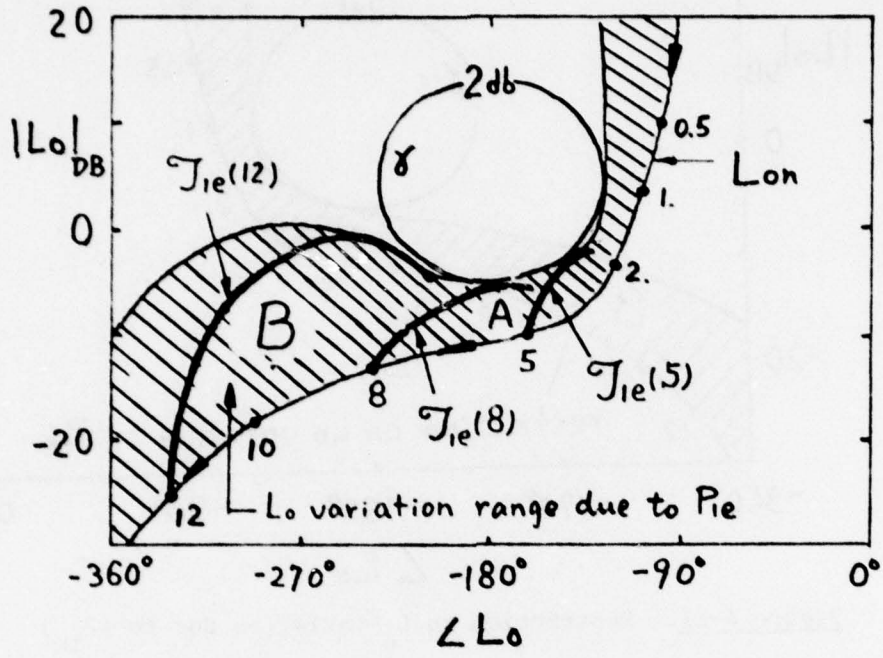

Figure 4-10(a). L_o variation range due to $\{P_{1e}\}$

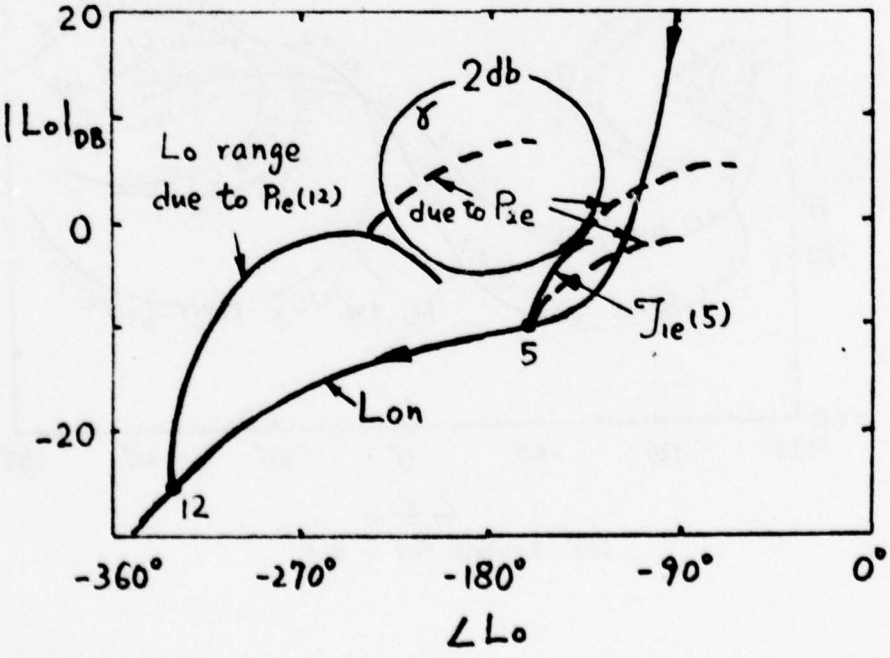

Figure 4-10(b). L_{on} and range of L_o due to $\{P_{1e}\}, \{P_{2e}\}$

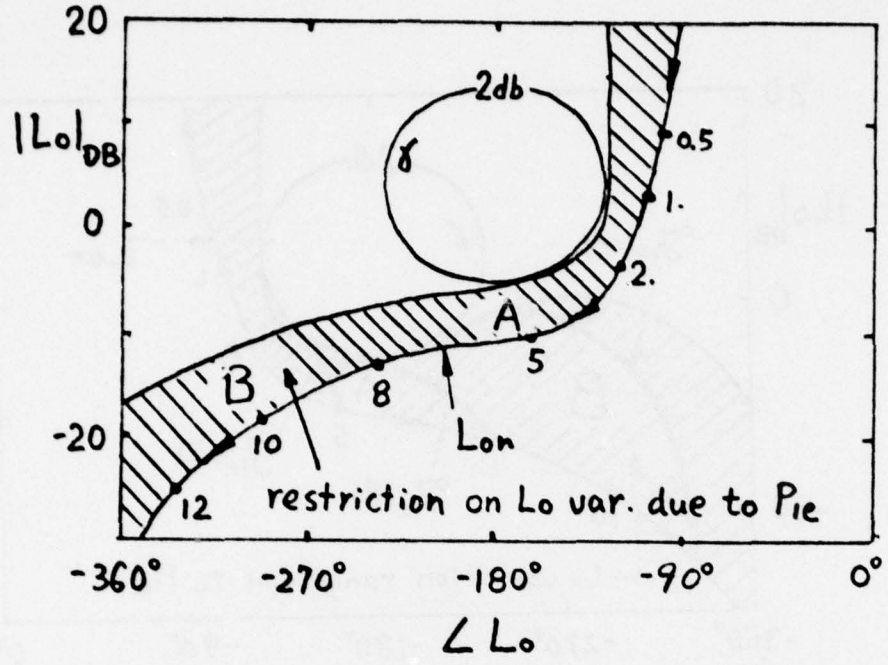

Figure 4-11. Restriction on L_o variation due to $\{P_{le}\}$

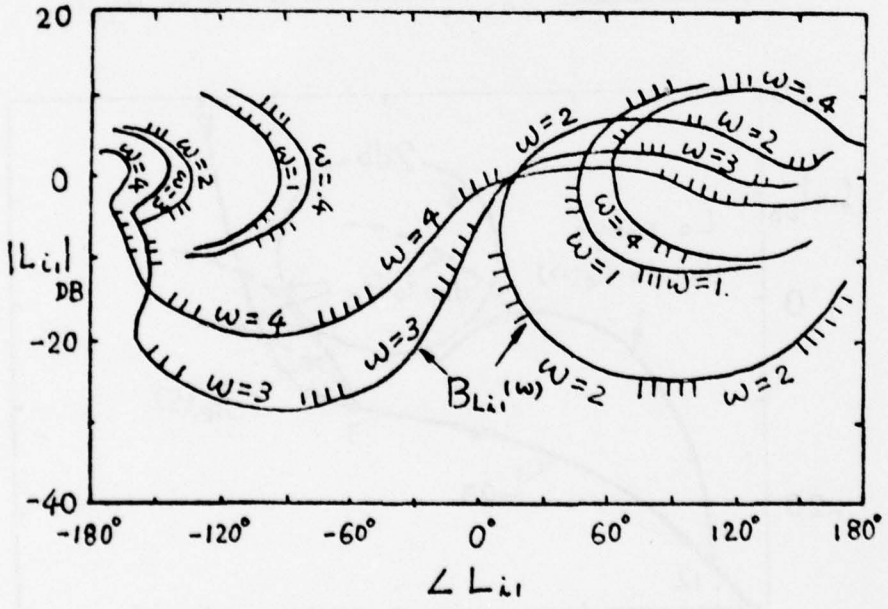

(a) Bounds for $\omega \leq 4$

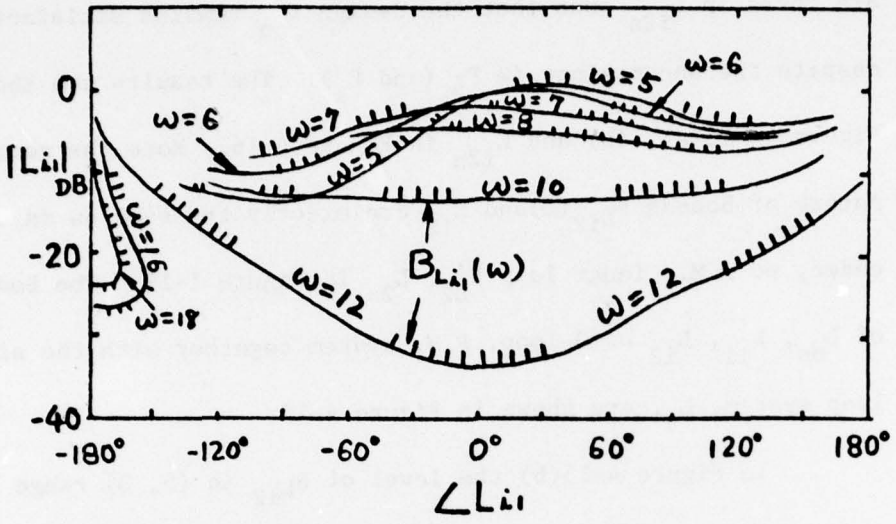

(b) Bounds for $\omega \geq 5$

Figure 4-12. Bounds on L_{i1}

compare $B_{L_{i1}}$ in Figures 4-9(a), (b) giving Figure 4-10(a) and the $B_{L_{i1}}$ of Figures 4-12(a), (b) due to Figure 4-11. There is no difference between Figures 4-9(a) and 4-12(a), because the modification in Figure 4-11 is for $\omega>6$ approximately, but there is a definite difference between Figures 4-12(b) and 4-9(b). L_{i1} is next designed to satisfy the new bounds of Figure 4-12 and is shown in Figure 4-13.

4.2.7 Inner loop $L_{i2} = P_2H_2$

The inner loop L_{i2} is designed exactly the same way as the inner loop in a cascaded, no P.M. system (section 1.4.3) except for

replacing P_1 by P_{1e}, as shown in Figure 4-14, i.e., bounds $B_{L_{i2}}(\omega)$ are found in L_{i2n} such that the design L_{on} remains satisfactory despite the uncertainty in P_2 (and P_1). The results are shown in Figures 4-15(a), (b) and L_{i2n} in Figure 4-16. Note the general nature of bounds $B_{L_{i2}}(\omega)$and L_{i2} are exactly the same as in the cascaded, no P.M., inner loop B_{L2}, L_{2n} in Figure 1-19. The Bode plots of L_{on}, L_{i1}, L_{i2} of 3-loop, P.M. system together with the single loop system, L_s, are shown in Figure 4-17.

In Figure 4-15(b) the level of $B_{L_{i2}}$ in [5, 8] range is so much higher than for $B_{L_{i1}}$ (in Figure 4-9(b)) because the 5 db margin in this range (Figures 4-10, 11) was used entirely for L_{i1}. Hence, $|L_{i2n}|$ is correspondingly $>|L_{i1n}|$ (see Figure 4-17) in this range and its effect persists for higher frequencies. This was done here to emphasize the trade-off possibilities between L_{i1} and L_{i2}.

4.2.8 Time response of the 3-loop, P.M. system

CSMP digital simulation of the 3-loop, P.M. system at four extreme parameter cases are shown in Figure 4-18. The time domain bounds of Figure 3-2(a) are included as dashed lines. It is seen the results satisfy the time specifications.

4.2.9 The bandwidth propagation effect

In the multiple-loop design, there is a significant effect of increasing the number of inner loops. This is the steadily

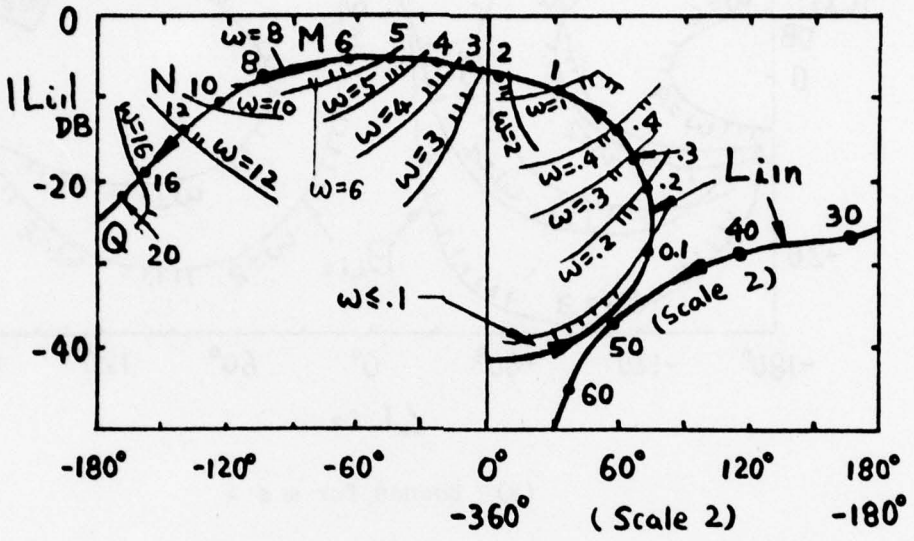

Figure 4-13. L_{iln} with bounds B_{Lil}

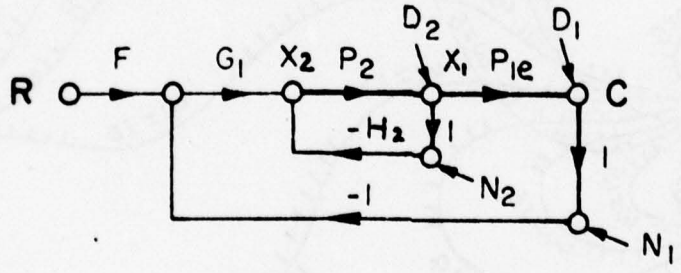

$$P_{le} = P/(1+L_{il})$$

Figure 4-14. The equivalent system of Figure 4-4

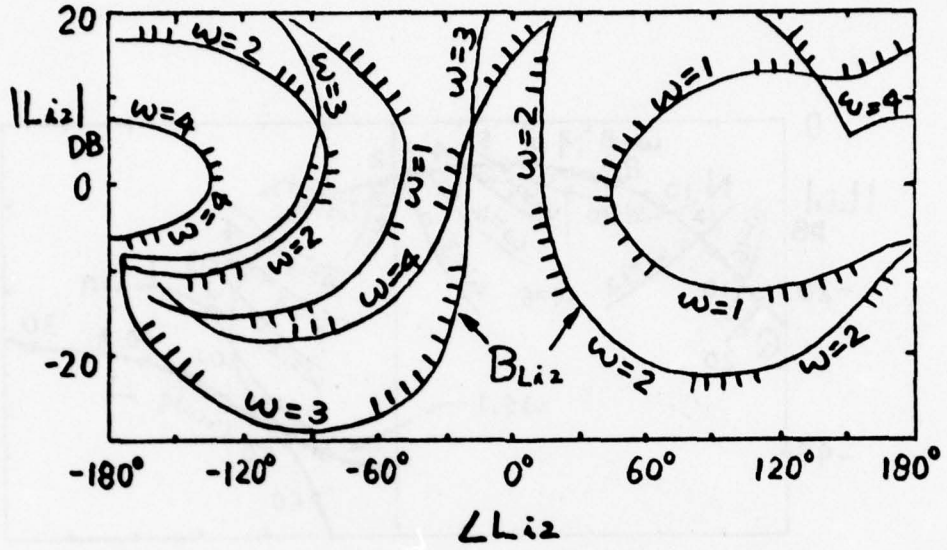

(a) Bounds for $\omega \leq 4$

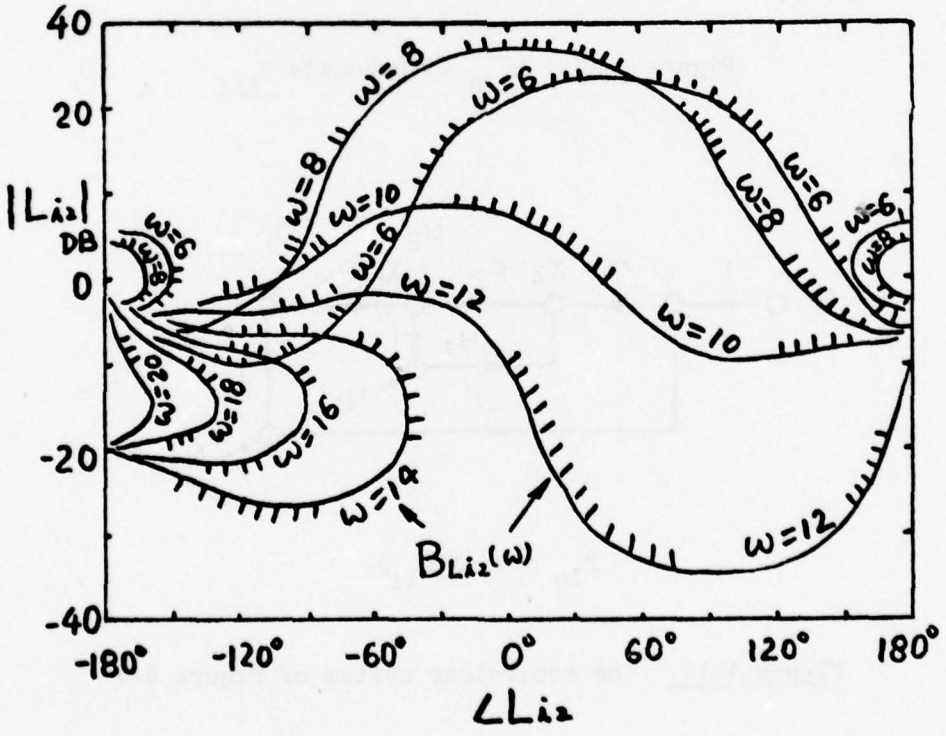

(b) Bounds for $\omega \geq 5$

Figure 4-15. Bounds on L_{i2}

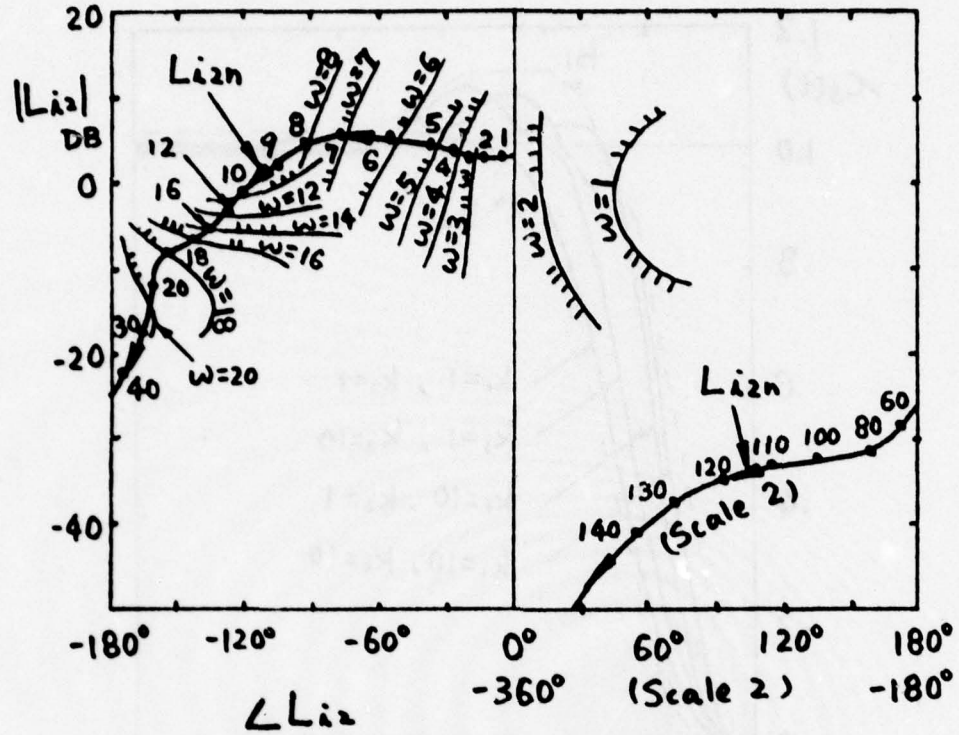

Figure 4-16. L_{i2n} with bounds

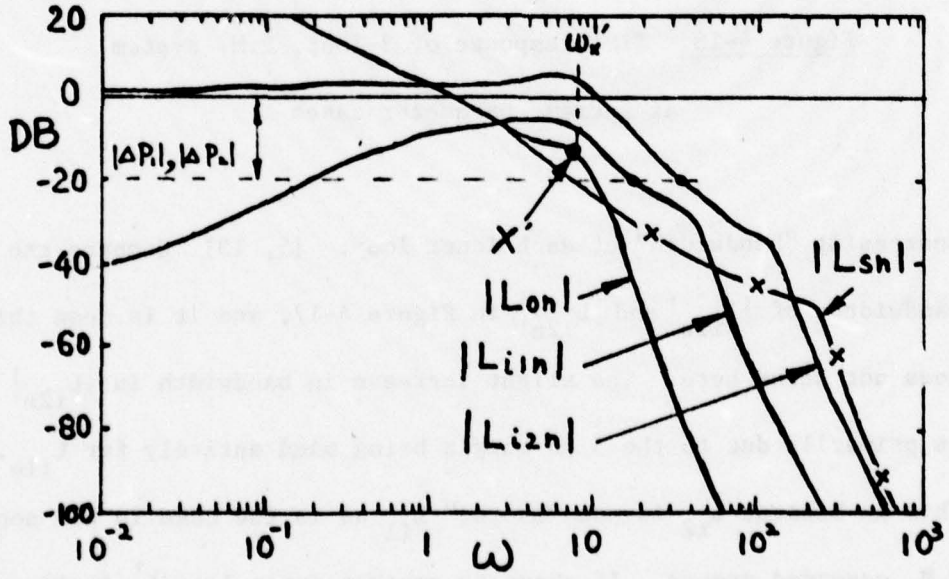

Figure 4-17. Bode plots of $|L_{sn}|$, $|L_{on}|$, $|L_{i1n}|$, $|L_{i2n}|$

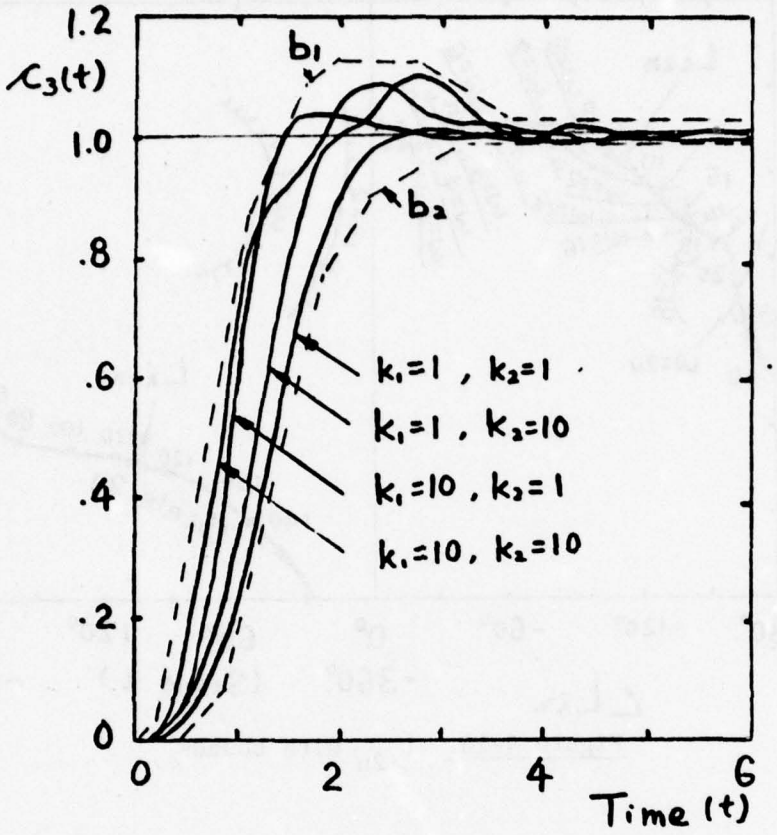

Figure 4-18. Time response of 3-loop, P.M. system at extreme parameter cases

increasing "bandwidth" of each inner loop. [5, 13] Compare the bandwidths of $|L_{i1n}|$ and $|L_{i2n}|$ in Figure 4-17, and it is seen this does not occur here. The slight increase in bandwidth in $|L_{i2n}|$ is primarily due to the 5 db margin being used entirely for L_{i1n}. This is because L_{i2} is not "inside" L_{i1} as is the case in the non P.M. cascaded system. If there is another inner loop L_i' inside L_{i1}, then the bandwidth propagation effect will occur (see section 4-4).

4.2.10 The signal level variation ratio (SLVR), ρ

Recall in section 2.2, the SLVR ρ, is defined

$$\rho = \frac{|C_{23}|_{max}}{|C_{2s}|_{max}} \frac{\left|\frac{L_o}{P_{1e}(1+L_o)}\right|_{max}}{\left|\frac{L_s}{P_1(1+L_s)}\right|_{max}} \cdot \frac{\left|\frac{L_s}{1+L_s}\right|_{max}}{\left|\frac{L_o}{1+L_o}\right|_{max}} \cdot \left(\frac{C_{3\ max}}{C_{s\ max}}\right) \quad (4.2\text{-}1.2)$$

The frequency ranges are redefined here (refer to section 2.3): $R_1' = [0., \omega_1']$, $|L_{sn}(j\omega_1')| = 25$ db, $\omega_1' = 0.08$; $R_2' = (\omega_1', \omega_2']$, $|L_{sn}(j\omega_2')| = 0$ db because P_2 is perfect in L_o, $\omega_2' = 1.6$; $R_3' = (\omega_2', \omega_3']$, $|L_{sn}(j\omega_3')| = -M_2 = -20$ db with M_2 is the hf uncertainty of P_2, $\omega_3' = 8$; $R_4' = (\omega_3', \omega_4']$, $\omega_4' = 10\omega_3' = 80$; $R_5' = (\omega_4', \infty)$.

We wish to simplify (1) (see section 2.4)

$$\rho = \alpha \cdot |1+L_{i1n}| \cdot \frac{|C_3|_{max}}{|C_s|_{max}} \quad (4.2\text{-}3)$$

Compare $(L_{on})_{3\text{-loop, P.M.}}$ with $(L_{on})_{2\text{-loop, P.M.}}$ in Figures 4-19 (a, ..., c). They are defined in the same way in R_1, R_2 and R_1', R_2' giving $\alpha \lesssim 1$ in R_1', R_2' as in sections 2.4.1, 2. Also, in the very hf region of R_5', $|L_{sn}|$, $|L_{on}|$, $|L_{i1n}|$, $|L_{i2n}| << 1$, so the result $\alpha \doteq 1$ of section 2.4.5 applies. There remain R_3', R_4'.

4.2.10.1 R_3', $\omega = (\omega_2', \omega_3']$, Figures 4-19(a), (c)

This region now corresponds to the latter part of R_2 in Figure 4-19(b). Recall in 2.4.2, $|L_s/(1+L_s)|$ is likely to reach its maximum at $|P_1|_{min}$ for $|L_{sn}| \gtrsim M_2$ db, where M_2 is the hf uncertainty

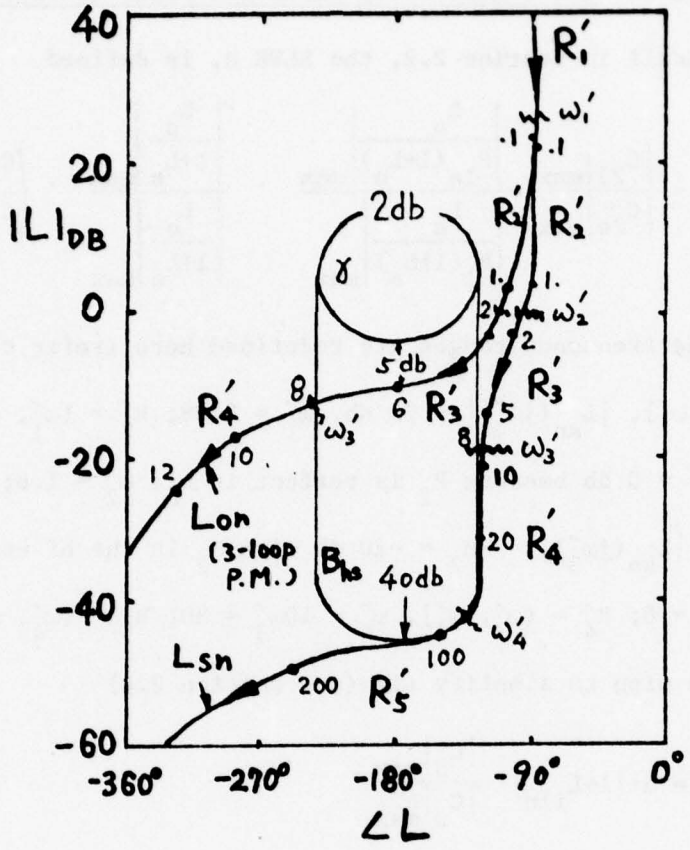

Figure 4-19(a). L_{on} of 3-loop P.M. system and L_{sn}

of P_2. But in the 3-loop, P.M. case, $|L_o/(1+L_o)|$ definitely cannot reach its maximum at $|P_{le}|_{min}$, so

$$\left|\frac{L_o}{P_{le}(1+L_o)}\right|_{max} < \frac{1}{|P_{le}|_{min}} \left|\frac{L_o}{1+L_o}\right|_{max} \qquad (4.2\text{-}4)$$

And the first two factors in (2) give

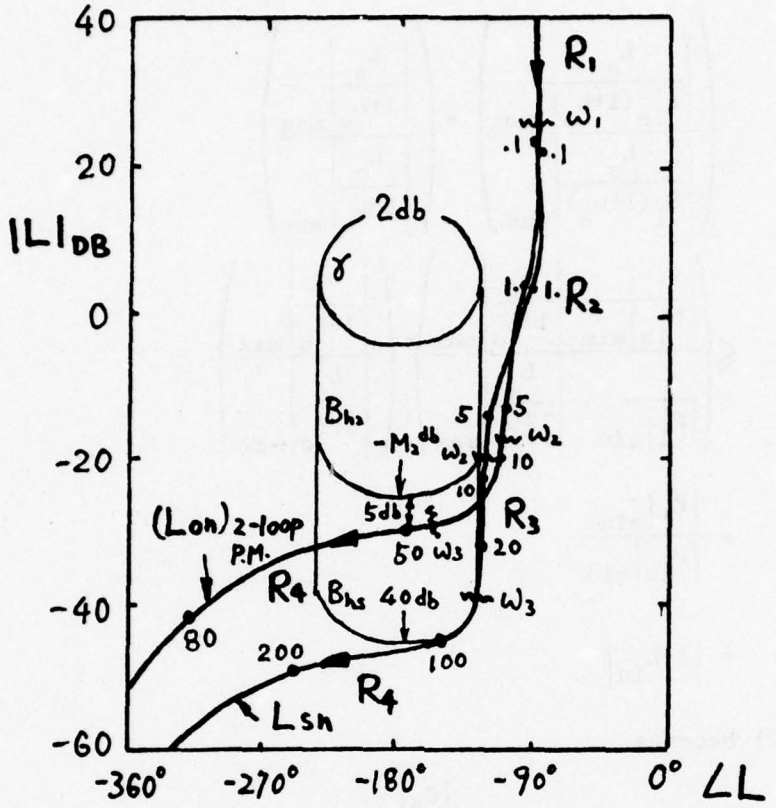

(b) L_{on} of 2-loop, P.M. system (Design A) and L_{sn}

Figure 4-19. Outer loops with defined regions

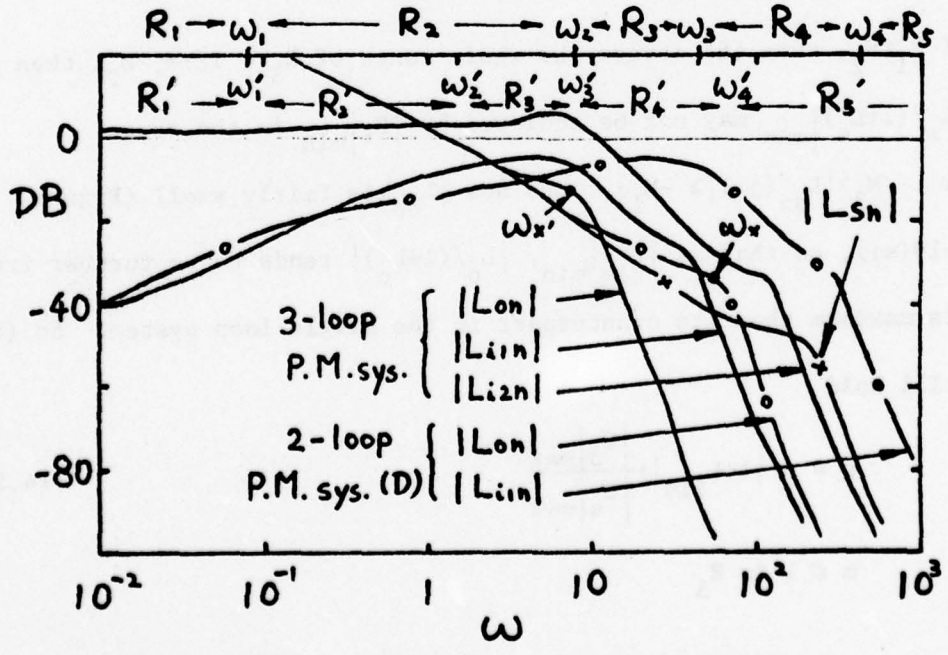

Figure 4-19(c). Bode plots of loop transmissions

$$\left(\frac{\left|\frac{L_o}{P_{le}(1+L_o)}\right|_{max}}{\left|\frac{L_s}{P_1(1+L_s)}\right|_{max}}\right)\cdot\left(\frac{\left|\frac{L_s}{1+L_s}\right|_{max}}{\left|\frac{L_o}{1+L_o}\right|_{max}}\right)$$

$$\leqslant\left(\frac{\left|\frac{1}{P_{le}}\right|_{min}\left|\frac{L_o}{1+L_o}\right|_{max}}{\left|\frac{1}{P_1}\right|_{min}\left|\frac{L_s}{1+L_s}\right|_{max}}\right)\cdot\left(\frac{\left|\frac{L_s}{1+L_s}\right|_{max}}{\left|\frac{L_o}{1+L_o}\right|_{max}}\right)$$

$$=\frac{|P_1|_{min}}{|P_{le}|_{min}}$$

$$\doteq |1+L_{in}| \qquad (4.2\text{-}5)$$

So (2) becomes

$$\rho = \alpha\,|1+L_{iln}|\cdot\frac{|C_3|_{max}}{|C_s|_{max}} \qquad (4.2\text{-}6)$$

$\alpha \leqslant 1$, for ω in $0 > |L_{sn}(j\omega)| \geqslant -M_2$.

If $M_1 \leqslant M_2$, then (6) covers the whole range of R_3. If $M_1 > M_2$, then $\left|L_s/(1+L_s)\right|_{max}$ may not be achieved by $|P_1|_{min}$ in the range $\{\omega \mid -M_2 > |L_{sn}(j\omega)| \geqslant -M_1\}$. But now $|L_{on}|$ is fairly small (Figure 4-19(a)), so that at $|P_{le}|_{min}$, $|L_o/(1+L_o)|$ tends to be further from its maximum than its counterpart in the single loop system. So (6) still hold

$$\rho = \alpha\,|1+L_{iln}|\cdot\frac{|C_3|_{max}}{|C_s|_{max}} \qquad (4.2\text{-}7)$$

$\alpha \leqslant 1$ in R_3

The result of the numerical example of a 3-loop, P.M. design is in Figure 4-20(a), and agrees with (7).

4.2.10.2 $R_4, \omega=(\omega_3', \omega_4']$, $|L_{sn}(j\omega_3')| = -M_1$ db, $|L_{sn}(j\omega_4') = -(M_1+M_2)$ db. (Figures 4-19(a), (c))

Compare $(L_{on})_{2\text{-loop}}$, $(L_{on})_{3\text{-loop}}$ in Figures 4-19(a), (b). R_4 in the 3-loop, P.M. system corresponds to the latter part of R_4 of the 2-loop, P.M. system. The nature of $|L_{sn}|$ in both cases is quite similar, because $|L_{sn}|$ is fairly small. So the results for the latter part of R_4 in the 2-loop system of section 2.4.4, applies, i.e.,

$$\rho = \alpha \cdot |1+L_{iln}| \cdot \frac{|C_3|_{max}}{|C_s|_{max}} \qquad (4.2\text{-}8)$$

$$\alpha \leq 1 \text{ in } R_4$$

which agrees with the result of the numerical example in Figure 4-20(a).

In conclusion, as $\alpha \leq 1$ for all ω, design based in $|1+L_{in}|$ is definitely conservative even more so than in the 2-loop design. Comparison of $|1+L_{iln}|$ with $\rho/[|C_3|_{max}/|C_s|_{max}]$ is shown in Figure 4-20(b), with Q = 1.26, which satisfies the specification $Q \leq 1.28$.

Comparison of α in the 2-loop and 3-loop P.M. systems is shown in Figure 4-21. In the 2-loop P.M. system (D), Q = 1.24 and in the 3-loop P.M. system, Q = 1.26.

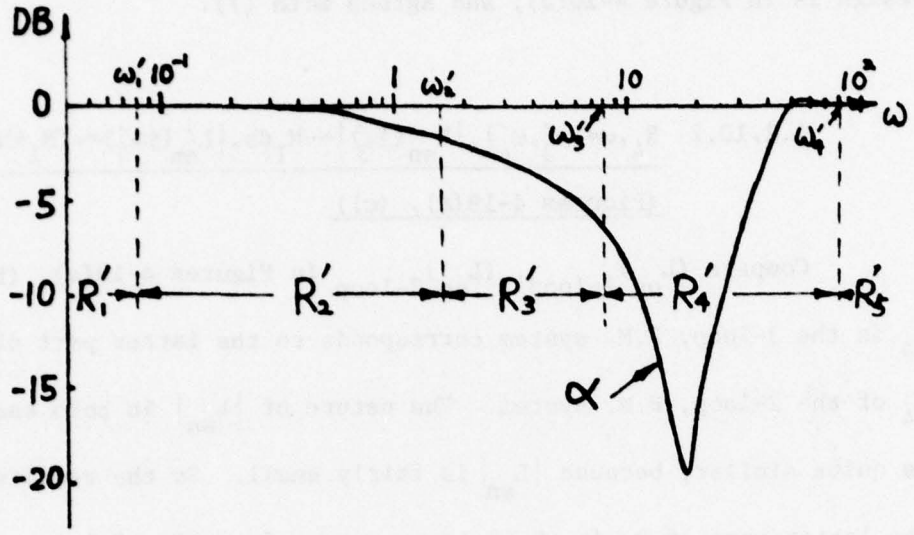

Figure 4-20(a). Nature of α in each frequency range

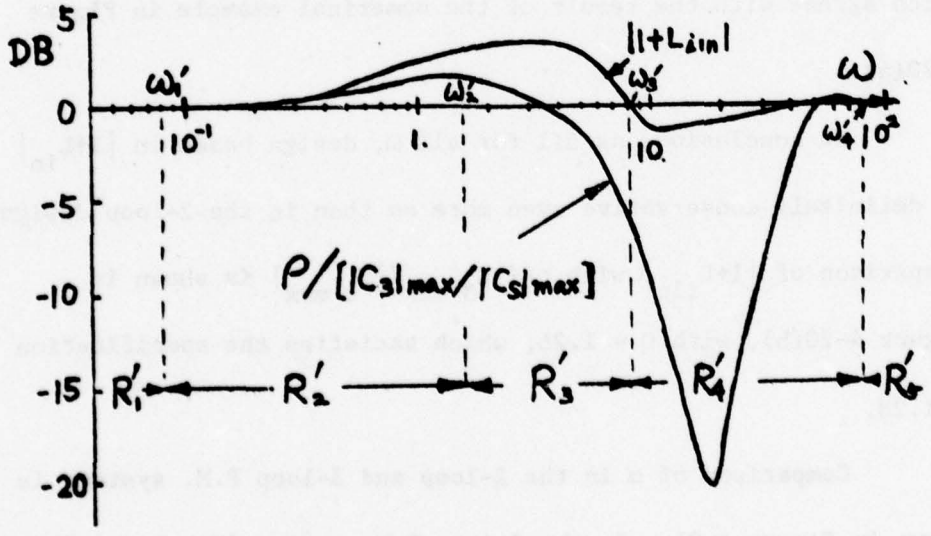

Figure 4-20(b). Nature of $|1+L_{iln}|$ and $\rho/[|C_s|_{max}/|C_3|_{max}]$

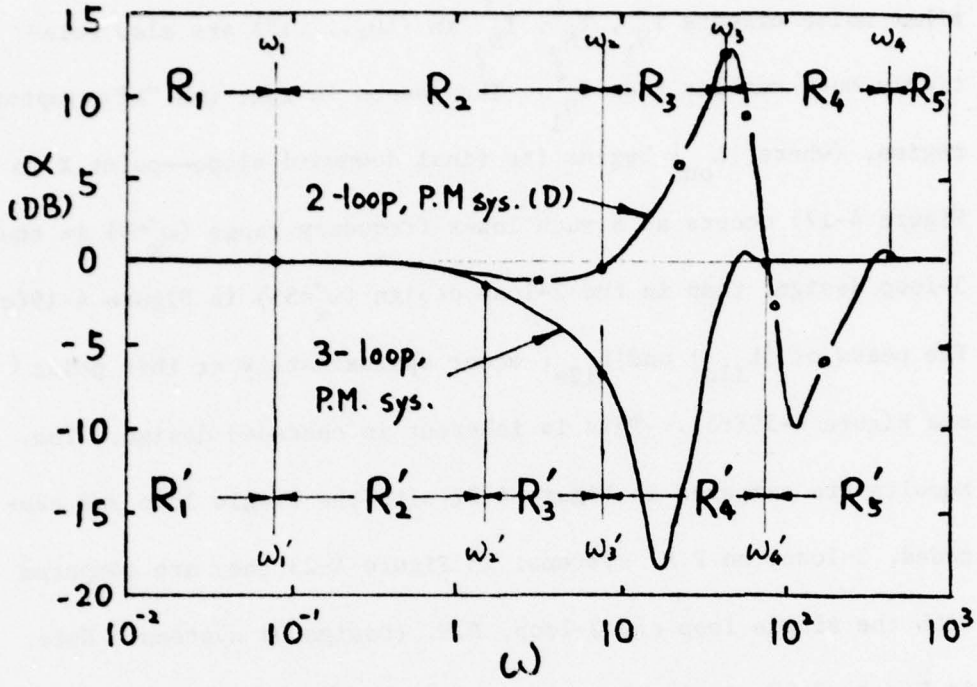

Figure 4-21. Nature of α for 2-loop and 3-loop P.M. systems

4.2.11 Sensor noise effect

We repeat the noise response function of section 1.6.3.

$$T_{N_1}^{2} \triangleq \frac{X_2}{N_1} \approx -\frac{L_o}{P_1 P_2}, \quad T_{N_1}^{1} \triangleq \frac{X_1}{N_1} \approx \frac{(L_{i1}+L_o)}{P_1}$$
$$T_{N_2}^{2} \triangleq \frac{X_2}{N_2} \approx -\frac{L_{i2}}{P_2}, \quad T_{N_2}^{1} \triangleq \frac{X_1}{N_2} \approx -L_{i2} \qquad (4.2.9\text{-}12)$$

at hf where $|L_o|$, $|L_{i1}|$, $|L_{i2}| \ll 1$.

In the hf range, all parameter uncertainties in P_1, P_2 are handled by the inner loops of L_{i1}, L_{i2}, so the bandwidth of L_{on} is fairly small (see Figure 4-17). Hence, the noise effect of $T_{N_1}^{2}$ in

(9) is considerably better than in the 2-loop P.M. design. The other noise effects $T_{N_1}^1$, $T_{N_2}^2$, $T_{N_2}^1$ in (10,...,12) are also relatively much smaller than $T_{N_1}^2$. The reason is that the "hf asymptotic region, (where $|L_{on}|$ begins its final downward slope--point X in Figure 4-17) occurs at a much lower frequency range ($\omega_x' \approx 8$) in the 3-loop design, than in the 2-loop design ($\omega_x' \approx 55$) in Figure 4-19(c). The peaks of $|L_{i1n}|$ and $|L_{i2n}|$ occur approximately at this point (see Figure 4-19(c)). This is inherent in cascaded design. The results are compared in Figure 4-22 with the single loop and cascaded, 2-loop, no P.M. systems; in Figure 4-23 they are compared with the single loop and 2-loop, P.M. (Design D) systems. Note, in Figure 2-23, Design D has Q = 1.24 and the 3-loop, P.M. system has Q = 1.26, so the signal level increases are quite similar, but the noise improvement is much bigger in the 3-loop P.M. than in the 2-loop P.M. system for the reason given above.

4.3 The 3-plant, 5-loop, P.M. system

4.3-1 Design philosophy

Design in Figure 4-24 commences exactly as in the 3-loop P.M. system (section 4.2.4). The bounds on L_i^ρ (i.e., on L_i in the lf range) are obtained to control the signal level increase at C_{25}. Then L_{i1}^ρ is obtained in the lf range, giving $P_{1e}(j\omega)$ in the lf region. The bounds on the outer loop L_{on} are obtained to handle the uncertainty in P_{1e} in lf only plus the safety margin (5 db in

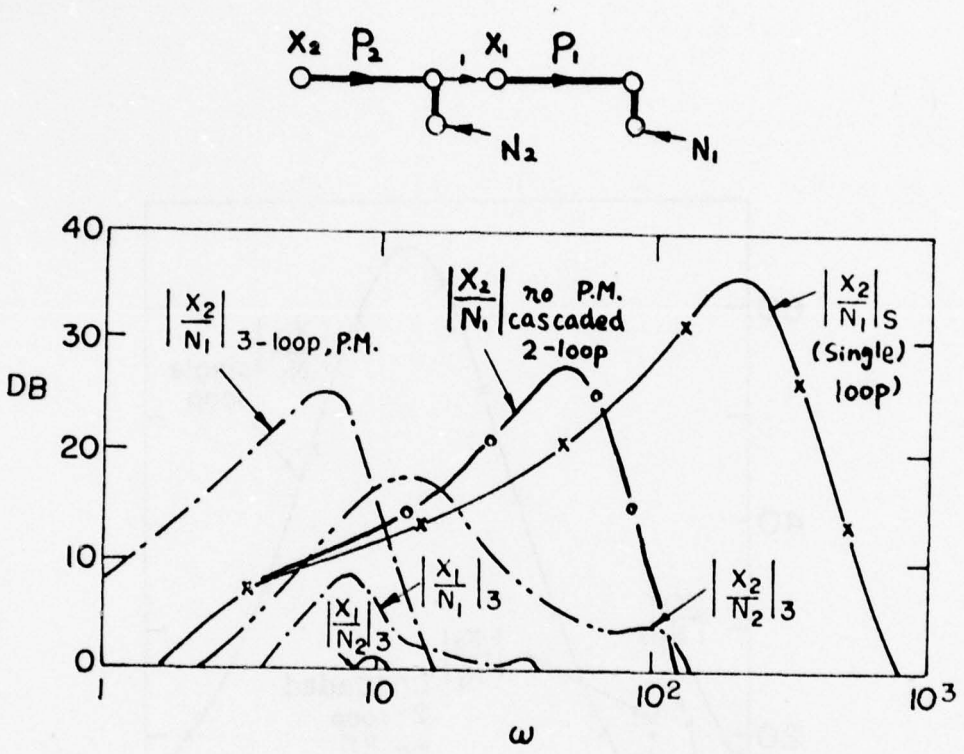

(a) In Log scale

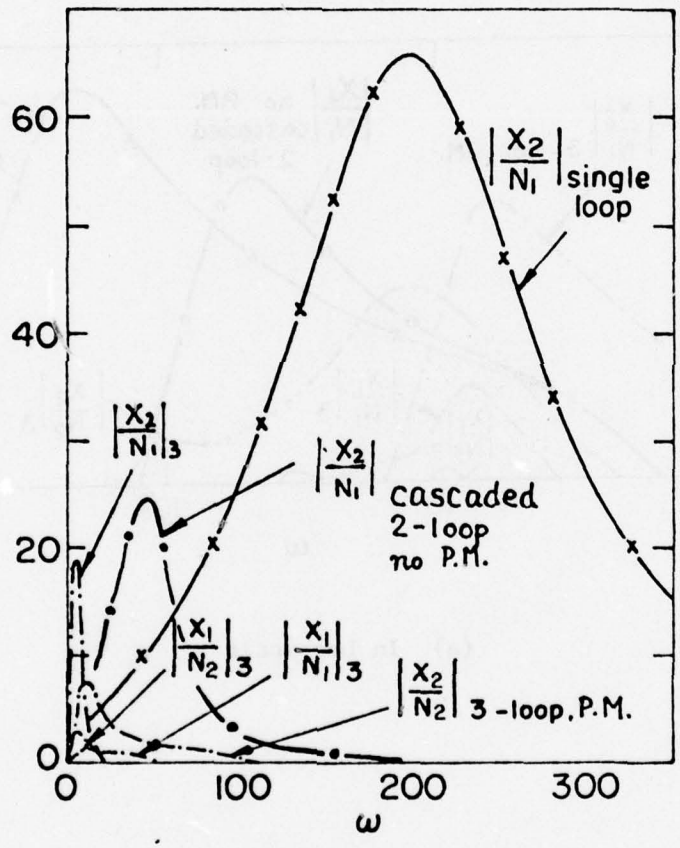

(b) In Arithematical scale

Figure 4-22. Comparison of noise effects

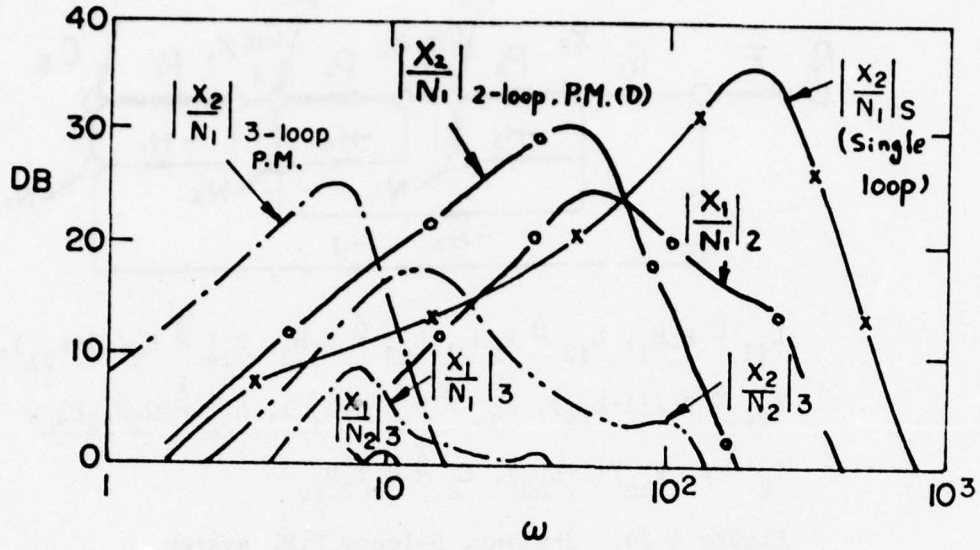

(a) In Log scale

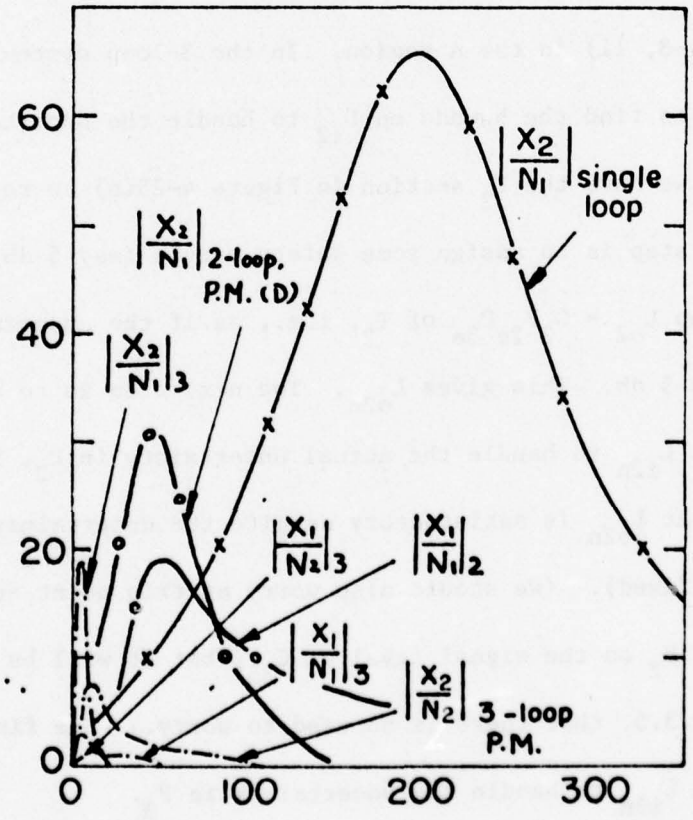

(b) In Arithematical scale

Figure 4-23. Comparison of noise effects

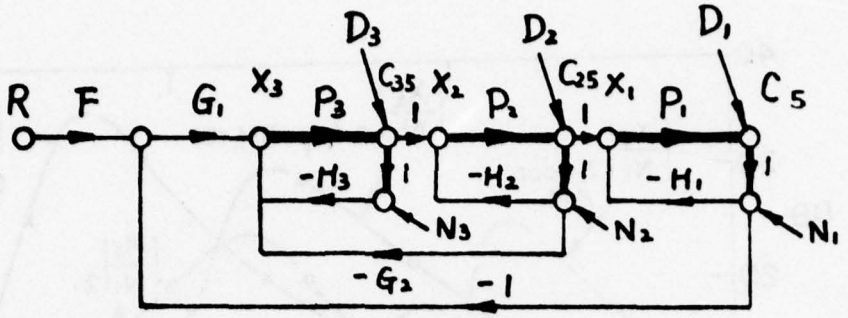

$L_{i1} \triangleq P_1H_1$, $L_{i2} \triangleq P_2H_2$, $L_{i3} \triangleq P_3H_3$, $P_{1e} \triangleq P_1/(1+L_{i1})$, $P_{2e} \triangleq P_2/(1+L_{i2})$, $P_{3e} \triangleq P_3/(1+L_{i3})$, $L_{o2} \triangleq G_2P_{2e}P_{3e}$, $T_2 \triangleq P_{2e}P_{3e}/(1+L_{o2})$, $L_o \triangleq G_1T_2P_{1e}$

Figure 4-24. 3-plant, 5-loop, P.M. system

Figures 4-8, 11) in the A region. In the 3-loop system the next step was to find the bounds on L_{i2} to handle the uncertainty in P_2. But here we have the T_2 section in Figure 4-25(a) to replace P_2H_2. Our next step is to assign some safety margin (say 5 db) $\forall\ \omega$ to the outer loop $L_{o2} = G_2P_{2e}P_{3e}$ of T_2, i.e., as if the uncertainty in $P_{2e}P_{3e}$ is 5 db. This gives L_{o2n}. The next step is to find the bounds on L_{i2n} to handle the actual uncertainty in P_2, i.e., to ensure that L_{o2n} is satisfactory despite the uncertainty in P_2, (at $P_3 = P_{3n}$ fixed). (We should also worry at this point about the effect of H_2 on the signal level at C_{35}, but it will be shown in section 4.3.5, that there is no need to worry.) The final step is to design L_{i3n} to handle the uncertainty in P_3.

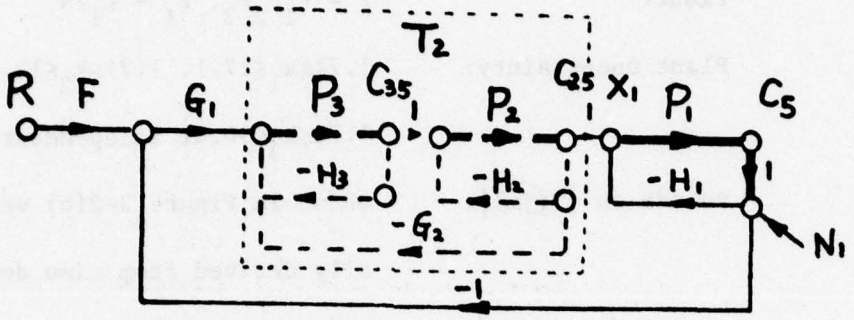

(a) Design of $L_{i1} \triangleq P_1 H_1$ and L_o

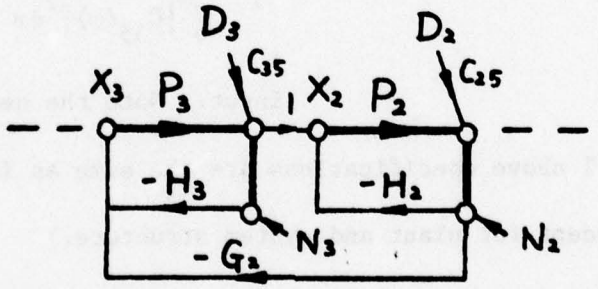

(b) An equivalent 3-loop, P.M. system

Figure 4-25. Design of 5-loop, P.M. system

4.3.2 Specifications on numerical examples

(Figures 4-24, ..., 27)

Plant: $P = P_1P_2P_3$, $P_i = k_i/s$

Plant uncertainty: $1.71 \leq k_1 \leq 17.1$, $1.71 \leq k_2 \leq 13.58$,

$1.71 \leq k_3 \leq 30.41$ independently

Bounds on $|T(j\omega)|$: shown in Figure 3-2(b) were originally derived from time domain bounds of Figure 3-2(a).

Disturbance Response: $\gamma \leq 2.0$ db

System structure: Figure 4-24.

Restriction on signal level: $Q_2 \triangleq \dfrac{\int_0^\infty |C_{23}(\omega)|^2 d\omega}{\int_0^\infty |C_{2s}(\omega)|^2 d\omega} \leq 1.28$,

$Q_3 \triangleq \dfrac{\int_0^\infty |C_{33}(\omega)|^2 d\omega}{\int_0^\infty |C_{35}(\omega)|^2 d\omega} \leq 1.30$ for unit input. Note the need for $Q_3 > Q_2$.

(All above specifications are the same as in section 4.2.2 except for plant and system structure.)

(The rational function values of the compensation functions in Figure 4-24 are given in Appendix II.)

4.3.3 Single loop and cascaded, 3-loop, no P.M. systems

The single loop system (Figure 4-26) and cascaded, 3-loop, no P.M. system (Figure 4-27) are also designed here in order to

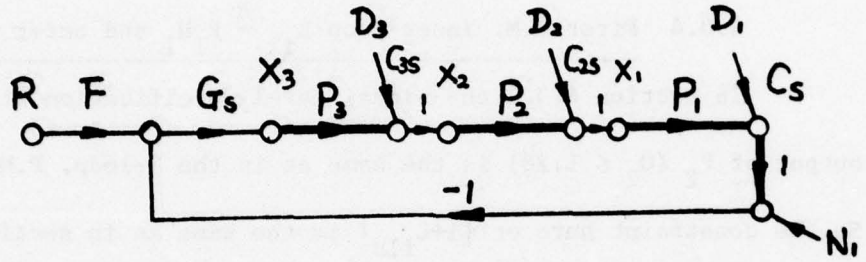

$|\Delta P_1| = 20$ db, $|\Delta P_2| = 18$ db, $|\Delta P_3| = 25$ db

Figure 4-26. The 3-plant, single loop system

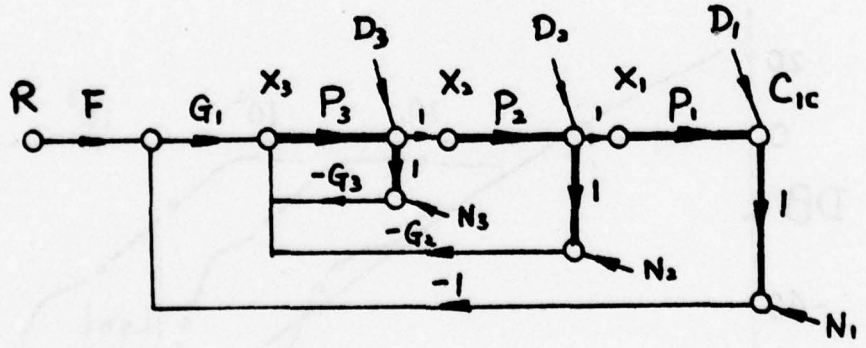

$$L_1 = G_1 P_1 P_{2e}, \quad P_{2e} = \frac{P_2 P_{3e}}{1+G_2 P_2 P_{3e}}, \quad P_{3e} = \frac{P_3}{1+P_3 G_3}$$

Figure 4-27. The 3-plant, cascaded, no P.M. system

compare with the 5-loop, P.M. system in SLVR, Q and sensor noise effects. The Bode plots are shown in Figure 4-28

4.3.4 First P.M. inner loop $L_{i1} \triangleq P_1 H_1$ and outer loop L_o

In section 4.3.2 the signal level specification at the output of P_2 ($Q_2 \lesssim 1.28$) is the same as in the 3-loop, P.M. case. So the constraint here on $|1+L_{i1n}|$ is the same as in section 4.2.4 We do not consider the signal level at C_{35}, knowing that it will only be slightly more than at C_{25} in a proper 5-loop design. The design of L_o and L_{i1} (ΔP_1 = 20 db) is exactly the same as in the 3-loop, P.M. system (sections 4.2.4-6), because at this point the uncertainty in all that precede P_1, is ignored. So Figures 4-5, ..., 13 apply here, including the trade-off of Figures 10, 11.

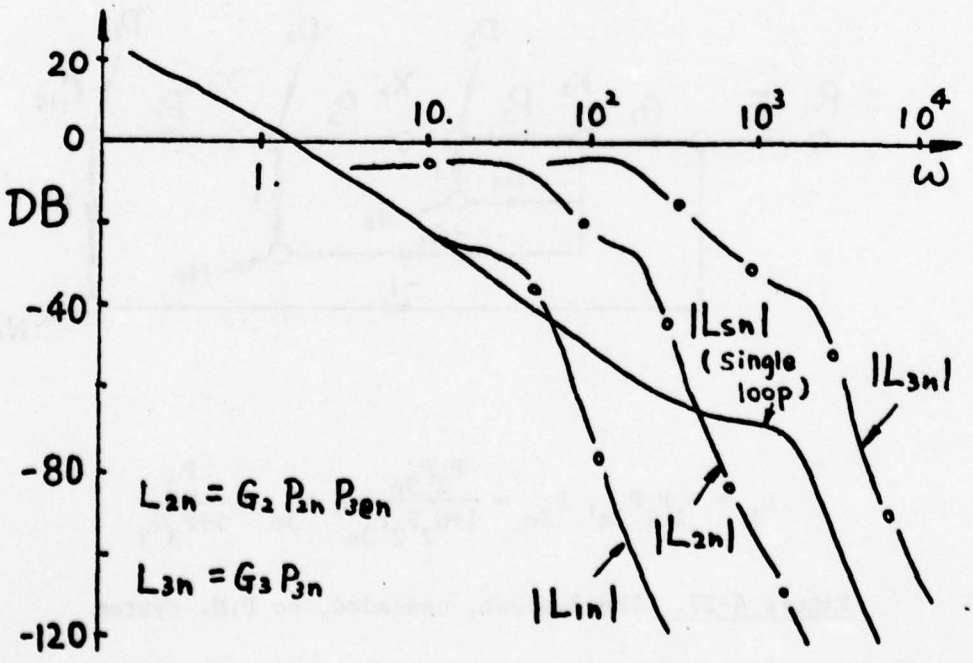

Figure 4-28. Bode plots of $|L_{sn}|$, $|L_{1n}|$, $|L_{2n}|$, $|L_{3n}|$

4.3.5 Second outer loop $L_{o2} = G_2P_{2e}P_{3e}$, second P.M. inner loop $L_{i2} \triangleq P_2H_2$ and the third inner loop $L_{i3} \triangleq P_3H_3$

The dash box (T_2) in Figure 4-25(a) is considered next. At this stage the problem is to control the T_2 variation such that the designed L_o and L_{iln} are satisfactory despite the fact that P_2, P_3 uncertainties were neglected in their design. Three loops are available for this purpose: L_{o2}, L_{i2}, L_{i3}.

4.3.5.1 Design of L_{o2} (Figure 4-29)

In the 3-loop system of sections 4.2.4-7 and Figure 4-1, the outer loop L_o had to handle the P_{1e} lf uncertainty (analogous to P_{2e} here) and P_{1e} lf design was dominated by consideration of signal level at C_{23} (C_{35} in Figure 4-24). So, presumably similar precautions must be taken here. Fortunately this is not so. It is recalled from chapter 3, section 3.3.7 (Figures 3-9, 10) that L_{il} design shifted the template which L_o had to handle, to the left where it could cross B_{h_2}, facing L_o to be more conservative. But here ABC in Figure 4-29(a) replace B_{h_2}, so excursions of the template of the new P_{1e} (i.e., P_{2e} of Figure 4-24) to the left are acceptable.

The second point is that in the 3-loop design L_{1i} could not handle entirely the lf uncertainty of P_1 (in Figure 4-1) because of the signal level problem. But here because of the 'bandwidth

propagation effect' discussed in section 4.3.7, we can neglect the signal level problem of the new P_{1e} (i.e., P_{2e} of Figure 4-24). Thus, the frequency corresponding to ω_M of Figure 3-24 is much larger (50 in Figure 4-30(c) cf 6 in Figure 4-13). Hence, there is very little obligation on the new outer loop (i.e., L_{o2} of Figure 4-24). However, as a safety factor, we design L_{o2} as if it has to handle a few db uncertainty over all ω (somewhat analagous to the 5 db safety margin used in Figure 4-8 for L_o there). In this design example 5 db was used.

A third factor is the analog of the trade-off (Figures 4-10, 11) between L_{i1} and L_{i2} in the 3-loop P.M. design. Here the trade-off is between L_{i1} and L_{o2}, and can be made in accordance with the levels of N_1, N_2. In this specific example, the 5 db region in A was given to L_{i1} and the region in B was split roughly equally between L_{i1} and L_{o2}.

4.3.5.2 Design of L_{i2} (Figure 4-30)

Special design of L_{i2}^{ρ} in the lf range in order to control SLVR at C_{35}, is not necessary because of the bandwidth propagation effect discussed in section 4.3.5.1. L_{i2} is designed simply to handle the uncertainty of P_2, i.e., bounds B_{Li2} in Figures 4-30(a, b) are obtained such that L_{o2n} is satisfactory for P_2 uncertainty (18 db here) despite the fact that L_{o2n} was designed on the basis of 5 db uncertainty. L_{i2n} is then obtained to satisfy B_{1i2}, as shown in Figure 4-30(c).

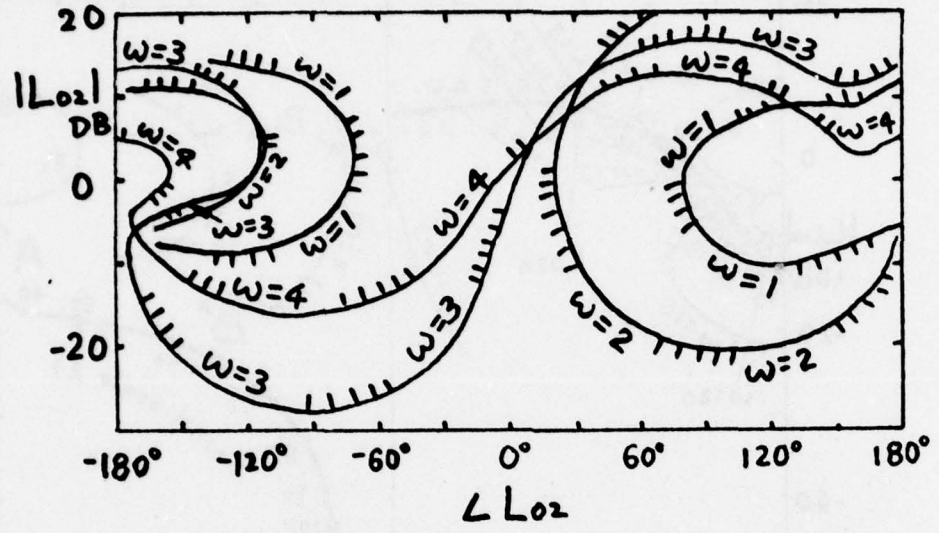

(a) B_{Lo2} for $\omega \leq 4$

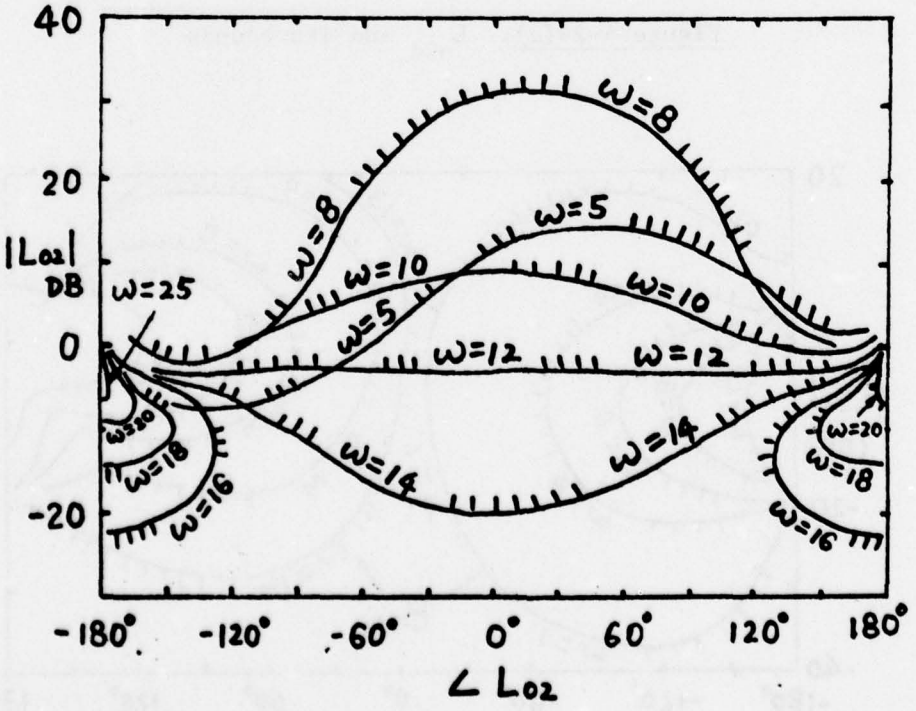

(b) B_{Lo2} for $\omega \leq 5$

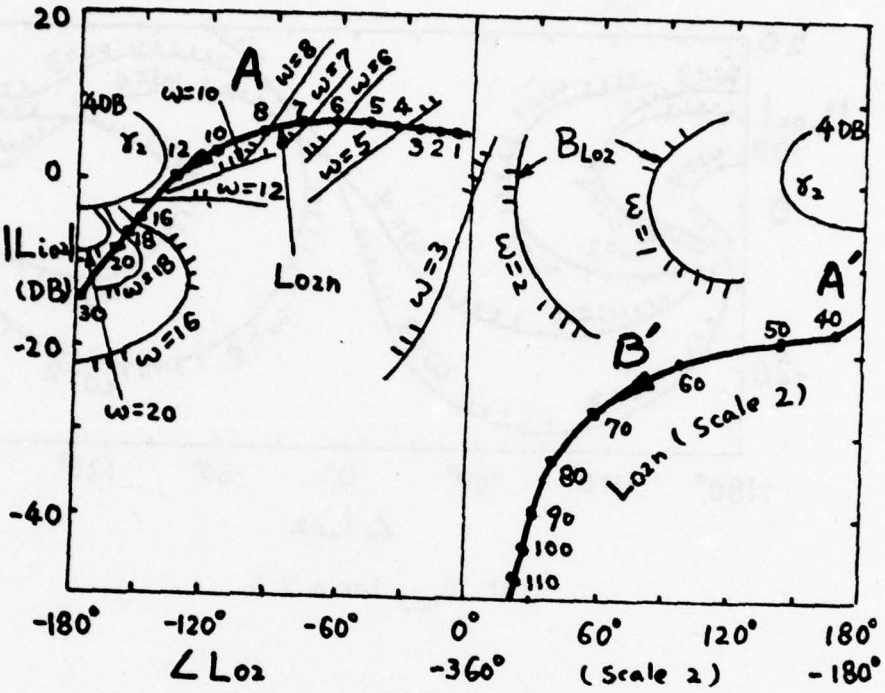

Figure 4-29(c). L_{o2n} and its bounds

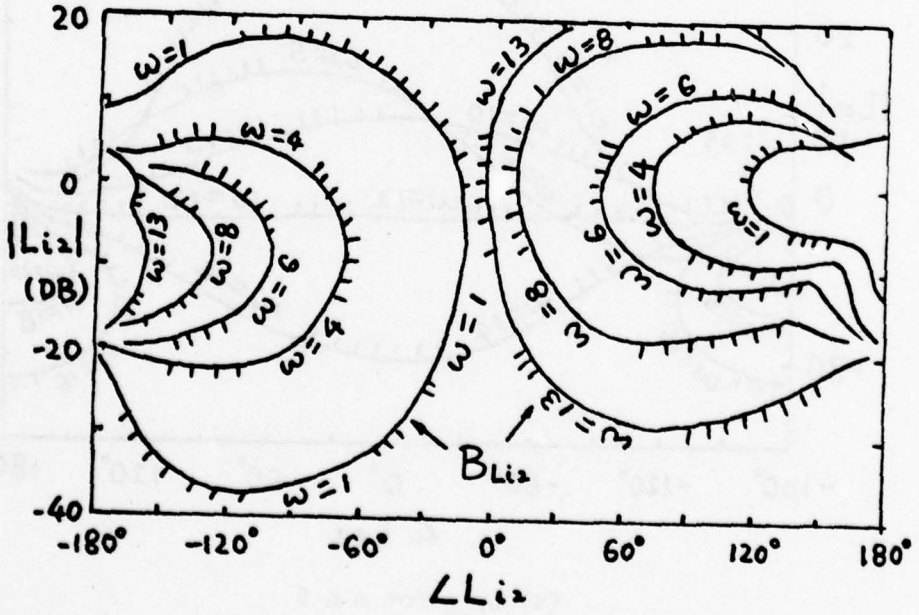

(a) $B_{L_{i2}}$ for $\omega \leq 13$

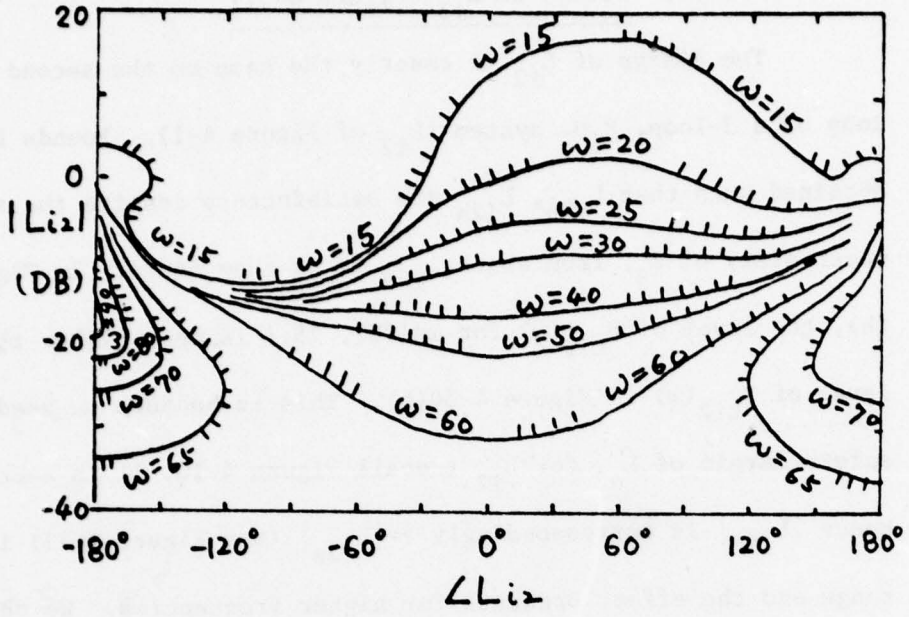

(b) $B_{L_{i2}}$ for $\omega \geq 15$

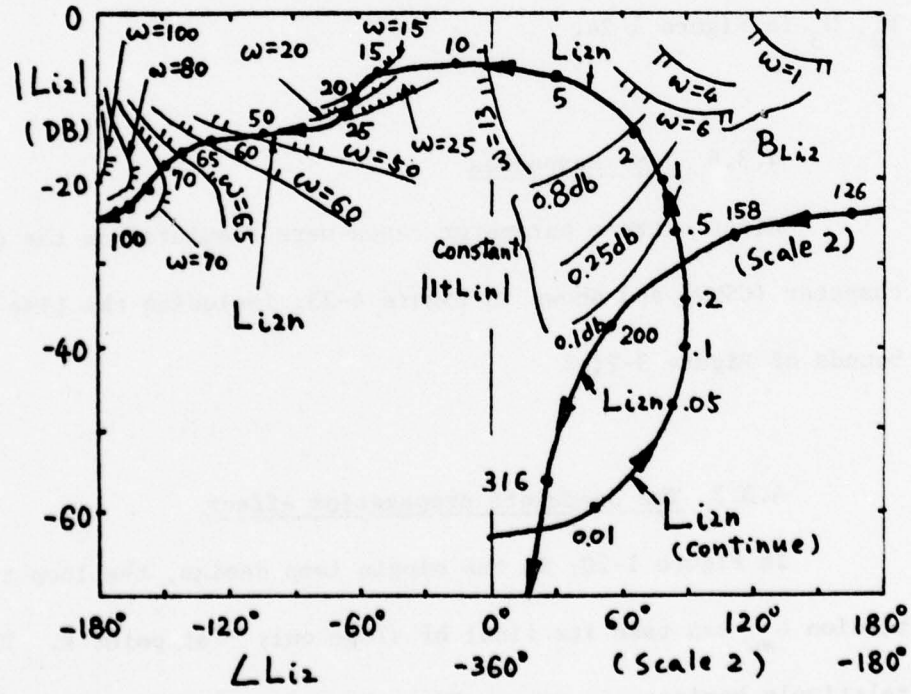

Figure 4-30(c). L_{i2n} and bounds

4.3.5.3 Design of L_{i3} (Figure 4-31)

The design of L_{i2} is exactly the same as the second inner loop of a 3-loop, P.M. system (L_{i2} of Figure 4-1). Bounds B_{Li3} are obtained such that L_{o2n}, L_{i2n} are satisfactory despite the actual uncertainty of P_3, from which L_{i3n} is as then found. In Figure 4-31 (b), the level of $B_{Li3}(\omega)$ for $\omega\in[20., 75.]$ is much higher than the level of $B_{Li2}(\omega)$ in Figure 4-30(b). This is because we used all the safety margin of L_{o2} for L_{i2} (recall Figure 4-10, 11 in section 4.2.6). Hence $|L_{i3n}|$ is correspondingly $>>|L_{i2n}|$ (see Figure 4-32) in this range and the effect presents for higher frequencies. We thereby emphasize the possibilities for trade-off between L_{i2} and L_{i3}, which is useful in the case of significant differences in the levels of N_2, N_3 in Figure 4-24.

4.3.6 Time Responses

Eight extreme parameter cases were simulated on the digital computer (CSMP) and shown in Figure 4-33, including the time domain bounds of Figure 3-2(a)

4.3.7 The bandwidth propagation effect

In Figure 1-20, in the single loop design, the loop transmission L_{sn} can take its final hf slope only ~ at point E. The relatively horizontal segment XE is a preparation for the final breakpoint. In the 2-loop design, E is replaced by ω_b

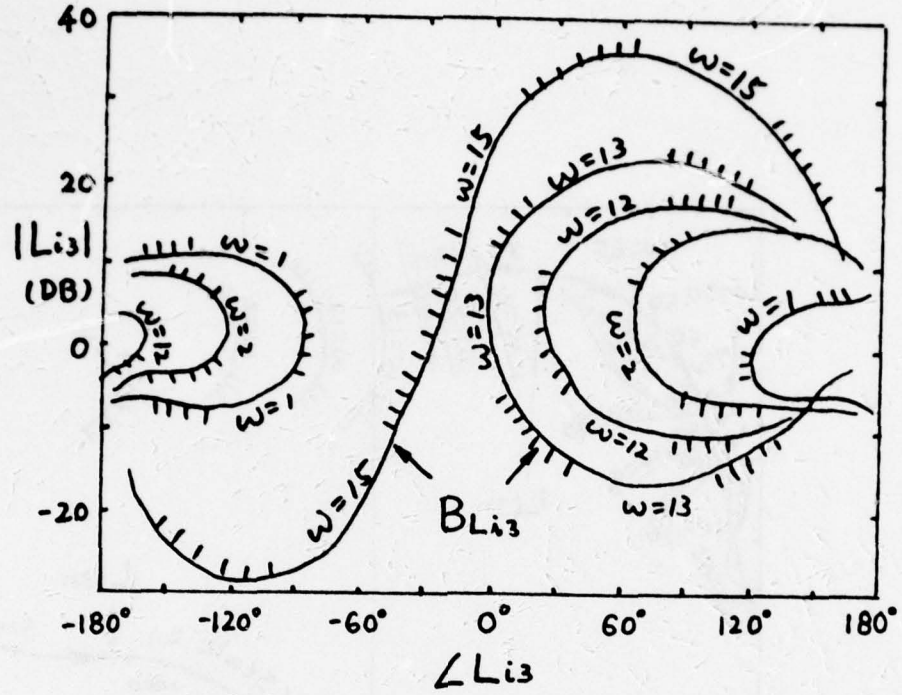

(a) $B_{L_{13}}$ for $\omega \leq 15$

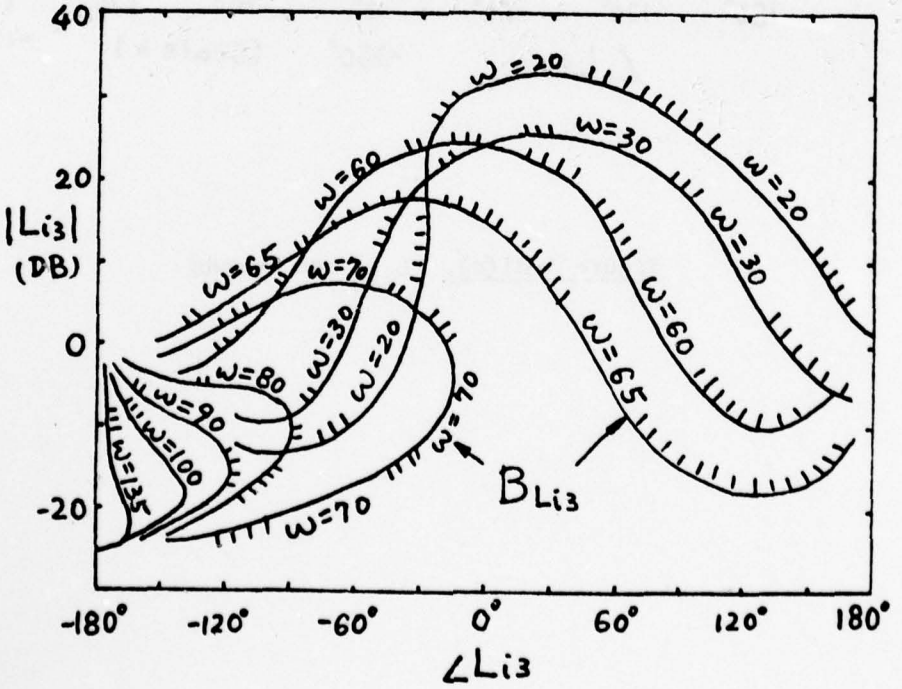

(b) $B_{L_{13}}$ for $\omega \geq 20$

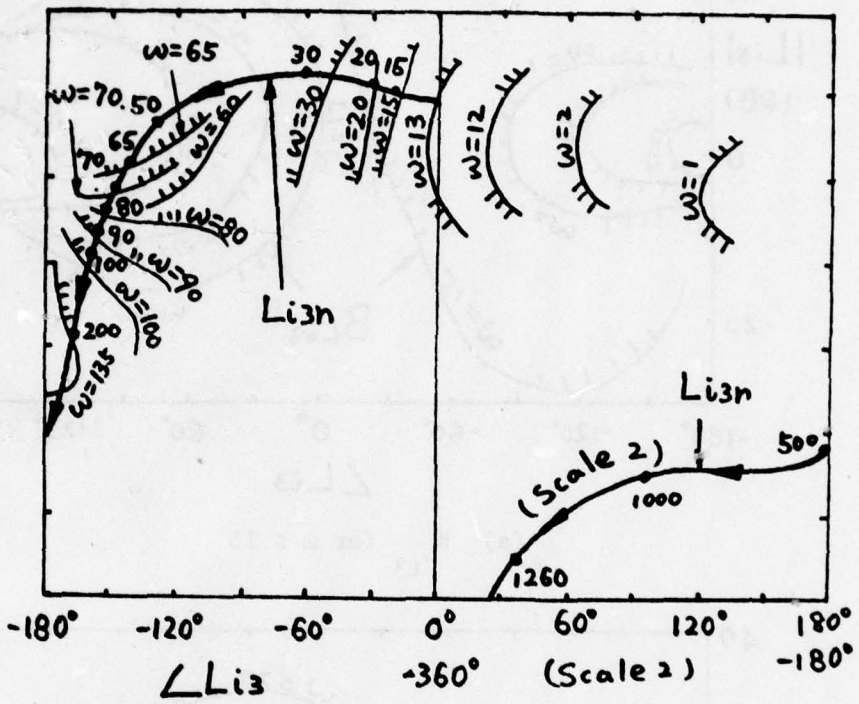

Figure 4-31(c). L_{i3n} and bounds

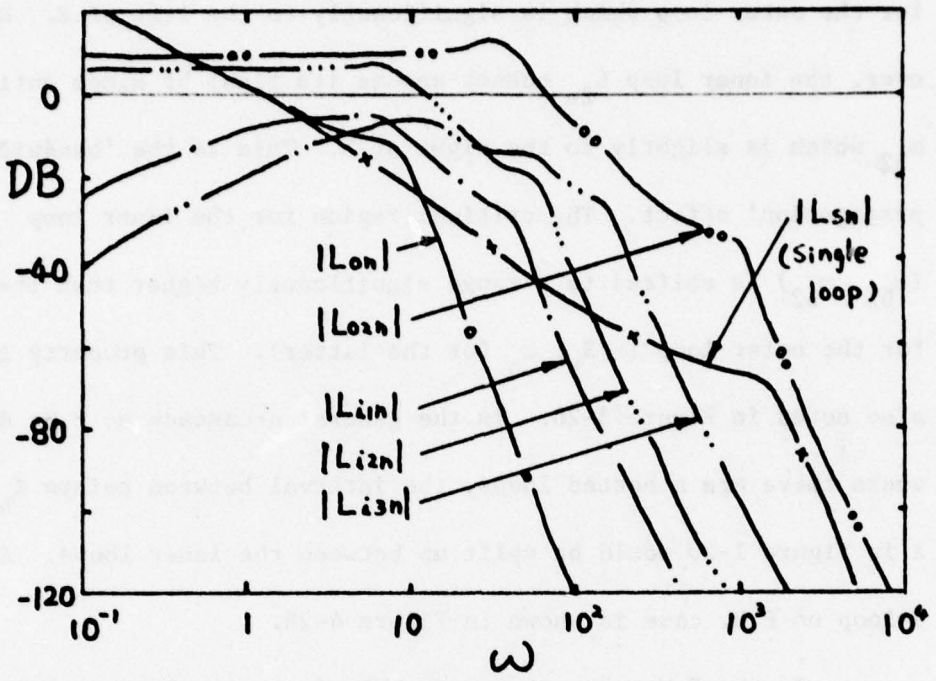

Figure 4-32. Loop transmissions of the 5-loop, P.M. system

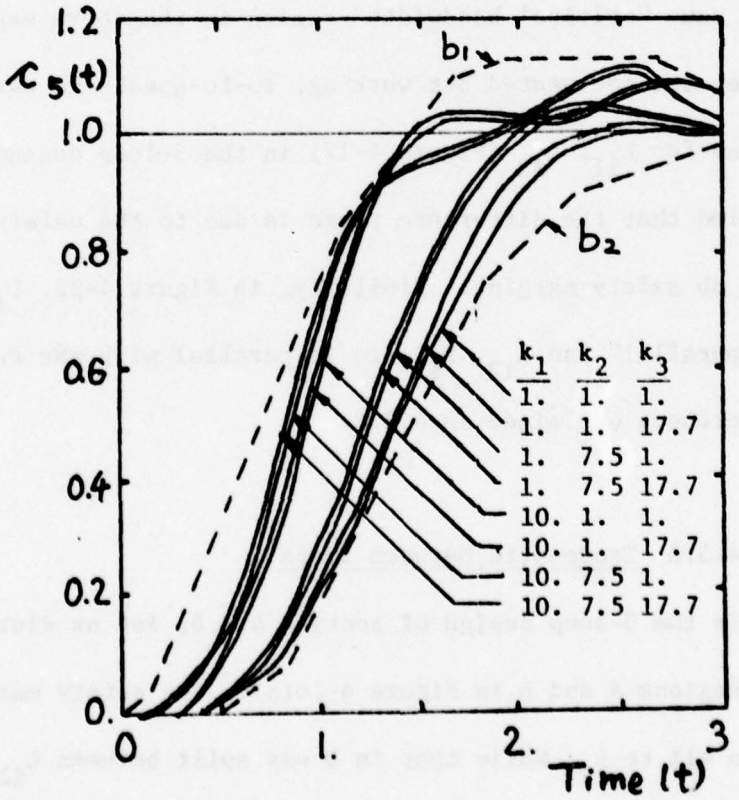

Figure 4-33. Time response of the 5-loop P.M. system

for the outer loop which is significantly to the left of E. However, the inner loop L_{2n} cannot assume its final hf slope until ω_{b2} which is slightly to the right of E. This is the 'bandwidth propagation' effect. The critical region for the inner loop (ω_{b1}, ω_{b2}) is shifted to a range significantly higher than that for the outer loop (~ X_b, ω_b for the latter). This property is also noted in Figure 3-28. In the general n-cascade no P.M. design where there are n nested loops, the interval between points X_b and X in Figure 1-20 would be split up between the inner loops. A 3-loop no P.M. case is shown in Figure 4-28.

In the P.M. case it is possible for several inner loops to have the same "critical bandwidth" region in the above sense, because they are not nested but working, so-to-speak, in parallel. This is so for L_{i1}, L_{i2} (Figure 4-17) in the 3-loop design. (It is recalled that the difference there is due to the unfair division of the 5 db safety margin). Similarly, in Figure 4-32, L_{i1} and L_{o2} are in "parallel" and L_{i2}, L_{i3} are in parallel with the reason for the differences explained in 4.3.8.

4.3.8 Trade-offs between loops

In the 3-loop design of section 4.2.6, let us distinguish between regions A and B in Figure 4-1o(a). The safety margin in A was given all to L_{i1} while that in B was split between L_{i1} and L_{i2}.

The result was significantly larger level of L_{i2n} than L_{i1n} (Figure 4-17), in the ω range corresponding to A (Figure 4-10(a)) which persisted in its effect to higher ω (because $|L_{i2n}|$ must then decrease over a larger interval). This was repeated precisely in the 5-loop design of section 4.3.4, between L_{i1n} and L_{o2n} (which effectively replaces L_{i2n} in this matter), leading to the significantly larger $|L_{o2n}|$ (Figure 4-32) than $|L_{i1n}|$.

The above problem was repeated in the design of $L_{i2n}, L_{i3n}. L_{o2n}$ is shown Figure 4-29(c). Because of the 'bandwidth propagation' effect A' is now at a higher ω range than A. Again some extra margin is assigned to L_{o2n} in A' (just as such was assigned to L_o in A). And again we let L_{i2n} have all of it in A', while that in B' was split between L_{i2n} and L_{i3n}. The result is L_{i3n} level significantly larger than L_{i2n} level in Figure 4-32 and which persists as before. The difference between L_{i3n} and L_{i2n} in Figure 4-32 is > between L_{i1n} and L_{i2n} in Figure 4-17, because in the former the uncertainty of P_3 > uncertainty of P_2 (25 db cf 18 db), whereas in Figure 4-17, the uncertainty of P_1, P_2 are equal (20 db each).

As previously noted, the above can be used as trade-off between the loops, to compensate for significant differences between sensor noise levels.

4.3.9 The signal level variation ratio (SLVR), ρ

The definition of SLVR is extended to account for the additional plant modification in the 5-loop case, over and above that in the 3-loop case. (Figures 4-24, 26).

$$\rho_2 = \frac{|C_{25}|_{max}}{|C_{2s}|_{max}}, \quad \rho_3 = \frac{|C_{35}|_{max}}{|C_{3s}|_{max}} \tag{4.3-1}$$

Recall section 4.2.10, it was proven

$$\rho_2 = \alpha_2 \cdot |1+L_{i1n}| \cdot \frac{|C_5|_{max}}{|C_s|_{max}} \tag{4.3-2}$$

$$\alpha_2 \leq 1$$

The frequency ranges for our numerical example are (section 4.2.10): $R_1' = [0, \omega_1']$, $|L_{sn}(j\omega_1')| = 25$ db, $\omega_1 = 0.08$; $R_2' = (\omega_1', \omega_2']$, $|L_{sn}(j\omega_2')| = 0$ db, $\omega_2' = 1.6$; $R_3' = (\omega_2', \omega_3']$, $L_s(j\omega_3') = -(M_2+M_3) = -43$ db, with M_2, M_3 the hf uncertainties of P_2, P_3 respectively, $\omega_3' = 55$; $R_4' = (\omega_3', \omega_4']$, $\omega_4' = 10\,\omega_3' = 550$; $R_5' = (\omega_4', \infty)$. The results of the 5-loop numerical example is shown in Figure 4-34(a), and agrees with (2).

The SLVR for C_{35} is

$$\rho_3 = \frac{|C_{35}|_{max}}{|C_{3s}|_{max}} = \frac{|C_{35}|_{max}/|C_{25}|_{max}}{|C_{3s}|_{max}/|C_{2s}|_{max}} \cdot \rho_2 \tag{4.3-3}$$

$$= \alpha_{32} \cdot |1+L_{i2n}| \cdot \rho_2 \tag{4.3-4}$$

with $\alpha_{32} \leq 1$, because the dashed part T_2 in Figure 2-25(a) acts as another 3-loop, P.M. system. Combining (2, 4)

$$\rho_3 = \alpha_3 \cdot |1+L_{i1n}| \cdot |1+L_{i2n}| \cdot (|C_5|_{max}/|C_s|_{max}) \qquad (4.3\text{-}5)$$

$$\alpha_3 = \alpha_{23} \cdot \alpha_2 \leq |$$

The results of the example are shown in Figure 4-34(b) and agree with (5). The nature of $|1+L_{i1n}|$, $\rho_2/(|C_5|_{max}/|C_s|_{max})$, $|1+L_{i1n}| \cdot |1+L_{i2n}|$ and $\rho_3/(|C_5|_{max}/|C_s|_{max})$ are shown in Figures 4-35 (a), (b), respectively.

4.3.10 Sensor noise effects

The sensor noise functions of the single loop and the cascaded, no P.M. system for a 3-section plant (Figures 4-26, 27) are:

(1) single-loop system

$$T^3_{N_1} \triangleq \left|\frac{X_3}{N_1}\right| \simeq \left|\frac{L_s}{P_1P_2P_3}\right|, \quad T^2_{N_1} \triangleq \left|\frac{X_2}{N_1}\right| \simeq \left|\frac{L_s}{P_1P_2}\right|,$$

$$T^1_{N_1} \triangleq \left|\frac{X_1}{N_1}\right| \simeq \left|\frac{L_s}{P_1}\right|, \quad \text{all at hf where } |L_s| \ll 1. \qquad (4.3\text{-}6)$$

(2) cascaded, no P.M. system

$$T^3_{N_1} \triangleq \left|\frac{X_3}{N_1}\right| \simeq \left|\frac{L_1}{P_1P_2P_3}\right|, \quad T^2_{N_1} \triangleq \left|\frac{X_2}{N_1}\right| \simeq \left|\frac{L_1}{P_1P_2}\right|,$$

$$T^1_{N_1} \triangleq \left|\frac{X_1}{N_1}\right| \simeq \left|\frac{L_1}{P_1}\right|, \quad \text{all at hf where all } |L| \ll 1. \qquad (4.3\text{-}7)$$

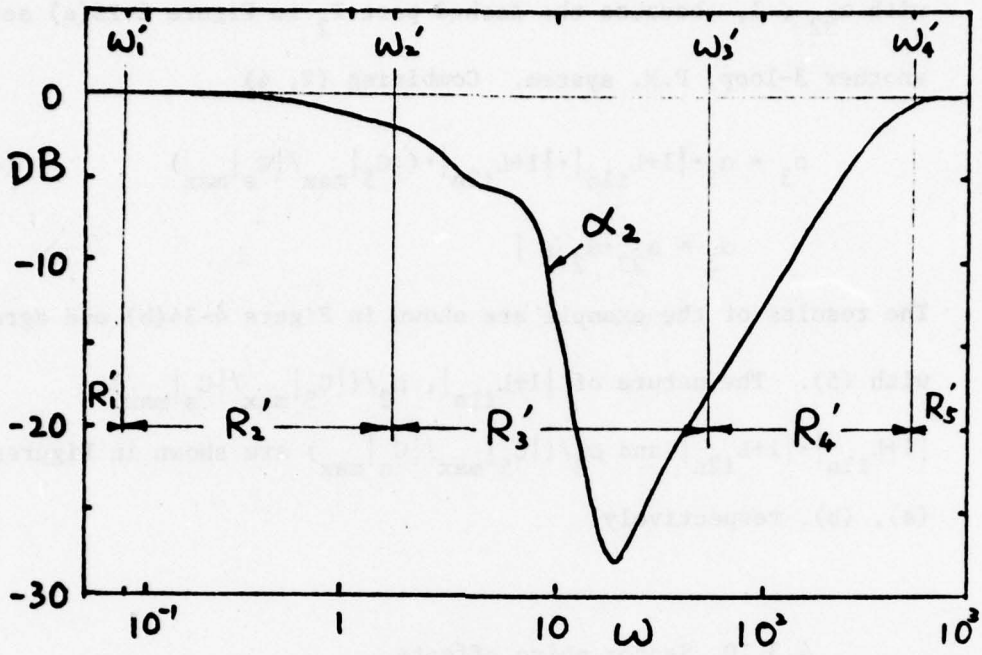

(a) Nature of α_2

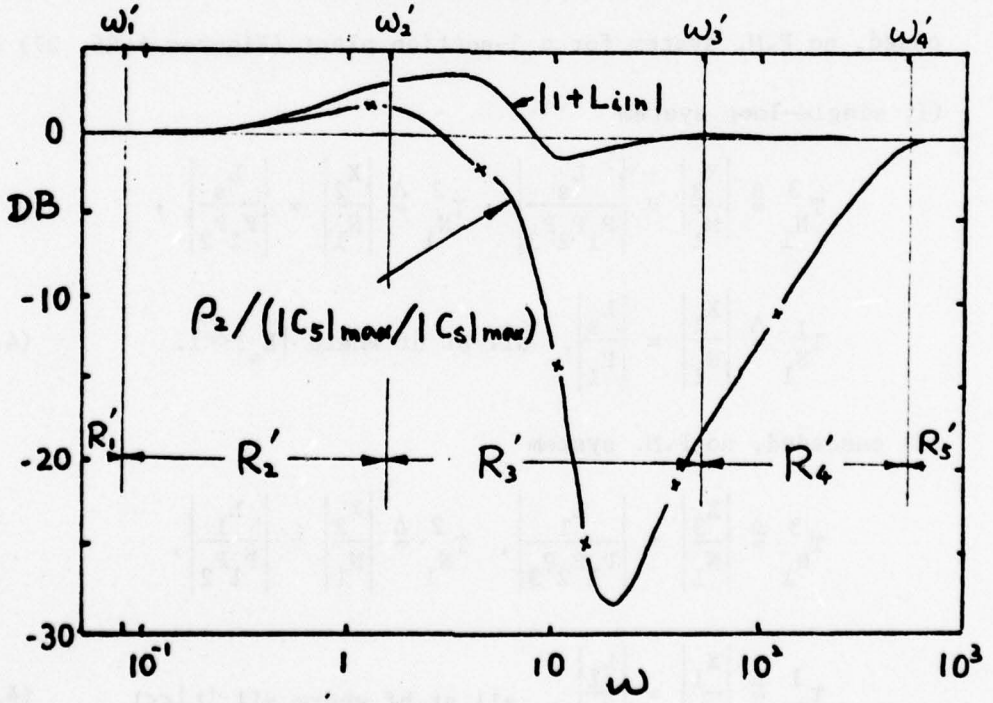

(b) Nature of $|1+L_{iln}|$ and $\rho/(|C_5|_{max}/|C_s|_{max})$

Figure 4-34. SLVR at C_{25}

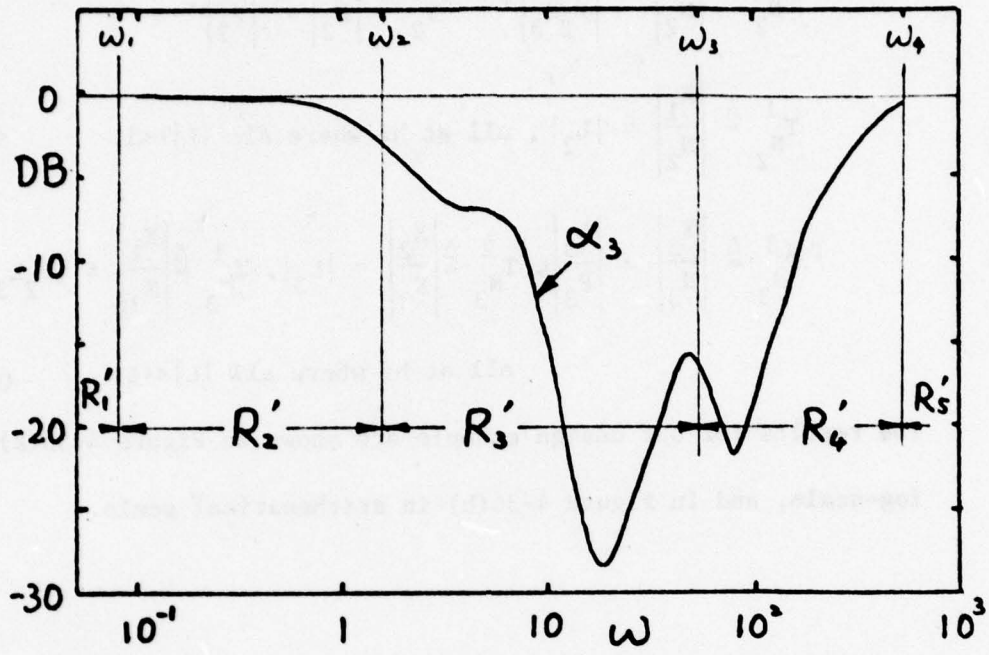

(a) Nature of α_3

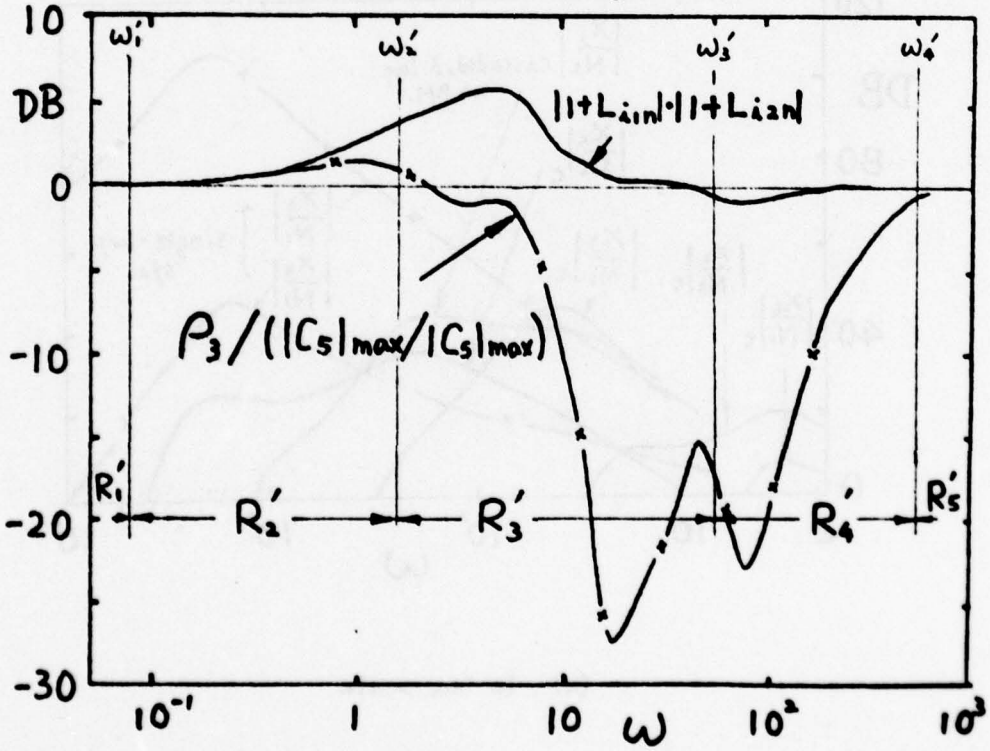

(b) Nature of $|1+L_{i1n}|\cdot|1+L_{i2n}|$ and $\rho_3/(|C_5|_{max}/|C_s|_{max})$

Figure 4-35. SLVR at C_{35}

$$T_{N_2}^{3} \triangleq \left|\frac{X_3}{N_2}\right| \simeq \left|\frac{L_2}{P_2P_3}\right|, \quad T_{N_2}^{2} \triangleq \left|\frac{X_2}{N_2}\right| \simeq \left|\frac{L_2}{P_2}\right|,$$

$$T_{N_2}^{1} \triangleq \left|\frac{X_1}{N_2}\right| \simeq |L_2|, \text{ all at hf where all } |L|<<1. \qquad (4.3\text{-}8)$$

$$T_{N_3}^{3} \triangleq \left|\frac{X_3}{N_3}\right| \simeq \left|\frac{L_3}{P_3}\right|, \; T_{N_3}^{2} \triangleq \left|\frac{X_2}{N_3}\right| \simeq |L_3|, \; T_{N_3}^{1} \triangleq \left|\frac{X_1}{N_3}\right| \simeq |P_2L_3|,$$

all at hf where all $|L|<<1$. (4.3-9)

The results for our design example are shown in Figure 4-36(a) in log-scale, and in Figure 4-36(b) in arithematical scale.

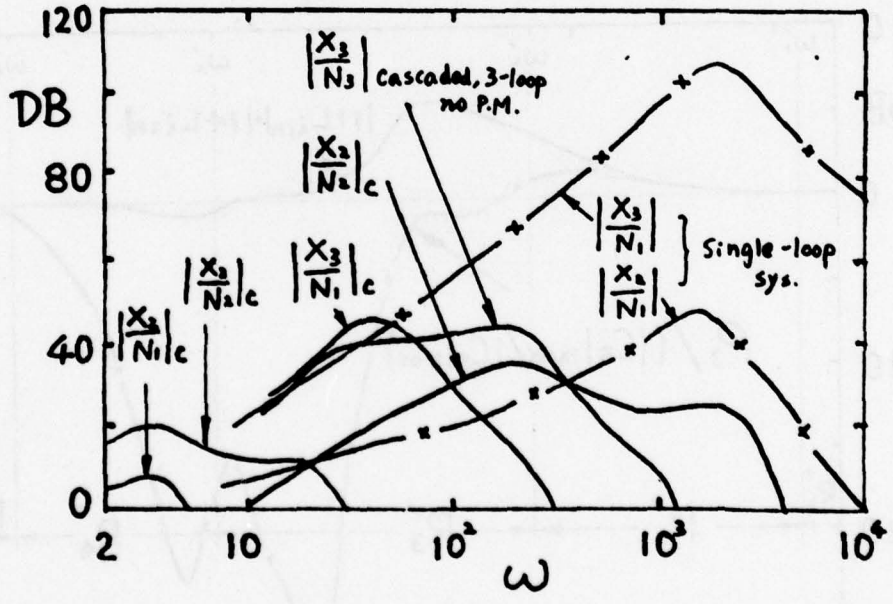

(a) In Log scale

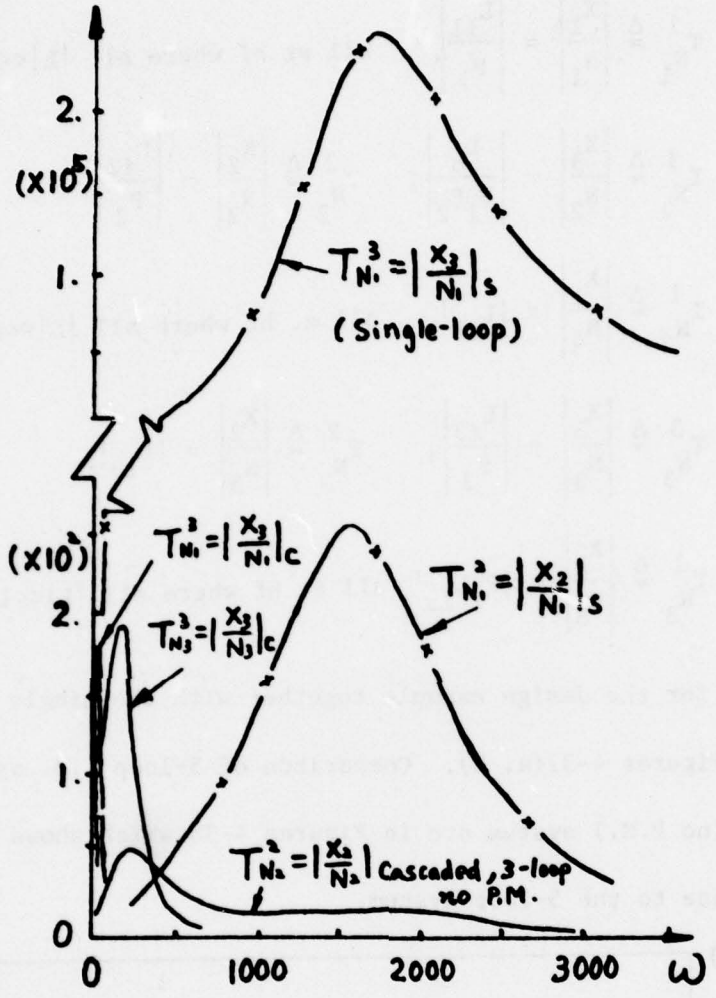

(b) In Arithematical scale

Figure 4-36. Noise responses of the single loop system and the cascaded, 3-loop, no P.M. system

The sensor noise functions for the 5-loop, P.M. system (Figure 4-24) are:

$$T_{N_1}^3 \triangleq \left|\frac{X_3}{N_1}\right| \simeq \left|\frac{L_o}{P_1P_2P_3}\right|, \quad T_{N_1}^2 \triangleq \left|\frac{X_2}{N_1}\right| \simeq \left|\frac{L_o}{P_1P_2}\right|,$$

$$T_{N_1}^{1} \triangleq \left|\frac{X_1}{N_1}\right| \simeq \left|\frac{L_{i1}}{P_1}\right| \quad \text{all at hf where all } |L|<<1. \tag{4.3-10}$$

$$T_{N_2}^{3} \triangleq \left|\frac{X_3}{N_2}\right| \simeq \left|\frac{L_o}{P_1P_2}\right|, \quad T_{N_2}^{2} \triangleq \left|\frac{X_2}{N_2}\right| \simeq \left|\frac{L_{i2}}{P_2}\right|,$$

$$T_{N_2}^{1} \triangleq \left|\frac{X_1}{N_2}\right| \simeq |L_{i2}| \quad \text{all at hf where all } |L|<<1. \tag{4.3-11}$$

$$T_{N_3}^{3} \triangleq \left|\frac{X_3}{N_3}\right| \simeq \left|\frac{L_{i3}}{P_3}\right|, \quad T_{N_3}^{2} \triangleq \left|\frac{X_2}{N_3}\right| \simeq |L_{i3}|,$$

$$T_{N_3}^{1} \triangleq \left|\frac{X_1}{N_3}\right| \simeq |P_2L_{i3}| \quad \text{all at hf where all } |L|<<1. \tag{4.3-12}$$

Results for the design example together with the single loop system are in Figures 4-37(a, b). Comparison of 5-loop P.M. system and 3-loop (no P.M.) system are in Figures 4-38 which shows the big saving due to the 5-loop system.

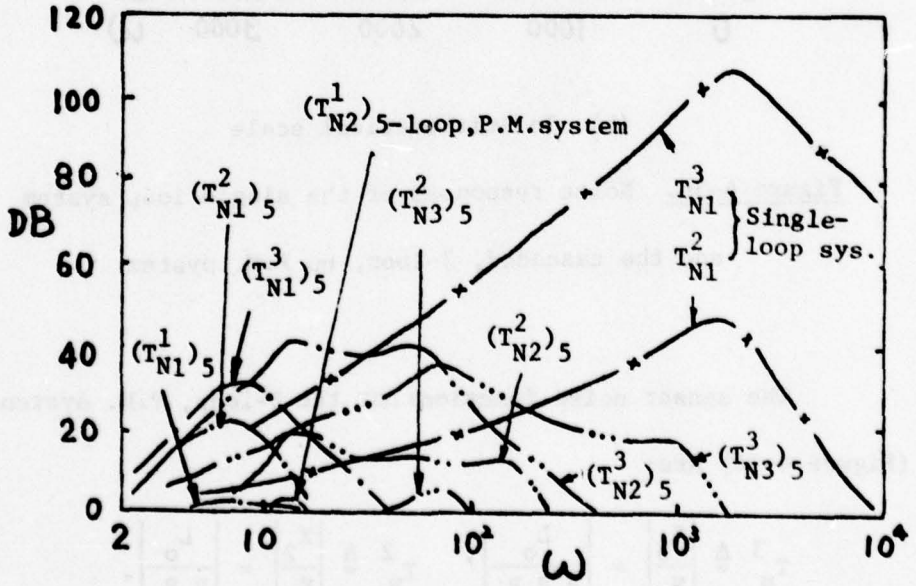

(a) In Log scale

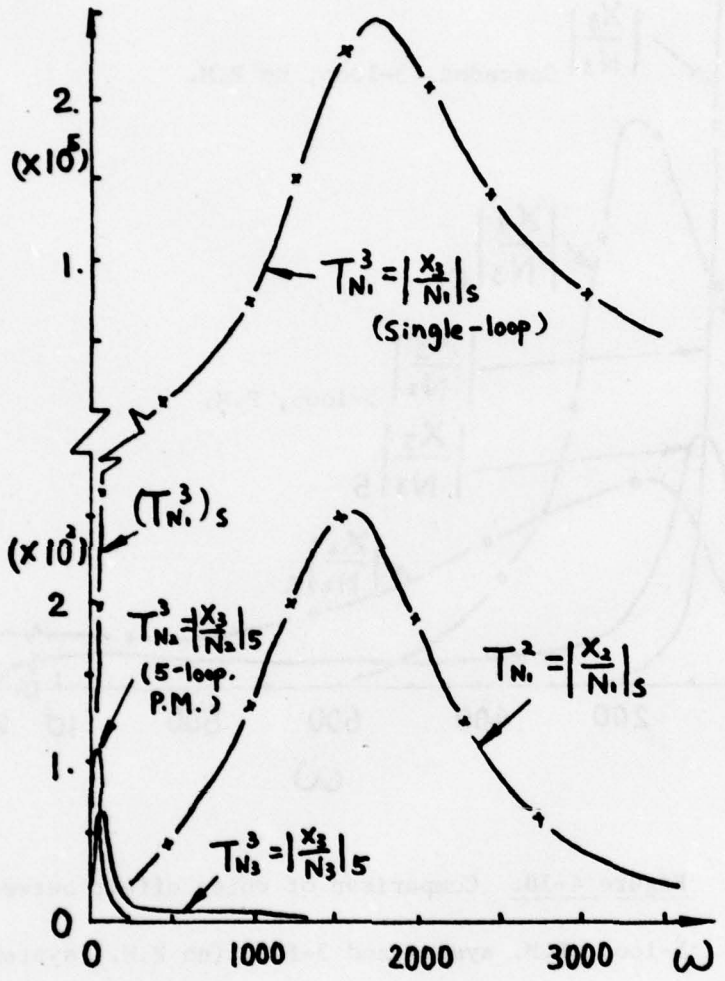

(b) In Arithematical scale

Figure 4-37. Noise response of the single loop system and the 5-loop, P.M. system

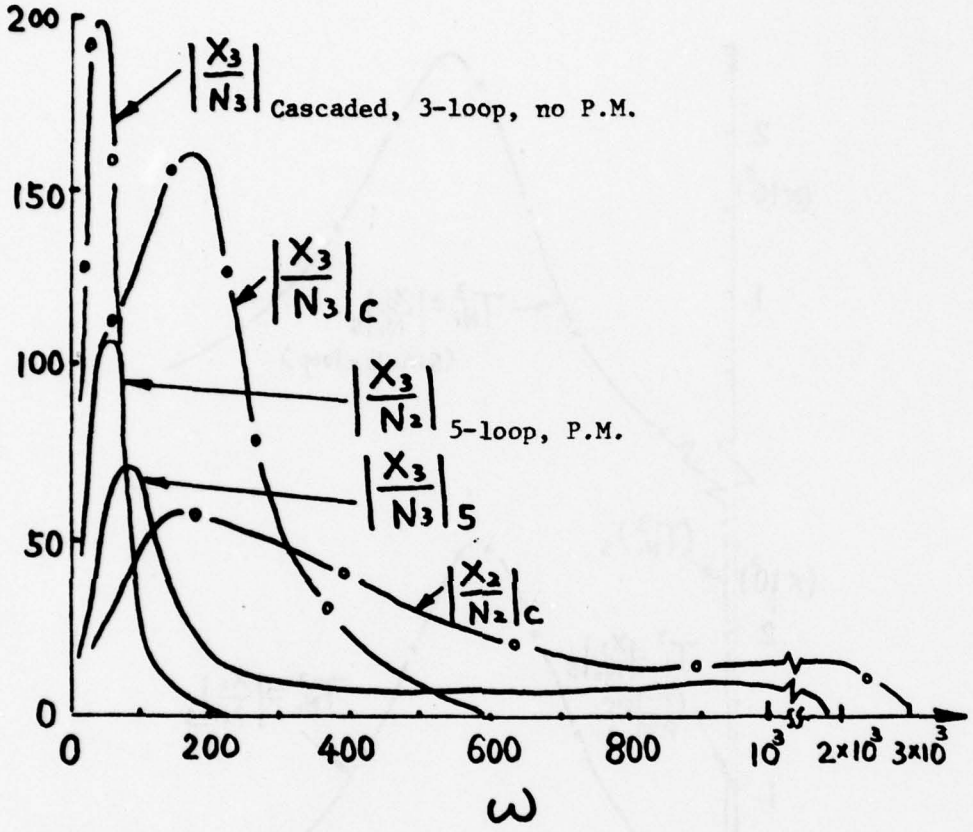

Figure 4-38. Comparison of noise effect between 5-loop, P.M. system and 3-loop (no P.M.) system

4.3.11 Signal level at plant input

In considering signal level increases, we have always gone backwards up to and including the output of the first plant section (X_{n-1} in Figure 39), but never bothered with input to the plant, X_n. The reason is that all feedback to X_n can proceed

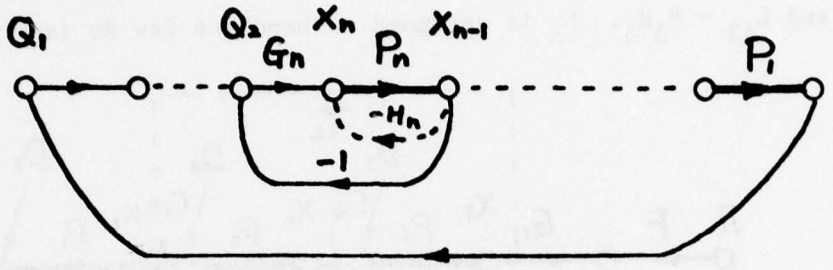

Figure 4-39 Cascaded, no P.M. multiple loop system

via a compensation network in cascade with the plant, e.g. G_n in Figure 4-39, rather than via P_n. The dimensions at Q_1, Q_2 can be electrical, not the physical ones of the plant (which may be chemical, aeronautical etc. as the case may be). Thus $X_n = X_{n-1}/P_n$ and in this way need not be affected by the feedback paths to X_n, which in this work we generally showed in the return path.

4.3.12 Design philosophy and perspective for second type 5-loop PM structure

The second type 5-loop PM structure is shown in Figure 4-40(b)(the first was Figure 4-24 and replotted in Figure 4-40(a)).

The outer loop $L_o = G_1 L_{o1} P_{3e}$ is designed first with $L_{o1} = G_2 P_{2e} P_{1e}$, ($P_{1e} = P_1/(1 + L_{i1})$, $P_{2e} = P_2/(1 + L_{i2})$, $L_{i1} = P_1 H_1$, $L_{i2} = P_2 H_2$) and $L_{i3} = P_3 H_3$. L_o is assigned to handle a few db (say 8db)

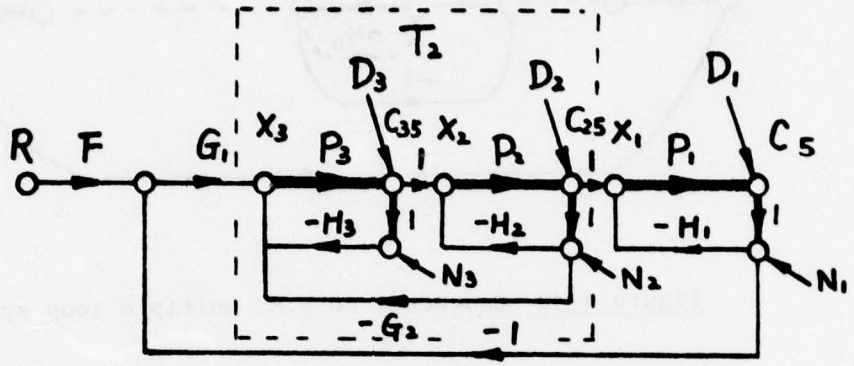

$L_{o2} \triangleq P_{3e} P_{2e} G_2$, $T_2 \triangleq P_{3e} P_{2e}/(1 + L_{o2})$, $L_o \triangleq T_2 P_{1e}$

(a) Structure I

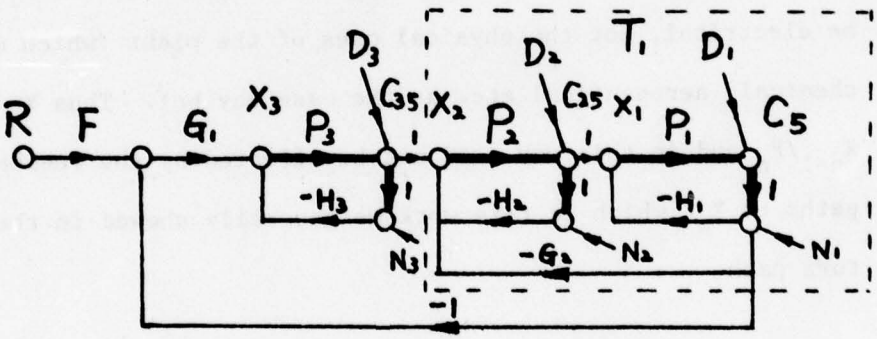

$L_{o1} \triangleq P_{2e} P_{1e} G_2$, $T_1 \triangleq P_{2e} P_{1e}/(1+L_{o1})$, $L_o \triangleq P_{3e} T_1$

(b) Structure II

$L_{i1} \triangleq P_1 H_1$, $L_{i2} \triangleq P_2 H_2$, $L_{i3} \triangleq P_3 H_3$, $P_{1e} \triangleq P_1/(1+L_{i1})$, $P_{2e} \triangleq P_2/(1+L_{i2})$, $P_{3e} \triangleq P_3/(1+L_{i3})$

Figure 4-40 5-loop, P.M. systems

uncertainty as a safety margin for the next step. Suppose we take the specific problem in Figure 4-40(b) where the hf uncertainty is 63 db, and a single-loop design gives L_{sn} in Figure 4-41. Measure 63-8 = 55 db up from the plateau of L_{sn} at A in Figure 4-41 to give L_{on} with new plateau at A' the nominal outer loop of our 5-loop design.

The loop $L_{o1} = P_{1e}P_{2e}G_2$ and $L_{i3} = P_3H_3$ now constitute two "parallel" inner loops (the first inner loops) next designed. Normally we would design L_{o1} in the same manner as L_{i1} was designed in Figure 4-13, i.e. SLVR considerations dominate. However, here L_{o1} need not handle the entire P_1P_2 uncertainty (whereas in Figure 4-13 L_{i1} did have to handle the P_1 uncertainty entirely), because here loops P_1H_1, P_2H_2 are available.

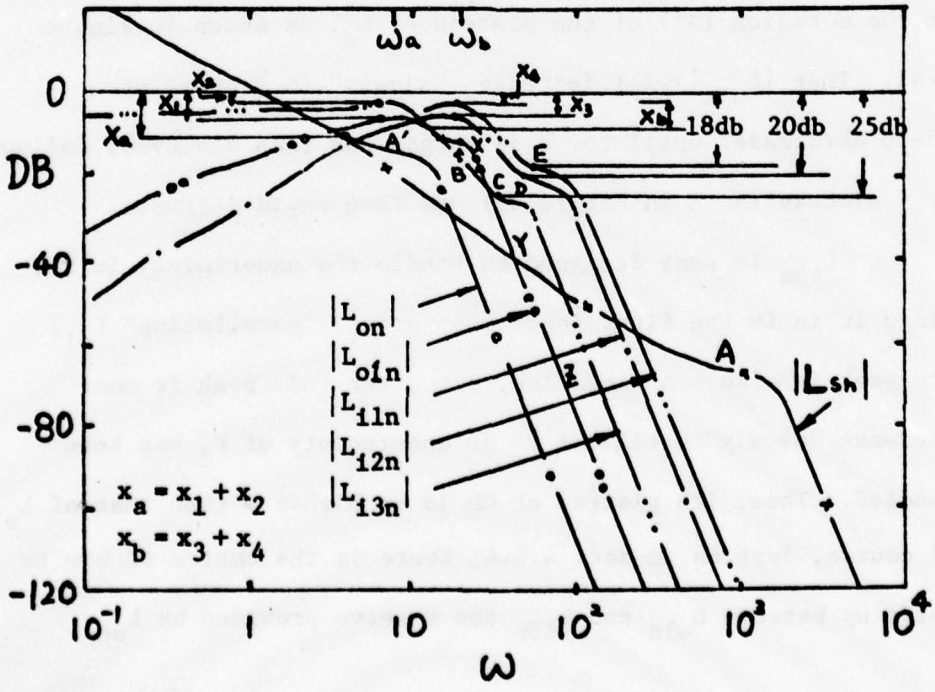

Figure 4-41 The perspective design of Structure II

SLVR considerations due to the other loops is considered later. We could assign some few db safety margin (say 8 db) for L_{o1} to handle. We now recall Figure 3-24 where we considered use of "positive feedback", locus A'B'C'MNQ for L_i, which is much better than A'''B'''C'''MNQ in terms of SLVR. There it was not useable because L_i had to handle bf uncertainty of $P_1 \sim 20$ db and a positive feedback path could not achieve it (recall the discussion in Section 3.5.4). However, here L_{o1} need handle only a token small uncertainty factor, so the "positive feedback" path is feasible. Hence we can pretty well ignore the SLVR problem in design of L_{o1}.

We can make a good estimate of L_{o1n} without a detailed design. It is an inner loop following L_o, so its peak will be in the ω region (A') of the plateau of L_o, as shown in Figure 4-41. Then $|L_{o1n}|$ will decrease "slowly" ($\sim$ average of 25-30 db/decade) until the 8 db margin has been achieved, followed by a plateau (at X in Figure 41) and then rapid decrease.

L_{i3n} is next designed to handle the uncertainty in P_3. Since it is in the first inner loop group, "paralleling" L_{o1}, its peak is also $\sim$ A' location, but after this peak it must decrease "slowly" until the 25 db uncertainty of P_3 has been handled. Thus, its plateau at CD is at higher ω than that of L_{o1n}. Of course, just as in Sec. 4.2.6, there is the choice of how to split up between L_{o1n} and L_{i3n} the reserve provided by L_{on}.

We next turn to the two "parallel" second inner loops $L_{i1} = P_1G_1$, $L_{i2} = P_2G_2$. L_{i1n} is designed to handle the uncertainty of P_1, and L_{3n} that of P_3; and the reserve due to L_{oln} design can be split up as desired. In Fig. 4-41, note that the peaks of L_{i1n}, L_{i2n} occur in the ω range ($\sim$ X) of the plateau of L_{oln}, inasmuch as this parallel inner-loop pair branch off from L_{oln}. L_{oln}, L_{o2n} were drawn as if there was even division of the L_{oln} reserve.

Note how the inner loops can be drawn approximately, without the need for a detailed design, - at most only of L_{sn}, the single - loop transmission. We should next consider the relative merits of Structures I (Figure 4-40(a)) and II (Figure 4-40(b)), but will first consider more fully the SLVR situation in Figure 4-40(b).

4.3.13 SLVR in structures I, II (Figures 4-40(a,b)

It is readily found that

$$C_{35}/C_5 = [(1+L_{o1})(1+L_{i1})(1+L_{i2})]/(P_1P_2) \qquad \text{in II}$$

$$C_{35}/C_5 = [(1+L_{i1})(1+L_{i2})]/(P_1P_2) \qquad \text{in I}$$

The effect of $(1+L_{o1})$ has been previously mentioned as not being dominant, so it would appear that the SLVR problem with respect to C_{35} is basically the same in I, II. There is, however, a difference. In I, L_{i1} is in the first inner loop pair, so the

$|1 + L_{i1}|>1$ factor is effective in a lower frequency range than in II where L_{i1} is in the second inner loop pair (bandwidth propagation effect). Hence SLVR would be bigger in Case I, because L_{i2} is in the second inner pair for both I and II. Consider $C_{25}/C_5 = (1+1_{i1})\ C_f$ for both I,II. As L_{i1} is in second inner loop pair in Case II (in first for Case I), SLVR tends to be bigger for Case I.

4.3.14 Noise response comparisons between structures I,II

The noise responses of Structures I,II are compared in Table 4-1. For example, at hf $X_2/N_3 \tilde{\sim} L_{i3}$ for both. However, in II, L_{i3} is in the first inner loop, so its final asymptotic descent begins earlier than in I. Hence, in the hf range $|L_{i3}|_I > |L_{i3}|_{II}$. The significance of a,b,c,d,e,g depend, of course, on the respective L/P ratios. If $|P|$ is large, then the effects are unimportant but in large uncertainties it is more likely that the L_i/P_j are large. If the level at X_3 is the major factor, then item (b) (as far as sensor noise is concerned) is the one to examine, but of course, the total RMS level due to all sources must be considered, so even if the difference is very large in (b), it does not matter much if (b) is still small compared to (a). If the X_2 level is important, then (d) should be contrasted with (f).

	Structure I		Structure II	Comparison
a) X_3/N_1	$L_o/(P_1P_2P_3)$	$\simeq$	$L_o/(P_1P_2P_3)$	Same
b) X_3/N_2	$\frac{L_{o2}+L_{i2}L_o}{P_2P_3}$	$>$	$\frac{L_{i2}L_o}{P_1P_2}$	Both L_{i2} in 2nd inner loop prs (ilp), L_{o2} in 1st ilp
c) X_3/N_3	L_{i3}/P_3	$>$	L_{i3}/P_3	In I, L_{i3} in 2nd ilp In II, L_{i3} in 1st ilp
d) X_2/N_1	$L_o/(P_1P_2)$	$<$	$\frac{L_o+L_{o1}}{P_1P_2} \simeq \frac{L_{o1}}{P_1P_2}$	L_{o1} in 1st ilp
e) X_2/N_2	$\frac{L_{i2}+L_{o2}}{P_2} \simeq \frac{L_{i2}}{P_2}$	$\simeq$	$\frac{L_{i2}}{P_2}$	
f) X_2/N_3	L_{i3}	$>$	L_{i3}	In I, L_{i3} in 2nd ilp In II, L_{i3} in 1st ilp
g) X_1/N_1	$\frac{L_{i1}+L_o}{P_1} \simeq \frac{L_{i1}}{P_1}$	$<$	$\frac{L_{i1}}{P_1}$	In I, L_{i1} in 1st ilp In II, L_{i1} in 2nd ilp
h) X_1/N_2	$L_{i2} + L_{o2} \sim L_{i2}$	$\simeq$	L_{i2}	L_{o2} in 1st ilp
i) X_1/N_3	P_2L_{i3}	$>$	P_2L_{i3}	In I, L_{i3} in 2nd ilp In II, L_{i3} in 1st ilp

Table 4-1 Noise responses (in hf range where $|1+L| \sim 1$)

Abbreviations

hf	high frequence
ℓf	low frequence
iℓp	inner loop pair
ℓti	linear time invariant
ℓtv	linear time varying
ℓhs	left hand side
rhs	right hand side
ISLV	ignoring signal level variation
N.P.R.	noise power ratio
P.M.	plant modification
S.L.	signal level
SLVR	signal level variation ratio
RMS	root mean square

REFERENCES

[1] Bode, H.W., Network Analysis and Feedback Amplifier Design. Van Nostrand, N.Y. (1945).

[2] Horowitz, I. and Sidi, M., Synthesis of feedback systems with large plant ignorance for prescribed time domain tolerances. Int. J. Control, 16, pp 287-309, 1972.

[3] Horowitz, I., Optimum loop transfer function in single-loop minimum-phase feedback systems. Int. J. Control, 18, pp 97-113, 1973.

[4] Horowitz, I. Synthesis of Feedback Systems. Academic Press, 1963.

[5] Horowitz, I. and Sidi, M., Synthesis of cascaded multiple-loop feedback systems with large plant parameter ignorance. Automatica, 9, pp 589-600, 1973.

[6] Sidi, M. Synthesis of linear feedback systems for prescribed time domain tolerances. Ph.D. Thesis, Weizmann Institute of Science, Israel, 1973.

[7] Rosenbaum, P. Reduction of the cost of feedback in systems with large parameter uncertainty. Ph.D. Thesis, Weizmann Institute of Science, Israel, 1978.

[8] Horowitz, I. and Rosenbaum, P., Nonlinear design for cost of feedback reduction in systems with large parameter uncertainty. Int. J. Control, 21, pp 977-1001, 1975.

[9] Horowitz, I., Smay, J., and Shapiro, A. A synthesis theory for self-oscillating adaptive systems (SOAS), Automatica, 10, pp 381-392, 1974.

[10] Horowitz, I., Smay, J. and Shapiro, A. A synthesis theory for the externally excited adaptive system (EEAS). IEEE Trans. AC-19, No.2, April, 1974.

[11] Krishnan, K.R. and Horowitz, I. Synthesis of a non-linear feedback system with significant plant-ignorance for prescribed system tolerances. Int. J. Control, 19, No.4, pp 689-706, 1974.

[12] Horowitz, I., and Wang, T.S. A synthesis theory for a class of multiple-loop systems with plant uncertainty. Int. J. Control. To appear.

[13] Wang, T.S. A synthesis theory for a class of single input-output multiple-loop feedback systems. Ph.D. Thesis, Weizmann Institute of Science, Israel, 1978.

[14] Krishnan, K.R. and Cruickshank, A. Frequency domain design of feedback systems for specified insensitivity of time-domain response to parameter variation. Int. J. Control, 25, pp 609-620, 1977.

[15] Horowitz, I. Synthesis of feedback systems with nonlinear time-varying uncertain plants to satisfy quantitative performance specifications. Proceedings of IEEE, 64, No. 1, Jan. 1976.

[16] Horowitz, I. A synthesis theory for linear time-varying feedback systems with plant uncertainty. IEEE Trans., AC-20, pp 454-464, Aug. 1975.

APPENDIX I

Patterns of Templates

Seven typical patterns of templates P_1 and P_2 are considered. They can be divided into three categories. The first category extends upward and to the right from the nominal point P_{in} (see Section 2.2.1), as shown in Figure I-1(a). And the

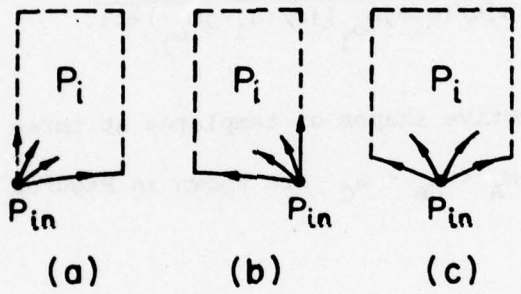

Figure I-1. Three categories of template.

second category extends upward and to the left from P_{in}, as shown in Figure I-1(b). The third one extends both the right and to the left from P_{in}, as shown in Figure I-1(c). The following three plant functions give templates of the shape of Figure I-1(a).

(1) $$P^a(s) = \frac{k}{s(s/p+1)}, \quad k = [k_1, k_2], \quad p = [p_1, p_2] \qquad \text{(I-1)}$$

$$P_n^a(s) = \frac{k_1}{s(s/p_1+1)} \qquad \text{(I-2)}$$

(2) $$P^b(s) = \frac{k(s/z+1)}{s(s/p_a+1)(s/p_b+1)}, \quad k = [k_1, k_2]$$

$$z = [z_1, z_2] \ , \quad p_a = [p_{a_1}, p_{a_2}] \ , \quad p_b = [p_{b_1}, p_{b_2}] \tag{I-3}$$

$$P_n^b(s) = \frac{k_1(s/z_2+1)}{s(s/p_{a_1}+1)(s/p_{a_2}+1)} \tag{I-4}$$

(3) $$P^c(s) = \frac{k}{s[s/(\sigma+j\omega_o)+1][s/(\sigma-j\omega_o)+1]}$$

$$k = [k_1, k_2] \ , \quad \omega_o = [\omega_{o_1}, \omega_{o_2}] \ , \quad \sigma = [\sigma_1, \sigma_2] \tag{I-5}$$

$$P_n^c(s) = \frac{k_1}{s[s/(\sigma_1+j\omega_{o_1})[s/(\sigma_1-j\omega_{o_1})+1]} \tag{I-6}$$

And the respective shapes of templates at three different frequencies $\omega_A < \omega_B < \omega_C$ are shown in Figures I-2,...,4. Note

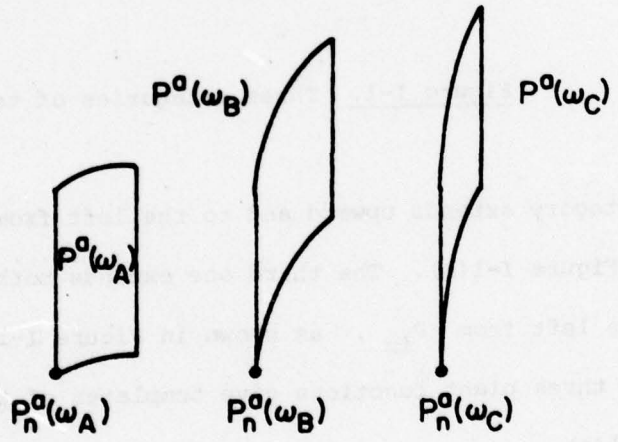

Figure I-2. Typical templates of $P^a(s)$, Case (1).

in Case (3) the pole-pair ranges inside MNQU and M'N'Q'U' in S-plane of Figure I-4(a). Three templates, Figures I-4(b),...,(d), are plotted with $\omega \geq \omega_{o_1}$. If $\omega < \omega_{o_1}$, then

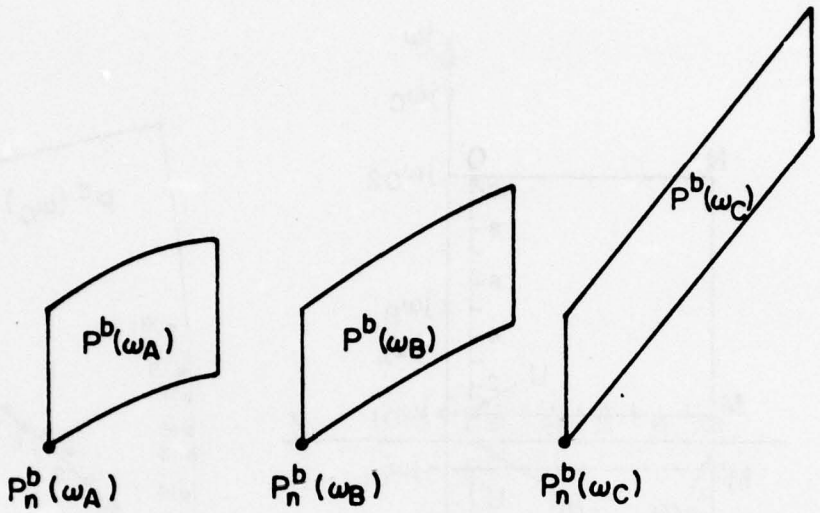

Figure I-3. Typical templates of $P^b(s)$, Case(2).

the template extends to the left which puts it in the second category.

The next three typical structures have the shape of Figure I-1(b).

(4) $$P^d(s) = \frac{k}{s(s+a)} \ , \ k = [k_1,k_2] \ , \ a = [a_1,a_2] \qquad \text{(I-7)}$$

$$P_n^d(s) = \frac{k_1}{s(s+a_2)} \qquad \text{(I-8)}$$

(5) $$P^e(s) = \frac{k(s+z)}{s(s+p_a)(s+p_b)} \ , \quad k = [k_1,k_2]$$

$$z = [z_1,z_2] \ , \ p_a = [p_{a_1},p_{a_2}] \ , \quad p_b = [p_{b_1},p_{b_2}] \qquad \text{(I-9)}$$

$$P_n^e(s) = \frac{k_1(s+z_1)}{s(s+p_{a_2})(s+p_{b_2})} \qquad \text{(I-10)}$$

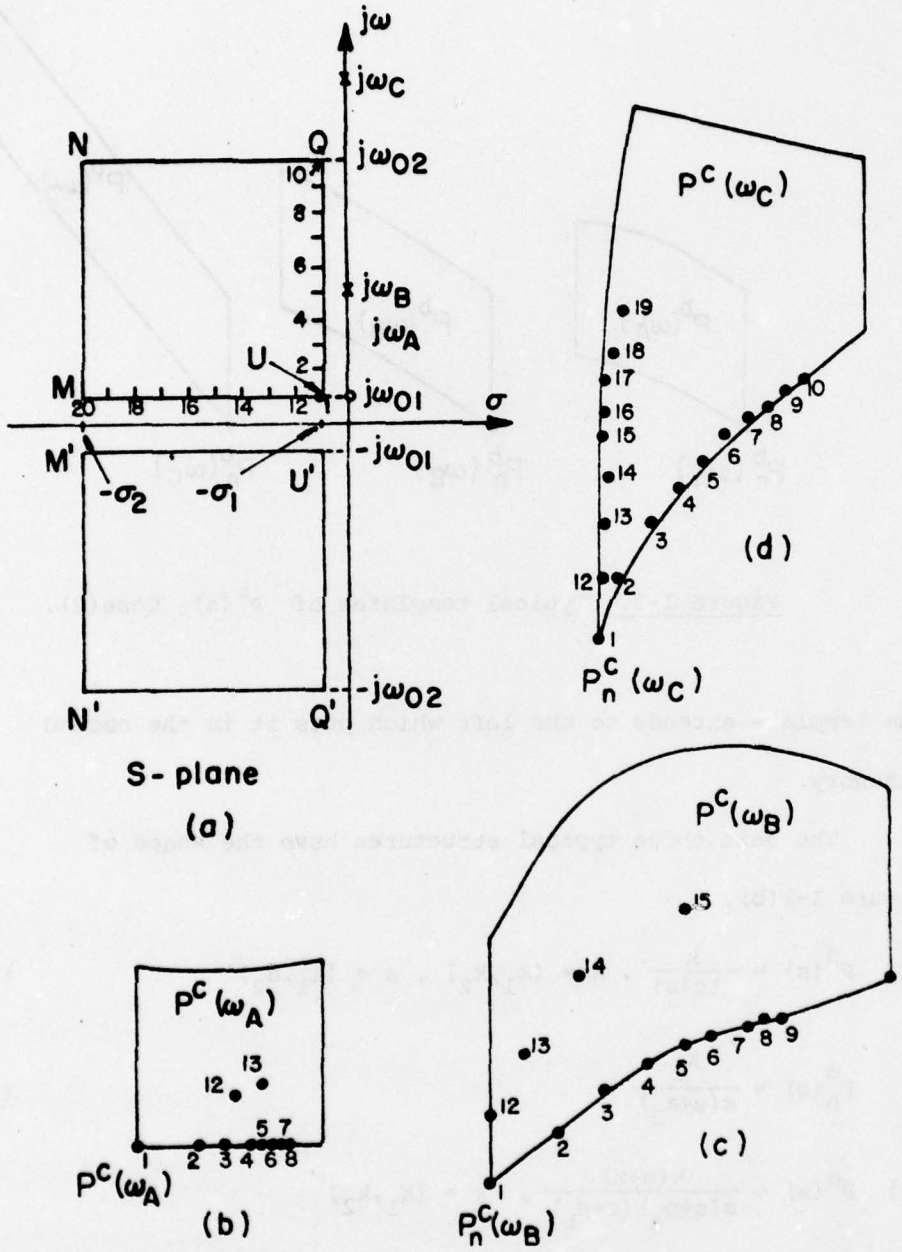

Figure I-4 (a). P^C parameter uncertainty in S-plane.

(b),...,(d). Typical templates of $P^C(s)$, Case 3.

$$(6)\quad P^f(s) = \frac{k}{s(s+\sigma+j\omega_o)(s+a-j\omega_o)}\ ,\quad k = [k_1,k_2]\ ,$$

$$\sigma = [\sigma_1,\sigma_2]\ ,\quad \omega_o = [\omega_{o_1},\omega_{o_2}] \qquad \text{(I-11)}$$

$$P_n^f(s) = \frac{k_1}{s(s+\sigma_2+j\omega_{o_2})(s+\sigma_2-j\omega_{o_2})}\ . \qquad \text{(I-12)}$$

Similarly, the respective shapes of templates at three different frequencies are shown in Figures I-5,...,7.

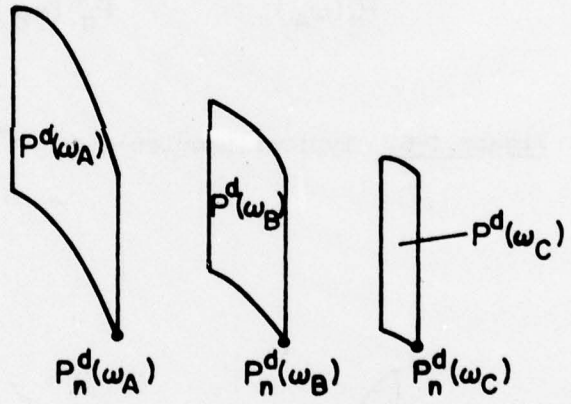

Figure I-5. Typical templates of $P^d(s)$, Case (4).

Note, in case (6), the complex pole-pair ranges within MNQU and M'N'Q'U' in the S-plane of Figure I-4(a). Three frequencies, $\omega_A < \omega_B < \omega_C$ in Figure I-7 are shown in Figure I-4(a). Again, if $\omega < \omega_{o_1}$, the template extends to the right which puts it in the first category.

The third category is the template extending both to the

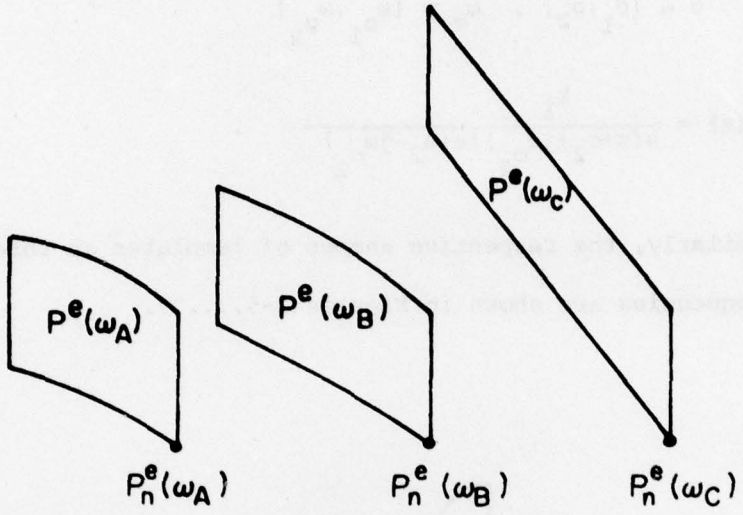

Figure I-6. Typical templates of $P^e(s)$, Case (5)

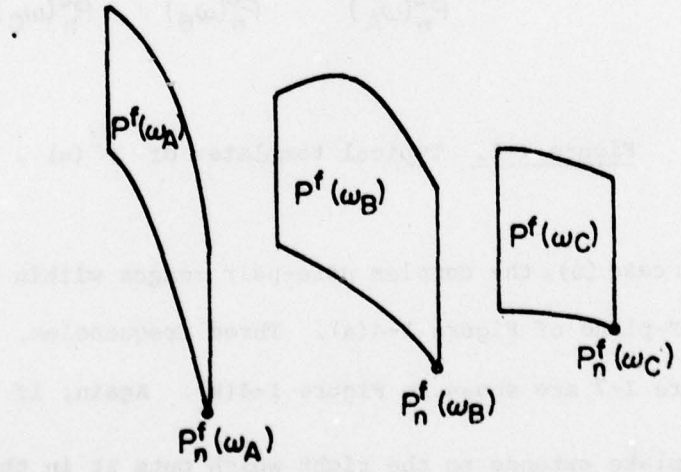

Figure I-7. Typical templates of $P^f(s)$, Case (6) with parameter uncertainty in Figure 2-14(a).

right and left of $P_n(j\omega)$. Such templates definitely occur when the plant set includes both minimum and nonminimum-phase elements, or both stable and unstable elements, or both, as illustrated by

$$(7)\quad P^g(s) = \frac{k}{s(s^2+as+b)}\ ,\quad k = [k_1,k_2] \qquad \text{(I-13)}$$

and the complex pole-pair of $P^g(s)$ ranging in MNQU , M'N'Q'U' of Figure I-8(a). Three typical templates at different frequencies $\omega_A < \omega_B < \omega_C$ in Figure I-8(a), are shown in Figures I-8(b),...,(d).

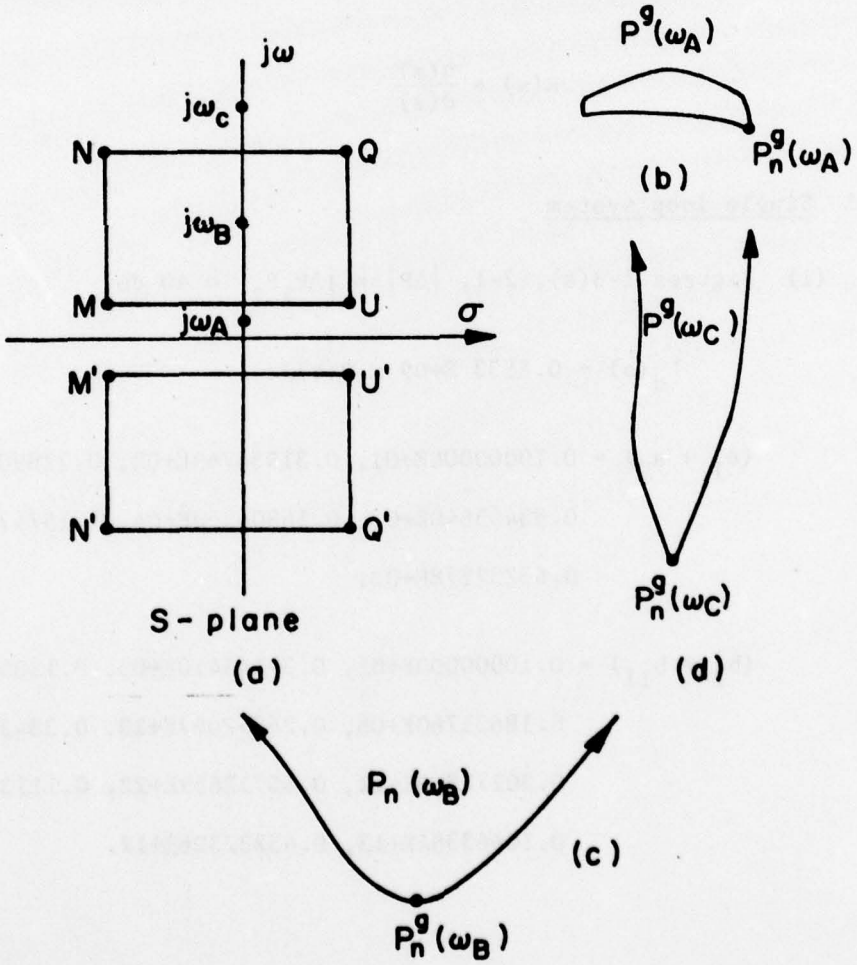

Figure I-8 (a) Range of complex pole-pair of $P^g(s)$

(b),(c),(d) Typical templates of $P^g(s)$, Case (7).

APPENDIX II

Rational Functions of Numerical Examples

The following expressions

$$n(s) = a_1 s^n + a_2 s^{n-1} + \ldots + a_{n-1} s + a_n$$

$$d(s) = b_1 s^m + b_2 s^{m-1} + \ldots + b_{m-1} s + b_m$$

represent the numerator and denominator of a rational function

$$R(s) = \frac{n(s)}{d(s)}$$

II.1 Single loop system

(1) Figures 1-3(a), 2-1, $|\Delta P| = |\Delta P_1 P_2| = 40$ db

$$L_s(s) = 0.8533 \text{ E+09 x } R(s)/s$$

$(a_1 \rightarrow a_7)$ = 0.10000000E+01, 0.31934769E+02, 0.22690730E+03, 0.83455640E+03, 0.15804253E+04, 0.15747661E+04, 0.65232178E+03.

$(b_1 \rightarrow b_{11})$ = 0.10000000E+01, 0.37145410E+03, 0.13052187E+06, 0.18631760E+08, 0.24542067E+10, 0.38433726E+11, 0.20272860E+12, 0.65712659E+12, 0.11138572E+13, 0.10663364E+13, 0.45332398E+12.

(2) Figure 4-26, $|\Delta P_1 P_2 P_3|$ = 63 db

$$L_s(s) = 0.2469E+13 \times R(s)/s$$

$(a_1 \rightarrow a_8)$ = 0.10000000E+01, 0.56891708E+02, 0.53505396E+03,
0.25187393E+04, 0.67933555E+04, 0.10429051E+05,
0.86928672E+04, 0.30754795E+04.

$(b_1 \rightarrow b_{12})$ = 0.10000000E+01, 0.28619253E+04, 0.80363180E+07,
0.86478725E+10, 0.90781117E+13, 0.23453811E+15,
0.15893765E+16, 0.63699863E+16, 0.15216227E+17,
0.21976691E+17, 0.17419455E+17, 0.63546876E+16.

II.2 Cascaded no P.M. system (Figure 1-15(a))

$$L_1(s) = 0.4513E+07 \times R(s)/s$$

$(a_1 \rightarrow a_5)$ = 0.10000000E+01, 0.12530328E+02, 0.45847092E+02,
0.70532761E+02, 0.41426315E+02.

$(b_1 \rightarrow b_9)$ = 0.10000000E+01, 0.92955902E+02, 0.78720469E+04,
0.28583481E+06, 0.91296180E+07, 0.59384608E+08,
0.18004706E+09, 0.22596626E+09, 0.12587678E+09.

$$L_2(s) = \frac{0.4 \times 40^2 \times 250^2}{(s^2 + 0.7 \times 40\, s + 40^2)(s^2 + 0.6 \times 250\, s + 250^2)}$$

II.3 2-loop P.M. system (Figures 2-2, 3-1)

(1) Design A

$$L_o(s) = 0.1500E+08 \times R(s)/s$$

$(a_1 \rightarrow a_7)$ = 0.10000000E+01, 0.20409637E+02, 0.15927747E+03,
0.67827539E+03, 0.16129690E+04, 0.19764927E+04,
0.10958235E+04.

$(b_1 \rightarrow b_{11})$ = 0.10000000E+01, 0.13237906E+03, 0.13798289E+05,
0.69865088E+06, 0.27376240E+08, 0.36934195E+09,
0.24605775E+10, 0.89491988E+10, 0.19679154E+11,
0.20897321E+11, 0.11361743E+11

$$L_{11}(s) = P_1(s)H_1(s)$$

$$= \frac{0.6(s+2)(40s+1) \times 45^2 \times 300^2}{(s+7.6)(40s+16.67)(s^2+45s+45^2)(s^2+0.7 \times 300s+300^2)}$$

(2) Design B

$$L_o(s) = 0.6371E+07 \times R(s)/s$$

$(a_1 \rightarrow a_5)$ = 0.10000000E+01, 0.11242662E+02, 0.42154068E+02,
0.67147141E+02, 0.40464294E+02.

$(b_1 \rightarrow b_9)$ = 0.10000000E+01, 0.99096939E+02, 0.86820664E+04,
0.33085312E+06, 0.10836760E+08, 0.71286944E+08,
0.23882952E+09, 0.32160640E+09, 0.20816880E+09.

$$L_{11}(s) =$$

$$\frac{0.68(1.25+3)(100s+1)(48s+1) \times 45^2 \times 250^2}{(1.2s+7)(100s+3)(48s+16.67)((1.2s)^2+1.2x45s+45^2)(s^2+0.7x250s+250^2)}$$

(3) Design C

$$L_o(s) = 0.2174E+08 \times R(s)/s$$

$$(a_1 \rightarrow a_5) = 0.10000000E+01,\ 0.10000282E+02,\ 0.35892151E+02,$$
$$0.56468002E+02,\ 0.33795563E+02.$$

$$(b_1 \rightarrow b_9) = 0.10000000E+01,\ 0.13268655E+03,\ 0.14712281E+05,$$
$$0.72320231E+06,\ 0.29226304E+08,\ 0.20516770E+09,$$
$$0.64369638E+09,\ 0.89944986E+09,\ 0.58078003E+09.$$

$$L_{11}(s) = \frac{0.5(s+3)(30s+1) \times 53^2 \times 330^2}{(s+9)(30s+25)(s^2+53s+53^2)(s^2+0.7 \times 330s+330^2)}$$

(4) Design D

$$L_o(s) = 0.1062E+08 \times R(s)/s$$

$$(a_1 \rightarrow a_5) = 0.10000000E+01,\ 0.11204820E+02,\ 0.41860794E+02,$$
$$0.66633072E+02,\ 0.40388687E+02.$$

$$(b_1 \rightarrow b_9) = 0.10000000E+01,\ 0.11282556E+03,\ 0.11241965E+05,$$
$$0.48381150E+06,\ 0.17928832E+08,\ 0.11999072E+09,$$
$$0.39335680E+09,\ 0.54214912E+09,\ 0.35039437E+09.$$

$$L_{11}(s) = \frac{0.5(s+2)(65s+1) \times 45^2 \times 300^2}{(s+5.5)(65s+16.67)(s^2+45s+45^2)(s^2+0.7 \times 300s+300^2)}$$

(5) Design E

$$L_o(s) = 0.4527E+08 \times R(s)/s$$

$$(a_1 \rightarrow a_4) = 0.10000000E+01,\ 0.72563848E+01,\ 0.17384796E+02,\ 0.13756199E+02.$$

$$(b_1 \rightarrow b_8) = 0.10000000E+01,\ 0.15459435E+03,\ 0.19788469E+05,\ 0.11070540E+07,\ 0.50771584E+08,\ 0.27372518E+09,\ 0.59020390E+09,\ 0.46127872E+09.$$

$$L_{i1}(s) = \frac{0.5(s + 4.5)(16s + 1) \times 60^2 \times 450^2}{(s + 10)(16s + 30)(s^2 + 60s + 60^2)(s^2 + 0.7 \times 450s + 450^2)}$$

(6) Design ISLV

$$L_o(s) = 0.4513E+07 \times R(s)/s$$

$$(a_1 \rightarrow a_5) = 0.10000000E+01,\ 0.12530328E+02,\ 0.45847092E+02,\ 0.70532761E+02,\ 0.41426315E+02.$$

$$(b_1 \rightarrow b_9) = 0.10000000E+01,\ 0.92955902E+02,\ 0.78720469E+04,\ 0.28583481E+06,\ 0.91296180E+07,\ 0.59384608E+08,\ 0.18004706E+09,\ 0.22596626E+09,\ 0.12587678E+09.$$

$$L_{i1} = \frac{0.4 \times 40^2 \times 250^2}{(s^2 + 0.7 \times 40s + 40^2)(s^2 + 0.6 \times 250s + 250^2)}$$

II.4 <u>3-loop P.M. system</u> (Figures 1-24, 4-1)

$$L_o(s) = 0.8331E+04 \times R(s)/s$$

$$(a_1 \rightarrow a_4) = 0.10000000E+01,\ 0.66346006E+01,\ 0.14799875E+02,\ 0.11100864E+02.$$

$$(b_1 \rightarrow b_8) = 0.10000000E+01,\ 0.22659241E+02,\ 0.35483521E+03,\ 0.31348845E+04,\ 0.19470348E+05,\ 0.66803438E+05,\ 0.10434300E+06,\ 0.64274535E+05.$$

$$L_{11}(s) = P_1(s)H_1(s) = \frac{4.125E+04 \times (s + 0.0153)}{(s^2 + 7s + 49)(s + 0.92)(s^2 + 0.4 \times 42s + 42^2)}$$

$$L_{12}(s) = P_2(s)H_2(s) = \frac{100 \times 120^2}{s^2 + 0.4 \times 120s + 120^2} \times R(s)$$

$$(a_1 \rightarrow a_{19}) = 0.10000000E+01,\ 0.14082841E+03,\ 0.83792813E+04,\ 0.31943319E+06,\ 0.83721440E+07,\ 0.17572984E+09,\ 0.27825651E+10,\ 0.35667821E+11,\ 0.36489101E+12,\ 0.30564963E+13,\ 0.20548717E+14,\ 0.11304564E+15,\ 0.48994571E+15,\ 0.17120134E+16,\ 0.44708156E+16,\ 0.90310750E+16,\ 0.11800826E+17,\ 0.99326917E+16,\ 0.15471337E+16.$$

$(b_1 \rightarrow b_{21})$ = 0.10000000E+01, 0.14528056E+03, 0.94655234E+04,
0.39388550E+06, 0.11540478E+08, 0.26542619E+09,
0.48147415E+10, 0.70719570E+11, 0.85274945E+12,
0.85201749E+13, 0.70939019E+14, 0.49207494E+15,
0.28397371E+16, 0.13527785E+17, 0.52607418E+17,
0.16437946E+18, 0.39902693E+18, 0.73407265E+18,
0.91156008E+18, 0.70823165E+18, 0.12667604E+18.

II.5. 5-loop P.M. system (type I) (Figure 4-24)

$L_o(s)$ and $L_{11}(s)$ are the same in 3-loop P.M. system

$$L_{02}(s) = \frac{2 \times 8^2 \times 60^2}{(s^2 + 8s + 8^2)(s^2 + 0.4 \times 60s + 60^2)}$$

$$L_{12}(s) = \frac{1.17E+07(s + 0.01)(s + 0.08)}{(0.1s + 1)(10s + 1)(s^2 + 0.4 \times 160s + 160^2)} \times R(s)$$

$(a_1 \rightarrow a_{14})$ = 0.10000000E+01, 0.21468179E+03, 0.21766156E+05,
0.16546280E+07, 0.80722400E+08, 0.29849879E+10,
0.82077090E+11, 0.16920483E+13, 0.27214205E+14,
0.31784369E+15, 0.27451995E+16, 0.15689971E+17,
0.55914070E+17, 0.89149159E+17.

$(b_1 \rightarrow b_{16})$ = 0.10000000E+01, 0.25456444E+03, 0.31895910E+05,
0.27528480E+07, 0.17333214E+09, 0.80436388E+10,
0.28532185E+12, 0.77741834E+13, 0.16361775E+15,
0.26835680E+16, 0.33811868E+17, 0.32018864E+18,
0.22259569E+19, 0.10466948E+20, 0.30991538E+20,
0.41061024E+20

$$L_{13}(s) = \frac{5.4E+09(s + 180)}{(s + 250)(s^2 + 2 \times 0.38 \times 36s + 36^2)(s^2 + 400s + 10^6)}$$

UNCLASSIFIED

SECURITY CLASSIFICATION OF THIS PAGE (When Data Entered)

REPORT DOCUMENTATION PAGE		READ INSTRUCTIONS BEFORE COMPLETING FORM
1. REPORT NUMBER AFOSR-TR- 78-1341	2. GOVT ACCESSION NO.	3. RECIPIENT'S CATALOG NUMBER
4. TITLE (and Subtitle) SYNTHESIS OF MULTIPLE LOOP FEEDBACK SYSTEMS WITH PLANT MODIFICATION		5. TYPE OF REPORT & PERIOD COVERED Interim 6. PERFORMING ORG. REPORT NUMBER
7. AUTHOR(s) Bor-Chyun Wang and Isaac M. Horowitz		8. CONTRACT OR GRANT NUMBER(s) AFOSR 76-2946
9. PERFORMING ORGANIZATION NAME AND ADDRESS University of Colorado Department of Electrical Engineering Boulder, Colorado 80309		10. PROGRAM ELEMENT, PROJECT, TASK AREA & WORK UNIT NUMBERS 61102F 2304/A1
11. CONTROLLING OFFICE NAME AND ADDRESS Air Force Office of Scientific Research/NM Bolling AFB, Washington, DC 20332		12. REPORT DATE August 1978 13. NUMBER OF PAGES 270
14. MONITORING AGENCY NAME & ADDRESS(if different from Controlling Office)		15. SECURITY CLASS. (of this report) UNCLASSIFIED 15a. DECLASSIFICATION/DOWNGRADING SCHEDULE

16. DISTRIBUTION STATEMENT (of this Report)

Approved for public release; distribution unlimited.

17. DISTRIBUTION STATEMENT (of the abstract entered in Block 20, if different from Report)

18. SUPPLEMENTARY NOTES

19. KEY WORDS (Continue on reverse side if necessary and identify by block number)

Multiple-loop systems
plant modification
internal feedback loops

20. ABSTRACT (Continue on reverse side if necessary and identify by block number)

Consider the constrained part (denoted as the Plant) of a control system, consisting of n coacoded sections, each of whose outputs can be sensed for feedback purposes. Feedback from these points is to be used to achieve apriori specified tolerances on the system response, despite great uncertainty in plant parameter values. In this first quantitative work of its kind, the feedback is permitted to proceed directly to internal plant variables, constituting "plant modification". The reason is that the internal plant signal levels

DD FORM 1 JAN 73 1473

UNCLASSIFIED

20. Abstract continued.

needed to achieve a specific output are now affected by the feedback loops. This is in contrast to previous quantitative research in which the feedback was confined to the plant input. The plant signal levels needed to achieve a specific output were then not influenced by the feedback.

Plant modification feedback permits greater reduction in the "cost of feedback", in terms of feedback loop bandwidths and effect of sensor noise, at the cost of increase in plant internal signal levels. In this work, the maximum permitted increase Q in signal level, is part of the design specifications. A step by step design procedure is presented for satisfying this Q requirement and the system response tolerances over the given range of plant uncertainty, and doing so at sensibly minimum "cost of feedback". This permits the designer to achieve desired trade-off between increased plant signal level and cost of feedback.